



Copyright Undertaking

This thesis is protected by copyright, with all rights reserved.

By reading and using the thesis, the reader understands and agrees to the following terms:

1. The reader will abide by the rules and legal ordinances governing copyright regarding the use of the thesis.
2. The reader will use the thesis for the purpose of research or private study only and not for distribution or further reproduction or any other purpose.
3. The reader agrees to indemnify and hold the University harmless from and against any loss, damage, cost, liability or expenses arising from copyright infringement or unauthorized usage.

IMPORTANT

If you have reasons to believe that any materials in this thesis are deemed not suitable to be distributed in this form, or a copyright owner having difficulty with the material being included in our database, please contact lbsys@polyu.edu.hk providing details. The Library will look into your claim and consider taking remedial action upon receipt of the written requests.

The Hong Kong Polytechnic University

Department of Applied Biology and Chemical Technology

**THE EFFECT OF FTSZ INHIBITORS ON THE B-LACTAM RESISTANT
ACTIVITY IN METHICILLIN-RESISTANT *STAPHYLOCOCCUS AUREUS***

CHEUNG KWAN CHOI

A Thesis Submitted in Partial Fulfillment of the Requirements

for the Degree of Master of Philosophy

December 2016

Certificate of Originality

I hereby declare that this thesis is my own work and that, to the best of my knowledge and belief, it reproduces no material previously published or written, nor material that has been accepted for the award of any other degree or diploma, except where due acknowledgement has been made in the text.

CHEUNG Kwan-Choi

December 2016

Abstract

The rapid emergence of antibiotic resistance in bacteria urges the need of new drugs to fight against bacterial infections caused by pathogenic microbes. The FtsZ protein is an essential cytoskeleton element involved in most bacterial cell divisions and has been shown to be a promising drug target. Previous studies indicated that derivatives of 3-methoxybenzamide (3-MBA) are inhibitors of the FtsZ protein and they can effectively inhibit the growth of Gram-positive rod-shaped *Bacillus subtilis* (*B. subtilis*) and exhibit synergistic effects when used in combination with β -lactams.

The aims of this project are to determine the antibacterial activities of 3-MBA derived FtsZ inhibitors (F332 and PC190723) and their combinations with β -lactams against methicillin-resistant *Staphylococcus aureus* (MRSA). 3-MBA derived FtsZ inhibitors were found to possess excellent growth inhibition effect on MRSA when used alone, and synergistically when used together with β -lactams. The bactericidal effects of individual and combinations of FtsZ inhibitors and β -lactams reveal that FtsZ inhibitors can restore the bactericidal and bacteriolysis activities of β -lactams against MRSA.

Delocalization of FtsZ protein as well as newly grown lipid-linked peptidoglycan precursor from their normal position were observed in *S. aureus* when it was treated with FtsZ inhibitors and in combination with β -lactams. Treatment by a combination of FtsZ inhibitor and β -lactam also caused cell enlargement of *S. aureus* which is a well-known physiological change when FtsZ activity is being interfered. It is believed that this change is related to a decrease in peptidoglycan crosslinking resulting from the delocalization of lipid-linked peptidoglycan precursors over the entire cell.

Acknowledgements

I would like to express my sincere gratitude to my chief supervisor, Prof. K. Y. Wong for his support, encouragement, supervision, invaluable suggestion and his valuable comments on this project.

Moreover, I would like to give my deepest gratitude to Dr. W. H. Chung for his invaluable advice and patience throughout my whole study. I would particularly like to thank Dr. H. K. Yap for teaching me molecular biology technique and his kind comments, Dr. K. F. Chan for providing chemical compounds, Dr. L. Y. So for teaching me basic laboratory techniques, Dr. Y. J. Gu for her generous assistance in high resolution and super-resolution microscopies, Mr. K. K. Tang for his expertise in microscopy, and Dr. H. Y. Chow for teaching me basic microscopy technique. Professor Elizabeth Harry and her group fellow Dr. Andrew T. F. Liew of University of Technology are thankful for the generous gift of plasmids and advice.

In addition, I am also greatly indebted to my groupmates, Dr. Y. W. Chen, Dr. Y. Wang, Mr. W. L. Cheong, Dr. Warrick K. C. Lo, Dr. N. Sun, Dr. Lawrence Y. S. Lee, Dr. K. C. Cheung, Dr. E. Ha, Miss R. L. Du, Mr. H. W. Man and all of my friends who have given me valuable suggestion and encouragement.

Furthermore, I would like to acknowledge the Research Committee of the Hong Kong Polytechnic University for the award of a postgraduate studentship from 2014 to 2016.

Last, but not least, my heartiest thanks go to my adorable son, and my beloved husband for sharing all the sweet and bad time with me, and my family for their persistent love, support, patient, guidance and encouragement.

Table of Content

CERTIFICATE OF ORIGINALITY	I
ABSTRACT	II
ACKNOWLEDGEMENTS	III
TABLE OF CONTENT	IV
ABBREVIATIONS	VII
LIST OF TABLES AND FIGURES	XII
CHAPTER 1. INTRODUCTION	1
1.1 <i>STAPHYLOCOCCUS AUREUS</i> INFECTION AND ANTIBIOTIC RESISTANCE	2
1.2 REGULATION OF CELL WALL SYNTHESIS	5
1.2.1 Cell morphology and cell shape	5
1.2.2 Role of FtsZ protein in cell division	7
1.2.3 Depletion of FtsZ protein	12
1.2.4 From cytoskeletal elements to membrane-bound protein	13
1.3 FTSZ INHIBITORS	14
1.3.1 Natural product inhibitors of FtsZ	14
1.3.2 Synthetic inhibitors of FtsZ	20
1.4 BIOSYNTHESIS AND STRUCTURE OF PEPTIDOGLYCAN OF <i>S. AUREUS</i>	27
1.4.1 Penicillin binding proteins (PBPs)	30
1.4.2 PBP in <i>S. aureus</i>	33
1.5 B-LACTAM ANTIBIOTIC	39
1.5.1 Acylation of PBP2 by β -lactam	39
1.5.2 β -lactam-resistant <i>S. aureus</i> (methicillin-resistant <i>S. aureus</i>)	39

1.6	AIMS AND OBJECTIVES OF THIS PROJECT-----	42
CHAPTER 2. ANTIBACTERIAL SUSCEPTIBILITY TESTS-----		44
2.1	INTRODUCTION -----	45
2.2	EXPERIMENTAL -----	48
2.2.1	Materials -----	48
2.2.2	Instrumentation and software -----	50
2.2.3	Minimum inhibitory concentration (MIC) assay-----	50
2.2.4	Study on the combination effect of FtsZ inhibitors and β -lactam antibiotics -----	51
2.2.5	Minimal bactericidal concentration (MBC) assay -----	52
2.2.6	Time-kill kinetic studies -----	53
2.2.7	Bacteriolysis assay -----	54
2.3	RESULTS AND DISCUSSION-----	54
2.3.1	Minimum inhibitory concentration (MIC) assay-----	54
2.3.2	Study on the combination effect of FtsZ inhibitors and β -lactam antibiotics -----	57
2.3.3	Minimal bactericidal concentration (MBC) assay -----	59
2.3.4	Time-kill kinetics -----	61
2.3.5	Bacteriolytic assay-----	68
2.4	CONCLUDING REMARKS -----	74
CHAPTER 3. TARGET LOCALIZATION AND MORPHOLOGICAL STUDIES -----		75
3.1	INTRODUCTION -----	76
3.2	EXPERIMENTAL -----	78

3.2.1	Materials -----	78
3.2.2	Instrumentation and software -----	80
3.2.3	Localization of FtsZ protein in <i>S. aureus</i> -----	80
3.2.4	Localization of transpeptidase substrate in <i>S. aureus</i> -----	85
3.2.5	Morphological studies -----	87
3.3	RESULTS AND DISCUSSION-----	89
3.3.1	Localization of FtsZ protein-----	89
3.3.2	Localization of transpeptidase substrate in <i>S. aureus</i> -----	93
3.3.3	Morphological studies -----	105
3.4	CONCLUDING REMARKS -----	117
CHAPTER 4. CONCLUSION -----		118
APPENDIX I VISUALIZATION OF NEWLY GROWN PEPTIDOGLYCAN -----		121
APPENDIX II HISTOGRAM SHOWING THE FREQUENCY DISTRIBUTION OF CELL VOLUME IN MRSA -----		158
REFERENCES -----		172

Abbreviations

ATCC	American Type Culture Collection
BHI	Brain-heart infusion
<i>B. subtilis</i>	<i>Bacillus subtilis</i>
°C	Degree Celsius
CA-MHB	Cation-adjusted Müller-Hinton broths
CaCl ₂	Calcium chloride
CFU	Colony forming unit
CLSI	Clinical and Laboratory Standards Institute
CPase	Carboxypeptidase
d	Diameter
DMSO	Dimethyl sulfoxide
DNA	Deoxyribonucleic acid
<i>E. coli</i>	<i>Escherichia coli</i>
F	Farad
FICI	Fractional inhibitory concentration index
Fts/ <i>fts</i>	Filamenting temperature sensitive
GDP	Guanosine-5'-diphosphate
GFP	Green fluorescence protein

GlcNAc	<i>N</i> -acetylglucisamine
Gly ₅	Pentaglycine
GTase	Transglycosylase
GTP	Guanosine-5' triphosphate
h	Hour(s)
HMW	High-molecular-weight
HUVEC	Human umbilical vein endothelial cell
IC ₅₀	The half maximal inhibitory concentration
IPTG	Isopropyl-β-D-1-thiogalactopyranoside
L	Liter
LB broth	Luria-Bertani broth
LD ₅₀	Median lethal dose
LMW	Low-molecular-weight
LTA	Lipoteichoic acid
m	Milli- (10^{-3})
M	Mole per liter
MATE	Multidrug and toxin extrusion transport protein
Mgts	Monofunctional transglycosylases
MBC	Minimal bactericidal concentration

MDRSA	Multi-drug resistant <i>Staphylococcus aureus</i>
MIC	Minimum inhibitory concentration
mL	Milliliter
mol	Mole(s)
MRSA	Methicillin-resistant <i>Staphylococcus aureus</i>
MurNAc	N-acetylmuramyl
<i>M. tuberculosis</i>	<i>Mycobacterium tuberculosis</i>
<i>M. smegmatis</i>	<i>Mycobacterium smegmatis</i>
n	Nano- (10^{-9})
NMR	Nuclear magnetic resonance
OD _x	Optical density at wavelength of x nm
<i>oriC</i>	Origin of replication
PBP _s	Penicillin binding proteins
PBS	Phosphate-buffered saline
PDB	Protein Data Bank
RNA	Ribonucleic acid
rpm	Revolution per minutes
<i>S. aureus</i>	<i>Staphylococcus aureus</i>
SBT	Serum bacterial test

SgtA	Second putative transglycosylase
SIM	Structured illumination microscopy
<i>S. pneumonia</i>	<i>Streptococcus pneumonia</i>
STORM	Stochastic optical reconstruction microscopy
STD	Saturation transfer difference
TSB	Trypticase soy broth
TPase	Transpeptidase
T7-loop	Tubulin-like loop No. 7
<i>Ter</i>	Terminus region
UDP	Undecaprenyl pyrophosphate
V	Volt
<i>V</i>	Volume
v/v	Volume per volume
Van/Van-FL	Vancomycin: Vancomycin BODIPY@FL conjugate pre-mixed solution
VREF	Vancomycin-resistant <i>Enterococcus faecium</i>
VRSA	Vancomycin-resistant <i>Staphylococcus aureus</i>
W	Watt
WTA	Wall teichoic acid

YFP	Yellow fluorescent protein
ZipA	FtsZ ring interacting protein A
ZapA	Z-ring association proteins A
3-MBA	3-Methoxybenzamide
μ	Micro- (10^{-6})
Ω	Ohm

List of Tables and Figures

Tables

Table 1.1 A list of natural product inhibitors FtsZ	16
Table 1.2 A list of synthetic and semi-synthetic compounds inhibitors of FtsZ	22
Table 1.3 A summary of <i>S. aureus</i> PBPs.....	34
Table 2.1 Structure of testing compounds	49
Table 2.2 MIC determination of FtsZ inhibitors and β -lactam antibiotics against <i>S. aureus</i> strains RN4220 (MSSA), ATCC 29213 (MSSA) and ATCC BAA-41 (MRSA) respectively.	56
Table 2.3 Susceptibility test results, in combination effects determination of FtsZ inhibitors and β -lactam antibiotics against MRSA ATCC BAA-41.....	58
Table 2.4 MBC determination of FtsZ inhibitors, β -lactam antibiotics and their combinations against MRSA ATCC BAA-41.....	60
Table 3.1 Antibiotic selection of various plasmid in different bacterial strains	82
Table 3.2 Cell volume at mode, mean and standard deviation of MRSA ATCC BAA-41 in the absence of antibacterial compound.....	108
Table 3.3 Cell volumes at mode, mean and standard deviation of MRSA ATCC BAA-41 in the presence of FtsZ inhibitor F332 at a range of concentrations.....	109
Table 3.4 Cell volumes at mode, mean and standard deviation of MRSA ATCC BAA-41 in the presence of FtsZ inhibitor PC190723 at a range of concentrations....	110
Table 3.5 Cell volumes at mode, mean and standard deviation of MRSA ATCC BAA-41 in the presence of oxacillin at a range of concentrations.....	111
Table 3.6 Cell volumes at mode, mean and standard deviation of MRSA ATCC BAA-41 in the presence of methicillin at a range of concentrations.....	112

Table 3.7 Cell volumes at mode, mean and standard deviation of MRSA ATCC BAA-41 in the presence of F332 and oxacillin combination at a range of concentrations..	113
Table 3.8 Cell volumes at mode, mean and standard deviation of MRSA ATCC BAA-41 in the presence of F332 and methicillin combination at a range of concentrations..	114
Table 3.9 Cell volumes at mode, mean and standard deviation of MRSA ATCC BAA-41 in the presence of PC190723 and oxacillin combination at a range of concentrations..	115
Table 3.10 Cell volumes at mode, mean and standard deviation of MRSA ATCC BAA-41 in the presence of PC190723 and methicillin combinations at a range of concentrations..	116

Figures

Figure 1.1 Antibiotic resistant mechanism of bacteria.	4
Figure 1.2 Crystal structure of <i>S. aureus</i> FtsZ monomer (PDB ID code: 3VOB) (prepared by ICM Molsoft LCC).....	9
Figure 1.3 Biosynthetic pathway of peptidoglycan	29
Figure 1.4 Enzymatic reaction of transglycosylation and transpeptidation for polymerization and crosslinking of glycan stands respectively.....	31
Figure 1.5 PBP2 is maintained by PBP2a in MRSA.	38
Figure 1.6 The crystal structure of the PBP2a of <i>S. aureus</i> (PDB ID code: 4DKI). ...	41
Figure 2.1 Time-kill curve for <i>S. aureus</i> ATCC BAA-41 in the precense or absence of FtsZ inhibitor F332..	63

Figure 2.2 Time-kill curve for <i>S. aureus</i> ATCC BAA-41 in the presence or absence of FtsZ inhibitor PC190723..	63
Figure 2.3 Time-kill curve for <i>S. aureus</i> ATCC BAA-41 in the presence or absence of β -lactam antibiotic oxacillin..	64
Figure 2.4 Time-kill curve for <i>S. aureus</i> ATCC BAA-41 in the presence or absence of β -lactam antibiotic methicillin..	64
Figure 2.5 Time-kill curve for <i>S. aureus</i> ATCC BAA-41 in the presence or absence of the F332 and oxacillin.....	65
Figure 2.6 Time-kill curve for <i>S. aureus</i> ATCC BAA-41 in the presence or absence of the F332 and methicillin..	65
Figure 2.7 Time-kill curve for <i>S. aureus</i> ATCC BAA-41 in the presence or absence of the PC190723 and oxacillin.....	66
Figure 2.8 Time-kill curve for <i>S. aureus</i> ATCC BAA-41 in the presence or absence of the PC190723 and methicillin.....	66
Figure 2.9 Time-kill curve for <i>S. aureus</i> ATCC BAA-41 in the presence or absence of the vancomycin.....	67
Figure 2.10 Time-kill curve for <i>S. aureus</i> ATCC BAA-41 in the presence or absence of the chloramphenicol.....	67
Figure 2.11 Growth profile of <i>S. aureus</i> ATCC BAA-41 in the presence of FtsZ inhibitor F332 in MIC values and sub-lethal concentrations.....	71
Figure 2.12 Growth profile of <i>S. aureus</i> ATCC BAA-41 in the presence of FtsZ inhibitor PC190723 in MIC values and sub-lethal concentrations.....	71
Figure 2.13 Growth profile of <i>S. aureus</i> ATCC BAA-41 in the presence of β -lactam antibiotic oxacillin in MIC values and sub-lethal concentrations.....	72

Figure 2.14 Growth profile of *S. aureus* ATCC BAA-41 in the presence of β -lactam antibiotic methicillin in MIC values and sub-lethal concentrations 72

Figure 2.15 Growth profile of *S. aureus* ATCC BAA-41 in the presence of FtsZ inhibitors and β -lactam antibiotic combinations in MIC values..... 73

Figure 2.16 Growth profile of MRSA ATCC BAA-41 in the presence of vancomycin and chloramphenicol in MIC \times 4 concentration. 73

Figure 3.1 *S. aureus* RN 4220-FtsZ-GFP mutant was (A) expressed with FtsZ-GFP protein, (B) stained for visualizing nucleus acid (blue) and (C) a merged image in the absence of antibiotic compound..... 90

Figure 3.2 *S. aureus* RN 4220-FtsZ-GFP mutant was (A) expressed with FtsZ-GFP protein, (B) stained for visualizing nucleus acid (blue) and (C) a merged image in the presence of FtsZ inhibitors (i) F332 and (ii) PC190723 with a concentration of MIC \times 4..... 91

Figure 3.3 *S. aureus* RN 4220-FtsZ-GFP mutant was (A) expressed with FtsZ-GFP protein, (B) stained for visualizing nucleus acid (blue) and (C) a merged image in the presence of β -lactam antibiotic (i) oxacillin and (ii) methicillin at a concentration of MIC \times 4. 92

Figure 3.4 MRSA BAA-41 was stained with single channel (A) for visualizing (i) lipid II of newly grown cell wall (green), (ii) nucleus acid (blue), (iii) cell membrane (red), (iv) DIC image; (C) (i) merage image of (A)(i) and (A)(ii); and (C) (ii) merage image of (A)(i), (A)(ii) and (A)(iii) in the absence of antibiotic compound 96

Figure 3.5 MRSA BAA-41 was stained with single channel (A) for visualizing (i) lipid II of newly grown cell wall (green), (ii) nucleus acid (blue), (iii) cell membrane (red), (iv) DIC image and (C) (i) merage image of (A)(i) and (A)(ii); and (C) (ii)

merage image of (A)(i), (A)(ii) and (A)(iii) in the presence of FtsZ inhibitor F332 at MIC × 2.....	97
Figure 3.6 MRSA BAA-41 was stained with single channel (A) for visualizing (i) lipid II of newly grown cell wall (green), (ii) nucleus acid (blue), (iii) cell membrane (red), (iv) DIC image and (C) (i) merage image of (A)(i) and (A)(ii); and (C) (ii) merage image of (A)(i), (A)(ii) and (A)(iii) in the presence of FtsZ inhibitor PC190723 at MIC × 2.....	98
Figure 3.7 MRSA BAA-41 was stained with single channel (A) for visualizing (i) lipid II of newly grown cell wall (green), (ii) nucleus acid (blue), (iii) cell membrane (red), (iv) DIC image and (C) (i) merage image of (A)(i) and (A)(ii); and (C) (ii) merage image of (A)(i), (A)(ii) and (A)(iii) in the presence of oxacillin at MIC × 2.....	99
Figure 3.8 MRSA BAA-41 was stained with single channel (A) for visualizing (i) lipid II of newly grown cell wall (green), (ii) nucleus acid (blue), (iii) cell membrane (red), (iv) DIC image and (C) (i) merage image of (A)(i) and (A)(ii); and (C) (ii) merage image of (A)(i), (A)(ii) and (A)(iii) in the presence of methicillin at MIC × 2.....	100
Figure 3.9 MRSA BAA-41 was stained with single channel (A) for visualizing (i) lipid II of newly grown cell wall (green), (ii) nucleus acid (blue), (iii) cell membrane (red), (iv) DIC image and (C) (i) merage image of (A)(i) and (A)(ii); and (C) (ii) merage image of (A)(i), (A)(ii) and (A)(iii) in the presence of F332 and oxacillin combination at MIC × 1.....	101
Figure 3.10 MRSA BAA-41 was stained with single channel (A) for visualizing (i) lipid II of newly grown cell wall (green), (ii) nucleus acid (blue), (iii) cell membrane (red), (iv) DIC image and (C) (i) merage image of (A)(i) and (A)(ii); and (C) (ii)	

merage image of (A)(i), (A)(ii) and (A)(iii) in the presence of F332 and methicillin combination at MIC \times 1..... 102

Figure 3.11 MRSA BAA-41 was stained with single channel (A) for visualizing (i) lipid

II of newly grown cell wall (green), (ii) nucleus acid (blue), (iii) cell membrane (red), (iv) DIC image and (C) (i) merage image of (A)(i) and (A)(ii); and (C) (ii)

merage image of (A)(i), (A)(ii) and (A)(iii) in the presence of PC190723 and oxacillin combination at MIC \times 1..... 103

Figure 3.12 BAA-41 was stained with single channel (A) for visualizing (i) lipid II of

newly grown cell wall (green), (ii) nucleus acid (blue), (iii) cell membrane (red), (iv) DIC image and (C) (i) merage image of (A)(i) and (A)(ii); and (C) (ii) merage

image of (A)(i), (A)(ii) and (A)(iii) in the presence of PC190723 and methicillin combination at MIC \times 1..... 104

Chapter 1. Introduction

1.1 *Staphylococcus aureus* infection and antibiotic resistance

The virulent pathogen *Staphylococcus aureus* (*S. aureus*) has been considered a major cause of health care-associated and community-acquired infections ever since its discovery [1]. The death rate of *S. aureus* infection was 80 % in the pre-antibiotic era [2]. Even with significantly improved infection treatments these days, the mortality rate of certain *S. aureus* infections, such as bacteremia, is still as high as 13 %. Indeed, there has been a considerable increase in incidences of *S. aureus* infection recently [3], and most cases are related to methicillin-resistant *S. aureus* (MRSA). MRSA is now considered to be the most common example of antibiotic-resistant bacteria caused by the abuse and overuse of antibiotics [4, 5].

In the evolution of antibiotic resistance, bacteria develop four major mechanisms (Figure 1.1). The first one is the enzymatic inactivation of drug. For instance, β -lactamase hydrolyzes β -lactam antibiotics which then lose their binding activity to penicillin-binding proteins (PBPs) [6]. The second mechanism is the activation of a drug exporter. For example, multidrug-resistant *S. aureus* contains *mepA* and *mepB* genes that encode an efflux pump in the form of the multidrug and toxin extrusion transport protein (MATE) in the plasma membranes [7, 8]. The third mechanism is to decrease the permeability of drug. For instance, the vancomycin tolerant *staphylococci* possesses a thick cell wall that acts as a buffer to absorb vancomycin before it further penetrates the cell wall [9]. The fourth antibiotic resistant mechanism is the modification of drug target. Vancomycin-resistant *S. aureus* (VRSA) is an example of this mechanism in which the last two amino acid residues (D-alanyl-D-alanine dipeptide) of stem peptide of peptidoglycan are altered to D-alanyl-D-lactate or D-alanyl-D-serine, resulting in a decrease in vancomycin binding [9]. The bacterial cell is sometimes protected by an alternative target that is resistant to the antibiotics,

which then provides an alternative pathway to bypass the antibiotic action. For instance, in MRSA, the *mecA* gene encodes the penicillin binding protein PBP2a that can bypass the effect of the β -lactam [10].

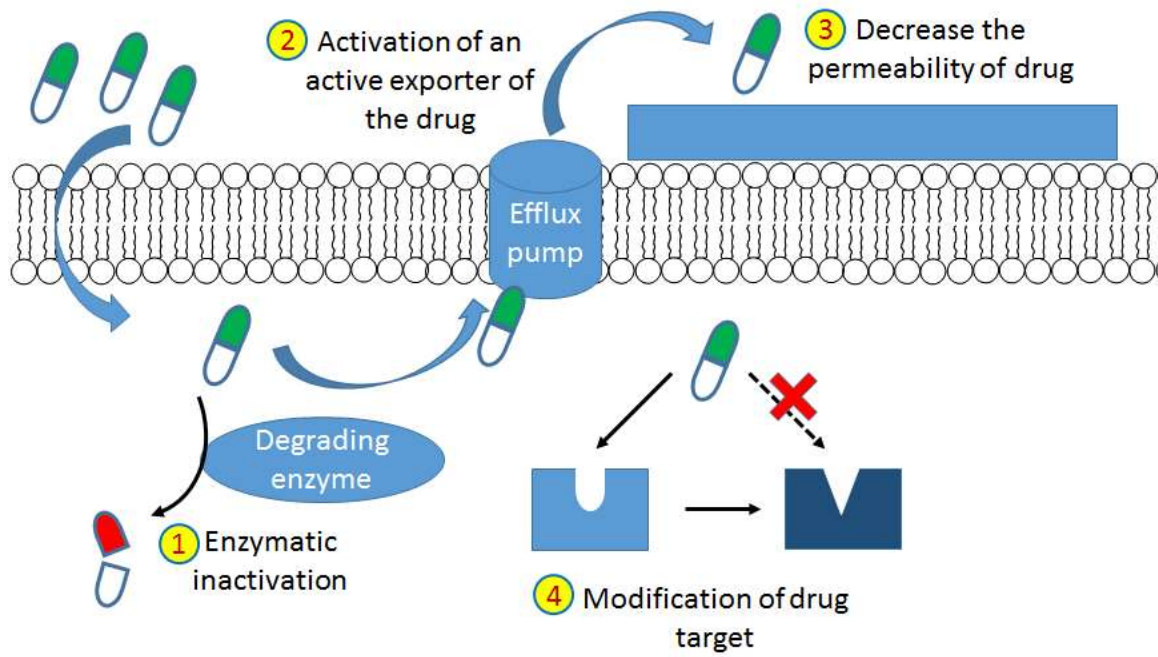


Figure 1.1 Antibiotic resistant mechanism of bacteria [10]. 1) Enzymatic inactivation or modification. 2) Activation of an active exporter of the drug. 3) Decrease the permeability of drug. 4) Modification of drug target.

Owing to the evolution of bacterial antibiotic resistance, new antibacterial agents are needed urgently. One strategy is to combine two or more drugs to provide a synergistic effect [11-13]. Augmentin is an example of this drug combination strategy. It consists of an irreversible β -lactamase inhibitor potassium clavulanate and β -lactam amoxicillin, in which clavulanate protects amoxicillin from hydrolysis by β -lactamase [14, 15]. In the case of FtsZ inhibitor, it has been previously reported that FtsZ inhibitor and β -lactam antibiotic showed synergistic antibacterial effect against MRSA [16], while FtsZ protein is the first cytoplasmic element to regulate cell division, PBP is the last protein for peptidoglycan crosslinking in the synthesis of cell wall. Thus, the role of FtsZ protein and its inhibitors and the role of PBP and β -lactam antibiotics will be discussed below.

1.2 Regulation of Cell wall synthesis

1.2.1 Cell morphology and cell shape

Staphylococcus aureus is a spherical-shaped (coccus) Gram-positive bacterium. It is divided into three alternating perpendicular planes with the daughter cells remaining attached, leading to its grape-like cluster arrangement, and hence its name “*staphylo-*” [17]. It produces a yellow carotenoid derivative, staphyloxanthin, which gives the colonies a golden appearance, and thus its species name “*aureus*” [18]. Similar to most cocci, the absence of flagella or other motile machinery leads to non-motile *S. aureus*. The small-sized cell has an average diameter of only 0.5 to 1.5 μm but is covered by a thick cell wall (20 to 40 nm) [19, 20]. The spherical shape indicates that the biosynthesis of cell wall is different from that of the rod cell.

Generally, bacterial cell wall synthesis of the rod-shaped cell model such as *Escherichia coli* (*E. coli*) and *Bacillus subtilis* (*B. subtilis*) involves two modes: (1) MreB and Mbl-associated elongation of the lateral cell wall (peripheral mode) and (2) cell division involving the FtsZ-driven peptidoglycan synthesis during septation (septal mode) [21]. Both cell growth and cell division require the synthesis of the peptidoglycan [22]. The peripheral mode for cell elongation contributes to the rod shape of the cell. On the other hand, “true” cocci bacteria such as *S. aureus* do not have the peripheral mode for elongation in lateral cell wall synthesis. Ovococci like *Streptococcus pneumonia* (*S. pneumonia*) are not perfectly round, and the cell wall synthesis occurs not only at the septum, but also at the equatorial ring [22], thus both lateral and septal modes are involved [23].

1.2.1.1 Peripheral mode of cell wall synthesis in rod-shaped cell

In rod-shaped bacteria, the cell shape and elongation growth are governed by the *mreB* or *mreB*-like gene. They encode MreB or MreB-like proteins for the cytoskeletal structure of the cells. MreB is an eukaryotic actin homologue and a composition of internal helical scaffolding in rod-shaped bacteria [24]. The X-ray structure of MreB shows a structure similar to that of actin [25]. In *E. coli*, MreB directly binds to the inner membrane [26]. The deletion of the *mreB* gene in *E. coli* results in an irregular cell morphology [27], showing that MreB is essential for shape regulation. In *B. subtilis*, there are two *mreB*-like genes that affect cell shape. They encode the MreB and Mbl proteins [24, 28, 29]. The role of cell shape determination of the MreB and Mbl proteins can be revealed using fluorescence microscopy. Disruption of the *mbl* gene in *B. subtilis* results in cell bending, irregular twisting and curves in the cell width [30]. It was observed that the helical structure of MreB and Mbl proteins encircle themselves just

under the cytoplasmic membrane [30]. However, high-resolution fluorescence microscopy showed that MreB forms a small filament and was involved in cell elongation by inserting new peptidoglycan into multiple sites in the lateral cell wall [31, 32]. On the other hand, the tubulin-like cell division protein FtsZ governs the preseptal phase of cell elongation for cell division and daughter cell separation in septum synthesis [33].

1.2.1.2 Septal mode of cell wall synthesis in true cocci

Cocci cells like *S. aureus* do not contain MreB protein for cell elongation [30] and therefore the cells are spherical in shape. The cell wall synthesis of *S. aureus* mainly occurs at the division septum and seems to display only septal peptidoglycan synthesis [34, 35]. The cell wall synthesis of *S. aureus* therefore depends solely on the bacterial cytoskeletal element, FtsZ [36].

1.2.2 Role of FtsZ protein in cell division

FtsZ protein is the first identified cytoskeletal element in bacterial cell division [37, 38]. It is an essential cell division protein that forms a Z-ring at the cell division site during cell division [36]. FtsZ is a bacterial ancestor of tubulin and has been identified as a highly conserved cell division protein in most species of the prokaryotic cell. The protein is encoded by the *ftsZ* gene in all eubacteria, archaea and chloroplasts [39]. During cell division, the tubulin-like protein FtsZ is the first protein to align at the division septum and activate the cell division process [40]. After the localization of FtsZ at the division site, it polymerizes to form a dynamic FtsZ ring with GTP

hydrolysis. [41, 42]. It acts as a framework for recruitment of other proteins to form a divisome.

1.2.2.1 Structural and functional characteristic of FtsZ

The structure of FtsZ is homologous to eukaryotic tubulin [43-45] (Figure 1.2), even though the amino acid sequence is different [46]. FtsZ is a cytoplasmic protein that contains two domains arranged around a central core helix H7 [47]. The N-terminal domain contains the signature motif GGGTGTG [48], which is highly conserved and is similar to the tubulin signature motif known as G-box, GGGTGSG, and possesses GTPase activity by providing the nucleotide-binding site [49]. The C-terminal domain, on the contrary, does not show any sequence that's similar to that of tubulin [44, 46, 50]. FtsZ polymerizes by inserting the C-terminal T7 loop into the N-terminal H7 to form a GTPase binding site [51, 52].

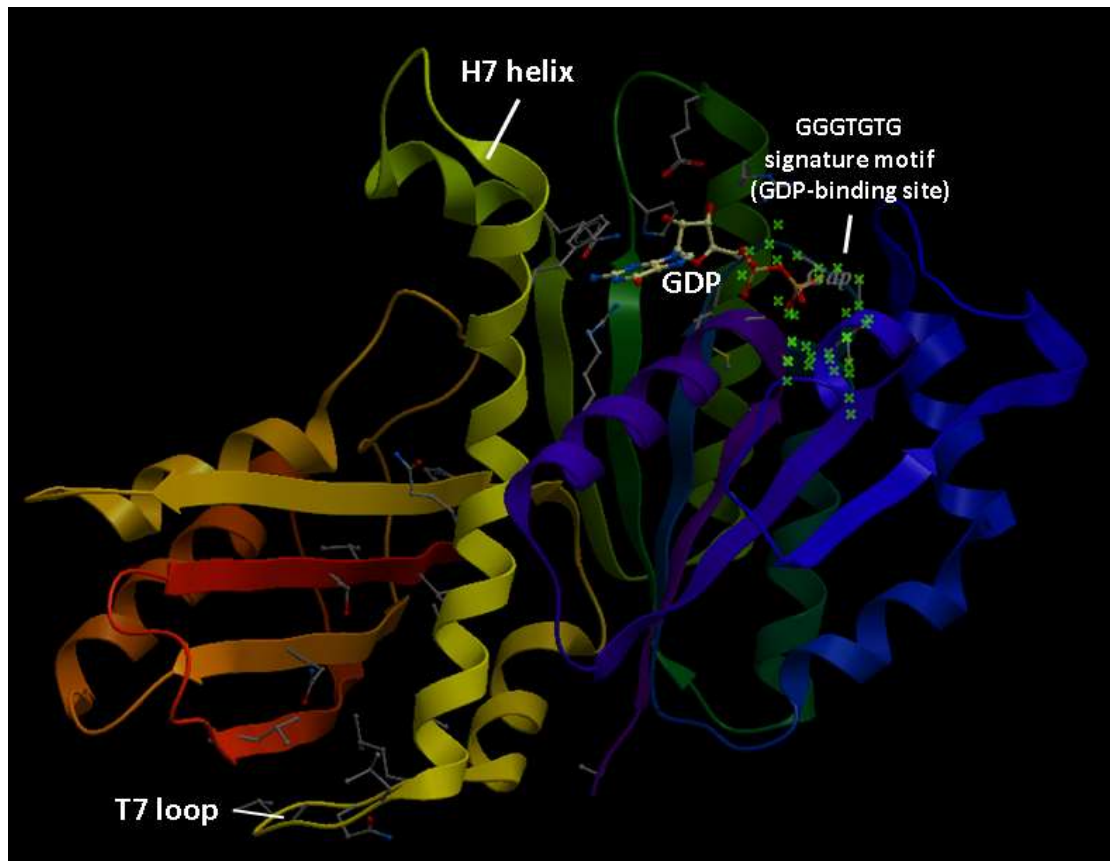


Figure 1.2 Crystal structure of *S. aureus* FtsZ monomer (PDB ID code: 3VOB) (prepared by ICM Molsoft LCC) [52]. Two independently folding domains and a core helix, H7, are the main components of FtsZ monomer. The N-terminal domain contains a signature motif, GGGTGTG for the nucleotide-binding site, while the C-terminal domain is the catalytic T7 loop and binding site for several division proteins.

1.2.2.2 Selection of division site in rod-shaped cells

Before cell division is initiated, the bacteria cell needs to ensure that the division site is correctly placed at the mid-cell for chromosome segregation and for the two daughter cells to divide into equal size. FtsZ proteins align at the correct division site and initiate the FtsZ ring polymerization. Two major mechanisms are involved to maintain the highly accurate localization of FtsZ proteins for cell division: the Min system and the nucleoid occlusion [53, 54].

The Min system can be observed in rod-shaped bacteria such as *E. coli* and *B. subtilis* [53, 54]. In *E. coli*, three Min proteins - MinC, MinD, MinE - are responsible for the restriction of the FtsZ assembly only at the mid-cell [55]. MinC interacts directly with the FtsZ protein to inhibit the assembly of the FtsZ ring [56]. On the other hand, MinC binds with MinD most of the time to form a complex MinCD. The MinE ring present at the center of the cell pushes MinCD out of the mid-cell, which then accumulates in the cell pole. The concentration of the negative regulator MinC is lowest at mid-cell, where the FtsZ ring is assembled [57, 58].

The nucleoid occlusion effector of *B. subtilis* and *E. coli* has been identified as Noc [59] and SlmA [60], respectively. It prevents the FtsZ ring assembly at the mid-cell before the completion of chromosome segregation. It also coordinates the timing of the cell division with chromosome segregation [61]. During chromosome segregation, nucleoid occlusion effector (Noc) binds at the origin of replication (*oriC*)-proximal region on the chromosome, but not at the terminus region (*Ter*). The binding of the effector protects the DNA by moving away from mid-cell and inhibiting the assembly of the FtsZ ring. After chromosome segregation of the protected regions has completed, FtsZ polymerization is allowed at the mid-cell [61].

In *S. aureus*, no MinC and MinD or their homologues are found, but it processes a Noc homologous protein which is similar to that of *B. subtilis*. The Noc homolog in *S. aureus* plays an important role in the placement of the FtsZ ring as well as the division septum in orthogonal planes. It also helps to prevent septum formation over the DNA chromosome. Septum formation in *S. aureus* occurs by three consecutive division cycle in three orthogonal planes. [62].

1.2.2.3 Assembly of the FtsZ ring

With the help of the well-managed localization of the FtsZ protein, FtsZ monomers are polymerized by the head-tail association at the septal division site. As mentioned earlier, the FtsZ protein and tubulin are structurally homologous. Their similarity is not only limited to their structure, but also their polymerization mechanism [21]. During the polymerization of FtsZ, the tubulin-like loop No. 7 (T7-loop) interacts with the γ -phosphate of GTP and inserts into the nucleotide-binding site of the adjacent FtsZ monomer [43, 63]. This process depends on the GTP binding by self-activation of the GTPase [42, 64]. The FtsZ ring undergoes a rapid turnover dynamic that depends on the concentration of the GTP and is regulated by GTP hydrolysis [65, 66], showing that an abundance of GTP is essential for polymer stabilization [21, 67].

1.2.2.4 Recruitment of FtsZ downstream proteins

After FtsZ polymerizes into the FtsZ ring, the ring then serves as a scaffold for the recruitment of downstream cell division proteins and assembly of the accessory divisome complex [68]. The FtsZ ring interacting proteins such as ZipA [69-72], Z-ring association proteins such as ZapA, ZapB [73-75], ZapC [75-77] and FtsA [72, 78-80] are proteins that directly interact with FtsZ at the cytoplasmic membrane. They play significant roles in stabilizing and protecting of the FtsZ ring structure from degradation. After the assembly of the FtsZ ring, the ring then directly interacts and recruits downstream proteins such as FtsK, FtsQ (DivIB in *B. subtilis* and *S. aureus*) [81], FtsL (DivIC in *B. subtilis* and *S. aureus*), and FtsN rely on the presence of ZipA [82]. Indeed, FtsK is localized at the division septum [83] and is a chromosome segregation coordinating protein to ensure the moving of unsegregated DNA to the daughter cells before the closure of the late stages of the cell cycle. FtsQ, FtsL and FtsN [84] are membrane spanning proteins [85]. FtsI (PBP3 for *E. coli*) [86] and FtsW [87, 88] are proteins that are involved in the process of septal mode of peptidoglycan synthesis and they also interact with each other [89]. In *S. aureus*, FtsW also plays an important role in septal peptidoglycan synthesis machinery. It properly aligns at septum and flips lipid-linked peptidoglycan to cell wall for peptidoglycan synthesis [90]. All of the aforementioned proteins are downstream proteins of FtsZ. Their alignments strongly depend on the proper localization of FtsZ [91].

1.2.3 Depletion of FtsZ protein

Since FtsZ is the key cell division protein, the depletion of FtsZ causes a failure of cell division. In rod-shaped cells, only the peripheral mode can function and thus, cells

generates a long filament without septa [92, 93]. In cocci cells such as *S. aureus*, the FtsZ-depleted cells show dispersing patches over the entire surface of the cells, this leads to an increase in size. The cells eventually lysed [35]. From this point of view, the FtsZ protein is a promising target for antibiotic development and has therefore been extensively investigated over the past decade [42, 43, 63-66, 68, 91-93].

1.2.4 From cytoskeletal elements to membrane-bound protein

Cytoskeletal elements such as MreB, Mbl and FtsZ carry the shape mode information which are the elongation mode and the septal mode, respectively [94]. This information needs to be transmitted outward to the cytoplasmic membrane by the membrane-bound and membrane-associated proteins. These membrane-bound and membrane-associated proteins can be penicillin binding proteins (PBPs) or other cell shape maintenance proteins [95]. In *E. coli*, PBP2 and RodA are required in the elongation mode [96, 97], while PBP3 and FtsW are required during the cell dividing septal mode [98]. In *S. aureus*, cell wall synthesis occurs at the septum division site only [34]. The formation of the septal peptidoglycan depends on the recruitment of the FtsZ protein. FtsZ recruits PBP2 as membrane-bound proteins for peptidoglycan synthesis [35]. After PBP2 is recruited, peptidoglycan chains are polymerized by the transglycosylase domain of PBP2 and then the transpeptidase domain of PBP2 works on peptidoglycan crosslinking. Cell wall synthesis involves both peptidoglycan synthase (PBP, for instance) and peptidoglycan hydrolase (autolysin) to break down part of the peptidoglycan to shape the cell morphology and then build up the peptidoglycan.

1.3 FtsZ inhibitors

1.3.1 Natural product inhibitors of FtsZ

The nature provides rich sources of drug leads in pharmaceutical research. There are many natural products that are FtsZ inhibitors and bioactive. Sanguinarine is a benzophenanthridine alkaloid derived from rhizomes of *Sanguinaria canadensis*. It causes FtsZ filamentation by inducing FtsZ conformational changes and weakens the protofilament interactions. It also exhibits growth inhibition on *B. subtilis* at 3.32 µg/mL and *E. coli* at 23.26 µg/mL [99]. However, it is toxic to mammalian cells by inhibiting tubulin assembly into microtubules. Sanguinarine binds to FtsZ with dissociation constants of 5.98 µg/mL to 9.97 µg/mL, but the binding site is unknown [100, 101]. Totarol, a diterpenoid phenol from *Podocarpus totara*, on the other hand, was identified to target at the GTP binding site. It was shown to inhibit the growth of *Mycobacterium tuberculosis* (*M. tuberculosis*) and *B. subtilis*, with low toxicity to mammalian cells [102].

Chrysophaentin A is a natural product isolated from the marine chrysophyte alga *Chrysophaeum taylori*. It is predicted to bind to the GTP binding site of FtsZ by *in silico* docking and saturation transfer difference-NMR. Chrysophaentin A inhibits FtsZ assembly and GTPase activity and bacteria growth in clinically relevant Gram-positive bacteria such as MRSA, multi-drug resistant *Staphylococcus aureus* (MDRSA) and vancomycin-resistant *Enterococcus faecium* (VREF) [103]. Viriditoxin was identified as an FtsZ inhibitor by screening over thousands of microbial fermentation broths and plant extracts [104]. It was isolated from *Aspergillus viridinutans* and showed inhibition of GTPase activity with an IC₅₀ of 7 µg/mL. It inhibited FtsZ polymerization at 8.2 µg/mL [105]. However, the high toxicity of viriditoxin with

myotoxic and hemorrhagic activities made it impossible to proceed to clinical trials [106, 107]. Curcumin is a polyphenolic compound extracted from the root of Turmeric (*Curcuma longa*). It is widely used as a spice, food preservative and coloring material in Asia. It showed inhibition of *B. subtilis* FtsZ polymerization. Unlike other FtsZ inhibitor, curcumin increased 35 % of GTPase activity at a concentration of 11.05 µg/mL instead of decreasing it [108]. Curcumin was shown to bind preferentially to the GTP-binding site by *in silico* molecular docking [109]. Cytotoxicity tests of curcumin indicated that the toxicity of curcumin increases with increasing uptake [110].

The high toxicity of the above-mentioned FtsZ inhibitors calls for the search of natural product inhibitors of FtsZ with low cytotoxicity. Berberine not only destabilizes FtsZ protofilaments and inhibits the FtsZ GTPase activity, but also inhibits the growth of *B. subtilis*. The GTP-binding mode was suggested by *in silico* molecular docking. Berberine does not induce human erythrocytes hemolysis below 2 mg/mL [111, 112]. Most FtsZ inhibitors perturb the function of FtsZ by binding to the N-terminal GTP-binding site of FtsZ, while some targeted on the T7 loop of FtsZ. Trans-cinnamaldehyde is a product extracted from the spice *Cinnamomum cassia*. The GTPase activity of FtsZ was reduced by cinnamaldehyde. Cinnamaldehyde binds FtsZ at the C-terminal region involving the T7 loop as predicted by *in silico* docking and saturation transfer difference-NMR. It also exhibits low cytotoxicity. Its hemolytic activity toward erythrocytes was observed at a concentration of 2 mg/mL [113]. Plumbagin is another natural product that binds to the C-terminal T7 loop of FtsZ [114]. It is a secondary metabolite in carnivorous plants such as *Nepenthes insignis* and *Drosera rotundifolia* [115, 116]. It shows inhibition of growth of *B. subtilis* and *Mycobacterium smegmatis* (*M. smegmatis*). Inhibition of GTPase activity and FtsZ ring formation was observed. However, it is highly toxic to keratinocytes with a IC_{50} of 3.39 µg/mL [117].

Table 1.1 A list of natural product inhibitors of FtsZ

Compound	Binding site	Detection method	GTPase activity	FtsZ assembly	Antibacterial activity (MIC values)	Cytotoxicity IC ₅₀
Sanguinarine (benzophenanthridine alkaloid) [99]	Unknown binding site: dissociation constant of 5.98-9.97 $\mu\text{g/mL}$	NA	NA	Perturbation of FtsZ ring formation Inhibit assembly of <i>EcFtsZ</i>	Against <i>B. subtilis</i> : 3.32 $\mu\text{g/mL}$; against <i>E. coli</i> : 23.26 $\mu\text{g/mL}$	Toxic to mammalian cells by inhibit tubulin assembly into microtubules [100, 101]
Totarol (diterpenoid phenol) [102]	GTP binding of <i>MtbFtsZ</i> : dissociation constant of $3.15 \pm 0.6 \mu\text{g/mL}$	Experimental	Suppressed <i>MtbFtsZ</i> GTPase activity	Inhibit assembly of <i>MtbFtsZ in vitro</i>	Against <i>B. subtilis</i> : 0.57 $\mu\text{g/mL}$	Low toxicity to mammalian cell (HeLa cell): $5.15 \pm 0.3 \mu\text{g/mL}$)

Compound	Binding site	Detection method	GTPase activity	FtsZ assembly	Antibacterial activity (MIC values)	Cytotoxicity IC ₅₀
Chtysohaentins A-H [103]	GTP	Docking, saturation transfer difference-NMR	Inhibit <i>EcFtsZ</i> GTPase activity (IC ₅₀ : 6.7 ± 1.7 µg/mL)	<i>EcFtsZ</i> assembly	MIC ₅₀ against MRSA: 1.5 ± 0.7 µg/mL; MIC ₅₀ against MDRSA: 1.3 ± 0.4 µg/mL; MIC ₅₀ against VREF: 2.9 ± 0.8 µg/mL	NA
Viriditoxin [105]	GTP	Docking from several thousand fermentation broths and plant extract [104]	Inhibit GTPase activity (IC ₅₀ : 7 µg/mL)	FtsZ polymerization IC ₅₀ : 8.2 µg/mL	Against MSSA CL9080: 4 µg/mL; against <i>E. coli</i> : >64 µg/mL	Mytotoxic [106, 107]

Compound	Binding site	Detection method	GTPase activity	FtsZ assembly	Antibacterial activity (MIC values)	Cytotoxicity IC ₅₀
Curcumin (1,7-bis (4-hydroxy-3-methoxyphenyl)-1,6-heptadiene-3,5-dione/diferuloyl methane) [108, 109]	GTP	Docking	Perturb FtsZ assembly by increasing 35 % GTPase activity (IC ₅₀ : 11.05 µg/mL) [108]	Perturb FtsZ assembly, induce filamentation in <i>B. subtilis</i> 168 by binding to T7 loop (IC ₅₀ : 11.05 µg/mL)	Against <i>B. subtilis</i> : MIC ₅₀ = 6.26 ± 1.1 µg/mL, MIC ₉₀ = 36.84 µg/mL; against <i>E. coli</i> K12 MG1655: MIC ₈₀ = 136.84 µg/mL	Toxicity to Fibroblast cell NIH3T3: 14.74 µg/mL (35 % cell death), but poorly bioavailability [110]
Berberine [111, 112]	GTP	Docking	Inhibit FtsZ GTPase activity (IC ₅₀ : 5.41 ± 1.69 µg/mL)	Destabilize FtsZ protofilaments	Against <i>B. subtilis</i> ATCC 663: 100 µg/mL; against <i>E. coli</i> : > 400 µg/mL; actively against MRSA	Toxicity to erythrocytes: 2 mg/mL

Compound	Binding site	Detection method	GTPase activity	FtsZ assembly	Antibacterial activity (MIC values)	Cytotoxicity IC ₅₀
Tran-cinnamaldehyde (Phenylpropanoid compound) [113]	T7-loop	Docking, saturation transfer difference-NMR	Inhibit <i>EcFtsZ</i> GTPase activity (IC ₅₀ : 0.77 ± 0.29 µg/mL)	Inhibit perturbation of FtsZ <i>in vivo</i> (0.91 ± 0.29 mg/mL)	Against <i>E. coli</i> : 1 mg/mL; against <i>B. subtilis</i> : 500 µg/mL; against <i>S. aureus</i> : 250 µg/mL	Toxicity to eukaryotic cell: 2 mg/mL
Plumbagin (5-hydroxy-2-methyl-1,4-naphthoquinone) [115]	C-terminal domain [114]	Experimental	NA	NA	Against <i>B. subtilis</i> 168: 5.47 µg/mL; against <i>M. smegmatis</i> : 5.83 µg/mL	Highly toxic to keratinocytes: 3.39 µg/mL [117]

1.3.2 Synthetic inhibitors of FtsZ

Natural products provide a clue on how the nature combats bacteria by targeting the FtsZ protein, while several synthetic and semi-synthetic compounds derived from natural products were also reported as FtsZ inhibitors. Semi-synthetic compounds may be prepared by modifying existing natural compounds. C8-substituted GTP derivatives such as 8-morpholino-GTP demonstrated inhibition to FtsZ assembly but without antibacterial activity [118]. Another type of GTP derivatives such as 8-bromoguanosine 5'-triphosphate (BrGTP) showed inhibition of FtsZ polymerization and GTPase activity. The GTP binding site was proved by displacing BrGTP with GTP in competition assay [119]. Amikacin is an aminoglycoside derived from kanamycin. It is a second-line drug for treating resistant *Mycobacterium* infection [120]. Perturbation of FtsZ ring assembly was observed at low concentration of amikacin. The low cytotoxicity to mammalian cells allowed amikacin to be developed into FtsZ-specific inhibitor [121]. *In silico* molecular docking indicated that amikacin most likely binds to the GTP-binding site [104].

Screening small molecule *in silico* not only predicts binding sites, but also identify potential compounds from libraries of chemicals. SRI-3072 and SRI-761 were identified by screening 200 of 2-alkoxycarbonylpyridines and they were found to inhibit the assembly of *M. tuberculosis* FtsZ and GTPase activity [122]. After screening 95,000 of 4-aminofurazan derivatives, A189 was found to inhibit FtsZ assembly and FtsZ ring formation as well as GTPase activity [123]. A high-throughput protein-based chemical screening approach was applied to identify the small molecules Zantrins (Z1 to Z5) which perturb FtsZ assembly and inhibit GTPase activity. Zantrins bind to a pocket between FtsZ subunits to push them apart, then the loop T7 in FtsZ monomer fails to optimize with the GTP bound to loops T1-T6 of the neighboring units [124].

Similarly, UCM05, UCM44, UCM53 were identified by screening virtual library to bind to a GTP-binding site of FtsZ. They inhibited GTPase activity and FtsZ polymerization. Among them, UCM53 inhibited the growth of *B. subtilis* at the lowest concentration and lowest cytotoxicity to human umbilical vein endothelial cells (HUVEC) [125].

A Cell-based antibiotic screening assay was applied to screen 105,000 synthetic compounds and PC58538 was found to inhibit GTPase activity. The binding pocket was suggested to be a GTP-binding pocket by mutation experiment. To improve the potency, the analogues of PC58538 such as PC170942 were synthesized, and showed antibacterial activity against both Gram-positive and Gram-negative bacteria [126]. So far, PC190723, a derivative from 3-methoxybenzamide (3-MBA), was found to be one of the most potent compounds against FtsZ. PC190723 inhibits GTPase activity in a dose-dependent manner, but it promotes FtsZ polymerization. It possesses potent activity against the resistant strains of *S. aureus*. Intravenous administration of PC190723 in a mouse model demonstrated that it is effective in treating *S. aureus* infection [127, 128]. The crystal structure showed that PC190723 binds to the T7 loop of the C-terminal domain of FtsZ [129]. PC190723 was then used as a lead compound for FtsZ inhibitor development.

Table 1.2 A list of synthetic and semi-synthetic compounds inhibitors of FtsZ

Compound	Binding site	Detection method	GTPase activity	FtsZ assembly	Antibacterial activity (MIC values)	Cytotoxicity IC ₅₀
8-morpholino-GTP [118]	GTP	NA	Inhibit FtsZ GTPase activity	FtsZ assembly: 53.12-265.59 μg/mL	No antibacterial activity	NA
8-bromoguanosine 5'-triphosphate (BrGTP) (C-8 bromine substituted GTP) [119]	GTP	Experimental	Inhibit <i>EcFtsZ</i> GTPase activity (IC ₅₀ : 16.47 μg/mL)	NA	Actively against <i>E. coli</i> and <i>S. aureus</i>	NA
Amikacin (aminoglycoside derived from kanamycin) [120]	GTP	Docking [104]	NA	Perturb FtsZ ring assembly <i>in vivo</i>	Against <i>E. coli</i> : 16 μg/mL	Low cytotoxicity [121]

Compound	Binding site	Detection method	GTPase activity	FtsZ assembly	Antibacterial activity (MIC values)	Cytotoxicity IC ₅₀
SRI-3072, SRI-7614 (2-alkoxycarbonyl-pyridines) [122]	Unknown	Screening 200 of alkoxy-carbonyl-pyridines	Inhibit <i>Mtb</i> FtsZ GTPase activity	<i>Mtb</i> FtsZ assembly of: SRI-3072 (IC ₅₀ : 28.27 ± 6.52 μg/mL)	Against <i>B. subtilis</i> : 0.15 μg/mL	NA
A189 (4-aminofurazan) [123]	Unknown	Screening 95,000 of 4-aminofurazan	Inhibit FtsZ GTPase activity (IC ₅₀ : 80 μg/mL)	FtsZ assembly <i>in vivo</i>	Against <i>E. coli</i> : 128 μg/mL; against <i>S. aureus</i> : 16 μg/mL	NA

Compound	Binding site	Detection method	GTPase activity	FtsZ assembly	Antibacterial activity (MIC values)	Cytotoxicity IC ₅₀
Zantrins (FtsZ <u>g</u> uanosine <u>t</u> riphosphatase <u>i</u> nhibitors) polyphenols derivatives (Z1, Z2, Z3, Z4, Z5) [124]	Loop T7	High-throughput protein-based chemical screening	Inhibit <i>Ec</i> FtsZ GTPase activity (IC ₅₀ values) of: Z1: 2.07 µg/mL; Z2: 4.88 µg/mL; Z3: 6.46 µg/mL; Z4: 15.13 µg/mL; Z5: 1.65 µg/mL	Z1, Z2, Z4: destabilize FtsZ assembly; Z3, Z5: hyperstabilize FtsZ assembly	Z1 against <i>S. aureus</i> : 1 µg/mL; Z1 against <i>E. coli</i> : 8 µg/mL	NA

Compound	Binding site	Detection method	GTPase activity	FtsZ assembly	Antibacterial activity (MIC values)	Cytotoxicity IC ₅₀
UCM05 [125]	GTP	Docking from virtual library	NA	NA	Against <i>B. subtilis</i> : 46.44 µg/mL	LD ₅₀ value to HUVEC: 13.93 ± 4.2 µg/mL
UCM44 [125]	GTP	Docking from virtual library	NA	NA	Against <i>B. subtilis</i> : 10.81 µg/mL	LD ₅₀ value to HUVEC: 19.02 ± 1.7 µg/mL
UCM53 [125]	GTP	Docking from virtual library	NA	NA	Against <i>B. subtilis</i> : 6.10 µg/mL	LD ₅₀ value to HUVEC: 23.46 ± 0.5 µg/mL
PC58538 [126]	GTP	Experimental	Inhibit FtsZ GTPase activity (IC ₅₀ : 136 µg/mL)	NA	Against <i>B. subtilis</i> : 128 µg/mL	NA

Compound	Binding site	Detection method	GTPase activity	FtsZ assembly	Antibacterial activity (MIC values)	Cytotoxicity IC ₅₀
PC170942 [126]	GTP	Screening 105,000 synthetic compounds in cell-based antibiotic screening	Inhibit GTPase activity (IC ₅₀ : 24 µg/mL)	NA	Against <i>B. subtilis</i> : 16 µg/mL; against <i>S. aureus</i> : 64 µg/mL; against <i>E. coli</i> : > 256 µg/mL	NA
PC190723 [127]	T7-loop	Crystal structure (PDB ID code: 3VOB) [129]	Inhibit <i>Sa</i> GTPase activity (IC ₅₀ : 55 ng/mL)	<i>Sa</i> FtsZ ring formation	Against <i>B. subtilis</i> 168: 4 mg/mL; against <i>S. aureus</i> : 1 µg/mL; against <i>E. coli</i> : > 64 µg/mL	NA

1.4 Biosynthesis and structure of peptidoglycan of *S. aureus*

The cell wall is essential for maintaining cell integrity, rigidity and viability, especially for bacteria that are under osmotic pressure [130, 131]. The cell wall is a dynamic structure that undergoes peptidoglycan synthesis, degradation and regeneration [132, 133]. In *S. aureus*, highly cross-linked peptidoglycan polymer constitutes the main scaffold of cell wall with a thickness of 20 to 40 nm [20]. The *S. aureus* cell wall consists of ~70 % peptidoglycan with wall teichoic acid (WTA), lipoteichoic acid (LTA) and cell wall-associated surface proteins [134-137]. Peptidoglycan, also called murein, is a polymeric glycan chain with a peptide cross-linked bridge. The *S. aureus* cell wall contains 20 layers of peptidoglycan to provide a flexible and elastic structure to protect bacteria against highly stressful osmotic pressure [130].

The biosynthesis of peptidoglycan generally occurs in three steps at different locations of the cell, the cytoplasm, the cell membrane and the external side of the cell membrane (Figure 1.3). The first step occurs in the cytoplasm, where nucleotide sugar-link precursors UDP-N-acetylmuramyl (UDP-MurNAc)-pentapeptide and UDP-N-acetylglucosamine (UDP-GlcNAc) are synthesized. (UDP-MurNAc)-pentapeptide is then linked to a transport lipid (undecaprenyl pyrophosphate) to form lipid I in the plasma membrane (second step). By adding GlcNAc, lipid I becomes lipid II. In *S. aureus*, the crossbridge pentaglycine (Gly₅) is added to the third amino acid residue (L-lysine). Lipid II-Gly₅ is then flipped to the external side of the plasma membrane. The third step of peptidoglycan synthesis occurs at the external side of the plasma membrane. Newly grown peptidoglycan is made by penicillin-binding proteins (PBPs). PBPs enzymatically carry out transglycosylation for glycan polymerization and transpeptidation for glycan stands crosslinking. PBPs play an important role in

peptidoglycan synthesis and therefore are popular drug targets in antibiotic development.

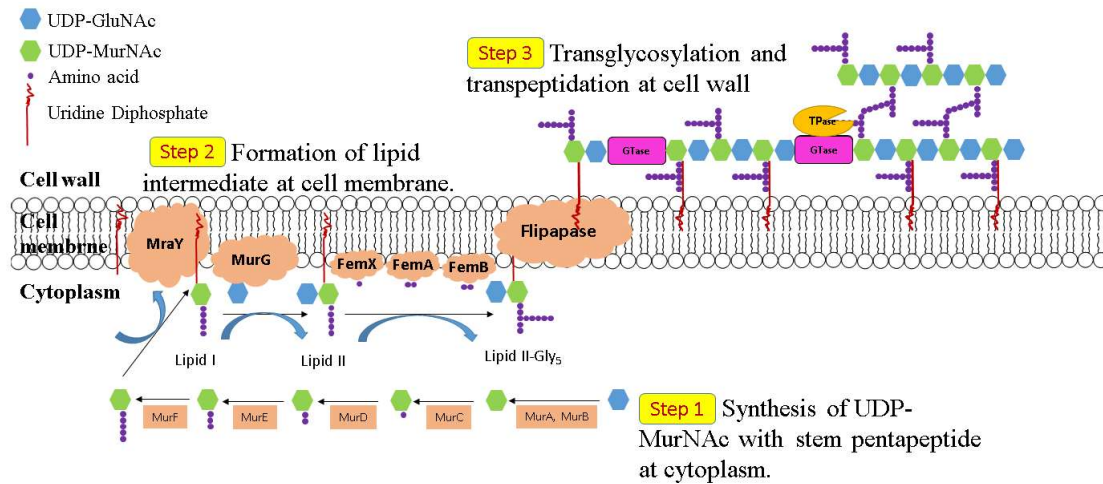


Figure 1.3 Biosynthetic pathway of peptidoglycan [23]. The biosynthetic pathway can be divided into three steps. **Step 1)** Synthesis of UDP-MurNAc (Uridine Diphosphate-N-Acetylmuramyl) from UDP-GluNAc (Uridine Diphosphate-N-Acetylglucosamine) by MurA and MurB at cytoplasm. The product is further catalyzed by MurC, MurD, MurE, and MurF to form four ATP-dependent amide bonds to give the stem peptide L-alanyl-D-glutamate-L-lysine-D-alanyl-D-alanine in *S. aureus*. **Step 2)** Formation of lipid intermediate at plasma membrane. This includes formations of lipid I by MraY and lipid II by MurG. Lipid II is further modified to form an pentaglycine inter-peptide bridge at the L-lysine of stem peptide. This process is catalyzed by the Fem family enzymes (FemX, FemA and FemB) in *S. aureus*. **Step 3)** Transglycosylation and transpeptidation are the last step that takes place at the cell wall. Glycan monomers are polymerized by transglycosylation, while stem peptides are cross-linked by transpeptidation.

1.4.1 Penicillin binding proteins (PBPs)

Penicillin binding proteins (PBPs) are members of acyl serine transferases. They were first identified when they contain a specific domain with the ability to bind to penicillin covalently [138]. The penicillin-interacting domains of PBPs either have transpeptidase or carboxypeptidase activities. Their enzymatic activities, as well as the penicillin binding ability, are related to the conserved signature motifs such as SXN, (K/H)(T/S)G and Serine-X-X-Lysine (SXXK) in the active site. In the action of transpeptidase, the hydroxyl group of active serine residue (SXXK) attacks the carbonyl of the fourth D-alanine residue of the stem peptide, which releases the last D-alanine residue to form a covalent acyl-PBP- complex (Figure 1.4). The carbonyl group of the fourth D-alanine residue forms an ester linkage temporarily with the serine residue in transpeptidase. The pentaglycine (Gly₅) extended from the third L-lysine residue is responsible for creating the cross-linkage bridge. During transpeptidation, the last glycine of the pentaglycine from one stem peptide attacks the ester linkage in between the D-alanine residue and the serine residue of PBP that has been formed in advanced. The last glycine of the pentaglycine finally binds with the fourth D-alanine residue of the stem peptide [139]. The penicillin-interacting activities make PBPs a group of critical enzymes that are involved in the activities of transpeptidation and DD-carboxypeptidation reaction, while some PBPs also contain a transglycosylation domain in the protein, which also plays a significant role in peptidoglycan chain polymerization. PBPs are divided into three classes according to the structural and functional difference of the enzymatic domains as well as the protein molecular weight. Classes A and B are high-molecular-weight (HMW) PBPs (> 45 kDa) whereas class C is low-molecular-weight (LMW) PBPs (< 45 kDa).

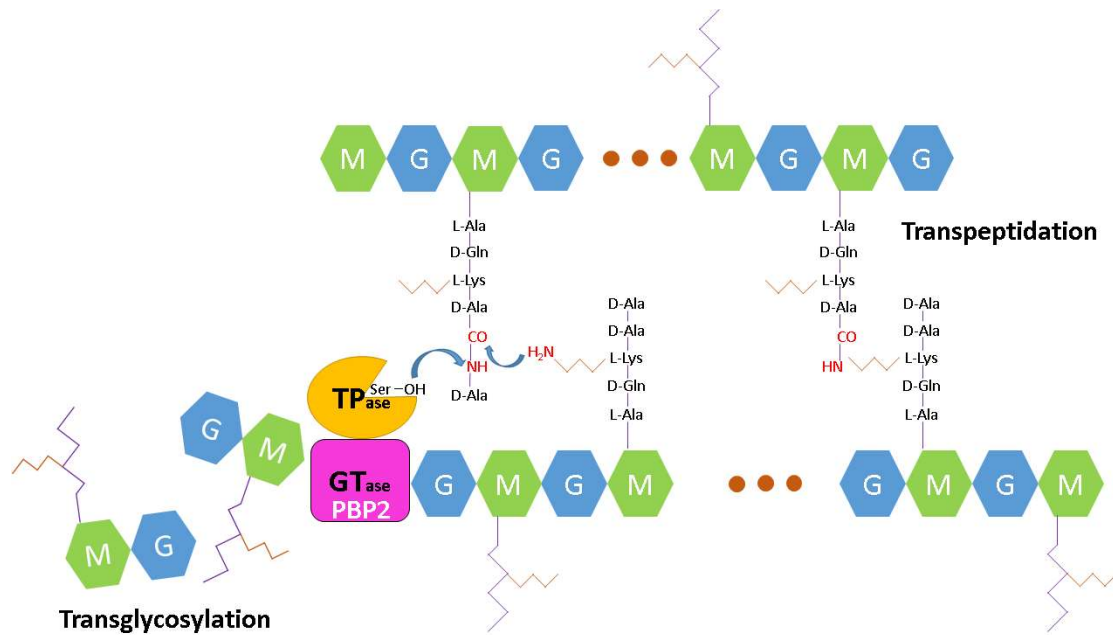


Figure 1.4 Enzymatic reaction of transglycosylation and transpeptidation for polymerization and crosslinking of glycan stands respectively [139]. “G” represents Uridine Diphosphate-N-Acetylglucosamine (UDP-GluNAc) while “M” is Uridine Diphosphate-N-Acetylmuramyl (UDP-MurNAc). They are polymerized by PBP that consists of a signature motif with serine in the active site. The serine attacks the carbonyl group of the fourth D-alanine residue of stem peptide and creates a cross-bridge with pentaglycine (Gly₅) that extends from the third L-lysine residue of another stem peptide.

1.4.1.1 High-molecular-weight (HMW) PBPs (Class A and B)

Most of the HMW PBPs are membrane-bound proteins that contain a short segment of non-cleavable peptide at the N-terminus followed by a transmembrane anchor domain attached to the outer surface of cytoplasmic membrane. They are classified into class A and class B. HMW class A PBPs are bifunctional peptidoglycan synthases containing two domains. The domain at the N-terminus is a transglycosylase (glycosyltransferase GTase) for linear glycan polymerization, whereas the C-terminal domain is a transpeptidase that catalyzes the cross-linking of pentapeptide. HMW class B PBPs are monofunctional transpeptidase (TPase) in which the active site is located at the C-terminus. Its N-terminal domain, however, is different from HMW Class A PBPs in that it has no known function. There is no sequence similarity between the N-terminal domains of different HMW class B PBPs, and the N-terminus is regarded to be involved in cell morphogenesis by protein-protein interaction during the cell cycle [90, 140, 141].

The HWM PBPs are involved in bacterial cell wall synthesis and are therefore named as peptidoglycan synthases. However, peptidoglycan synthases are not necessarily PBPs. Monofunctional TPases are another type of peptidoglycan synthases, which play a role similar to that of the glycosyltransferase domain of class A PBPs. In *S. aureus*, transglycosylation can be performed by monofunctional transglycosylase (MGT), second putative transglycosylase (SgtA), or the transglycosylases domain of PBP2. Both MGT and SgtA are not essential proteins in the survival of *S. aureus*. MGT can take over the role in the absence of PBP2, showing that either MGT or PBP2 is required for transglycosylase activity for cell survival [142].

1.4.1.2 Low-molecular-weight PBPs

Low-molecular-weight PBPs (LMW PBPs) are monofunctional DD-peptidases, many of which have carboxypeptidation activity [143], although in some species LMW PBPs act as transpeptidase [144] or endopeptidase [145]. Carboxypeptidase (CPase) controls the degree of peptidoglycan cross-linking by cleaving off a D-alanyl-D-alanine peptide bond of a stem peptide and trims it to a tetrapeptide. The tetrapeptide then loses its cross-linking ability, and no marked cross-linking takes place [146].

1.4.2 PBPs in *S. aureus*

The number of PBPs varies among different bacteria species. Rod-shaped bacteria tend to have more PBPs compared with cocci bacteria. For instance, *E. coli* and *B. subtilis* contain 12 and 16 PBPs, respectively. In *S. aureus*, there are four native PBPs, PBP1 to PBP4, while MRSA strains contain an additional PBP, PBP2a [147]. Among these PBPs, PBP2 is the only bifunctional HMW class A PBP that possesses both enzymatic activities of transglycosylation and transpeptidation, whereas PBP1, PBP2a (or PBP2') and PBP3 are HMW class B PBPs and PBP4 is a LMW PBP. Table 1.3 summarizes the gene information and localization of *S. aureus* PBPs.

Table 1.3 A summary of *S. aureus* PBPs

Class	Gene	Protein	Function, expression	Localization	Detection method of localization
HWM-B	<i>pbpA</i> [148]	PBP1	Growth	Site of cell division [149]	Immuno- fluorescence [149]
HWM-B	<i>pbpC</i> [150]	PBP3	Unknown	Entire periphery of the cell [90] or unknown	
HWM-B	<i>mecA</i> [151]	PBP2a / PBP2'	Horizontally acquired gene that confers β -lactam resistance [152, 153]	Unknown	
LWM-C TPase	<i>pbpD</i> / <i>pbp4</i> [154]	PBP4	Secondary cross- linking of peptidoglycan [144]	Site of cell division [155]	Fluorescence of a fused yellow fluorescent protein (YFP) [155]

1.4.2.1 PBP1 of *S. aureus*

Synthesis of peptidoglycan occurs at the septum and it involves at least both PBP1 and PBP2. The presence of PBP1 of *S. aureus* was reported to be essential for cell growth. This was demonstrated by the lethal result of the disruption of *pbpA* gene [156]. It has been reported that PBP1 might not to be a major protein in contributing to the cross-linking of peptidoglycan. However, it localizes at the division site and the role must be closely related to the mechanism of cell division [149]. Further investigation on the detailed role of PBP1 in the cellular process is still required to fully understand its function.

1.4.2.2 PBP3 of *S. aureus*

The crystal structure of PBP3 of *S. aureus* has been resolved in its apo form and as complex with cefotaxime [157]. Its localization has not yet been defined, but it is likely to catalyze cell wall synthesis from the beginning around the entire periphery of the cell [90]. Mutant without PBP3 encoded by *pbpC* gene did not show any major defects in morphology, or muropeptide composition of cell wall peptidoglycan, but a decrease in the rate of autolysis [150]. Investigation on the detailed roles and functions of PBP3 are still needed.

1.4.2.3 PBP4 of *S. aureus*

PBP4 is recruited to the septum for peptidoglycan cross-linking at the late step of the cell cycle. PBP4 of *S. aureus* was found to have “model” transpeptidase, DD-carboxypeptidase and β -lactamase activities. Its transpeptidase activity is involved in secondary cross-linking of peptidoglycan and is responsible for the high degree of cell

wall cross-linking. The lack of, or low activity of DD- and LD-carboxypeptidase [144], helps to maintain the cell with up to 90 % peptidoglycan cross-linking [158]. Mutants with PBP4 depletion, or cells which were treated with high binding affinity β -lactam cefoxitin, showed a marked reduction in the extent of peptidoglycan cross-linking. The absence of PBP4 also leads to the lack of activity of other PBPs, showing that PBP4 has an inter-relationship with other PBPs [144]. However, a lack of PBP4 did not lead to death of the organism and thus PBP4 was concluded to be a non-essential protein [159]. Because of the β -lactamase activity of PBP4, overexpression of this protein was reported to increase β -lactam resistance and thus cross-linking of the peptidoglycan [160, 161].

1.4.2.4 PBP2 and PBP2a of *S. aureus*

In *S. aureus*, PBP2 is the only bi-functional HMW class A PBPs having both enzymatic activities of transglycosylation and transpeptidation among the four native PBPs. Methicillin-resistant *S. aureus* contains an extra gene *mecA* to encode PBP2a that can compensate the loss of transpeptidase activity of PBP2 acrylated by β -lactam antibiotic.

In rod-shaped bacteria such as *E. coli*, the localization of the division-specific PBP3 (FtsI of *E. coli*) depends on the cell division proteins FtsZ, FtsA, FtsQ, FtsL and FtsW through protein-protein interactions [162], whereas in *B. subtilis*, PBP1 depends on other membrane-associated cell division proteins [163, 164].

Unlike *E. coli*, PBP2 in *S. aureus* can only function when it lines up at the division site (septum). It has been shown that PBP2 localization depends on its transpeptidation substrate recognition in the septum region [90, 165-167]. PBP2 is revealed to align at the septum for cell division [35]. β -Lactam antibiotics such as

oxacillin inactivate the transpeptidase domain of PBP2 by acylation. This leads to the failure of binding with its substrate, stem peptide of lipid II (lipid-linked peptidoglycan precursor at cell wall), and results in delocalization of PBP2. The division septum formation is then disrupted [165]. Addition of D-cycloserine inhibits the formation of D-alanine residues and creates a peptidoglycan without D-alanyl-D-alanine residues of stem peptide, whereas addition of vancomycin blocks the last two residues (D-alanyl-D-alanine) of stem peptide. Both treatments prevented the interaction between the D-alanyl-D-alanine residues and the transpeptidase domain of PBP2, leading to delocalization of PBP2 [165]. This suggests that proper localization of PBP2 depends on its transpeptidase substrate recognition.

In MRSA, the transpeptidase domain of PBP2a is responsible for substrate recognition. When a β -lactam antibiotic (e.g. oxacillin) is present, PBP2 is acylated and becomes dispersed. PBP2a, however, has a transpeptidase domain with low affinity for β -lactam, and can restore the action of transpeptidase activity. PBP2a can then be properly recruited to the division site by its substrate lipid II [165]. The incorporation of the transpeptidase domain of PBP2a and the transglycosylase domain of PBP2 in MRSA relies on the properly retention of acylated PBP2. Their incorporation restores peptidoglycan synthesis at the division septum [168]. This suggests that PBP2a not only provides an alternative transpeptidase that is resistant to β -lactam, but also maintains the acylated PBP2 to the division septum by protein-protein interaction (Figure 1.5) [90, 165].

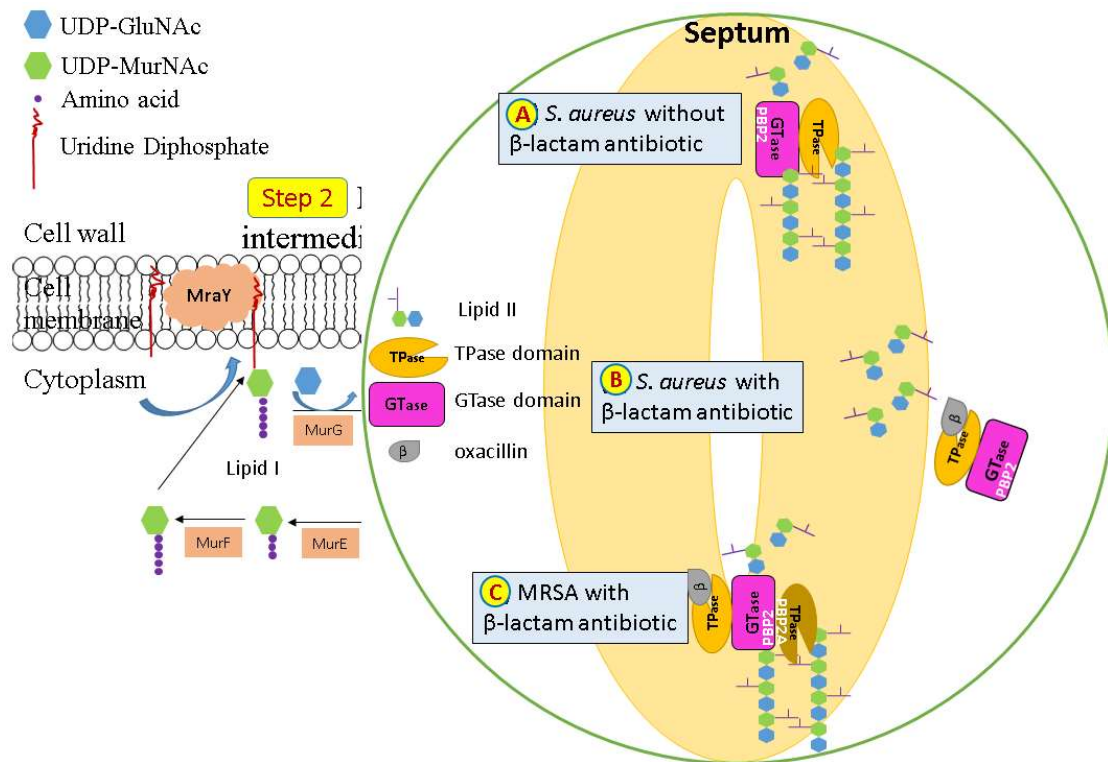


Figure 1.5 PBP2 is maintained by PBP2a in MRSA [165]. **(A)** In *S. aureus*, PBP2 localized in septum. The localization depends on TPase substrates (lipid II). **(B)** When β -lactam (oxacillin) is present in *S. aureus*, the transpeptidase (TPase) domain is acylated, PBP2 delocalizes and is dispersed from the septum, leading to a failure of cell wall cross-linking and finally cell dead (bactericidal effect). **(C)** In MRSA, however, β -lactam (oxacillin) is no longer effective. PBP2a restores the transpeptidase activity with low β -lactam binding affinity. PBP2a is localized by its substrate (lipid II) binding and maintains PBP2 at the septum position. In the case of MRSA, although transpeptidase domain of PBP2 is acylated, a proper localization of transglycosylase (domain on PBP2) is also important for glycan polymerization during the peptidoglycan synthesis.

1.5 β -lactam antibiotic

1.5.1 Acylation of PBP2 by β -lactam

PBP2 is a division-specific PBP involved in the last stage of the cell wall synthesis during cell division. β -Lactam is a commonly used drug that inhibits the transpeptidase of PBPs. β -Lactam antibiotics have an analogous structure to the transpeptidase substrate. They mimic the acyl-D-alanyl-D-alanine dipeptide located at the terminus of stem peptide in an elongated conformation [169, 170]. In the SXXX motif in the active site of the penicillin-interacting domains of PBPs, the lysine residue acts as a catalytic base to assist the serine residue in acylation. The hydroxyl group ($-OH$) of the serine residue is acylated by the β -lactam antibiotic. This causes the opening of the β -lactam ring and forms an acyl-enzyme complex. The active site of the transpeptidase domain is blocked when the PBP is acylated [171, 172].

S. aureus has evolved to produce β -lactamase (penicillinase) after the introduction of the first generation of penicillin in the 1960s [173]. In order to tackle the drug-resistance caused by β -lactamase, scientists have applied semi-synthetic penicillins such as methicillin. Methicillin has a bulky carbonyl side-chain so that it is protected from hydrolysis by β -lactamase. *S. aureus*, however, has further evolved to become MRSA by the expression of PBP2a.

1.5.2 β -lactam-resistant *S. aureus* (methicillin-resistant *S. aureus*)

Methicillin-resistant *S. aureus* contains an extra methicillin-resistant gene, *mecA*, which encodes the 78 kDa PBP2a. The β -lactam binding affinity of PBP2a is markedly lower than that of PBP2 because the transpeptidase binding pocket is closed and restraint the approach of β -lactam, which was shown by its X-ray structure [152, 153, 174]. An

allosteric binding domain was discovered to locate at 60 Å from the transpeptidase active site. It controls the opening of transpeptidase binding pocket (Figure 1.6). Ceftriaxone, an advanced generation of cephalosporin β -lactam antibiotics, was found to occupy the allosteric binding domain. This results in the multi-residue conformational changes of transpeptidase binding pocket and allows higher binding affinity of the β -lactam antibiotics [175].

When a β -lactam antibiotic is present in the cell, it tends to bind to the transpeptidase domain of PBP2 rather than to that of PBP2a. The active site of transpeptidase domain of PBP2 is acylated by the β -lactams, but the transglycosylase domain at the C-terminus remains active. The transpeptidation activity then relies on PBP2a, and the cross-linking between stem pentapeptides can be restored. The transpeptidase domain of PBP2a, together with the transglycosylase domain of PBP2, could complete the peptidoglycan synthesis [168].

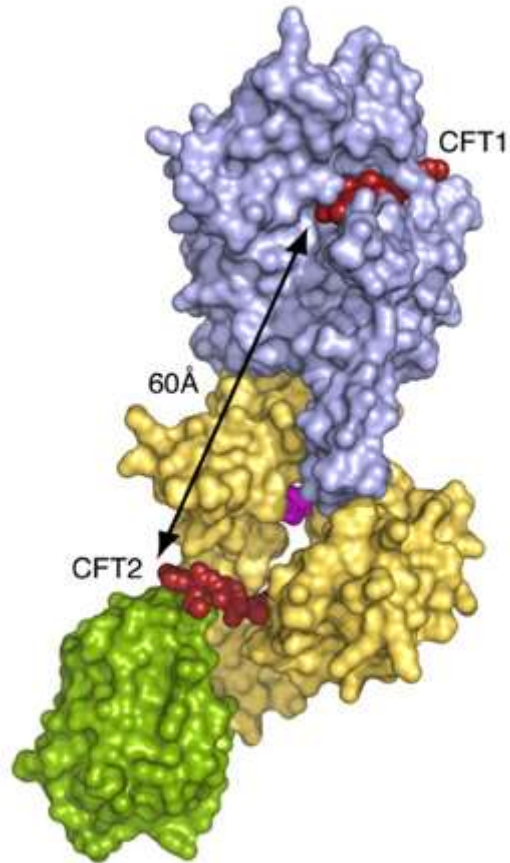


Figure 1.6 The crystal structure of the PBP2a of *S. aureus* (PDB ID code: 4DKI) [175]. The transpeptidase domain is colored in blue, while the allosteric domain is in gold, the green colour represents the N-terminal extension. The allosteric domain (CFT2) was identified to be located at 60 Å away from the transpeptidase domain (CFT1) active site.

1.6 Aims and objectives of this project

While FtsZ inhibitors and β -lactam antibiotics target on different proteins (FtsZ protein and transpeptidase domain of PBP) at different phases of cell division (early phase for FtsZ inhibitors and late phase for β -lactam antibiotics), some reported the synergistic antibacterial activity of FtsZ inhibitors with β -lactam antibiotics. This study aims to examine the role play by FtsZ inhibitor, β -lactam antibiotic, and a combination of them in the fight against bacteria. F332 [176], a FtsZ inhibitor developed by our research group; and PC190723, which had previously been proven as a potent FtsZ inhibitor [127, 129], were used in this study. Both β -lactam-antibiotic-sensitive (ATCC 29213) and resistant (ATCC BAA-41) strains of *S. aureus* were used as organism models in this study. The relatively simple cell division machinery of *S. aureus* reduces the complexity in the study of the antibacterial mechanism and drug-pathogen interaction.

Antibacterial susceptibility tests, which are commonly used for studying the potency of candidate inhibitors, were conducted on FtsZ inhibitors, β -lactam antibiotics, and their combination against MRSA to obtain the minimum inhibitory concentration (MIC). Minimal bactericidal concentration (MBC) and time-kill kinetic studies were applied to determine the bactericidal or bacteriostatic activities. If the compounds are fatal to bacteria, the way they are killed is important to refract the mode of action and mechanism. Hence, bacteriolysis assays were used to address whether cell lysis is the reason of death against MRSA.

Another objective of this study is the localization of the target of two distinct types of antibacterial compounds, FtsZ inhibitor, β -lactam antibiotic and their combinations in MRSA. Proteins that are involved in the control of cell division need to be recruited properly during the normal cell cycle. Introduction of FtsZ inhibitors

and β -lactam antibiotics could affect the localizations of various components of the cell-division machinery, resulting in cell lysis. The localization of two important components, FtsZ protein and lipid II, under the influence of FtsZ inhibitors, β -lactam antibiotics and their combination were performed in this project. The localization of FtsZ protein was visualized by FtsZ-GFP fusion induction and expression in *S. aureus* mutant, while localizations of lipid II was stained by a fluorescent vancomycin analogue. Both were visualized under a high resolution confocal microscope.

Chapter 2. Antibacterial Susceptibility Tests

2.1 Introduction

Derivatives of 3-methoxybenzamide (3-MBA) have been shown to inhibit FtsZ assembly and growth of Gram-positive bacteria like *Bacillus subtilis* (*B. subtilis*) and *Staphylococcus aureus* (*S. aureus*) [128, 177-179]. These compounds are potential antibacterial agents, especially for drug resistant bacteria such as methicillin-resistant *Staphylococcus aureus* (MRSA). Compound F332 is a newly developed derivative of 3-MBA, with proven antibacterial activity against Gram-positive bacteria and inhibition of FtsZ protein polymerization as determined by light scattering assay and GTP activity assay, respectively [176]. This chapter further extended the study on the antibacterial susceptibility of various compounds against antibiotic-resistant strains such as MRSA. Furthermore, since PC190723 had been reported to have synergistic antibacterial effect with β -lactam antibiotic against MRSA [16], antibacterial susceptibility tests on F332 together with antistaphylococcal β -lactam antibiotics such as methicillin and oxacillin against MRSA strain ATCC BAA-41 were also conducted.

Antibacterial activity can be described by several parameters including minimal inhibitory concentration (MIC), minimal bactericidal concentration (MBC), time-kill kinetic profiles and serum bacterial test (SBT) profile. MIC is a determination of the growth-inhibiting activity of bacteria and is defined as the minimal concentration of antibacterial compounds necessary inhibit the growth of a standard bacterial inoculum [10^5 colony forming unit per milliliter (CFU/mL)] up to 90 % as measured by optical density at wavelength of 600 nm (OD_{600}). MBC is the determination of bacterial-killing activity. It is defined as the minimal concentration of antibacterial compounds that reduces the standard bacterial inoculum not less than 99.9 % ($3 \log_{10}$ reduction) after subculturing MIC inoculum for 24 hours [178].

Both MIC and MBC are end-point determination of bacterial population after antimicrobial compounds exposure to antimicrobial compounds at different concentrations for an overnight incubation [180]. Unlike MIC or MBC, time-kill kinetic studies can examine the amount of bacteria that survive at various time points [181]. By monitoring the colony forming unit (CFU) at a particular time interval during 24-hour incubation, it is usually used to examine the rate of bactericidal activities and evaluate whether an antibacterial agent function in a concentration-dependent or time-dependent manner [182]. the SBT is concerned with a patient's serum which would be conducted in clinical trial phases [183]. The MIC volume is used to classify an antibacterial compound against a particular organism, whether the antibacterial compound is sensitive, intermediate or resistant, whereas the MBC value classifies antibacterial compounds into bactericidal or bacteriostatic agents. Time-kill kinetic studies is based on CFU measured by the OD of bacterial culture at the time of interest. These susceptibility tests can tell whether a compound is bactericidal or bacteriostatic. They can also identify the inhibitory activity and bactericidal activity of any antibacterial compound.

The bactericidal activity of an antibacterial compound is defining non-cultivable bacteria as a dead cell. Therefore, bactericidal assay on antibacterial compounds is not enough to provide information on the mode of action and whether cell lysis has occurred during the bacteria-drug interaction. For instance, daptomycin, a bactericidal lipopeptide, kills MRSA by inserting itself onto the cell membrane and alters membrane curvature to create ions leakage, which results in the death of bacterial cells without lysis [184, 185].

In light of the above, bacteriolytic assay had to be applied to reveal the antibacterial mechanism, i.e. whether cell lysis occurs during the action of FtsZ

inhibitors and β -lactam antibiotics in combination. In this assay, antibacterial compound would be applied when the culture was in the mid-log phase (high density of cells) instead of the lag phase (low density of cells). Changes in bacterial density were monitored by their OD_{600} values. Any decrease in OD_{600} value would reflect the decrease in live cell density, implying that cell lysis because of the antibacterial compounds.

2.2 Experimental

2.2.1 Materials

2.2.1.1 Bacterial strains

The *S. aureus* strains RN4220, ATCC 29213 and methicillin-resistant ATCC BAA-41 were used in the antibacterial susceptibility tests. *S. aureus* RN4220 was our laboratory's collection. *S. aureus* ATCC 29213 and methicillin-resistant *S. aureus* ATCC BAA-41 were purchased from American Type Culture Collection (USA).

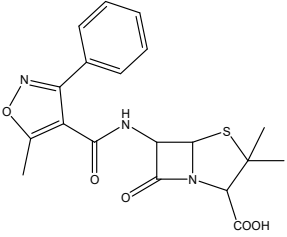
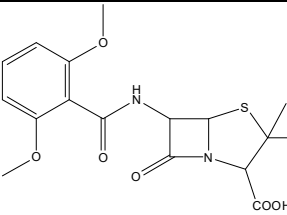
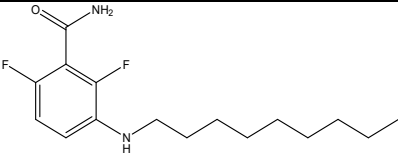
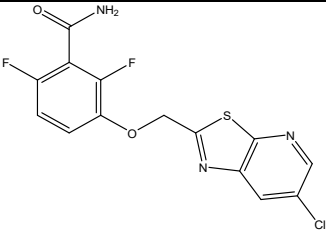
2.2.1.2 Media

Agar powder, tryptone and yeast extract were purchased from Oxoid Limited (Nepean, Ontario, Canada). Luria-Bertani broth was prepared by dissolving 10 g of tryptone, 5 g of yeast extract and 10 g of sodium chloride in deionized water [186]. Powder form of Cation-adjusted Müller-Hinton broths (CA-MHB) and trypticase soy broth (TSB), brain-heart infusion (BHI) were purchased from Becton, Dickinson and Company (New Jersey, USA). The broths were prepared according to the manufacturer's instructions. Solid form of different nutrient media was prepared by adding 15 g/L of agar powder to each broth before sterilization. Unless otherwise specified, all broths and agar were autoclaved before use.

2.2.1.3 Antibacterial compounds

Oxacillin, methicillin, and vancomycin were purchased from Sigma-Aldrich (United States). FtsZ inhibitors 3-MBA derivatives F332 and PC190723 [16] were our laboratory's collection. Their structures and details are given in Table 2.1.

Table 2.1 Structure of testing compounds

Testing compound	Molecular structure	Molecular weight (g/mol)
β -lactam antibiotic (anti-staphylococcal penicillin)	 <chem>CC1(C)SC(=O)N1C(=O)NC(=O)C2=CN=C(C2)c3ccccc3</chem>	401.426
	 <chem>CC1(C)SC(=O)N1C(=O)NC(=O)C2=CC(OC)=C(OC)C=C2</chem>	380.42
FtsZ inhibitors (derivatives of 3-MBA)	 <chem>CCCCCCCCCNc1ccc(F)c(C(=O)N)c1F</chem>	298.377
	 <chem>Clc1cn2c(s2)nc1COc3ccc(F)c(C(=O)N)c3F</chem>	355.743

2.2.2 Instrumentation and software

96-well microliter plates were purchased from Fisher Scientific and used in determination of MIC and in bacteriolysis assay. The optical density at 600 nm (OD_{600}) of bacterial culture was measured by a microplate reader Model 680 (Bio-rad Laboratories) or microplate spectrophotometer (CLARIOstar, BMG Labtech GmbH). Quantity One® 1-D Analysis Software (Bio-rad Laboratories) was used for counting colonies.

2.2.3 Minimum inhibitory concentration (MIC) assay

The minimum inhibitory concentration (MIC) value of the tested compounds was determined by a broth micro-dilution method according to the National Committee for Clinical and Laboratory Standards Institute (CLSI) Guidelines of which the procedure are listed below [187]:

A single colony of methicillin-sensitive *S. aureus* strain RN4220, ATCC 29213 or methicillin-resistant *S. aureus* ATCC BAA-41 was picked from TSB agar plate and inoculated in 5 mL of CA-MH broth at 37 °C with shaking at 250 rpm for 16 hours. Then, this culture was diluted 100-fold in 5 mL fresh CA-MH broth, and the cells were further incubated to achieve mid-log phase with OD_{600} at approximately 0.8. The cell culture was diluted to standard inoculum at approximately 5×10^5 CFU/mL in a fresh CA-MH broth, which was then transferred into a sterile 96-well microliter plate. Antibacterial compound or positive control (vancomycin) solutions of various concentrations (with serial two-fold dilution) was introduced into the broth.

The bacterium-antibacterial compound mixtures were incubated at 37 °C for 18 hours. OD₆₀₀ values were measuring UV absorbance wavelength 600 nm by a microplate reader with and the percentage inhibition of bacterial growth was calculated with respect to the bacterial control (culture with 1 % DMSO) by Equation 2.1.

$$\% \text{ Inhibition} = \left(1 - \frac{\text{OD}_{600} \text{ of bacteria - antibacterial compound mixture}}{\text{OD}_{600} \text{ of control culture}}\right) \times 100$$

.....Equation 2.1

The MIC is the lowest compound concentration of the tested compounds at which growth inhibition of target organism was up to 90 %. Each data set was repeated in triplicate.

2.2.4 Study on the combination effect of FtsZ inhibitors and β-lactam antibiotics

The methicillin-resistant *Staphylococcus aureus* strain ATCC BAA-41 was used in the experiment on the combination effect of β-lactams and FtsZ inhibitors. The MICs of each individual compound and the two compounds in combination were determined according to the National Committee for Clinical and Laboratory Standards Institute (CLSI) Guidelines [187]. The detailed procedure of the determination was described in Section 2.2.3, while two compounds (FtsZ inhibitor and β-lactam antibiotics) of equal amount were added in the same well of a sterile 96-well microtiter plate in the combination experiment. The combination effect of the FtsZ inhibitor and β-lactam antibiotic was indicated by checkerboard using fractional inhibitory concentration index (FICI), in which the index was calculated by Equation 2.2.

$$FICI = \frac{MIC\ drug_A\ in\ combination}{MIC\ drug_A\ in\ alone} + \frac{MIC\ drug_B\ in\ combination}{MIC\ drug_B\ in\ alone}$$

.....Equation 2.2

An FICI indexes less than 0.5 means synergistic effect; an index larger than or equal to 0.5 but less than or equal to 0.75 ($0.5 \leq FICI \leq 0.75$) is partial synergistic effect; an index larger or equal to 0.76 but less than or equal to 1 ($0.76 \leq FICI \leq 1$) indicates additive effect; an index larger or equal to 1 but less than or equal to 4 ($1 < FICI \leq 4$) is indifferent effect, while an index larger than 4 (>4) means antagonistic effect [188].

2.2.5 Minimal bactericidal concentration (MBC) assay

The minimum bactericidal concentration (MBC) value of the tested compounds was determined according to the National Committee for Clinical and Laboratory Standards Institute (CLSI) Guidelines M26-A and the procedure is described below [182]:

The experiment was conducted immediately after the MIC experiment as mentioned in Section 2.2.3. Inoculums with MICs of antibacterial compounds and their multiples ($MIC \times 1$, $MIC \times 2$, $MIC \times 4$, or above) were diluted in appropriate fraction and sub-cultured on the CA-MH agars without antibacterial compound, then, the agars were further incubated at 37 °C for 24 hours [189]. Colony counting was conducted by an imaging system with Quantity One® 1-D Analysis Software. The MBC is defined as the lowest concentration of an antibacterial agent that reduces the initial inoculum to or greater than 99.9 % ($3\log_{10}$) in the initial inoculum within 24 hours. Each data set was repeated in triplicate.

2.2.6 Time-kill kinetic studies

The time-kill kinetic studies of the antibacterial compounds were carried out according to the National Committee for Clinical and Laboratory Standards Institute (CLSI) Guidelines M26-A and the procedure is described [182]:

Standard inoculum of approximately 5×10^5 CFU/mL in fresh CA-MH broth was prepared as mentioned in Section 2.2.3, and then transferred into incubation tubes. The antibacterial compounds vancomycin (bactericidal antibiotic) and chloramphenicol (bacteriostatic control) were added at concentrations of MIC \times 1, MIC \times 2, MIC \times 4, or above. Control experiment was conducted in the absence of antibacterial compound. The bacterium-antibacterial compound mixtures were incubated at 37 °C with shaking at 250 rpm. The inoculum was sampled at various time intervals at 0 hour, 2.5 hours, 5 hours, 7.5 hours, 21 hours and 24 hours. The samples were diluted with the appropriate fractions and then sub-cultured on the CA-MH agars without antibacterial compounds, and the agars were further incubated at 37 °C for 24 hours [189]. Colony counting in various time intervals was carried out by imaging system with Quantity One® 1-D Analysis Software. A time-kill curve was plotted by \log_{10} of colony-forming unit per microliter (\log_{10} CFU/mL) against time with various MICs multiples. A bactericidal antibacterial compound should be able to kill more than or equal to 99.9 % or more of target organism ($3 \log_{10}$) from the initial inoculum, whereas a bacteriostatic antimicrobial compound kills less than 99.9 % of target organism ($3 \log_{10}$) when compared with the initial inoculum.

2.2.7 Bacteriolysis assay

A single colony of *S. aureus* ATCC BAA-41 was picked from the BHI agar plate and inoculated in 5 mL BHI at 37 °C with shaking at 250 rpm for 16 hours. Then, the culture was diluted 100 fold into 5 mL fresh BHI broth, and the cells were further incubated to achieve mid-log phase with OD_{600} values at approximately 0.8. The diluted bacterial suspension was dispensed in a 96-well microliter plate. The cell culture was then incubated at 37 ± 1 °C and monitored by a microplate reader at 600 nm (OD_{600}) for 24 hours at 15 minute intervals. The antibacterial compounds were added at sub-lethal concentration, $MIC \times 1$. The control experiment was conducted in the absence of antibacterial compound (see experimental section for details) when the bacteria grew to mid-log phase.

2.3 Results and discussion

2.3.1 Minimum inhibitory concentration (MIC) assay

Table 2.2 shows the MIC values of FtsZ inhibitors, β -lactam, vancomycin and chloramphenicol against methicillin-sensitive *S. aureus* (MSSA) (RN4220 and ATCC29213) and MRSA (ATCC BAA-41), respectively, while vancomycin and chloramphenicol were taken as bactericidal or bacteriostatic controls. According to the CLSI guidance, MIC values can be used to classify the susceptibility of testing compounds against particular bacteria ($MIC \leq 4$ $\mu\text{g/mL}$ is susceptible; 8 $\mu\text{g/mL}$ to 16 $\mu\text{g/mL}$ is intermediate; while ≥ 32 $\mu\text{g/mL}$ is resistant) [190].

Generally, MSSA are susceptible to β -lactam and FtsZ inhibitor with MIC values less than or equal to 1 (criteria: ≤ 4 $\mu\text{g/mL}$) [190]. Oxacillin and methicillin are synthetic penicillins to combat against MSSA. Oxacillin is the first isoxazolympenicillin

that performs better than 2,6-dimethoxyphenylpenicillin methicillin when applied against *S. aureus* [191][192]. Therefore, oxacillin generally showed a lower MIC value when compared with methicillin. The FtsZ inhibitor PC190723 generally showed a better antibacterial activity than F332 in table 2.2, while F332 has been reported to be less cytotoxic than PC190723 which may be more beneficial in clinical use [176].

MSRA with acquired transpeptidase PBP2a are resistant to β -lactams (MIC \geq 32 $\mu\text{g}/\text{mL}$), but are susceptible to FtsZ inhibitor (MIC \leq 4 $\mu\text{g}/\text{mL}$) [190]. Transpeptidase PBP2, a target of β -lactam, can be acylated by β -lactam (for example oxacillin and methicillin) in both MSSA and MRSA. However, the acquired PBP2a with low binding affinity with β -lactam in MRSA allows peptidoglycan synthesis to continue even in the presence of β -lactam, resulting in higher MIC values of β -lactam against MRSA.

On the other hand, MRSA are susceptible to FtsZ inhibitors because the inhibitors target on FtsZ protein. The antibiotic resistance of MRSA originates from PBP2a which is not the target of FtsZ inhibitors.

Table 2.2 MIC determination of FtsZ inhibitors and β -lactam antibiotics against *S. aureus* strains RN4220 (MSSA), ATCC 29213 (MSSA) and ATCC BAA-41 (MRSA) respectively.

		MIC ($\mu\text{g/mL}$)		
		RN4220	ATCC 29213	ATCC BAA-41
FtsZ inhibitor	F332	1	1	2
	PC190723	0.25	0.25	1
β -lactam antibiotic	Oxacillin	0.125	0.125	256
	Methicillin	1	1	512
Bactericidal antimicrobial	Vancomycin	/	/	2
Bacteriostatic antimicrobial	Chloramphenicol	/	/	1

2.3.2 Study on the combination effect of FtsZ inhibitors and β -lactam antibiotics

Table 2.3 shows the combination effects when FtsZ inhibitor F332 or PC190723 was used in combination with β -lactam antibiotics oxacillin and methicillin.

When oxacillin or methicillin was used in combination with F332, FICI value of 0.563 was obtained, indicating the combination effect is partial synergistic and F332 could restore the ability of oxacillin and methicillin.

On the other hand, when oxacillin or methicillin respectively was used in combination with PC190723, a FICI value of 0.375 was obtained, indicating a full synergistic effect. However, although the same FICI value was obtained for both oxacillin and methicillin, a lower concentration of PC190723 (0.125 $\mu\text{g}/\text{mL}$) is required in the case of oxacillin (see Table 2.3). Because of the low oral bioavailability and relatively higher cytotoxicity of PC190723 [127-129, 177-179], a combination of PC190723 and oxacillin with lower concentration of PC190723 is preferred.

By comparing the two FtsZ inhibitors, a combination of β -lactam antibiotics with F332 (partial synergistic effect) provide higher FICI than that of PC190723 (synergistic effect), reflecting that PC190723 has a larger capability restore the susceptibility of MRSA to oxacillin and methicillin.

Table 2.3 Susceptibility test results, in combination effects of FtsZ inhibitors and β -lactam antibiotics against MRSA ATCC BAA-41.

Antibacterial compound	MIC ($\mu\text{g/mL}$)		FICI	Combination effect
	Compound alone	Compound in combination		
Oxacillin	256	16	0.563	Partial synergistic
F332	2	1		
Methicillin	512	32	0.563	Partial synergistic
F332	2	1		
Oxacillin	256	64	0.375	Synergistic
PC190723	1	0.125		
Methicillin	512	64	0.375	Synergistic
PC190723	1	0.25		

2.3.3 Minimal bactericidal concentration (MBC) assay

The MIC results in Table 2.2 show that the ability of the antibacterial compounds to inhibit bacteria growth. The MBC values could be determined based on the MIC values. The bactericidal activities (bacteriostatic or bactericidal) of antibacterial compounds can then be classified. Table 2.4 shows the MBC values in term of the number of times of MIC.

Antibacterial compounds are regarded as bactericidal compounds when the MBC to MIC ratio is less than or equal to 4 [193]. Vancomycin, a member of glycopeptide antibiotic family that interferes with the cross-linking of peptidoglycan pentapeptide during peptidoglycan biosynthesis, is a standard bactericidal agent [194]. The β -lactam antibiotics oxacillin, methicillin and FtsZ inhibitor combinations show bactericidal activity against MRSA ATCC BAA-41 (Table 2.4).

When the ratio of MBC to MIC is higher than 4, the antibacterial compounds are classified as bacteriostatic compounds. Chloramphenicol, a protein synthesis inhibitor that reversibly binds to the 50S subunit of bacterial ribosome with a wide antimicrobial spectrum, is an example of bacteriostatic agents [194-197]. FtsZ inhibitor F332 has a MBC to MIC ratio equal to 16 and therefore is bacteriostatic. FtsZ inhibitor PC190723, β -lactam antibiotics and their combination have MBC to MIC ratios ≤ 2 and they are considered as bactericidal compounds.

Table 2.4 MBC determination of FtsZ inhibitors, β -lactam antibiotics and their combinations against MRSA ATCC BAA-41.

	Antimicrobial compound		MBC (Time of MIC)	Bactericidal activity
	FtsZ inhibitors	β -lactam antibiotics		
Compound alone	F332	/	MIC \times 16	Bacteriostatic
	PC190723	/	MIC \times 1	Bactericidal
	/	Oxacillin	MIC \times 1	Bactericidal
	/	Methicillin	MIC \times 2	Bactericidal
Compound in combination	F332	Oxacillin	MIC \times 1	Bactericidal
	F332	Methicillin	MIC \times 1	Bactericidal
	PC190723	Oxacillin	MIC \times 1	Bactericidal
	PC190723	Methicillin	MIC \times 1	Bactericidal
	Vancomycin		MIC \times 1	Bactericidal
	Chloramphenicol		MIC \times 8	Bacteriostatic

2.3.4 Time-kill kinetics

Time-kill kinetic studies are studies on the rate of bactericidal activity to monitor bacteria survival at various time points. The rate of bactericidal activity is a pharmacodynamic characteristic of antibacterial compounds. A bactericidal compound may either exhibit time-dependent killing or concentration-dependent killing. A bactericidal compound with time-dependent killing exhibits bactericidal activity continuously as long as the concentration of the bactericidal compound is in excess of MIC, and the bactericidal action is relatively slow. Thus, the frequency of drug administrations determines the drug efficacy. Concentration-dependent killing means the extent of killing would increase with the increase in the concentration of antibacterial compound. In this case, the dosage of drug, rather than the administration determines the efficacy [181, 182].

In all time-kill curves in Figure 2.1 to Figure 2.10, green line represents the control without antibacterial compound treatment. The quantity of bacteria decreased a bit in the first 2 hours, representing the lag phase under which the bacteria consumed nutrient and adapted to the new environment. Then, the number of bacteria increased from 2 hours to 8 hours representing the log phase that bacteria grow exponentially. After that, the number of bacteria become steady corresponding to the stationary phase.

The time-kill curves shown in indicate that FtsZ inhibitor F332 and chloramphenicol are bacteriostatic compounds, because they needed more than four times the concentration of MIC to kill all bacteria within 24 hours.

PC190723, however, exhibits a bactericidal activity at 1 X MIC in Figure 2.2. The effective time could be shortened when concentrations was increased to 2 X MIC

or 4 X MIC, indicating that PC190723 as a concentration dependent bactericidal. The stronger bactericidal activity consistence with the strong potency of PC190723 [16].

When MRSA was treated with oxacillin, the time kill curve as shown in Figure 2.3 shows a similar pattern with that of vancomycin in Figure 2.11, indicating a typical time dependent bactericidal activity. Methicillin shows a concentration dependent bactericidal with complete bactericidal activity observed in time-kill curve shown in Figure 2.4, which indicated a different bactericidal action compared with oxacillin.

F332 demonstrated bactericidal activity when used in combination with β -lactam antibiotics (Figure 2.5 and Figure 2.6). Bactericidal activities were also observed in the combinations of PC190723 and β -lactam antibiotics (Figure 2.7 and Figure 2.8) and β -lactam antibiotics alone (Figure 2.3 and Figure 2.4). All combinations exhibited bactericidal activities in concentration $\text{MIC} \times 1$, and effective from 20 hours to 24 hours. When the concentration is increased to $\text{MIC} \times 2$, bactericidal activity was also observed in between 20 and 24 hours, showing a time-dependent bactericidal activity.

The results demonstrated that FtsZ inhibitor would provide bactericidal activity when used in combination with β -lactam antibiotic. The bactericidal activity may be contributed by β -lactams and enhanced by FtsZ inhibitor. Using a combination of compounds as antibacterial agent can reduce the stock of harmful bacterial endotoxins when the cell lyses. A combination of antibacterial agents may also prevent genetic mutation and emergence of antibacterial resistance. [193, 198, 199].

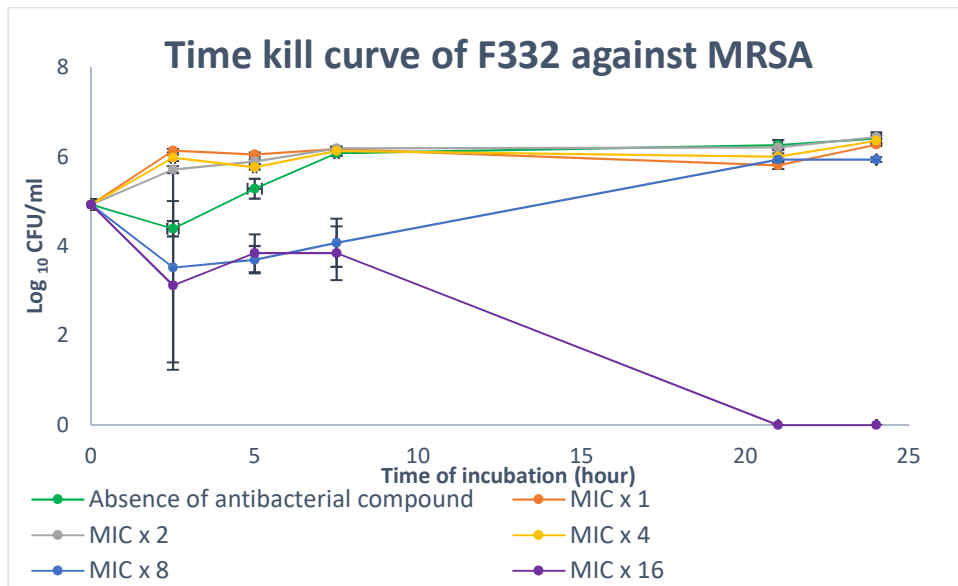


Figure 2.1 Time-kill curve for *S. aureus* ATCC BAA-41 in the presence or absence of FtsZ inhibitor F332. The error bars indicate standard deviations from measurements of triplicates.

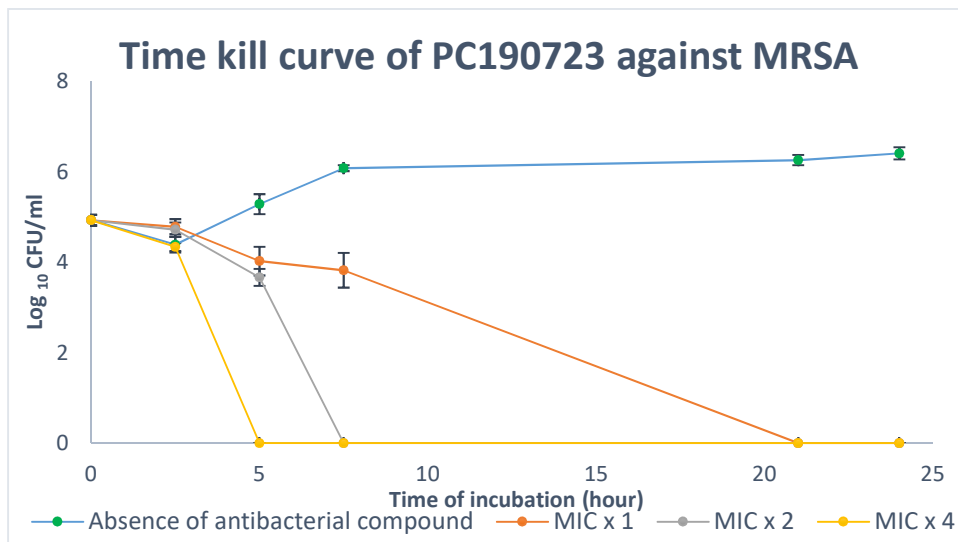


Figure 2.2 Time-kill curve for *S. aureus* ATCC BAA-41 in the presence or absence of FtsZ inhibitor PC190723. The error bars indicate standard deviations from measurements of triplicates.

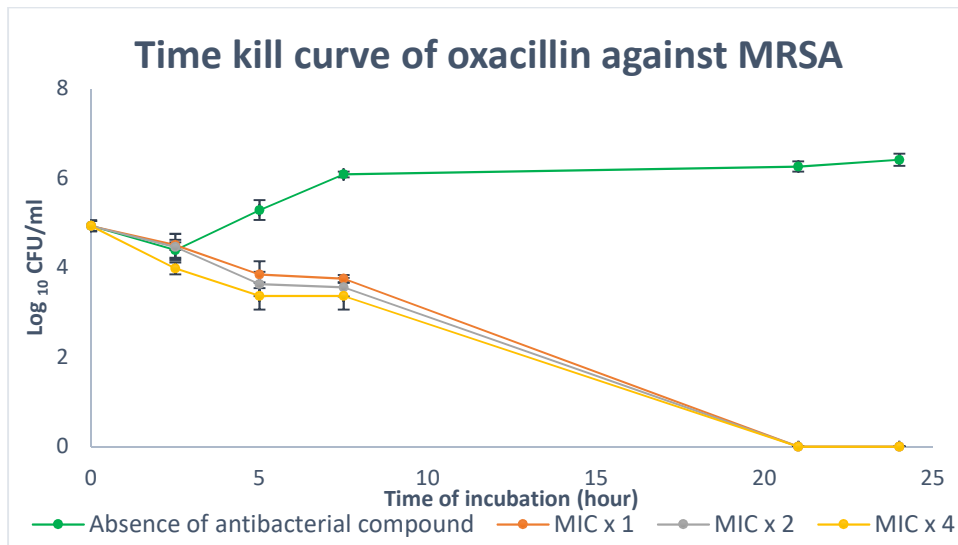


Figure 2.3 Time-kill curve for *S. aureus* ATCC BAA-41 in the presence or absence of β -lactam antibiotic oxacillin. The error bars indicate standard deviations from measurements of triplicates.

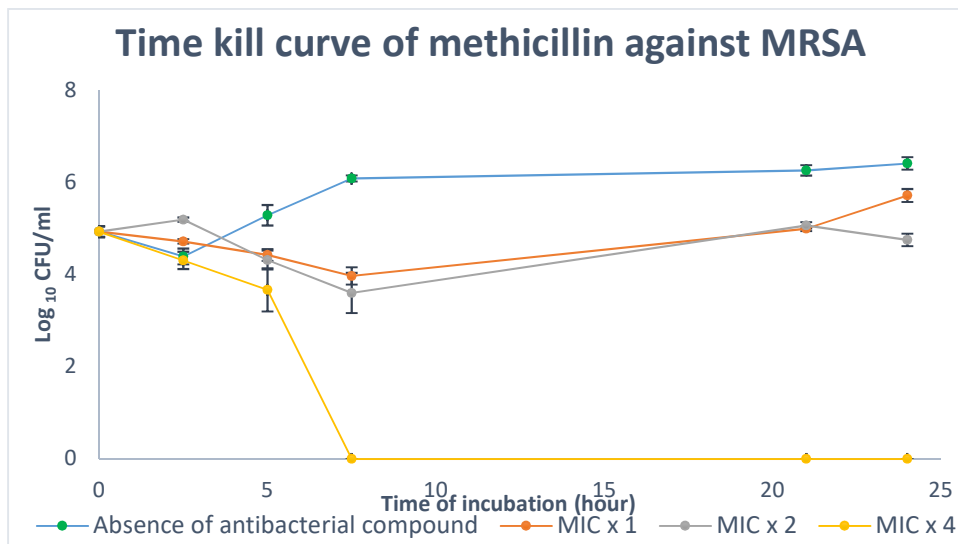


Figure 2.4 Time-kill curve for *S. aureus* ATCC BAA-41 in the presence or absence of β -lactam antibiotic methicillin. The error bars indicate standard deviations from measurements of triplicates.

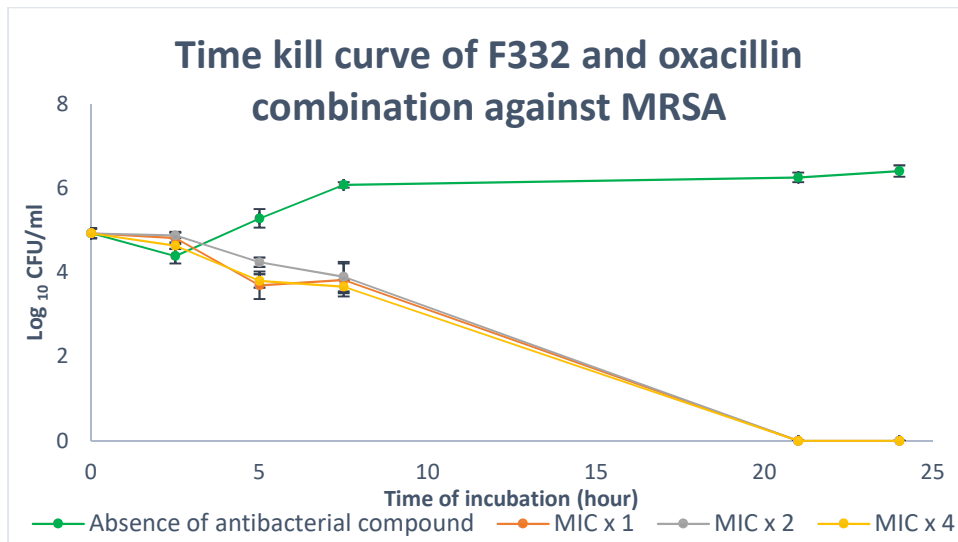


Figure 2.5 Time-kill curve for *S. aureus* ATCC BAA-41 in the presence or absence of the F332 and oxacillin. The error bars indicate standard deviations from measurements of triplicates.

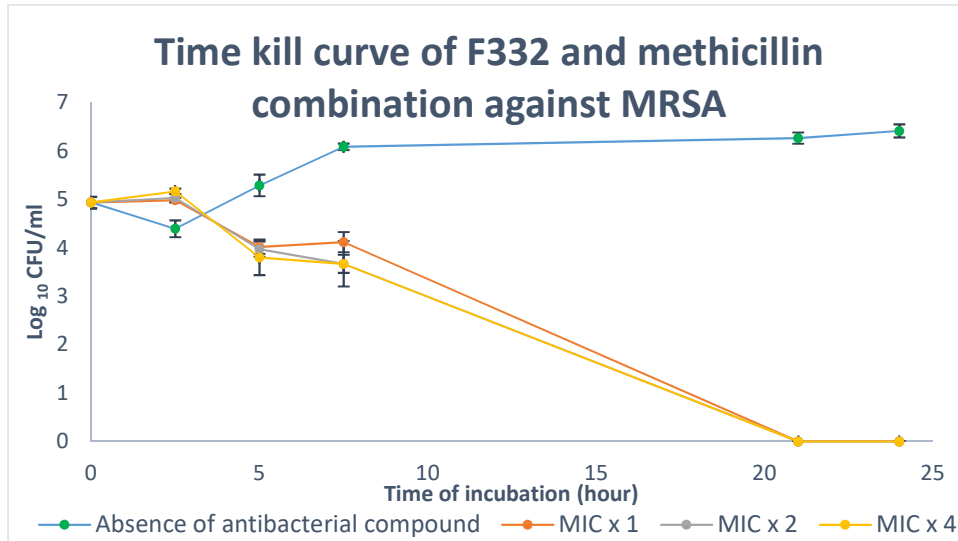


Figure 2.6 Time-kill curve for *S. aureus* ATCC BAA-41 in the presence or absence of the F332 and methicillin. The error bars indicate standard deviations from measurements of triplicates.

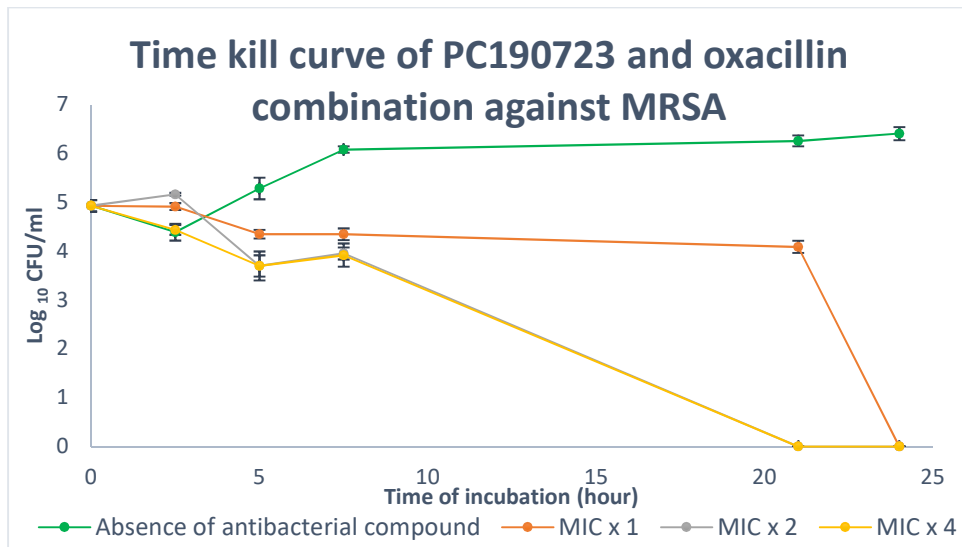


Figure 2.7 Time-kill curve for *S. aureus* ATCC BAA-41 in the presence or absence of the PC190723 and oxacillin. The error bars indicate standard deviations from measurements of triplicates.

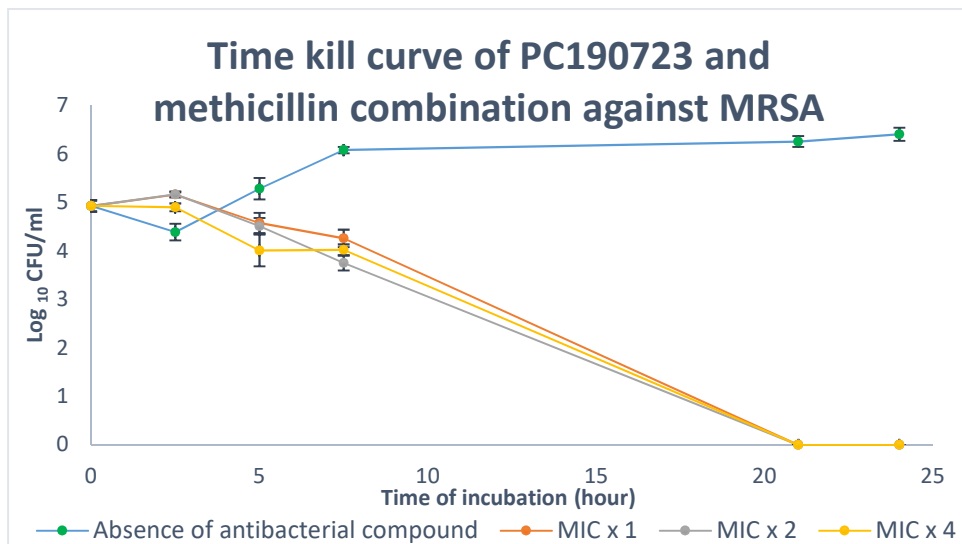


Figure 2.8 Time-kill curve for *S. aureus* ATCC BAA-41 in the presence or absence of the PC190723 and methicillin. The error bars indicate standard deviations from measurements of triplicates.

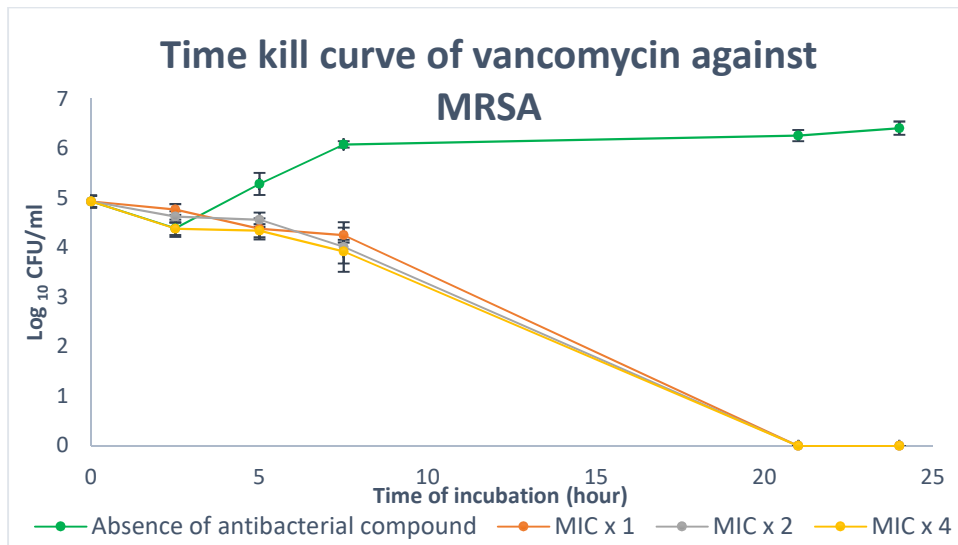


Figure 2.9 Time-kill curve for *S. aureus* ATCC BAA-41 in the presence or absence of the vancomycin. The error bars indicate standard deviations from measurements of triplicates.

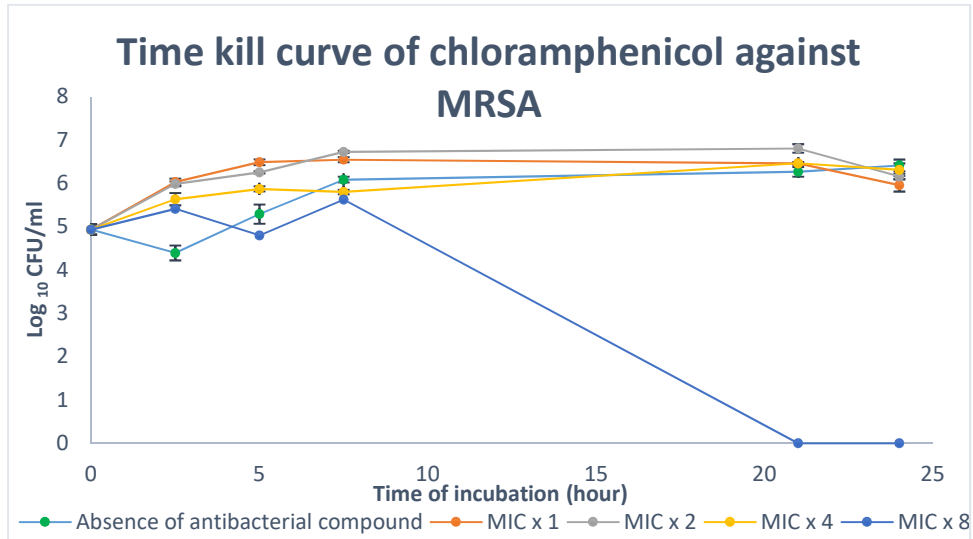


Figure 2.10 Time-kill curve for *S. aureus* ATCC BAA-41 in the presence or absence of the chloramphenicol. The error bars indicate standard deviations from measurements of triplicates.

2.3.5 Bacteriolytic assay

The experiment conditions under which the bacteriolytic experiment was performed were different from those in MIC, MBC and time-kill kinetic studies in two ways. Firstly, MIC or concentration that provided partial synergistic or synergistic effect (determined in table 2.3) of FtsZ inhibitor and β -lactam were applied in Figure 2.11 to Figure 2.14 and MICs in combination of FtsZ inhibitor of β -lactam were applied in Figure 2.15. Secondly, in bacteriolytic experiment, the compounds were applied at mid-log phase with high cell density of MRSA ($OD_{600} \sim 1.0$), whereas in MIC, MBC and time-kill studies, the compounds were applied at the incubation stage in the beginning with low cell density (standard inoculum 5×10^5 CFU/mL, with $OD_{600} \sim 0.01$). Because of these two differences, the concentrations of compounds used in bacteriolysis experiment may not effectively or completely lyse all bacteria. Also, re-growth of bacteria with increase in OD_{600} was observed after 15 hours for some concentrations. This could be due to that the bacteria reproduced much faster at mid-log phase than the bacteriolytic rate, or drug resistance was developed in the bacteria population..

Figure 2.11 and Figure 2.12 show the control experiment of how F332 and PC190723 respectively interacted with MRSA BAA-41 at various concentrations. The growth curves did not depend much the concentration of compound used. This is because the FtsZ inhibitor is only effective in inhibitory the growth of bacteria at low cell density of MRSA (standard inoculum 5×10^5 CFU/mL, with $OD_{600} \sim 0.01$), but not at high cell density MRSA ($OD_{600} \sim 1.0$). Moreover, the bacteriostatic or time-dependent bactericidal activity of FtsZ inhibitors may lead to only bacteriolytic effect.

Figure 2.13 and Figure 2.14 indicate how oxacillin and methicillin interacted with MRSA BAA-41 at various concentrations. In both curves, sub-MIC of β -lactam could reduce the population of bacteria by approximately 50 % (yellow and orange), compared with no treatment. Large reduction of bacteria population was observed when MIC of β -lactams were applied. These bacteriolysis curves suggest stronger bacteriolytic abilities of β -lactam compared with FtsZ inhibitor. Re-growth of bacteria was observed in MIC of methicillin but not in oxacillin, which is consistent with the fact that the bacterial strain was resistant to methicillin.

Figure 2.15 shows the decrease in OD_{600} when combinations of FtsZ inhibitor and β -lactam were applied at mid-log phase. The bacteria continued to grow after a combination of FtsZ inhibitor and oxacillin was applied (grey and orange), but the OD_{600} gradually decreased after 10 hours. On the other hand, the amount of bacteria decreased sharply right after applying a combination of FtsZ inhibitor and methicillin (yellow and blue) after 3 to 4 hours. These indicate that the FtsZ inhibitors restored the bacteriolytic ability of methicillin against MRSA faster than that of oxacillin. Interestingly, a combination of F332 and β -lactam (grey and yellow) showed a delay increase in OD_{600} after 23 hour and 15 hour for oxacillin and methicillin respectively. Again, this is probably due to the development of methicillin resistance in the MRSA strain.

In the cases of β -lactam antibiotics and β -lactam in combination with FtsZ inhibitors (Figure 2.13, Figure 2.14 and Figure 2.15), the growth profile generally kept in low cell density but not totally killed. This demonstrated that β -lactam antibiotics and β -lactam in combination with FtsZ inhibitors exhibited partial bactericidal effects at high cell density. On the other hand, sub-lethal concentrations of β -lactam antibiotics and β -lactam in combination with FtsZ inhibitors showed a high cell density against

time. The results showed that sub-lethal concentration did not have bactericidal effect in low nor high cell density. The growth profiles of vancomycin and chloramphenicol displayed the generally growth profile of bactericidal and bacteriostatic agent respectively when applied in high cell density (Figure 2.16).

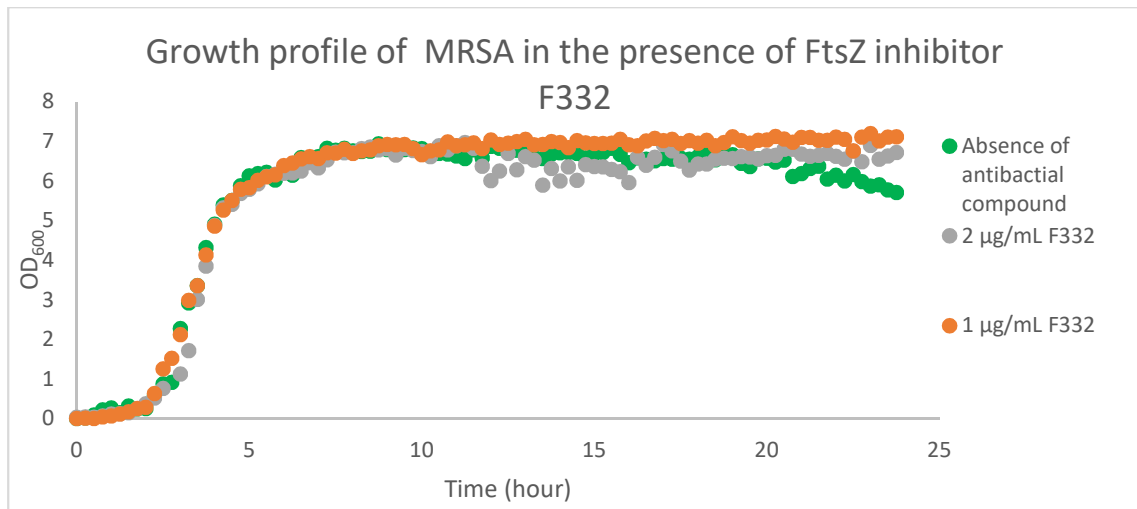


Figure 2.11 Growth profile of *S. aureus* ATCC BAA-41 in the presence of FtsZ inhibitor F332 in MIC values and sub-lethal concentrations.

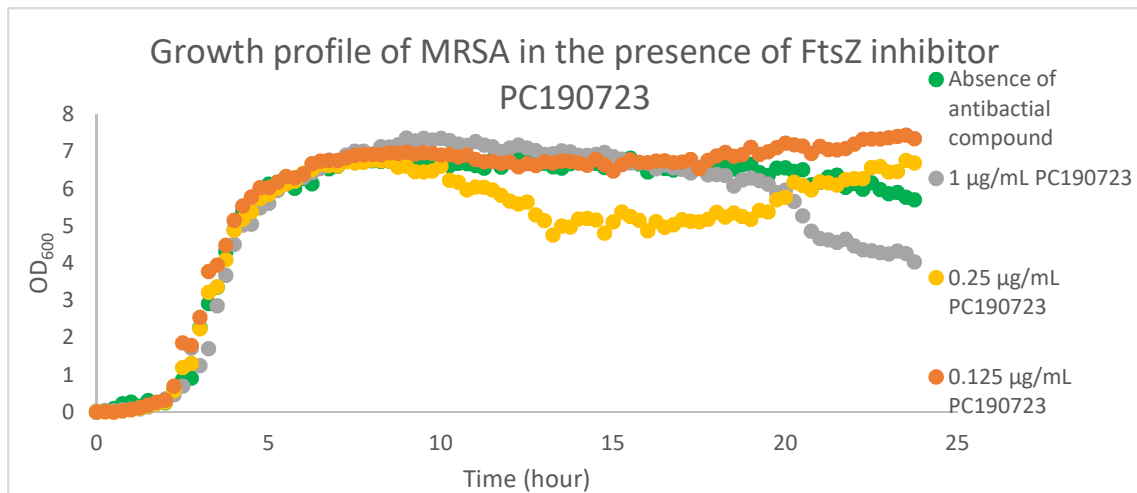


Figure 2.12 Growth profile of *S. aureus* ATCC BAA-41 in the presence of FtsZ inhibitor PC190723 in MIC values and sub-lethal concentrations.

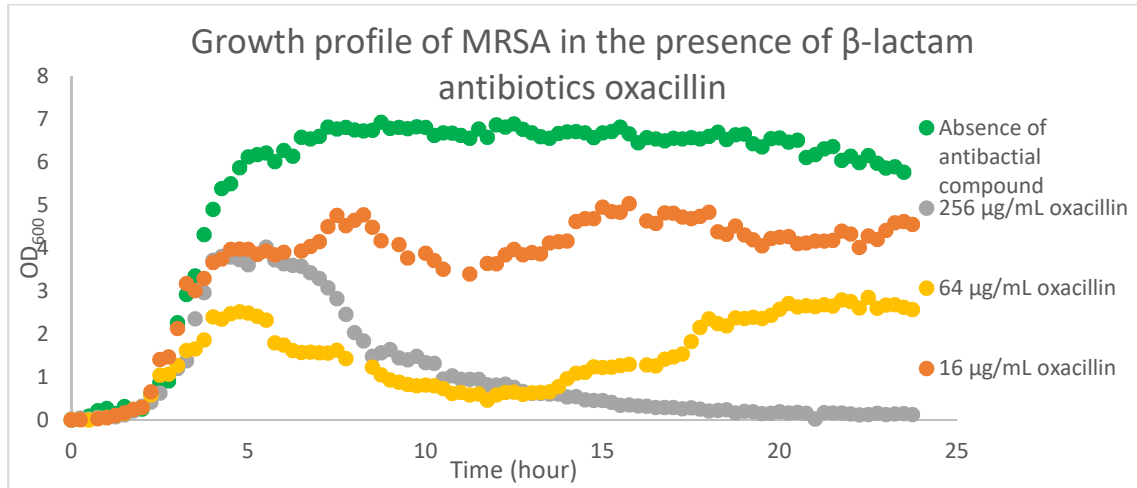


Figure 2.13 Growth profile of *S. aureus* ATCC BAA-41 in the presence of β -lactam antibiotic oxacillin in MIC values and sub-lethal concentrations

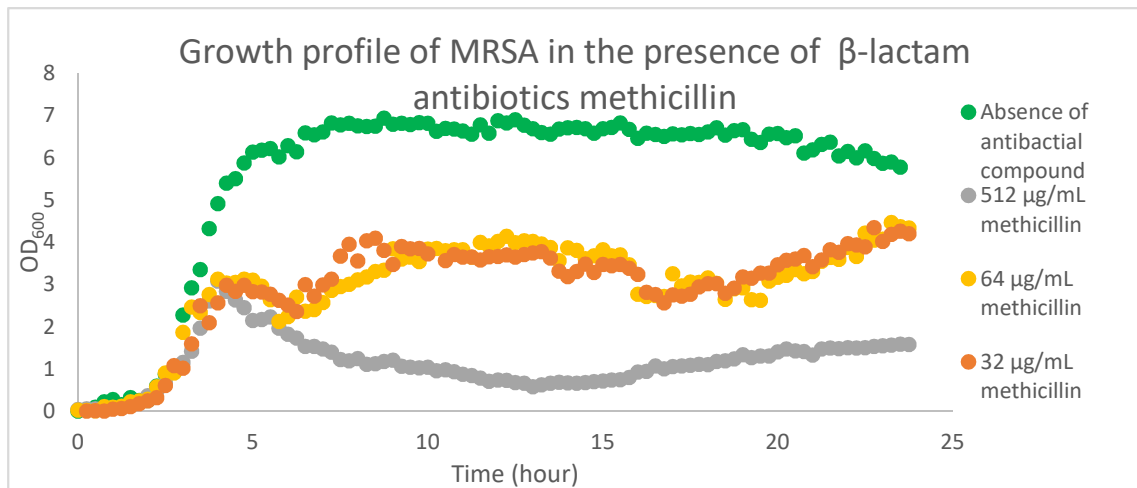


Figure 2.14 Growth profile of *S. aureus* ATCC BAA-41 in the presence of β -lactam antibiotic methicillin in MIC values and sub-lethal concentrations

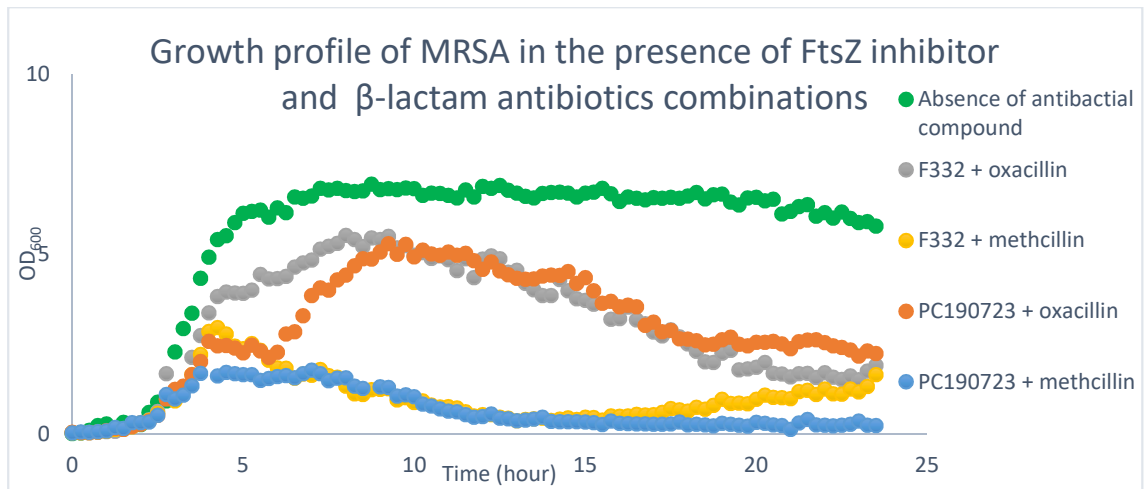


Figure 2.15 Growth profile of *S. aureus* ATCC BAA-41 in the presence of FtsZ inhibitors and β -lactam antibiotic combinations in MIC values.

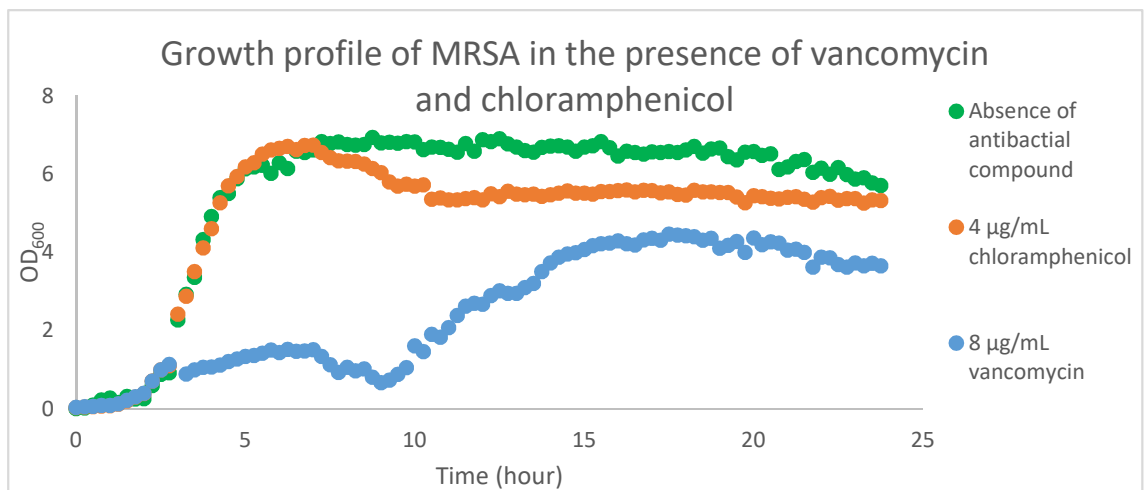


Figure 2.16 Growth profile of MRSA ATCC BAA-41 in the presence of vancomycin and chloramphenicol in MIC \times 4 concentration.

2.4 Concluding remarks

In this chapter, the FtsZ inhibitor F332 was firstly shown to have low value of MIC against the MRSA strain ATCC BAA-41, indicating that it is a good candidate to combat MRSA. When FtsZ inhibitor was used with β -lactam, partial synergistic effects or synergistic effects were observed against MRSA ATCC BAA-41. The MBC results indicated that FtsZ inhibitor F332 is a bacteriostatic antibacterial compound. However, bactericidal activities were displayed when FtsZ inhibitor in combinations with β -lactam antibiotics. The time-kill kinetic studies revealed the time-dependent bactericidal activities in the combination of FtsZ inhibitors and β -lactam.

The bacteriolysis assay demonstrated cell lysis occurred when the cells grew were treated with a combination of FtsZ inhibitor and β -lactam after entering mid-log phase. The bacteriolysis activities were time-dependent and became effective at 20 to 24 hours. Cell lysis was probably promoted by β -lactam and enhanced by FtsZ inhibitor. In order to examine the role played by FtsZ inhibitors, β -lactams and their combination, how FtsZ inhibitors, β -lactams and their combination affected the localization of their targets or related products was studied and the results would be reported in the next chapter.

Chapter 3. Target localization and morphological studies

3.1 Introduction

This chapter focuses on the effect of antibacterial compounds on the localization of their targets. FtsZ inhibitors target FtsZ protein while β -lactam antibiotics target on penicillin binding protein (PBP). PBP is a transpeptidase responsible for the crosslinking between two stem peptides of the lipid-linked peptidoglycan precursor (lipid II). The objectives of this chapter are to examine the effect of FtsZ inhibitors, β -lactam antibiotics and their combination on the localization of their targets.

Previous work from our group has shown that 3-MBA derivative FtsZ inhibitors delocalized FtsZ ring assembly. The delocalization of FtsZ protein in rod-shaped cell models such as *E. coli* and *B. subtilis* has been visualized in previous studies [165, 200, 201]. Delocalization of FtsZ proteins in *S. aureus* was observed upon treatment with 3-MBA derivative PC190723 [16]. However, visualization of *S. aureus* FtsZ ring was not yet observed upon the treatment of F332. Using *S. aureus* as a spherical model in FtsZ localization imaging could exclude the unknown and potential effects from elongation proteins (such as MreB related proteins) that appear in rod-shaped cells. Therefore, recombinant *S. aureus* expressing GFP-FtsZ fusion protein was developed to visualize FtsZ protein localization and FtsZ ring formation [16, 35].

The target of β -lactam antibiotics is the transpeptidase domain in PBP2 for *S. aureus* or PBP2a for MRSA. Their substrate is the D-alanyl-D-alanine amino acid residues on the lipid-linked peptidoglycan precursor (lipid II), while the lipid-linked peptidoglycan precursor is one of the downstream products of FtsZ present outside peptidoglycan. One of the objectives of this chapter is to visualize the localization of stem peptide region of lipid II with the use of a commercially available fluorescent vancomycin analogue probe [24]. D-serine supplemented in the culture medium

converted the last two amino acid residues of the stem peptide from D-alanyl-D-alanine to D-serine-D-serine and prevented the binding of fluorescent vancomycin analogue probe to the stem peptide. The cells were then transferred to normal medium without D-serine and incubated for one cell cycle, the newly grown peptidoglycan consists of stem peptide with D-alanyl-D-alanine will then allow the fluorescent vancomycin analogue probe to bind to this dipeptide. This pulse labelling method allows the visualization of the localization of newly grown peptidoglycan [165].

Cell elongation has been observed in rod-shaped models such as *E. coli* and *B. subtilis* under the treatment of FtsZ inhibitor F332 or other FtsZ inhibitors [176, 201, 202], while some studies have reported cell enlargement in *S. aureus* when treated with FtsZ inhibitors [35, 127]. The cell morphological changes (cell enlargement) in *S. aureus* were herein investigated. These were addressed by treating *S. aureus* with a full range of concentrations of FtsZ inhibitors, β -lactam antibiotics and their combinations. The change in cells volume were used as an indication of morphological change.

3.2 Experimental

3.2.1 Materials

3.2.1.1 Bacterial strains

E. coli Top 10 (ThermoFisher), DH5 α TM (ThermoFisher) or ER2566 (New England BioLabs Inc.) and *S. aureus* RN4220 competent cells were used for plasmid DNA propagation and amplification for examination of FtsZ protein localization *in vivo*. MRSA ATCC BAA-41 was used in examination of the localization of stem peptide of lipid II on newly grown peptidoglycans and its morphological changes. *S. aureus* RN4220 was our laboratory collection. MRSA ATCC BAA-41 was purchased from American Type Culture Collection (USA).

3.2.1.2 Media

Agar powder, tryptone and yeast extract were purchased from Oxoid Limited (Nepean, Ontario, Canada). Luria-Bertani broth was prepared by dissolving 10 g of tryptone, 5 g of yeast extract and 10 g of sodium chloride in deionized water [186]. Powder form of trypticase soy broth (TSB) and brain-heart infusion (BHI) were purchased from Becton, Dickinson and Company (New Jersey, USA). The broths were prepared according to manufacturers' instructions. Solid form of different nutrient media was prepared by an addition of 15 g/L agar powder to each broth before sterilization. Unless otherwise specified, all broths and agar were autoclaved before use.

3.2.1.3 Plasmids

Plasmids pGL485, pLOW-GFP control and pLOW FtsZ-GFP were the generous gifts from Professor Elizabeth Harry and group fellow Dr. Andrew Liew Tze Fui from University of Technology, Sydney [203].

3.2.1.4 Antibacterial compounds

Oxacillin, methicillin, and vancomycin were purchased from Sigma-Aldrich (United States). FtsZ inhibitors 3-MBA derivatives F332 and PC190723 [16], were our laboratory's collection. Their structures and details are listed in Table 2.1.

3.2.1.5 Chemicals and consumables

BODIPY FL vancomycin conjugated, Hoechst 33342 and FM® 4-64FX, which would stain nucleic acid, lipid II and cell membrane, respectively, were purchased from Thermofisher Scientific, Vancomycin (Sigma) and D-serine amino acid (Sigma) were applied in transpeptidase substrate assay. 0.1 cm electroporation cuvettes were purchased from Biorad Laboratory. Paraformaldehyde, purchased from Sigma-Aldrich was applied in cell fixing in microscopic slide preparation. Plastic frames (Gene Frame ®) were purchased from Life Technologies and high tolerance cover glass with thickness No. 1.5 H purchased from Mattek, USA, were used in microscope slide preparation.

3.2.2 Instrumentation and software

Confocal microscope Leica SP8 with software LAS X was used to capture images with high resolution, images treatment and 3-D image construction. The confocal microscope was equipped with a water immersion 63X objective HC PL APO 63/1.20 W CORR CS2 and a water immersion microscope dispenser for fixed live monolayer samples and an oil immersion 63X objective HC PL APO C52 63x/1.40 OIL for fixed monolayer samples. Huygens software from Scientific Volume Imaging was applied for image deconvolution. ImageJ software from National Institutes of Health was applied for cell diameter measurement.

3.2.3 Localization of FtsZ protein in *S. aureus*

3.2.3.1 Preparation of *E. coli* competent cell

A single colony of *E. coli* competent cells was picked from LB agar plate and inoculated in 5 mL of LB broth at 37 °C with shaking at 250 rpm overnight. Then, this culture was diluted 100-fold in 100 mL fresh LB broth, and the cells were further incubated until the OD₆₀₀ value reached between 0.3 and 0.4. The cells were harvested by centrifugation at 4,000 rpm at 4 °C for 15 minutes. The cell pellet was re-suspended in 10 mL of 0.1 M CaCl₂ and pelleted again at 4 °C. The cells were then incubated in 0.1 M CaCl₂ for half to one hour and centrifuged at 4 °C for 15 minutes. Finally, the cells were resuspended in 0.1 M CaCl₂. 50 % (v/v) solution of glycerol was added to the cell culture so that the final concentration of glycerol reached 15 %. The cells were aliquoted to 80 µL per microcentrifuge tube and used immediately or stored at -80 °C.

3.2.3.2 Transformation of *E. coli* competent cells by heat shock

The plasmids pGL485 and pLOW FtsZ-GFP were transformed into *E. coli* competent cells. The target plasmid DNA was introduced and gently mixed with 80 μ L *E. coli* competent cells. The mixture was incubated for 30 minutes in an ice bath. The mixture was heat shocked at 42 °C for 1 minute and stored in an ice bath for 2 minutes. 1 mL of LB broth was immediately added to the mixture. The cells were then incubated at 37 °C for 1 hour. After incubation, the cells were plated on LB agar with selection antibiotics listed in Table 3.1 and further incubated at 37 °C overnight. Any colonies formed were cells carrying antibiotic resistant plasmid. A single colony was picked and inoculated in 5 mL of LB broth with selection antibiotics. The plasmids in cells were extracted by Wizard® Plus SV Minipreps DNA Purification System (Promega) and further confirmed by sequencing services provided by BGI Co. Ltd. or Tech Dragon.

Table 3.1 Antibiotics selection of various plasmids in different bacterial strains

Bacterial competent cells	Antibiotics for selection	Selecting plasmids	Final concentrations of antibiotics
<i>E. coli</i> Top 10	Ampicillin	pLOW-GFP	100 µg/mL
<i>E. coli</i> Top 10	Spectinomycin	pLG485	100 µg/mL
<i>S. aureus</i> (RN4220)	Erythromycin	pLOW-GFP	20 µg/mL
	Lincomycin		100 µg/mL
<i>S. aureus</i> (RN4220)	Chloramphenicol	pLG485	40 µg/mL

3.2.3.3 Preparation of *S. aureus* competent cells

A single colony of *S. aureus* RN4200 was picked from BHI agar plate and inoculated in 5 mL of BHI broth at 37 °C with shaking at 250 rpm overnight. Then, this culture was diluted 100-fold in 50 mL fresh BHI broth, and the cells were further incubated until the OD₆₀₀ reached between 0.3 and 0.4. The cells were harvested by centrifugation at 4,000 rpm at 4 °C for 15 minutes. The cell pellet was re-suspended in 25 mL of deionized water, pelleted again at 4 °C, and repeated cell pellet resuspension and pelleting twice. The cells were centrifuged at 4,000 rpm at 4 °C for 15 minutes, re-suspended with 10 % (v/v) solution of glycerol and incubated with 10 % glycerol solution for half to one hour. The cells were finally pelleted again and re-suspended with 200 µL of 10 % (v/v) solution of glycerol. The cells were aliquoted to 80 µL per microcentrifuge tube and used immediately or stored at -80 °C.

3.2.3.4 Transformation of *S. aureus* competent cells by electroporation

The plasmids pGL485 and pLOW FtsZ-GFP were transformed sequentially into *S. aureus* competent cells by a reported method [204]. The target plasmid DNA was introduced and gently mixed with 80 µL *S. aureus* competent cells. The mixture was incubated for 30 minutes in an ice bath. It was then transferred to a 0.1 cm electroporation cuvette and underwent electroporation at 100 Ω resistance, 25 µF capacitance and 2.3 kV voltage and a time constant of approximately 2.5 ms. 1 mL of BHI broth was immediately added to the cell mixture and stored in an ice bath for 10 minutes. The cells were then incubated at 37 °C for 3 to 4 hours. After incubation, the cells were plated on BHI agar with selection antibiotics listed in Table 3.1 and further incubated at 37 °C overnight. Any colonies formed were cells carrying antibiotic-

resistant plasmid. A single colony was picked and inoculated in 5 mL of BHI broth with selection antibiotics. The cells with the first plasmids were incubated and the procedures of preparation of *S. aureus* competent cells and transformation of *S. aureus* competent cells were repeated by electroporation with another plasmid as mentioned above. The plasmids in cells were extracted by Wizard® Plus SV Minipreps DNA Purification System (Promega) and further confirmed by sequencing services provided by BGI Co. Ltd. or Tech Dragon.

3.2.3.5 Visualization of FtsZ-GFP protein in *S. aureus*

The visualization of FtsZ-GFP in *S. aureus* was performed based on a previous reported method [203]. The nucleus acids were stained with a blue fluorescent Hoechst 33342. This is a cell permeable bisbenzimidazole derivative that can bind to DNA with AT selectivity [205].

A single colony of *S. aureus* RN4220 with FtsZ-GFP fusion protein plasmid was picked from LB agar plate and inoculated in 5 mL of LB broth supplemented with the selection antibiotics (Table 3.1) and 400 μ M of isopropyl β -D-1-thiogalactopyranoside (IPTG) at 30 °C with shaking at 250 rpm overnight. Then, this culture was diluted 100-fold in 5 mL fresh LB broth. 400 μ M of IPTG and antimicrobial compounds (FtsZ inhibitors F332 and PC190723, β -lactam antibiotics oxacillin and methicillin) were added at concentration of MIC \times 4. The cells were further incubated at 30 °C with shaking at 250 rpm for 5 hours. Next, the cells were washed and re-suspended with PBP. 30 μ g/mL of Hoechst 33342 nucleus acid stain was added to each sample. They were further incubated at 25 °C for 15 minutes. Next, the samples were washed twice with PBS (phosphate-buffered saline) and mono-layer bacterial slides

were prepared for microscopic observation. In brief, a plastic frame was attached in the middle of a clean microscope glass slide, 1.5 % agarose was poured in the middle of the frame and another slide was loaded on top of the molten agarose. After the agarose had been frozen, the upper slide was carefully removed. 2 μ L of cells was loaded on an agarose pad. Any surplus liquid on the agarose pad was allowed to evaporate for 10 minutes. A cover glass was placed on the plastic frame.

FtsZ ring localization was visualized using a Leica TCS SP8 confocal microscope equipped with a 63X water objective (numerical aperture 1.2) with automatically optimized confocal pinhole apertures. Images were captured by a hybridized photomultiplier tube or a photomultiplier tube fluorescence detector. Fluorescence Z-scans were captured sequentially with a 405 nm diode laser (50 mW) for nucleus stain and 488 nm line argon laser (20 mW) for GFP. Deconvolution of captured images were processed by Huygens software and the contrast of images was adjusted by stack auto scale using the software Leica LAS X. Images were visualized by maximum projection using software Leica LAS X. This is a volume visualization method that projects 3D data in visualization plane with maximum intensity. All Z-stacks of 2D images were reconstructed to provide a good sense of 3D in a 2D image.

3.2.4 Localization of transpeptidase substrate in *S. aureus*

The visualization of transpeptidase substrate localization in *S. aureus* was achieved by BODIPY® FL Vancomycin with supplement of certain amino acid during the inoculation of the cells. The nucleic acids were stained with a blue fluorescent Hoechst 33342. FM® 4-64FX is a lipophilic styryl compound for cell membrane studies. It is

an aldehyde-fixable analog that utilize aliphatic amines for crosslinking by formaldehyde or glutaraldehyde during cell fixing.

Equal volumes of vancomycin and BODIPY FL conjugated vancomycin at sub-inhibitory concentration $MIC \times 0.5$ were mixed to form Vancomycin: Vancomycin BODIPY@FL conjugate pre-mixed solution (Van/Van-FL). The pre-mixed solution was added to the cells used in newly grown peptidoglycan staining to give a final concentration of 1 $\mu\text{g}/\text{mL}$ (1 $\mu\text{g}/\text{mL}$ of Van/Van-FL mixture) as previously described [35, 165].

A single colony of *S. aureus* BAA-41 was picked from BHI agar plate and inoculated in 5 mL BHI broth supplemented with 0.125 M D-serine amino acid at 37 °C with shaking at 250 rpm overnight. Supplemented D-serine amino acid was incorporated to the propagating synthesis of peptidoglycan. Then, this culture was diluted 100 times in 5 mL fresh BHI broth supplemented with 0.125 M D-serine amino acid, and the cells were further incubated to achieve mid-log phase with OD_{600} values at approximately 0.5. The antibacterial compounds (FtsZ inhibitors F332 and PC190723, β -lactam antibiotics oxacillin and methicillin, and their combination) were added at sub-lethal concentration, $MIC \times 0.5$, $MIC \times 1$, $MIC \times 2$ or in the absence of any antibacterial compounds (see experimental section for details). The samples were further incubated at 37 °C for 3 hours with shaking at 200 rpm. After that, the samples were washed twice with PBS and resuspended in BHI broth with the testing antibacterial compounds, then further incubated at 37 °C for 15 minutes so that the newly grown peptidoglycan could allow incorporation of D-alanine amino acids in the terminus of pentapeptide.

Next, the cells were fixed by re-suspending them in freshly prepared 4 % paraformaldehyde for 10 minutes. Then, the cells were washed with and re-suspended in PBS. Sub-inhibitory concentration of Van/Van-FL, 30 µg/mL of final concentration of Hoechst 33342 and 6 µg/mL of final concentration FM® 4-64FX were added to each sample. They were further incubated at 25 °C for 15 minutes. Next, the samples were washed twice with PBS and mono-layer bacterial slides were prepared for microscopic observation according to the method discussed in Section 3.2.3.5.

The stained *S. aureus* was visualized under a Leica TCS SP8 confocal microscope equipped with 63X oil objective (numerical aperture 1.4) with automatically optimized confocal pinhole apertures. Images were captured by a hybridized photomultiplier tube or a photomultiplier tube fluorescence detector. Fluorescence Z-scans were captured sequentially with a 405 nm diode laser (50 mW) for Hoechst 33342 nucleus stain, 488 nm line argon laser (20 mW) for fluorescent vancomycin analogues probe, a 633 nm line Helium, Neon laser (10 mW) for FM® 4-64 FX cell membrane stain. Deconvolution of captured images were processed by Huygens software and the contrast of images was adjusted by stack auto scale by the software Leica LAS X. Images were visualized by maximum projection using software Leica LAS X. This is a volume visualization method that projects 3D data in visualization plane with maximum intensity. All Z-stacks of 2D images were reconstructed to provide a good sense of 3D in a 2D image.

3.2.5 Morphological studies

A single colony of *S. aureus* BAA-41 was picked from BHI agar plate and inoculated in 5 mL BHI broth at 37 °C with shaking at 250 rpm overnight. Then, this culture was

diluted 100-fold in 5 mL fresh BHI broth, and the cells were further incubated at 37 °C with shaking at 250 rpm, until mid-log phase was achieved with OD₆₀₀ values at approximately 0.5. The antibacterial compounds (FtsZ inhibitors, β-lactam antibiotics, or their combinations) were added at sub-lethal concentration, MIC × 0.5, MIC × 1, MIC × 2 or in the absence of antibacterial compound (see Appendix I for details). The samples were further incubated at 37 °C with shaking at 200 rpm for 3 hours. Next, the cells were washed with and re-suspended in PBS and mono-layer bacteria were prepared according to the method discussed in Section 3.2.3.5.

S. aureus morphologies were viewed under Leica TCS SP8 confocal microscope with a under 63X oil objective (numerical aperture 1.4) with automatically optimized confocal pinhole apertures and the images were captured by a hybridized photomultiplier tube or a photomultiplier tube detector by differential interference contrast (DIC) or phase contract. The diameters of bacteria were measured by the software ImageJ. The diameters (d) were converted into spherical volume (V) by equation 3.1

$$V = \frac{4\pi(\frac{d}{2})^3}{3} \dots\dots\dots \text{Equation 3.1}$$

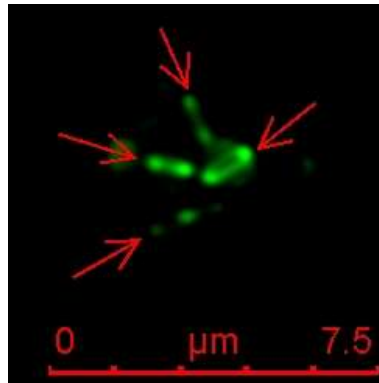
The frequency of volume in each treatment group was normalized by the highest frequency and then plotted as histograms of frequency distribution of cell volume, which are attached in appendix. The trend-lines of 5 average periods movement are indicated on the histograms. The mode (highest frequency) of volumes in histograms are peaks of the trend-lines. The mode, mean (average) of the volumes and the standard deviation are presented in the table in Section 3.3.3.

3.3 Results and discussion

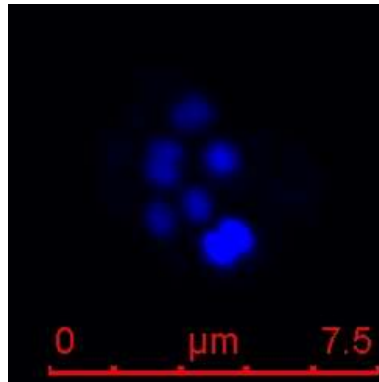
3.3.1 Localization of FtsZ protein

In normal bacterial cell cycle, FtsZ ring assembly is the initializing step of septum formation [36, 165, 206], which is followed by a series of biochemical processes and finally completion of cell division. Disruption of FtsZ ring formation, for instance by the presence of FtsZ inhibitor, will interfere with the normal cycle and cause cell death. Visualizing the FtsZ ring formation in cell cycle interfered by FtsZ can give information about the antibacterial mechanism of FtsZ inhibitor. In this study, visualization of the Z ring was done by applying *S. aureus* RN4220-FtsZ-GFP in fluorescent microscopic analysis. In the absence of antibacterial compounds, FtsZ-GFP fusion protein localized in the septum, forming an intact Z-ring (indicted with red arrows) (Figure 3.1). As expected, introducing F332 or PC190723 to *S. aureus* RN4220 FtsZ-GFP delocalized the FtsZ protein and disrupted the Z-ring assembly. The red arrows in Figure 3.2 indicate the dispersed FtsZ proteins that could not form a complete Z-ring. This was a direct proof of Z-ring disruption by F332. β -Lactam antibiotics (oxacillin or methicillin) were applied in this study. β -Lactam antibiotics had no direct interaction with FtsZ, and thus had no effect on Z-ring formation (Figure 3.3).

A



B



C

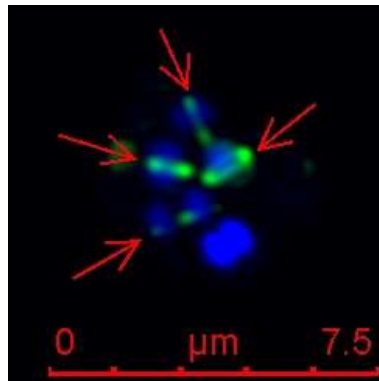


Figure 3.1 *S. aureus* RN 4220-FtsZ-GFP mutant was (A) expressed with FtsZ-GFP protein, (B) stained for visualizing nucleus acid (blue) and (C) a merged image in the absence of antibiotic compound. Scale bar is 7.5 μm .

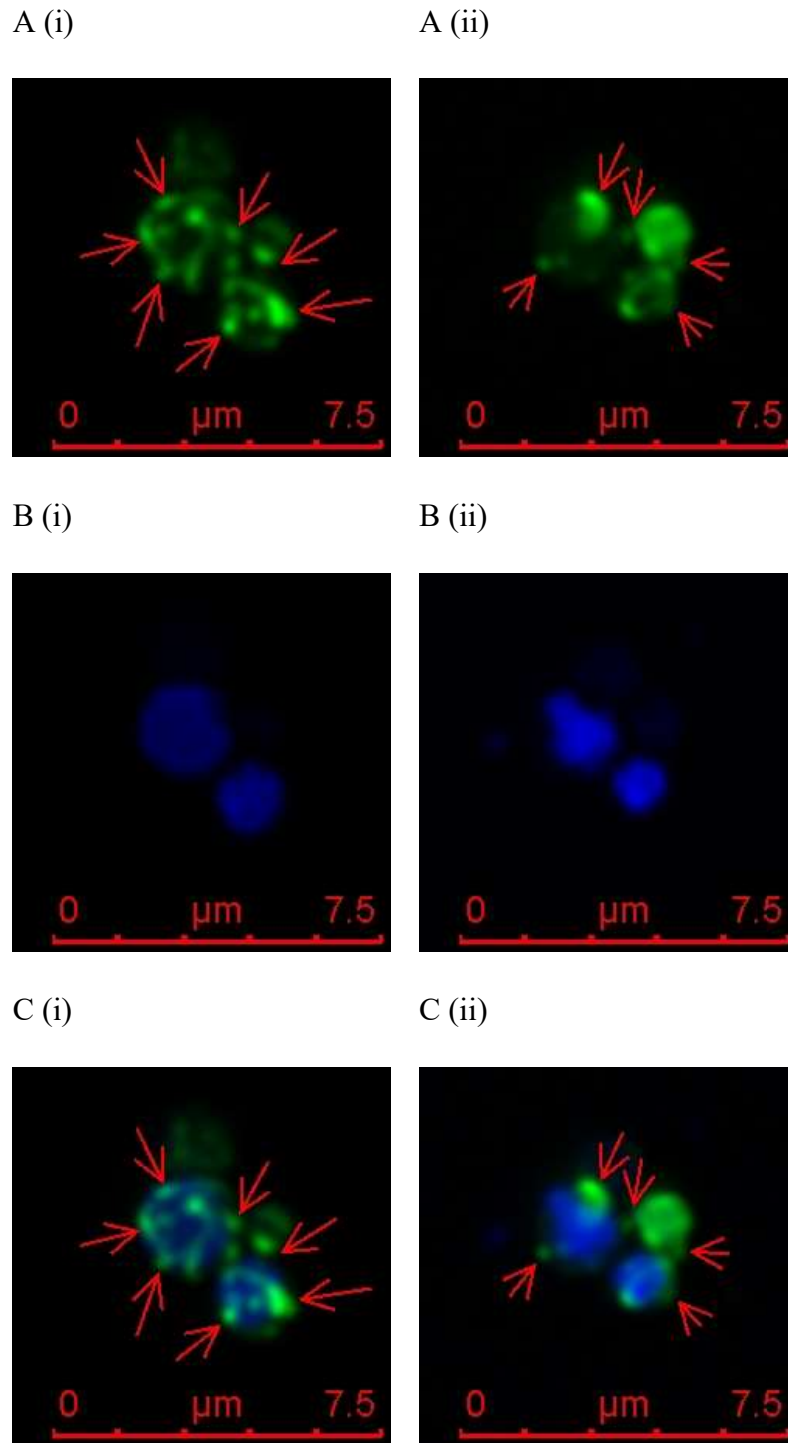


Figure 3.2 *S. aureus* RN 4220-FtsZ-GFP mutant was (A) expressed with FtsZ-GFP protein, (B) stained for visualizing nucleus acid (blue) and (C) a merged image in the presence of FtsZ inhibitors (i) F332 and (ii) PC190723 with a concentration of MIC \times 4. Scale bar is 7.5 μ m.

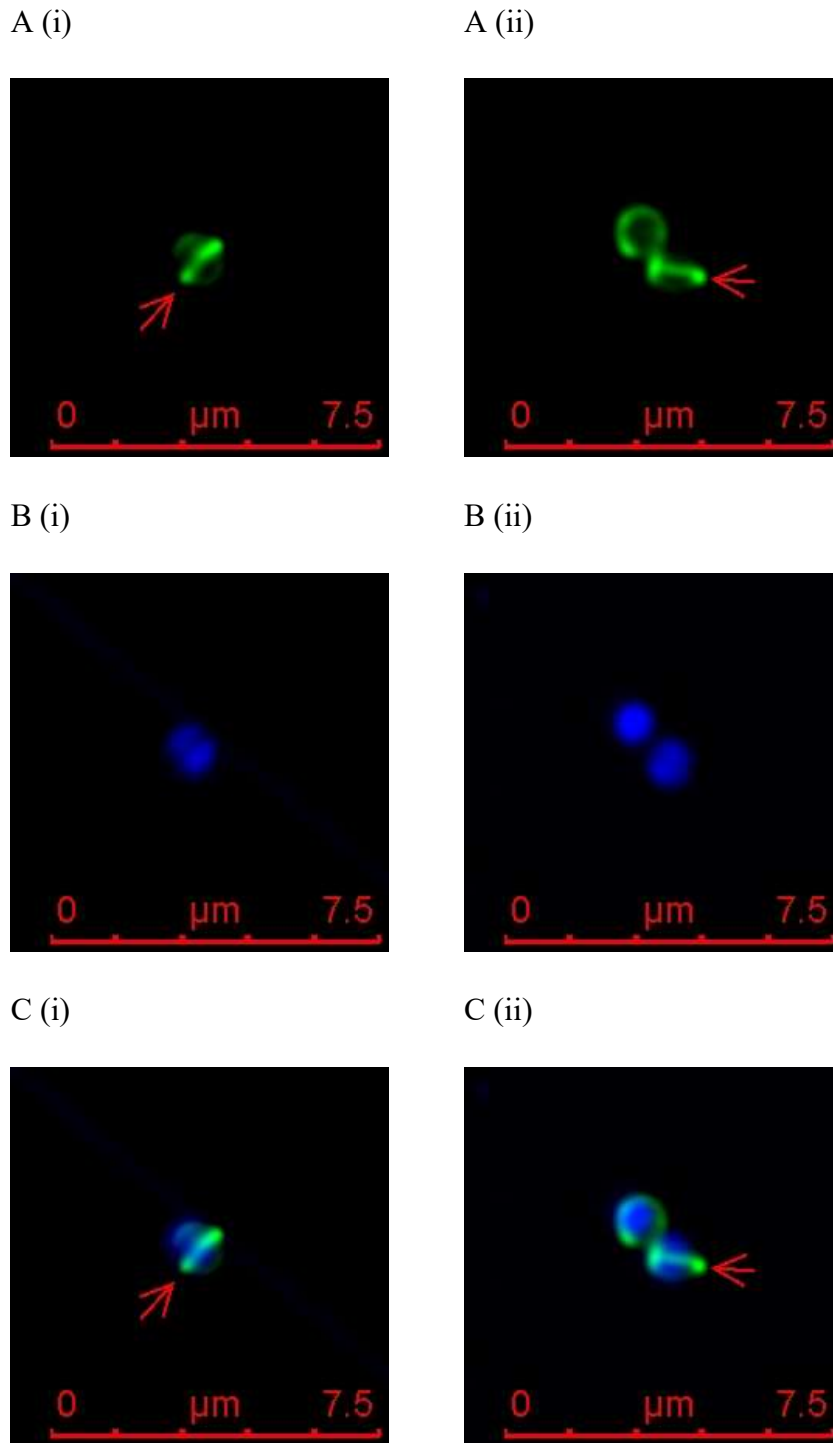


Figure 3.3 *S. aureus* RN 4220-FtsZ-GFP mutant was (A) expressed with FtsZ-GFP protein, (B) stained for visualizing nucleus acid (blue) and (C) a merged image in the presence of β -lactam antibiotic (i) oxacillin and (ii) methicillin at a concentration of $\text{MIC} \times 4$. Scale bar is 7.5 μm .

3.3.2 Localization of transpeptidase substrate in *S. aureus*

In the previous section, F332 and PC190723 were shown to inhibit FtsZ ring formation in living *S. aureus*. However, more experiments have to be conducted to reveal the effect of these inhibitors on the downstream biochemical process and the implication of FtsZ delocalization on antibacterial activity.

One of the most important downstream biochemical processes in the cell division cycle is the production of lipid II, the peptidoglycan precursor, and locating it in a suitable position. Successful synthesis of lipid II is obviously critical in peptidoglycan synthesis during cell division. In fact, some bactericidal agents, such as D-cycloserine, target lipid II synthase and can inhibit cell growth or cell division. Strong relationship has also been shown between cell death and the improper alignment of lipid II-linked peptidoglycan precursor (newly grown cell wall), which could be caused by introducing FtsZ inhibitor to *S. aureus* [165].

Fluorescent vancomycin analogue stain (Van-Van FL), which specifically binds to lipid II of newly grown peptidoglycan (cell wall) was used in the presence of F332 or PC190723 (3-MBA derivatives FtsZ inhibitor), β -lactam antibiotics or their combinations in various concentrations (Appendix I). In this study, the stain was especially suitable for Gram-positive *S. aureus* because vancomycin was unable to penetrate the outer membrane of Gram-negative bacteria. Due to the membrane impermeability of Van-Van FL, only D-alanyl-D-alanine amino acid residues of the terminus of stem peptide on the lipid-linked peptidoglycan precursors (lipid II) at the cell wall could be stained by Van-Van FL [24, 35].

In the absence of any antibacterial compounds, the division septum between parent cell and daughter cell was stained by Van-Van FL (Figure 3.4). This demonstrated that the newly grown cell wall II was polymerized to give a complete division septum in a normal cell cycle. On the other hand, lipid II of newly grown cell wall was found to delocalize from septum when the FtsZ inhibitor concentration was at $MIC \times 2$ for F332 or PC190723 (Figure 3.5 and Figure 3.6). The delocalization of lipid II was possibly due to the incapability of proper alignment of FtsZ proteins, rather than caused by direct interaction with FtsZ inhibitor.

This captured images were also similar to reported images using FtsZ-depleted *S. aureus* mutant without FtsZ protein expression [35]. The appearance of the newly grown lipid II in FtsZ-depleted *S. aureus* suggested that the synthesis of cell wall occurred in a non-regulated manner [35, 127, 207]. In both cases, the “FtsZ-downstream” process, i.e. lipid II *in situ* synthesis and localization, were indirectly interfered with.

It should be pointed out that improper localization of lipid II would result in improper alignment of PBP2, the sole class 1A PBP in *S. aureus* [16, 166], which shall align with the division septum in normal cell cycle. It is rational that delocalization of PBP2 would cause incorrect positioning of peptidoglycan synthesis, which shall play a critical role in cell death (lysis).

Pinho and co-workers also showed that delocalization of PBP2 could be caused by introducing β -lactam antibiotics to *S. aureus*. Acylation of the transpeptidase site of PBP2 by β -lactam antibiotics interfered with the interaction between PBP2 and peptide moiety of lipid II [165]. The interaction was believed to be essential for recruiting PBP2 to the division septum [165]. Thus, although lipid II aligned at the division septum,

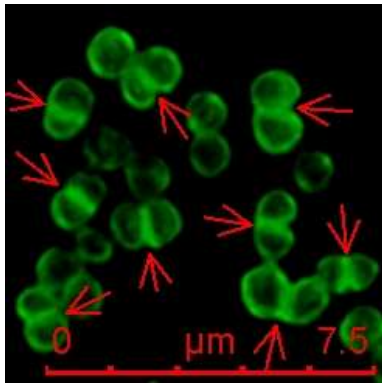
PBP2 without any functional transpeptidase could no longer be properly recruited at the septum unless the functional transpeptidase of the acquired PBP2a was present in MRSA. On the other hand, introducing β -lactam antibiotic to *S. aureus* would not cause delocalization of lipid II, suggesting that PBP2 was recruited under proper lipid II synthesis and localization (Figure 3.7 and Figure 3.8).

In samples treated with combinations of FtsZ inhibitors and β -lactam antibiotics, delocalizations of lipid II were also observed (Figure 3.9, Figure 3.10, Figure 3.11 and Figure 3.12). Cell membrane injuries (colored in red) or cell debris were observed [Appendix I.29 B(iii), I.26 B(iii), I.32 B(iii)], implying cell lysis had occurred. These observations are consistent with the result of bacteriolysis (Section 2.3.5). It is believed that delocalization of FtsZ protein contributed by FtsZ inhibitor, probably affect the localization of downstream product lipid II.

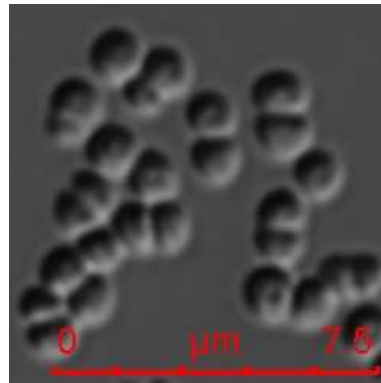
It was observed that FtsZ inhibitors led to delocalization of both FtsZ protein and lipid II. However, whether they delocalized at the same position is still unknown. The excitation and emission wavelength of GFP (in Section 3.3.1) and those of vancomycin analogues stains (in Section 3.3.2) overlapped, which is one of the limitation of the multicolor visualization in a cell. Fluorescent probes with emission wavelength other than that of GFP could be applied to replace the vancomycin analogue stain, but are not commercially available [208, 209].

Another limitation of this study was that images that were captured by confocal microscope had xy-resolution of around 200 nm while *S. aureus* under normal situation had a diameter of around 1 μ m. Thus, it would be difficult to use confocal microscope to resolve the localization of the two targets in *S. aureus*.

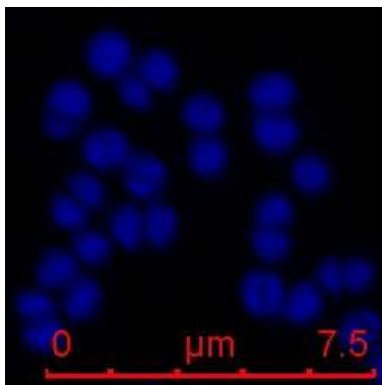
A (i)



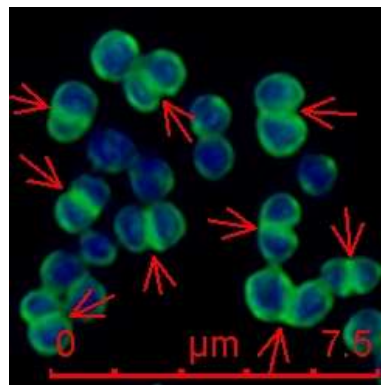
A (iv)



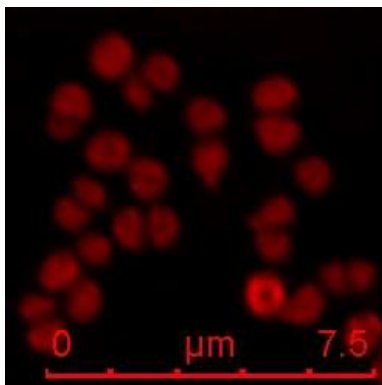
A (ii)



B (i)



A (iii)



B (ii)

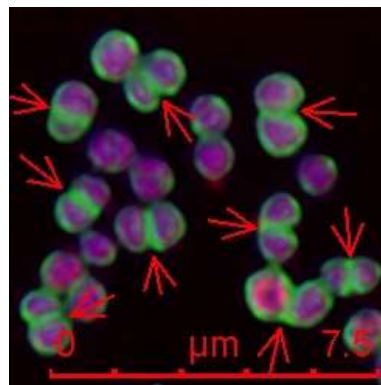


Figure 3.4 MRSA BAA-41 was stained with single channel (A) for visualizing (i) lipid II of newly grown cell wall (green), (ii) nucleic acid (blue), (iii) cell membrane (red), (iv) DIC image; (B)(i) merged image of (A)(i) and (A)(ii); and (B)(ii) merged image of (A)(i), (A)(ii) and (A)(iii) in the absence of antibiotic compound. Scale bar is 7.5 μm .

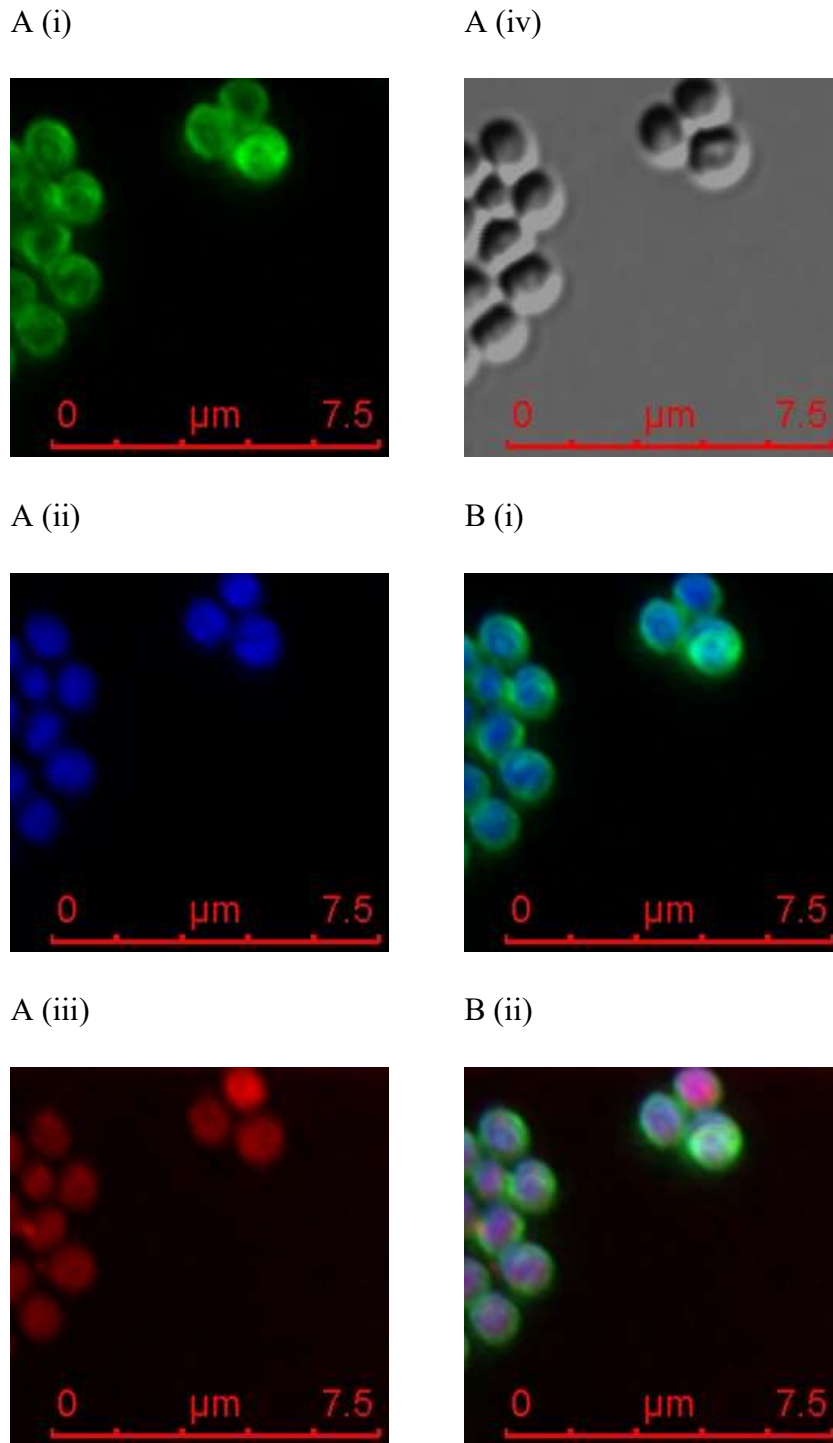
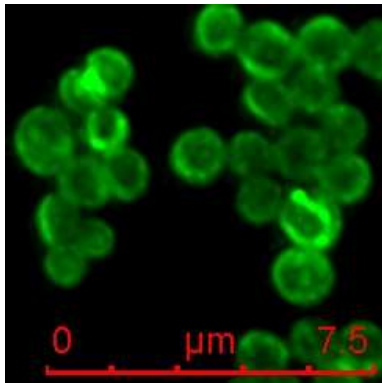
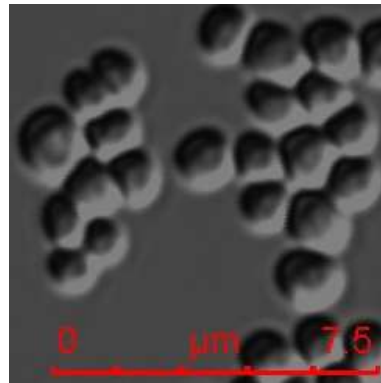


Figure 3.5 MRSA BAA-41 was stained with single channel (A) for visualizing (i) lipid II of newly grown cell wall (green), (ii) nucleus acid (blue), (iii) cell membrane (red), (iv) DIC image; (B)(i) merged image of (A)(i) and (A)(ii); and (B)(ii) merged image of (A)(i), (A)(ii) and (A)(iii) in the presence of FtsZ inhibitor F332 at MIC \times 2. Scale bar is 7.5 μ m.

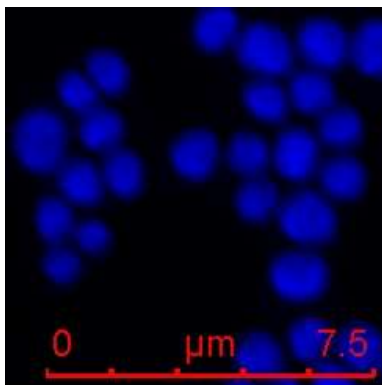
A (i)



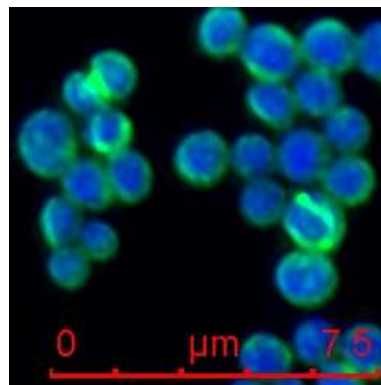
A (iv)



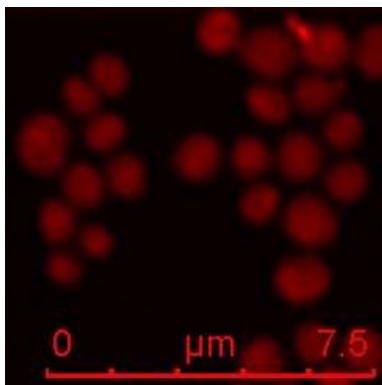
A (ii)



B (i)



A (iii)



B (ii)

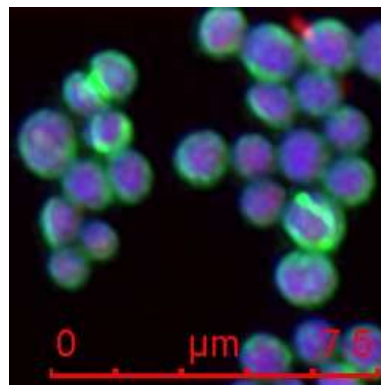
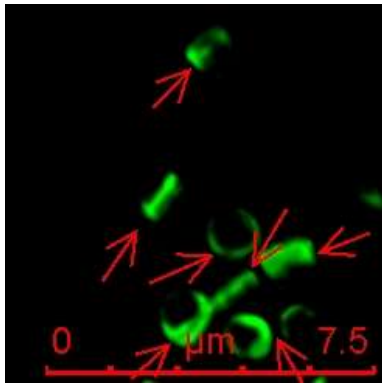
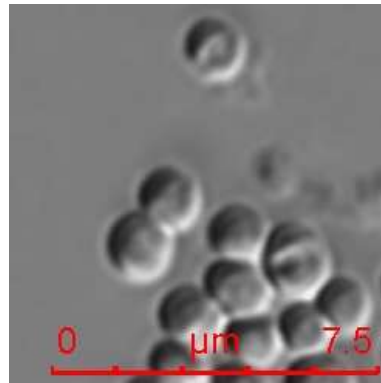


Figure 3.6 MRSA BAA-41 was stained with single channel (A) for visualizing (i) lipid II of newly grown cell wall (green), (ii) nucleus acid (blue), (iii) cell membrane (red), (iv) DIC image; (B)(i) merged image of (A)(i) and (A)(ii); and (B)(ii) merged image of (A)(i), (A)(ii) and (A)(iii) in the presence of FtsZ inhibitor PC190723 at MIC \times 2. Scale bar is 7.5 μ m.

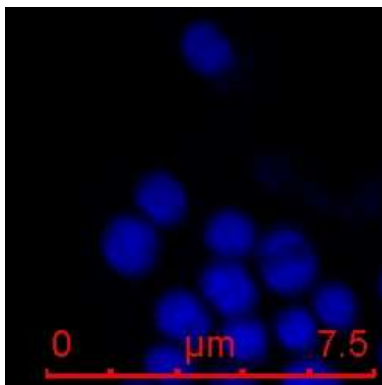
A (i)



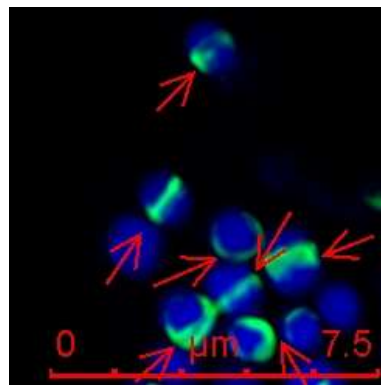
A (iv)



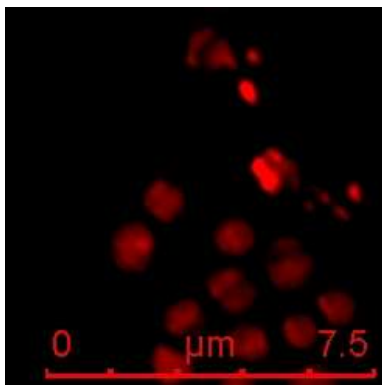
A (ii)



B (i)



A (iii)



B (ii)

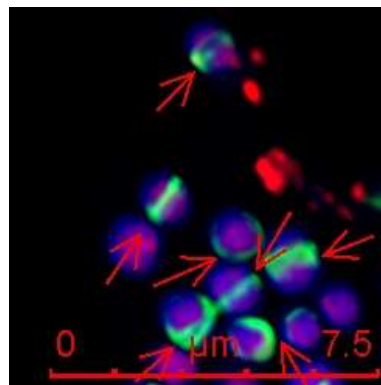
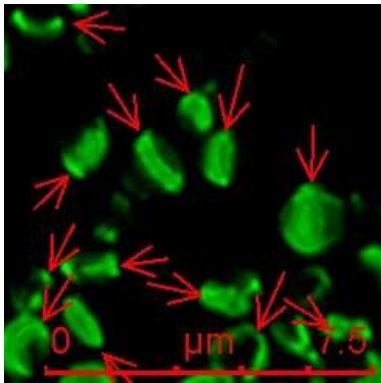
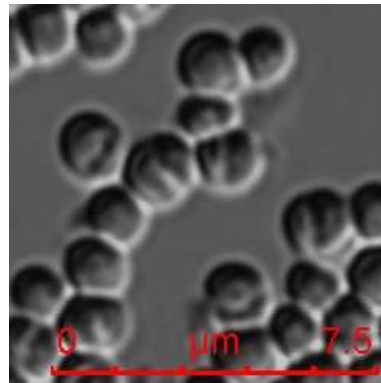


Figure 3.7 MRSA BAA-41 was stained with single channel (A) for visualizing (i) lipid II of newly grown cell wall (green), (ii) nucleus acid (blue), (iii) cell membrane (red), (iv) DIC image; (B)(i) merged image of (A)(i) and (A)(ii); and (B)(ii) merged image of (A)(i), (A)(ii) and (A)(iii) in the presence of oxacillin at $MIC \times 2$. Scale bar is 7.5 μm .

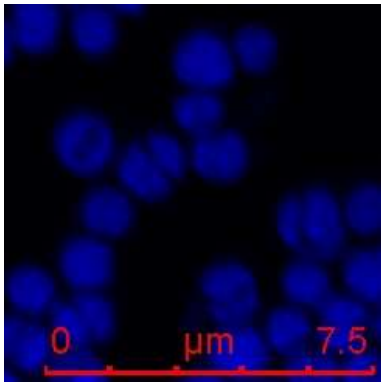
A (i)



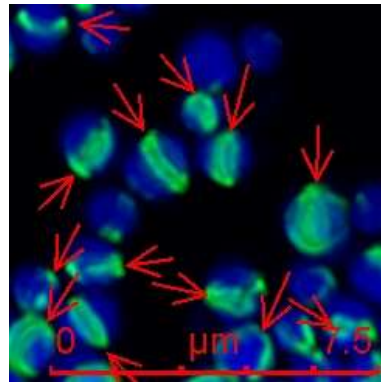
A (iv)



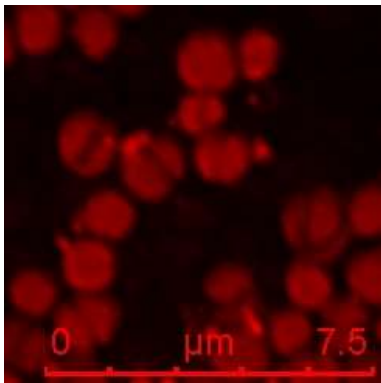
A (ii)



B (i)



A (iii)



B (ii)

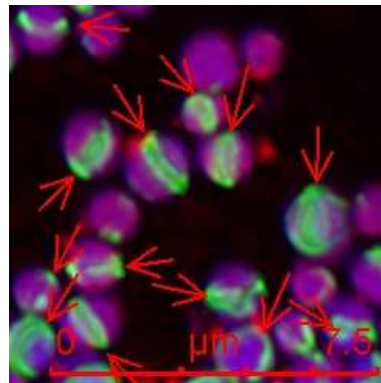
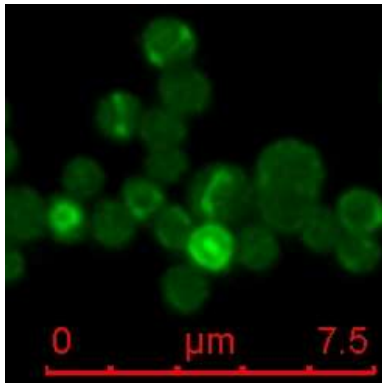
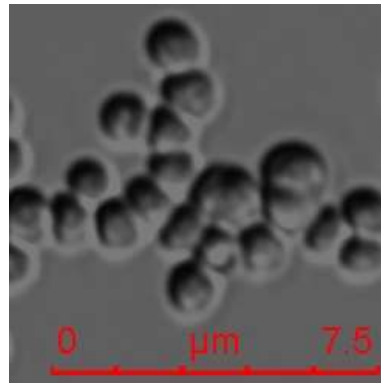


Figure 3.8 MRSA BAA-41 was stained with single channel (A) for visualizing (i) lipid II of newly grown cell wall (green), (ii) nucleic acid (blue), (iii) cell membrane (red), (iv) DIC image; (B)(i) merge image of (A)(i) and (A)(ii); and (B)(ii) merge image of (A)(i), (A)(ii) and (A)(iii) in the presence of methicillin at $\text{MIC} \times 2$. Scale bar is 7.5 μm .

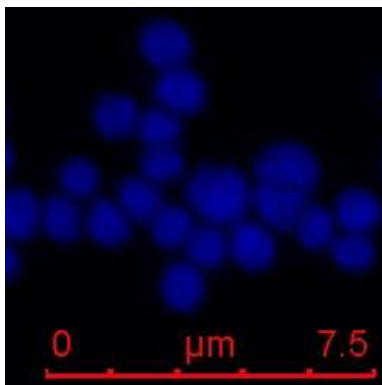
A (i)



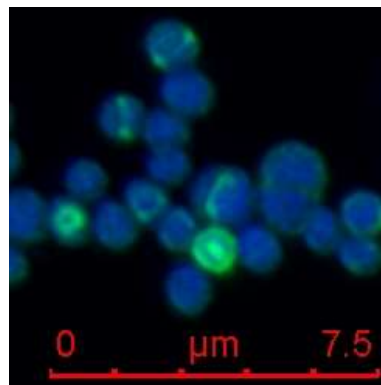
A (iv)



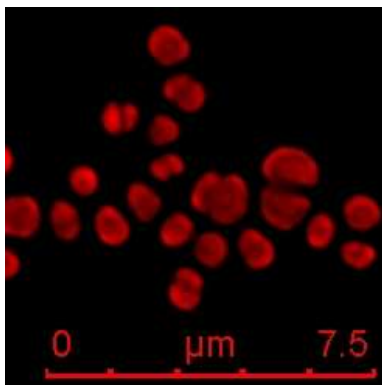
A (ii)



B (i)



A (iii)



B (ii)

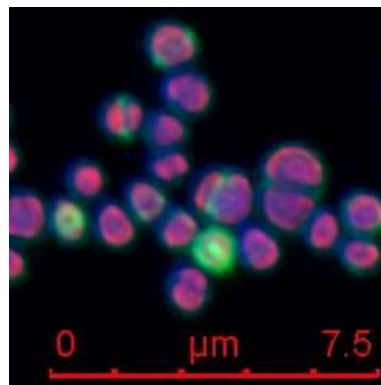


Figure 3.9 MRSA BAA-41 was stained with single channel (A) for visualizing (i) lipid II of newly grown cell wall (green), (ii) nucleus acid (blue), (iii) cell membrane (red), (iv) DIC image; (B)(i) merged image of (A)(i) and (A)(ii); and (B)(ii) merged image of (A)(i), (A)(ii) and (A)(iii) in the presence of F332 and oxacillin combination at MIC \times 1. Scale bar is 7.5 μ m

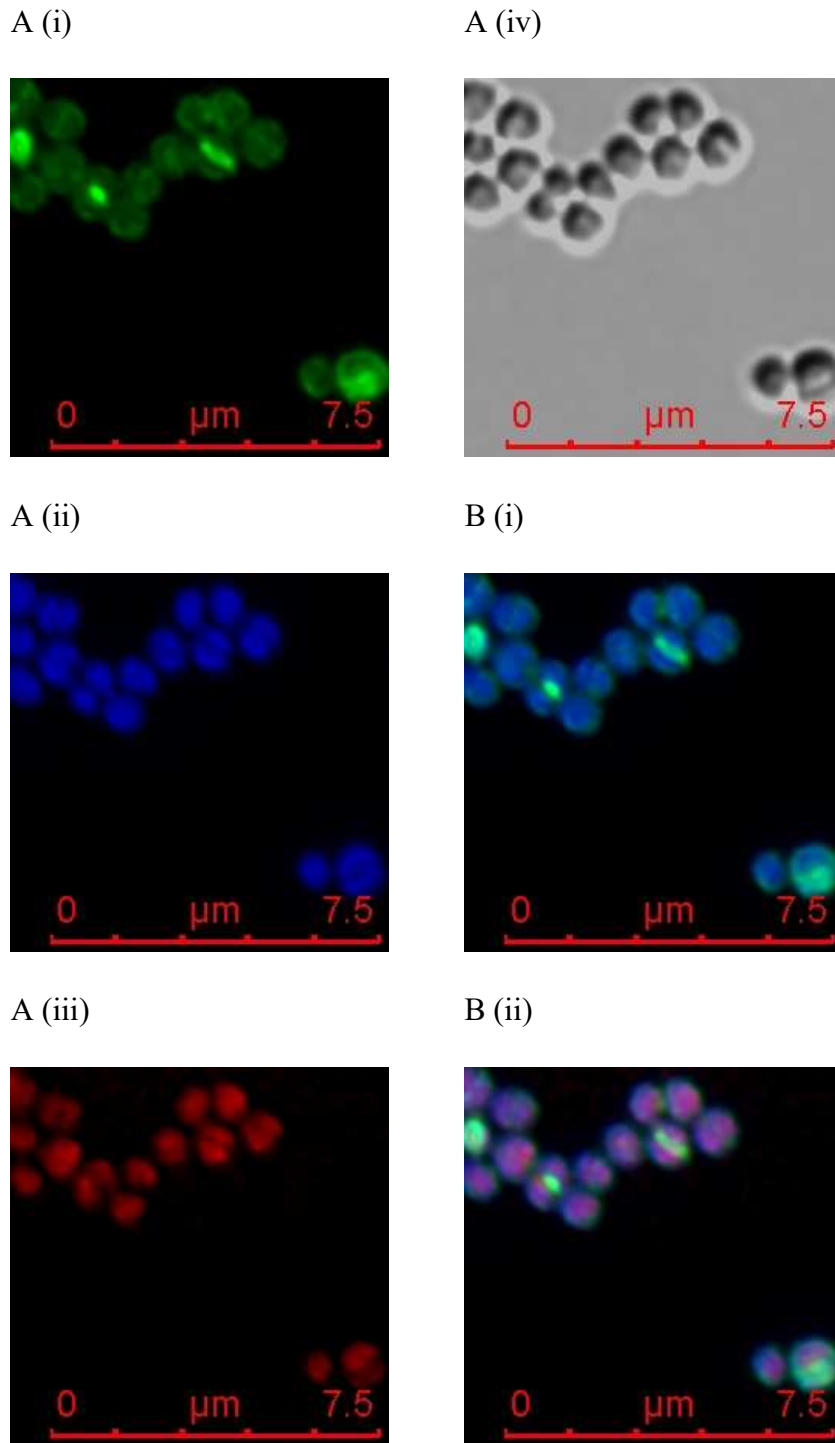


Figure 3.10 MRSA BAA-41 was stained with single channel (A) for visualizing (i) lipid II of newly grown cell wall (green), (ii) nucleus acid (blue), (iii) cell membrane (red), (iv) DIC image; (B)(i) merged image of (A)(i) and (A)(ii); and (B)(ii) merged image of (A)(i), (A)(ii) and (A)(iii) in the presence of F332 and methicillin combination at MIC \times 1. Scale bar is 7.5 μm .

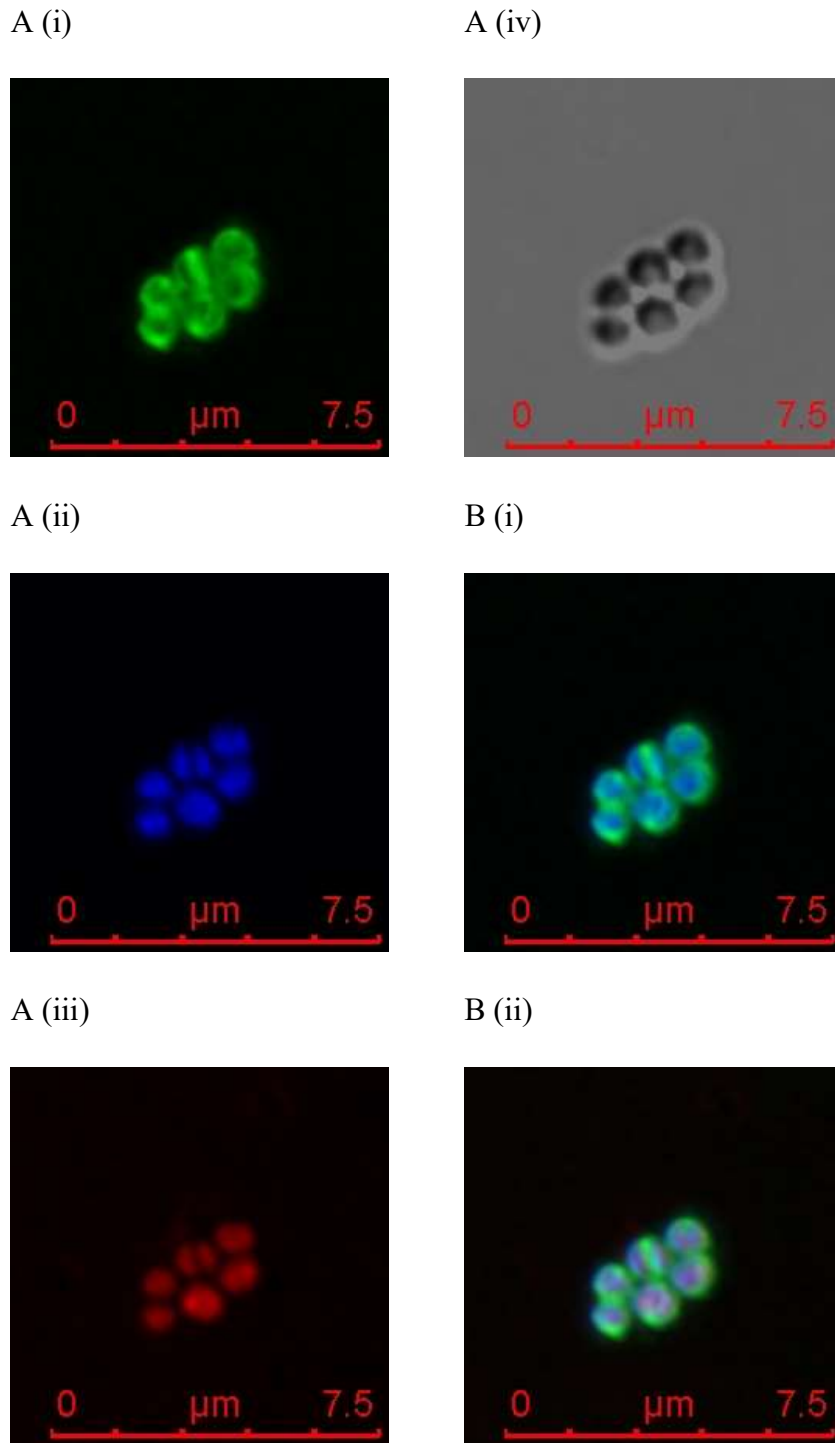


Figure 3.11 MRSA BAA-41 was stained with single channel (A) for visualizing (i) lipid II of newly grown cell wall (green), (ii) nucleus acid (blue), (iii) cell membrane (red), (iv) DIC image; (B)(i) merged image of (A)(i) and (A)(ii); and (B)(ii) merged image of (A)(i), (A)(ii) and (A)(iii) in the presence of PC190723 and oxacillin combination at MIC \times 1. Scale bar is 7.5 μ m.

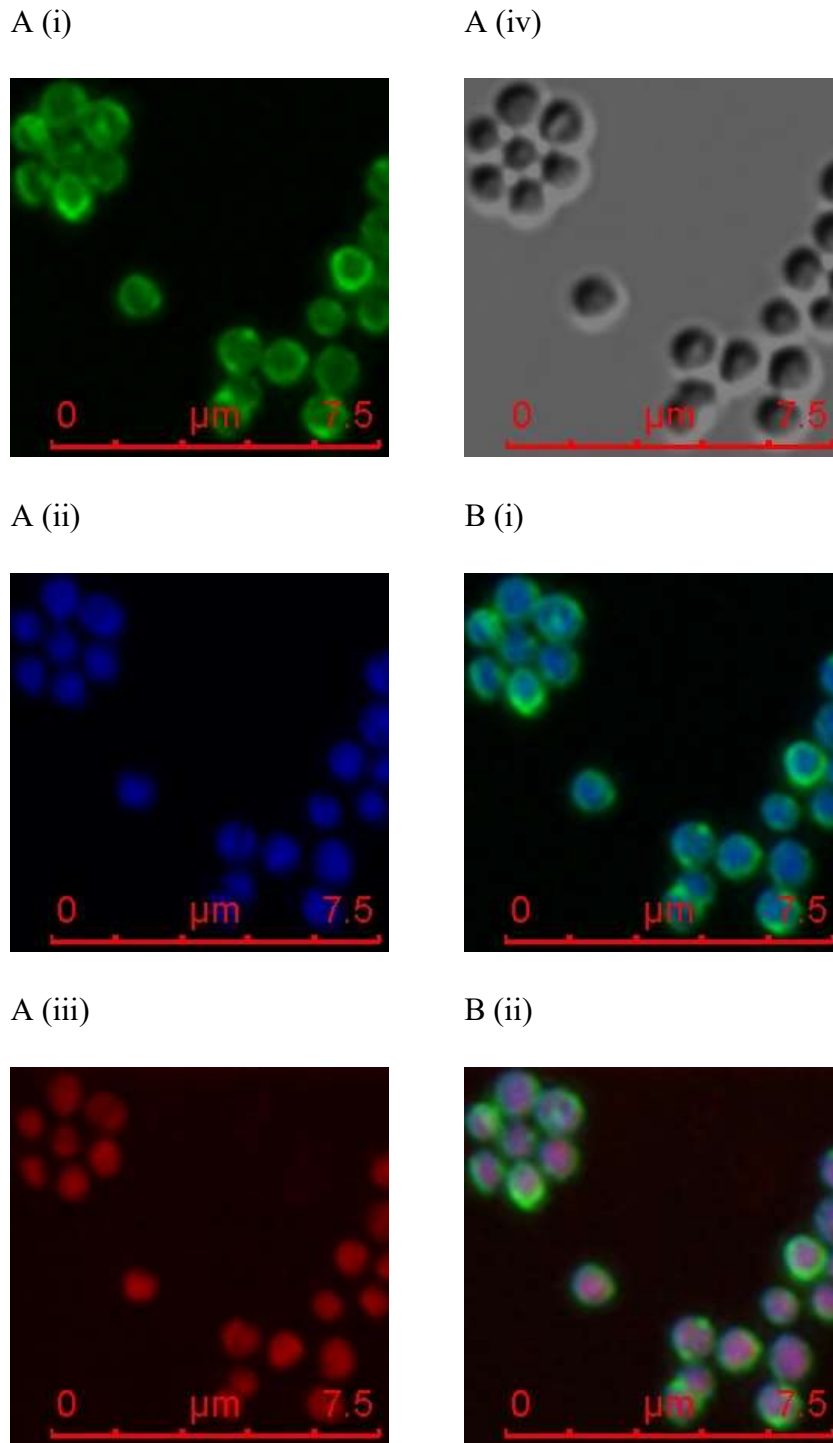


Figure 3.12 BAA-41 was stained with single channel (A) for visualizing (i) lipid II of newly grown cell wall (green), (ii) nucleus acid (blue), (iii) cell membrane (red), (iv) DIC image; (B)(i) merged image of (A)(i) and (A)(ii); and (B)(ii) merged image of (A)(i), (A)(ii) and (A)(iii) in the presence of PC190723 and methicillin combination at MIC \times 1. Scale bar is 7.5 μm .

3.3.3 Morphological studies

Apart from FtsZ and lipid II delocalization, cell enlargement was also observed when FtsZ inhibitors were used. During the division cycle of spherical cells such as *S. aureus*, the parent cell was transiently enlarged when the division septum was completely formed just before the parent cell splitting into two daughter cells. The introduction of FtsZ inhibitor into *S. aureus* would stop the division cycle at that stage, the size of each cells would be monitored.

The cell diameters were measured after treatment with various antibacterial compounds and then used to calculate the cell volumes. The volumes were converted by considering cell as spherical in shape, and then plotted as frequency distribution histogram, with the normalized frequency on the y-axis, and cell volume on the x-axis. The mode (highest frequency), mean and standard deviation of cell volume were indicated. The mode and mean were not equal to each other, reflecting an uneven distribution in histograms, which is also the reason for large standard deviation in some cases. Because of the uneven distribution of cell population, the modes of the cell volume provide more meaningful information compared with the average values.

In this experiment, the surviving cells were counted and the number of counted cells were indicated as sample size. The sample size may differs in each sample (fifty to hundreds) because the amount of cells is dependent on the captured image. Since only surviving cells were counted, samples with lethal-concentrations of FtsZ inhibitors of β -lactam may contain less surviving cells, so more images had to be captured for surviving cells counting, resulting in more cells being counted under lethal-concentrations.

In the absence of antibacterial compounds, the mode cell volume was $0.25 \mu\text{m}^3$ (Table 3.2). When the cells were treated with FtsZ inhibitors, the majority cell volume increased at high FtsZ inhibitors concentration. The volume reached to $0.35 \mu\text{m}^3$ and $0.40 \mu\text{m}^3$ at $\text{MIC} \times 1$ when treated with F332 and PC190723, respectively (Table 3.3 and Table 3.4). The increase in size under treatment with F332 was consistent with the morphological changes of FtsZ depletion or inhibition, which were conducted by other researches groups, suggesting exclusively autolytic activity with decreasing cross-linking of peptidoglycan, resulting in large cell surface area [35, 127]. FtsZ protein delocalization and lipid II delocalization in the presence of FtsZ inhibitors were observed as reported Section 3.3.1 and Section 3.3.2, respectively. Tan and co-workers have also observed delocalization of PBP2, an enzyme of transpeptidation, under the treatment of PC190723 [16].

In the case of β -lactam antibiotics, the majority cell volume increased with β -lactam antibiotics concentration. As shown in Table 3.5 and Table 3.6, the majority cell volumes were $0.45 \mu\text{m}^3$ at $\text{MIC} \times 1$ for both oxacillin and methicillin but increased dramatically to around $1.00 \mu\text{m}^3$ and $0.90 \mu\text{m}^3$ when the cells were treated with $\text{MIC} \times 2$ of oxacillin and methicillin, respectively. MRSA contained an acquired PBP2a to compensate for the loss of transpeptidase domain on PBP2 when PBP2 was acylated by β -lactam, which is a drug-resistant mechanism of MRSA [153, 168, 210, 211]. It was reported that PBP2 did not delocalize in MRSA but did delocalize in MSSA because of compensation of PBP2a in MRSA. PBP2a with a functional transpeptidase domain could guide itself to be properly recruited by lipid II [165, 212]. As shown in Section 3.3.1 and Section 3.3.2, β -lactam delocalized neither FtsZ protein nor lipid II, but literature showed β -lactam delocalized PBP2 in high concentration of β -lactam antibiotics [165, 212]. Thus, it is believed that the cell enlargement was contributed by

inhibition of transpeptidation and a marked decrease in peptidoglycan crosslinking in the entire cell surface when the cells was treated by β -lactam.

In the cases of a combination of FtsZ inhibitor and β -lactam, increase in cell volumes was also observed (Table 3.7, Table 3.8, Table 3.9 and Table 3.10). The majority of cells had a cell volume of more than $0.65 \mu\text{m}^3$ at $\text{MIC} \times 2$ of FtsZ inhibitor and β -lactam antibiotics used in combination. In the presence of both FtsZ inhibitors and β -lactam antibiotics used in combinations, FtsZ inhibitors led to delocalization of FtsZ protein and lipid II. Although β -lactam antibiotics induced expression of PBP2a, which can ensure the proper localization of cell wall synthesis machinery PBP2 to lipid II [90, 165, 166], the delocalization of lipid II offset the recruitment of PBP2a. Delocalization of FtsZ (division machinery) with concomitant delocalization of lipid II, PBP2 or PBP2a (cell wall synthesis machinery) was likely to be the reason of synergistic effect against MRSA. After FtsZ inhibitor interrupt the Z-ring formation, only low concentration of β -lactam antibiotics could be applied to acylate the residual and functional PBP2 or PBP2a that localized at the septum [16]. It was also suggested that cell enlargement was probably due to an incorrect alignment of FtsZ protein, lipid II and PBP2/2a. Delocalization not only led to a less extent of transpeptidation activity, but merely autolysin activity occur at septum. β -Lactam antibiotics synergistically reduced the crosslinking of peptidoglycan, which further led to an increase in cell surface. A further increase in cell volumes was already observed when FtsZ inhibitors and β -lactam antibiotics were used in combination. Less degree cross-linked peptidoglycan likely led to fragile cell walls and eventually cell lysis.

Table 3.2 Cell volumes at mode, mean and standard deviation of MRSA ATCC BAA-41 in the absence of antibacterial compound. Sample size is indicated.

Absence of antibacterial compound	
Mode (μm^3)	0.25
Mean (μm^3)	0.29
Standard Deviation (SD)	SD greater than the mean
Sample size	682

Table 3.3 Cell volumes at mode, mean and standard deviation of MRSA ATCC BAA-41 in the presence of FtsZ inhibitor F332 at a range of concentrations. Sample sizes are indicated.

	Sub-lethal concentration	MIC X 0.5	MIC X 1	MIC X 2
F332 ($\mu\text{g/mL}$)	0.5	1	2	4
Mode (μm^3)	0.35	0.25	0.35	0.50
Mean (μm^3)	0.36	0.27	0.39	0.62
Standard Deviation (SD)	0.16	SD greater than the mean	0.29	SD greater than the mean
Sample size	53	417	245	1015

Table 3.4 Cell volumes at mode, mean and standard deviation of MRSA ATCC BAA-41 in the presence of FtsZ inhibitor PC190723 at a range of concentrations. Sample sizes are indicated.

	Sub-lethal concentration	MIC X 0.5	MIC X 1	MIC X 2	
PC190723					
($\mu\text{g/mL}$)	0.065	0.25	0.5	1	2
Mode (μm^3)	0.40	0.30	0.30	0.40	0.65
Mean (μm^3)	0.43	0.21	0.30	0.40	0.63
Standard Deviation (SD)	SD greater than the mean	SD greater than the mean	SD greater than the mean	SD greater than the mean	SD greater than the mean
Sample size	98	433	174	281	131

Table 3.5 Cell volumes at mode, mean and standard deviation of MRSA ATCC BAA-41 in the presence of oxacillin at a range of concentrations. Sample sizes are indicated.

	Sub-lethal concentration				MIC X 0.5	MIC X 1	MIC X 2
Oxacillin ($\mu\text{g/mL}$)	8	16	32	64	128	256	512
Mode (μm^3)	0.50	0.55	0.95	0.40	0.65	0.45	1.00
Mean (μm^3)	0.42	0.53	0.88	0.38	0.75	0.57	0.88
Standard Deviation (SD)	0.19	SD greater than the mean	0.44	0.18	0.34	0.28	0.40
Sample size	145	118	85	211	177	294	329

Table 3.6 Cell volumes at mode, mean and standard deviation of MRSA ATCC BAA-41 in the presence of methicillin at a range of concentrations. Sample sizes are indicated.

	Sub-lethal concentration			MIC X 0.5	MIC X 1	MIC X 2
Methicillin						
($\mu\text{g/mL}$)	32	64	128	256	512	1024
Mode (μm^3)	0.80	0.40	0.95	0.70	0.45	0.90
Mean (μm^3)	0.54	0.38	0.89	0.83	0.50	0.84
Standard Deviation (SD)	SD greater than the mean	SD greater than the mean	SD greater than the mean	SD greater than the mean	0.22	0.41
Sample size	125	334	118	233	90	235

Table 3.7 Cell volumes at mode, mean and standard deviation of MRSA ATCC BAA-41 in the presence of F332 and oxacillin combination at a range of concentrations. Sample sizes are indicated.

	MIC X 0.5	MIC X 1	MIC X 2
F332 ($\mu\text{g/mL}$)	0.5	1	2
Oxacillin ($\mu\text{g/mL}$)	8	16	32
Mode (μm^3)	0.90	0.70	1.00
Mean (μm^3)	0.78	0.60	0.80
Standard Deviation (SD)	0.36	0.26	SD greater than the mean
Sample size	151	181	340

Table 3.8 Cell volumes at mode, mean and standard deviation of MRSA ATCC BAA-41 in the presence of F332 and methicillin combination at a range of concentrations.

Sample sizes are indicated.

	MIC X 0.5	MIC X 1	MIC X 2
F332 ($\mu\text{g/mL}$)	0.5	1	2
Methicillin ($\mu\text{g/mL}$)	16	32	64
Mode (μm^3)	0.90	0.70	1.05
Mean (μm^3)	0.83	0.60	0.94
Standard Deviation (SD)	SD greater than the mean	0.27	0.41
Sample size	149	93	258

Table 3.9 Cell volumes at mode, mean and standard deviation of MRSA ATCC BAA-41 in the presence of PC190723 and oxacillin combination at a range of concentrations. Sample sizes are indicated.

	MIC X 0.5	MIC X 1	MIC X 2
PC190723 ($\mu\text{g/mL}$)	0.0625	0.125	0.25
Oxacillin ($\mu\text{g/mL}$)	32	64	128
Mode (μm^3)	0.45	0.40	0.65
Mean (μm^3)	0.72	0.49	0.92
Standard Deviation (SD)	SD greater than the mean	SD greater than the mean	SD greater than the mean
Sample size	62	52	75

Table 3.10 Cell volumes at mode, mean and standard deviation of MRSA ATCC BAA-41 in the presence of PC190723 and methicillin combinations at a range of concentrations. Sample sizes are indicated.

	MIC X 0.5	MIC X 1	MIC X 2
PC190723 ($\mu\text{g/mL}$)	0.125	0.25	0.5
Methicillin ($\mu\text{g/mL}$)	32	64	128
Mode (μm^3)	0.75	0.50	1.05
Mean (μm^3)	0.83	0.45	1.23
Standard Deviation (SD)	SD greater than the mean	0.21	0.58
Sample size	92	255	127

3.4 Concluding remarks

In this chapter, localizations of FtsZ protein, and lipid II and morphological changes of MRSA cells were examined in the presence of FtsZ inhibitors and β -lactam antibiotics and in their combinations.

FtsZ-GFP fusion protein in *S. aureus* was applied to visualize the FtsZ protein assembly in the spherical cells. Lipid II was also visualized by staining with a fluorescent vancomycin analogue. FtsZ inhibitor was found to delocalize FtsZ protein and lipid II. β -Lactam antibiotics delocalized neither FtsZ protein nor lipid II, but was reported to delocalize PBP2 or PBP2a depending on the concentrations of β -lactam antibiotics [165]. On the other hand, when FtsZ inhibitor and β -lactam antibiotic were applied in combination, FtsZ protein and lipid II were found to have delocalized. The improper alignment of FtsZ and lipid II in the presence of both FtsZ inhibitor and β -lactam might be related to the delocalization of PBP2 in the cell wall synthesis machinery as reported previously [16, 165, 166].

Cell enlargements were observed when MRSA cells were treated with FtsZ inhibitors and β -lactams. As FtsZ inhibitors are believed to cause delocalization of cell division machinery and cell wall synthesis machinery, a reduction of transpeptidation activity was expected, except the autolysin activity at the septum. This led to a decrease in crosslinking and increase in cell surface area at the septum. β -Lactam antibiotics further lowered the peptidoglycan crosslinking in the delocalized position. The reduction in peptidoglycan crosslinking weakened the rigidity of cell wall and led to cell lysis.

Chapter 4. Conclusion

The antibacterial activities of FtsZ inhibitors, β -lactam antibiotics and their combinations were reported in this thesis. The inhibitory growth activities were determined by MIC and analyzed by FICI on FtsZ inhibitors, β -lactam antibiotics and in their combinations. The results revealed that MRSA was susceptible to 3-MBA FtsZ inhibitors but resistant to β -lactam antibiotics. Synergistic effect or partial synergistic effect were observed when FtsZ inhibitors and β -lactam antibiotics were used in combination. The bactericidal activities were evaluated by end-points mode (MBC) and kinetic mode (time-kill kinetic studies). All antibacterial candidates in this project demonstrated bactericidal activities except FtsZ inhibitor F332. Bacteriolysis activities were applied to examine whether the cells were lysed or not. Cell lysis was found to occur under the treatment of FtsZ inhibitors and β -lactam antibiotics in combination.

The role of antibacterial compounds on the localization of their targets was studied. FtsZ inhibitors F332 and PC190723 interfered the localization of their targets, FtsZ and its downstream lipid-linked peptidoglycan (lipid II), while β -lactam antibiotics affected neither of them. The targets were visualized by high resolution microscopic imaging. Changes in cell volume after treatment of various concentrations of the antibacterial compounds were measured. The synergistic effect of FtsZ inhibitor and β -lactam was most likely to be due to 1) the delocalization of division machinery (FtsZ protein) and cell wall synthesis machinery (lipid II, PBP2 and PBP2a) by FtsZ inhibitors, resulting in reduction of the septum transpeptidation activity but not the autolysin activity, and 2) the decrease in transepeptidation activity in peptidoglycan synthesis by β -lactam antibiotics by reducing the degree of peptidoglycan crosslinking. The weakened rigidity of cell wall results in cell lysis.

There are some implications arising from the result of this project. Firstly, the proper localization of division machinery is important to proper localization of cell wall

synthesis machinery during the cell division cycle. Delocalization of one of the proteins may affect the delocalization of downstream products as well as the cell morphology. When two compounds are applied to delocalize two products in the chain of cell division cycle, this may result in a synergistic effect.

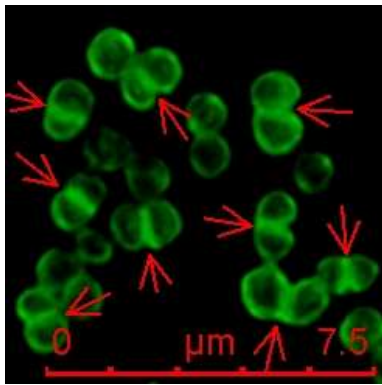
A possible direction for future research is to address the localization of the target of the β -lactam antibiotics. Co-localization studies between cell wall synthesis machinery PBP2 and PBP2a could be conducted. The interaction between two proteins could be visualized within a single cell by co-localization studies. Further, it will be interesting to study the co-localization between division machinery and cell wall synthesis machinery. The co-localization and dynamic interaction of these machineries could be observed with super resolution microscopy such as structured illumination microscopy (SIM) and stochastic optical reconstruction microscopy (STORM) with a resolution to about 100 nm. However, using super resolution microscopy may require further development on bacterial fixing technique under imaging buffer when STORM is applied.

Moreover, it will be worthwhile to study how cells respond to FtsZ inhibitor and β -lactam antibiotics. This could be done by immobilizing live bacteria and providing cultivable environment under real-time cell imaging, so the cell enlargement and the process of cell lysis could be visualized. The rapid protein dynamic would also require high resolution microscope equipped with a high speed scanner for image capturing.

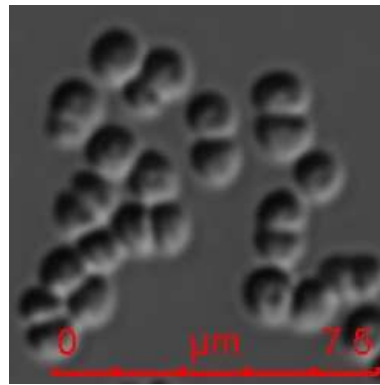
Appendix I

**Visualization of newly grown
peptidoglycan**

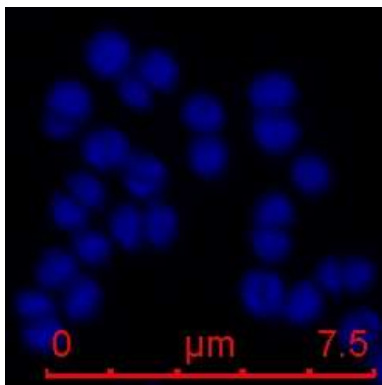
A (i)



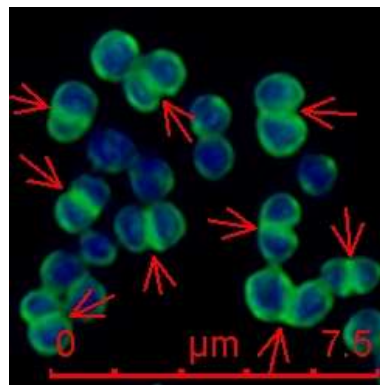
A (iv)



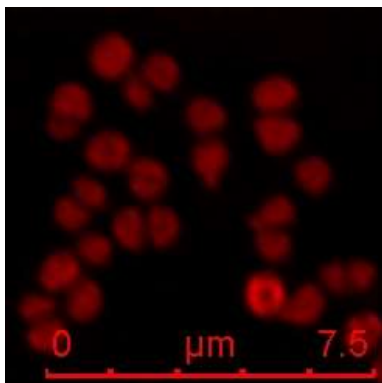
A (ii)



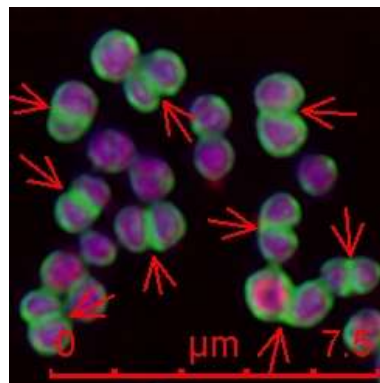
B (i)



A (iii)

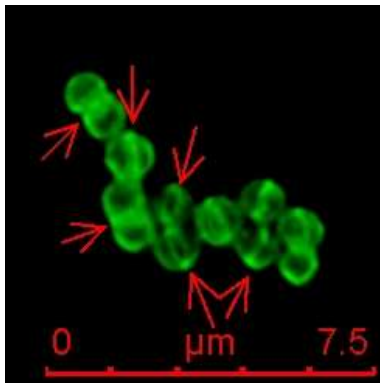


B (ii)

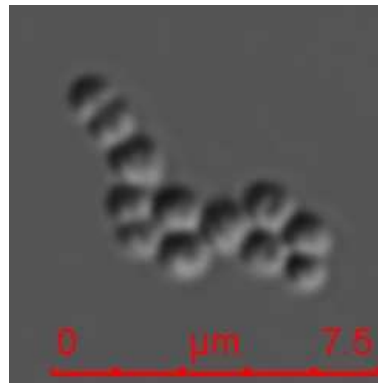


Appendix I. 1 MRSA BAA-41 was stained with single channel (A) for visualizing (i) lipid II of newly grown cell wall (green), (ii) nucleus acid (blue), (iii) cell membrane (red), (iv) DIC image; (B)(i) merged image of (A)(i) and (A)(ii); and (B)(ii) merged image of (A)(i), (A)(ii) and (A)(iii) in the absence of antibiotic compound. Scale bar is 7.5 μm .

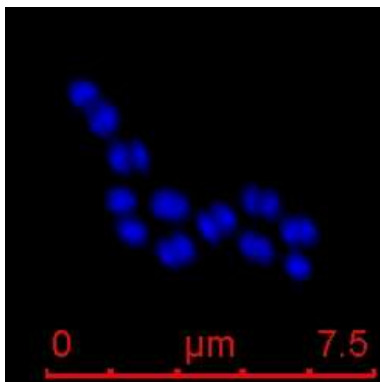
A (i)



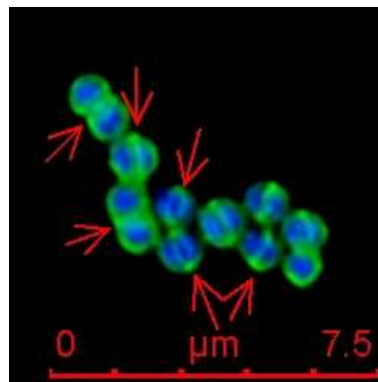
A (iv)



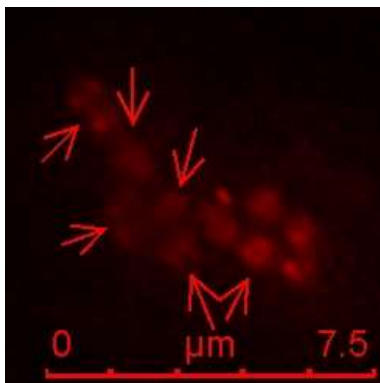
A (ii)



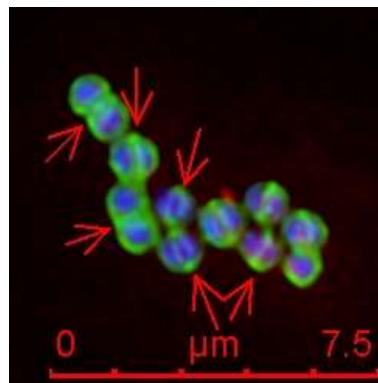
B (i)



A (iii)

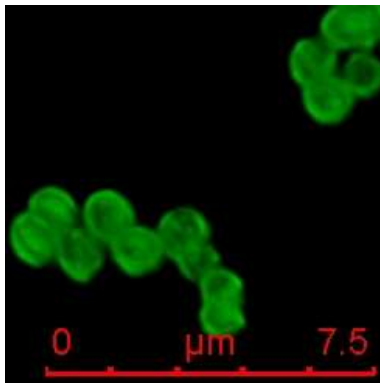


B (ii)

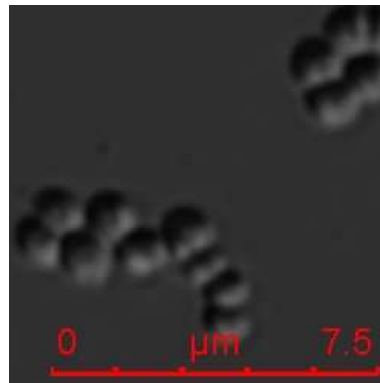


Appendix I. 2 MRSA BAA-41 was stained with single channel (A) for visualizing (i) lipid II of newly grown cell wall (green), (ii) nucleus acid (blue), (iii) cell membrane (red), (iv) DIC image; (B)(i) merged image of (A)(i) and (A)(ii); and (B)(ii) merged image of (A)(i), (A)(ii) and (A)(iii) in the presence of FtsZ inhibitor F332 at sub-lethal concentration 0.5 $\mu\text{g}/\text{mL}$. Scale bar is 7.5 μm .

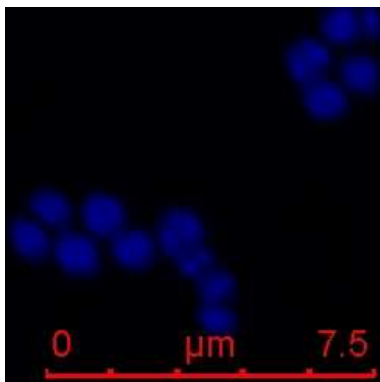
A (i)



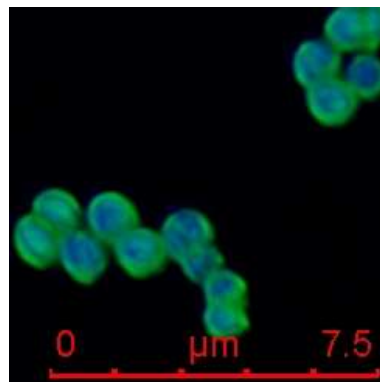
A (iv)



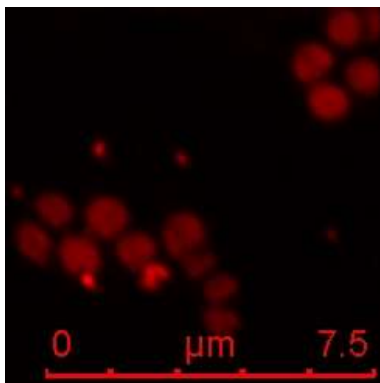
A (ii)



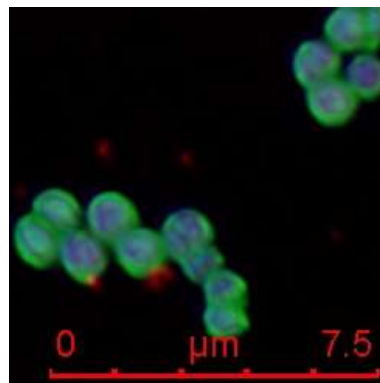
B (i)



A (iii)

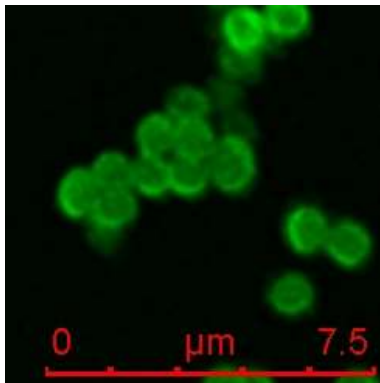


B (ii)

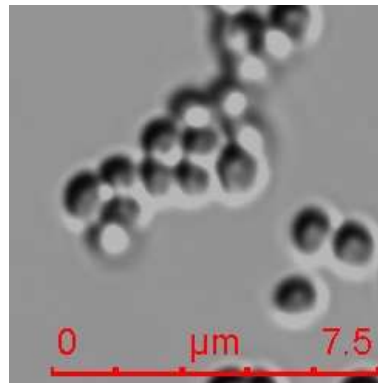


Appendix I. 3 MRSA BAA-41 was stained with single channel (A) for visualizing (i) lipid II of newly grown cell wall (green), (ii) nucleus acid (blue), (iii) cell membrane (red), (iv) DIC image; (B)(i) merged image of (A)(i) and (A)(ii); and (B)(ii) merged image of (A)(i), (A)(ii) and (A)(iii) in the presence of FtsZ inhibitor F332 at $MIC \times 0.5$ ($1 \mu\text{g/mL}$). Scale bar is $7.5 \mu\text{m}$.

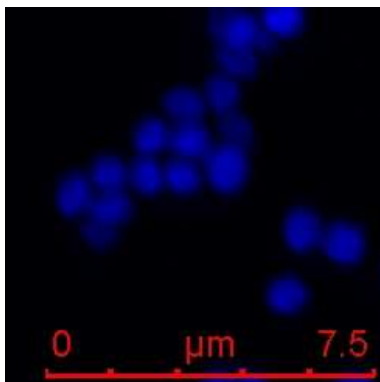
A (i)



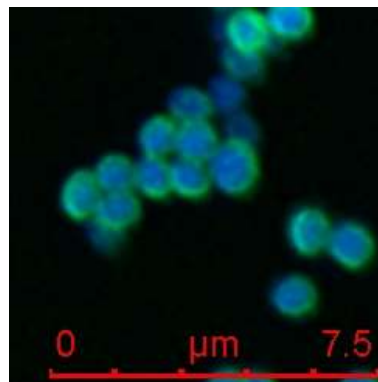
A (iv)



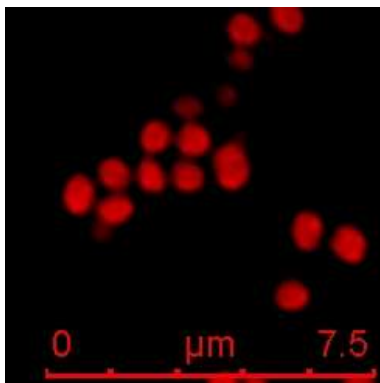
A (ii)



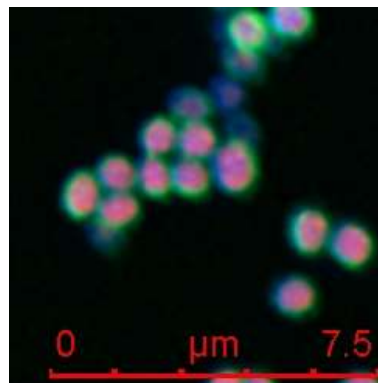
B (i)



A (iii)

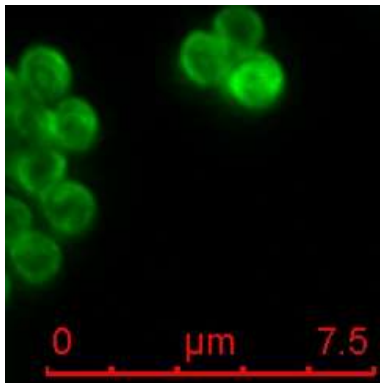


B (ii)

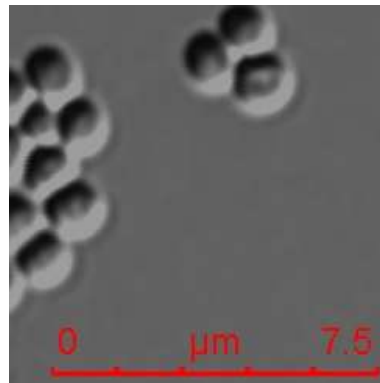


Appendix I. 4 MRSA BAA-41 was stained with single channel (A) for visualizing (i) lipid II of newly grown cell wall (green), (ii) nucleus acid (blue), (iii) cell membrane (red), (iv) DIC image; (B)(i) merged image of (A)(i) and (A)(ii); and (B)(ii) merged image of (A)(i), (A)(ii) and (A)(iii) in the presence of FtsZ inhibitor F332 at MIC \times 1 (2 $\mu\text{g}/\text{mL}$). Scale bar is 7.5 μm .

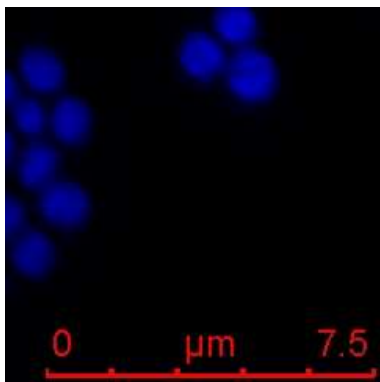
A (i)



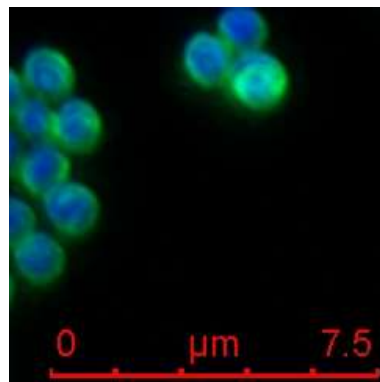
A (iv)



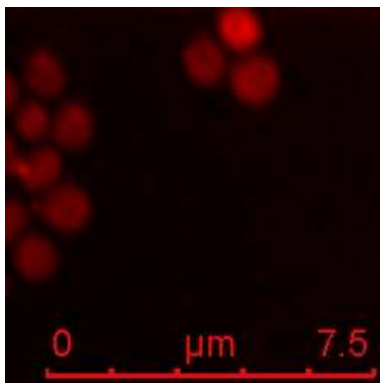
A (ii)



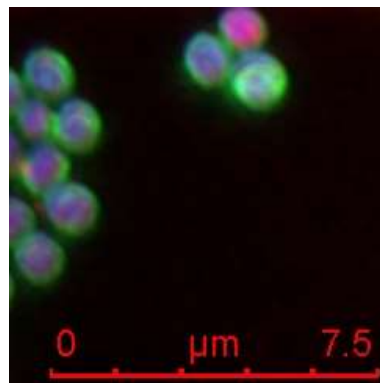
B (i)



A (iii)

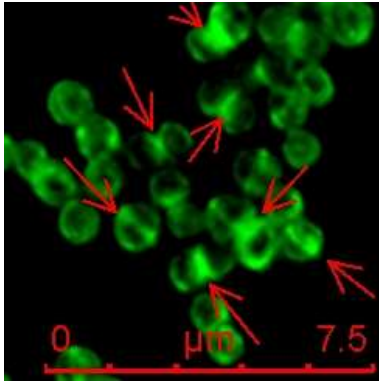


B (ii)

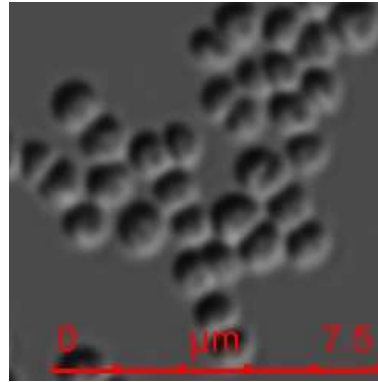


Appendix I. 5 MRSA BAA-41 was stained with single channel (A) for visualizing (i) lipid II of newly grown cell wall (green), (ii) nucleus acid (blue), (iii) cell membrane (red), (iv) DIC image; (B)(i) merged image of (A)(i) and (A)(ii); and (B)(ii) merged image of (A)(i), (A)(ii) and (A)(iii) in the presence of FtsZ inhibitor F332 at MIC \times 2 (4 μ g/mL). Scale bar is 7.5 μ m.

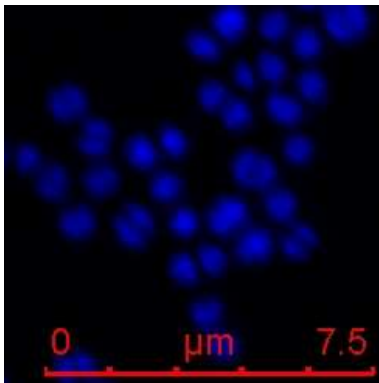
A (i)



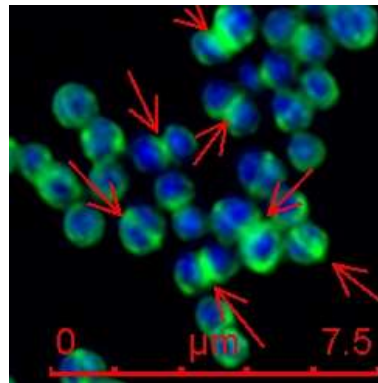
A (iv)



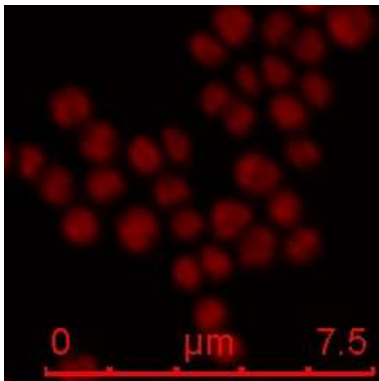
A (ii)



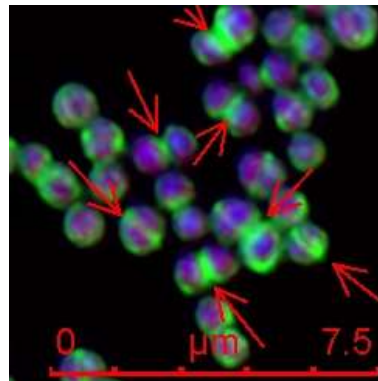
B (i)



A (iii)

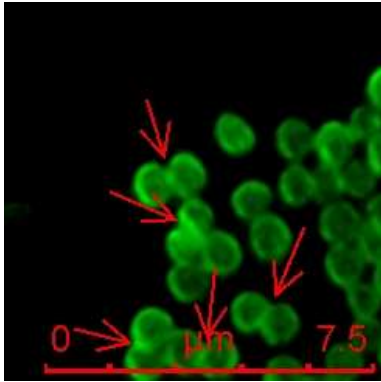


B (ii)

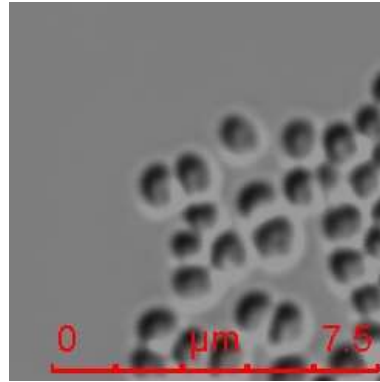


Appendix I. 6 MRSA BAA-41 was stained with single channel (A) for visualizing (i) lipid II of newly grown cell wall (green), (ii) nucleus acid (blue), (iii) cell membrane (red), (iv) DIC image; (B)(i) merged image of (A)(i) and (A)(ii); and (B)(ii) merged image of (A)(i), (A)(ii) and (A)(iii) in the presence of FtsZ inhibitor PC190723 at sub-lethal concentration 0.063 $\mu\text{g}/\text{mL}$. Scale bar is 7.5 μm .

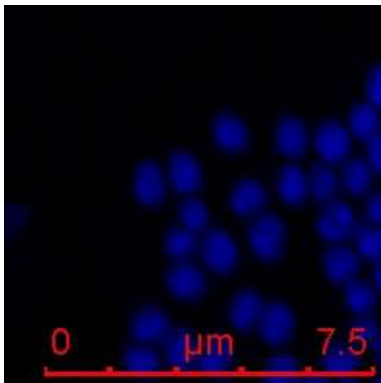
A (i)



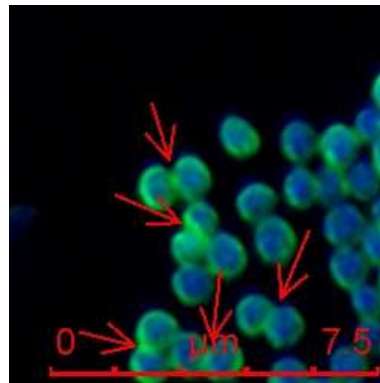
A (iv)



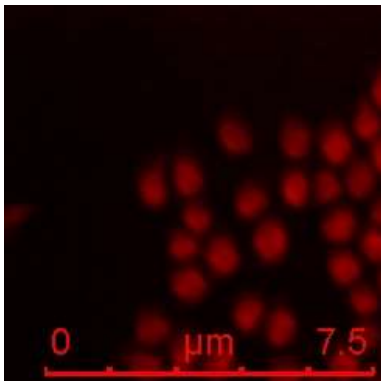
A (ii)



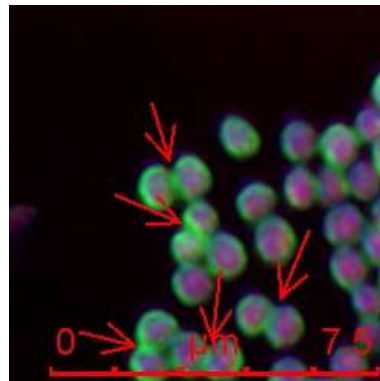
B (i)



A (iii)

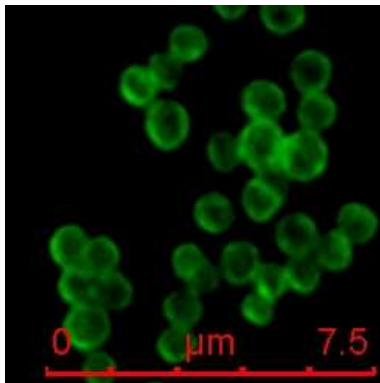


B (ii)

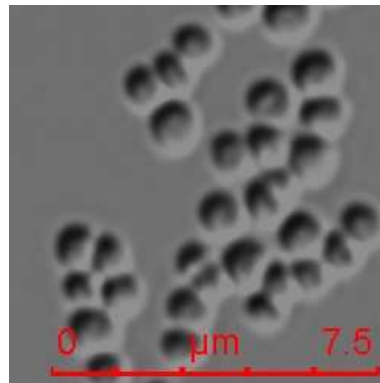


Appendix I. 7 MRSA BAA-41 was stained with single channel (A) for visualizing (i) lipid II of newly grown cell wall (green), (ii) nucleus acid (blue), (iii) cell membrane (red), (iv) DIC image; (B)(i) merged image of (A)(i) and (A)(ii); and (B)(ii) merged image of (A)(i), (A)(ii) and (A)(iii) in the presence of FtsZ inhibitor PC190723 at sub-lethal concentration 0.25 $\mu\text{g}/\text{mL}$. Scale bar is 7.5 μm .

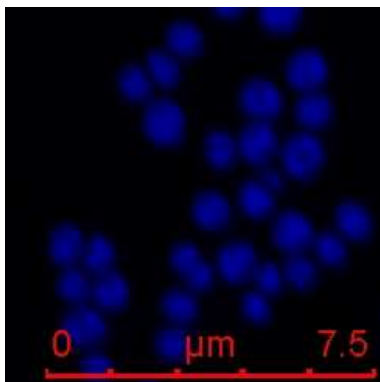
A (i)



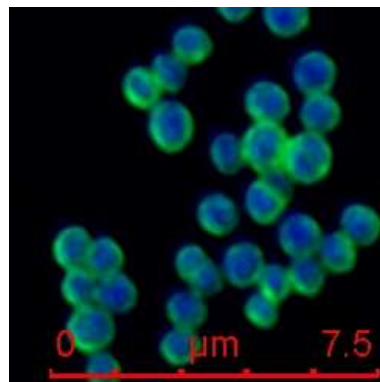
A (iv)



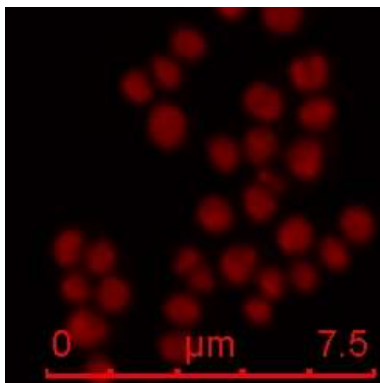
A (ii)



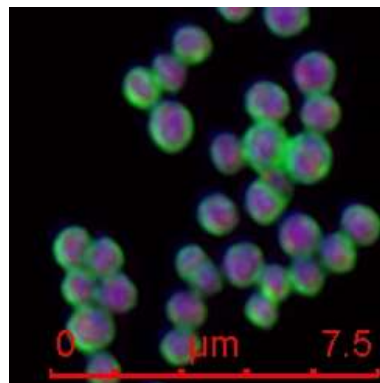
B (i)



A (iii)

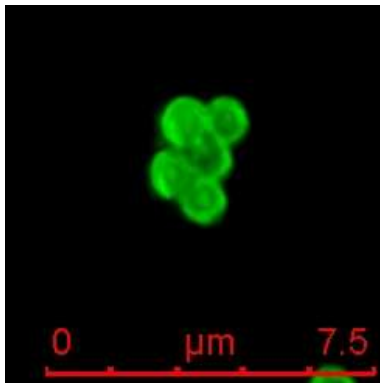


B (ii)

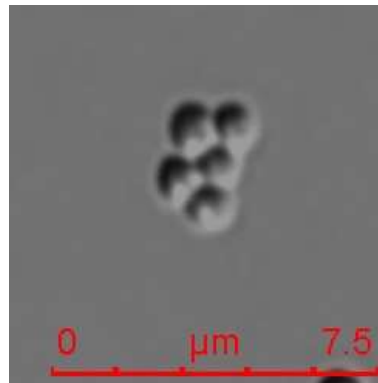


Appendix I. 8 MRSA BAA-41 was stained with single channel (A) for visualizing (i) lipid II of newly grown cell wall (green), (ii) nucleic acid (blue), (iii) cell membrane (red), (iv) DIC image; (B)(i) merged image of (A)(i) and (A)(ii); and (B)(ii) merged image of (A)(i), (A)(ii) and (A)(iii) in the presence of FtsZ inhibitor PC190723 at MIC \times 0.5 (0.5 $\mu\text{g}/\text{mL}$). Scale bar is 7.5 μm .

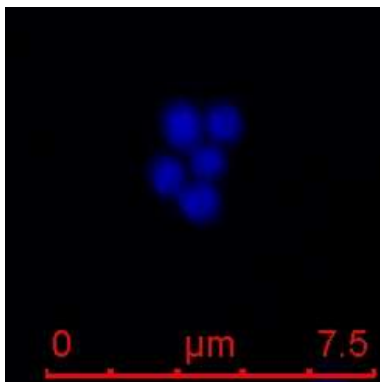
A (i)



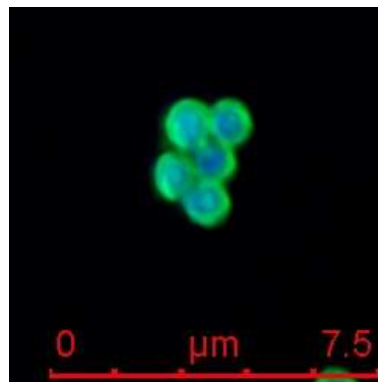
A (iv)



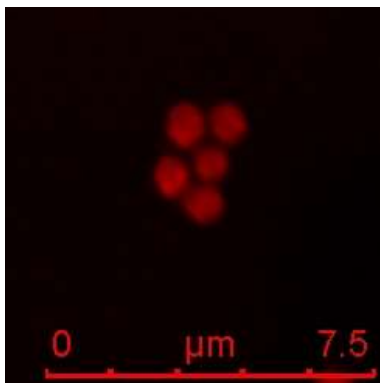
A (ii)



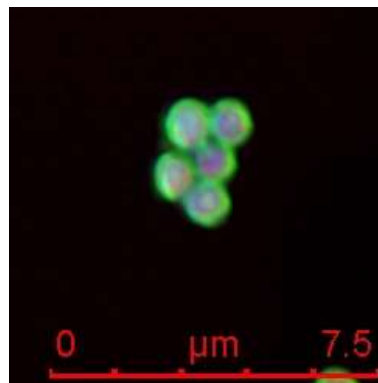
B (i)



A (iii)

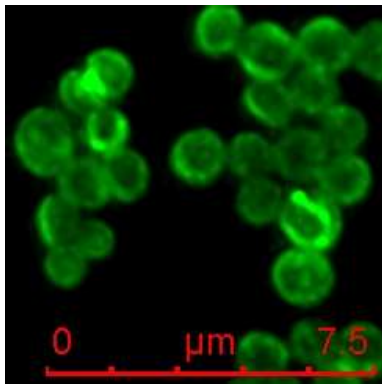


B (ii)

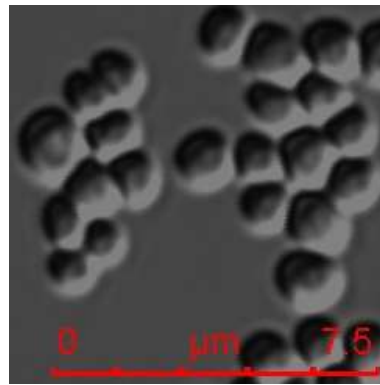


Appendix I. 9 MRSA BAA-41 was stained with single channel (A) for visualizing (i) lipid II of newly grown cell wall (green), (ii) nucleus acid (blue), (iii) cell membrane (red), (iv) DIC image; (B)(i) merged image of (A)(i) and (A)(ii); and (B)(ii) merged image of (A)(i), (A)(ii) and (A)(iii) in the presence of FtsZ inhibitor PC190723 at MIC \times 1 (1 $\mu\text{g}/\text{mL}$). Scale bar is 7.5 μm .

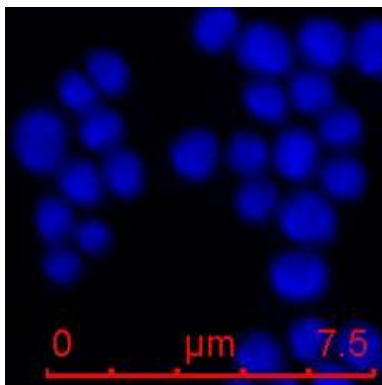
A (i)



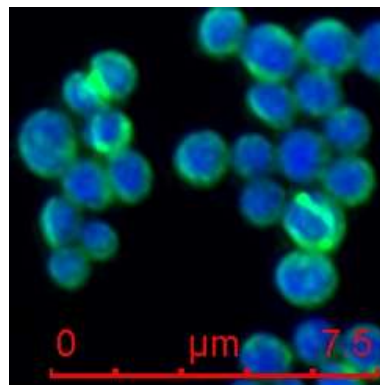
A (iv)



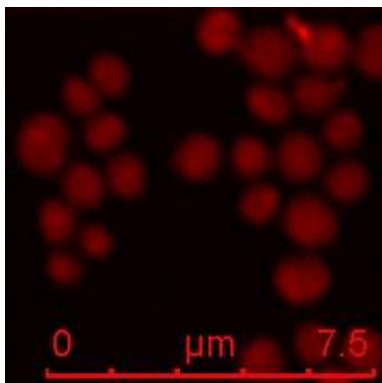
A (ii)



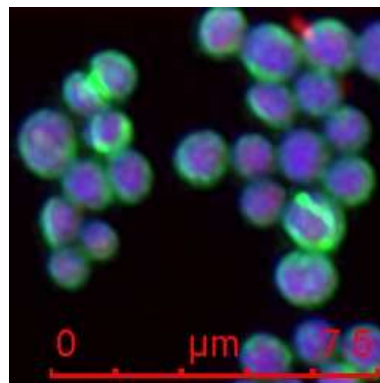
B (i)



A (iii)

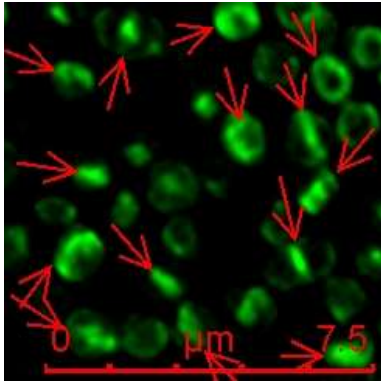


B (ii)

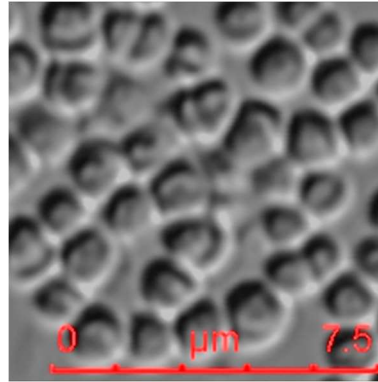


Appendix I. 10 MRSA BAA-41 was stained with single channel (A) for visualizing (i) lipid II of newly grown cell wall (green), (ii) nucleus acid (blue), (iii) cell membrane (red), (iv) DIC image; (B)(i) merged image of (A)(i) and (A)(ii); and (B)(ii) merged image of (A)(i), (A)(ii) and (A)(iii) in the presence of FtsZ inhibitor PC190723 at $MIC \times 2$ ($2 \mu\text{g/mL}$). Scale bar is $7.5 \mu\text{m}$.

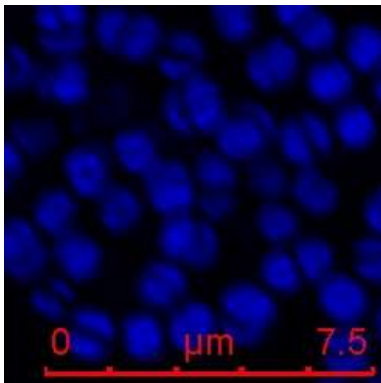
A (i)



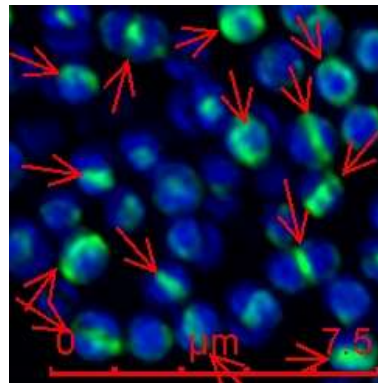
A (iv)



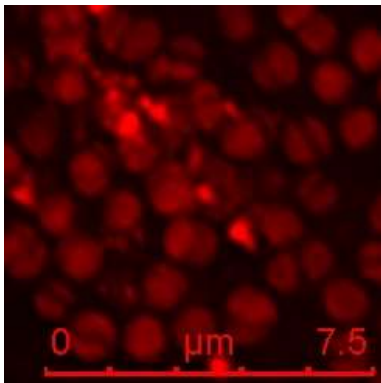
A (ii)



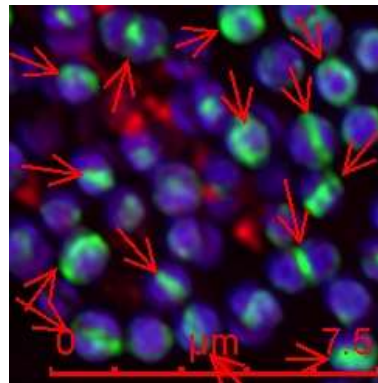
B (i)



A (iii)

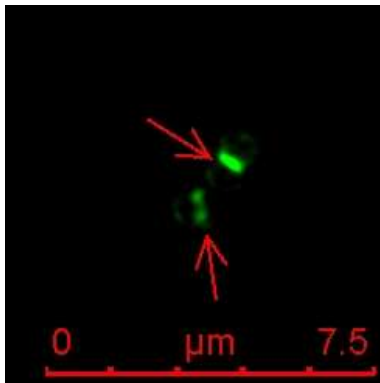


B (ii)

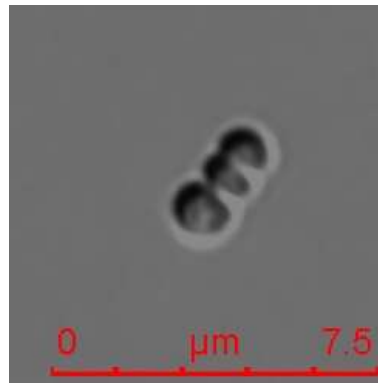


Appendix I. 11 MRSA BAA-41 was stained with single channel (A) for visualizing (i) lipid II of newly grown cell wall (green), (ii) nucleus acid (blue), (iii) cell membrane (red), (iv) DIC image; (B)(i) merged image of (A)(i) and (A)(ii); and (B)(ii) merged image of (A)(i), (A)(ii) and (A)(iii) in the presence of oxacillin at sub-lethal concentration 8 $\mu\text{g}/\text{mL}$. Scale bar is 7.5 μm .

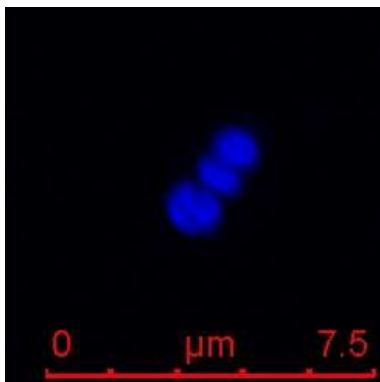
A (i)



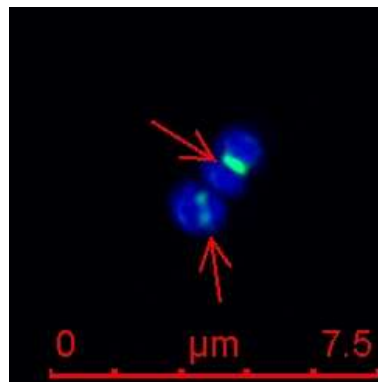
A (iv)



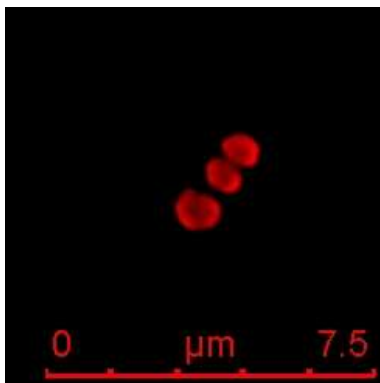
A (ii)



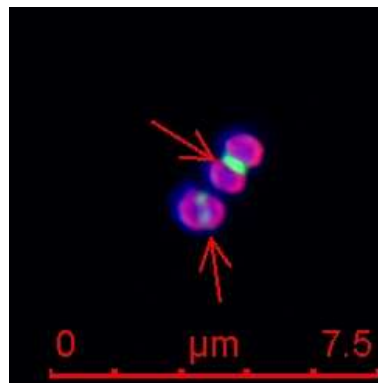
B (i)



A (iii)

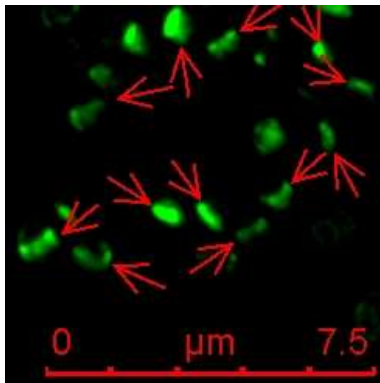


B (ii)

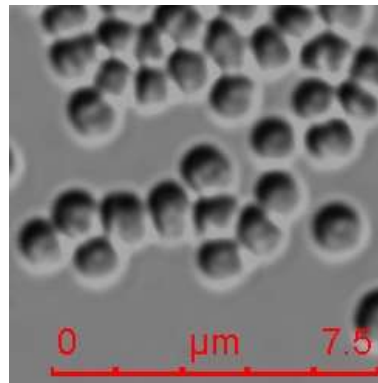


Appendix I. 12 MRSA BAA-41 was stained with single channel (A) for visualizing (i) lipid II of newly grown cell wall (green), (ii) nucleus acid (blue), (iii) cell membrane (red), (iv) DIC image; (B)(i) merged image of (A)(i) and (A)(ii); and (B)(ii) merged image of (A)(i), (A)(ii) and (A)(iii) in the presence of oxacillin at sub-lethal concentration 16 $\mu\text{g}/\text{mL}$. Scale bar is 7.5 μm .

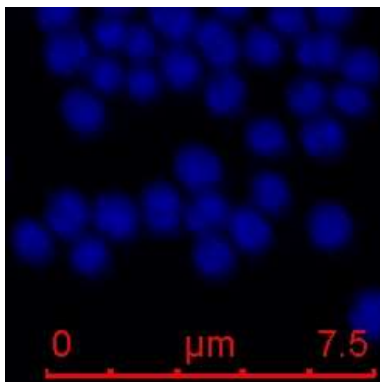
A (i)



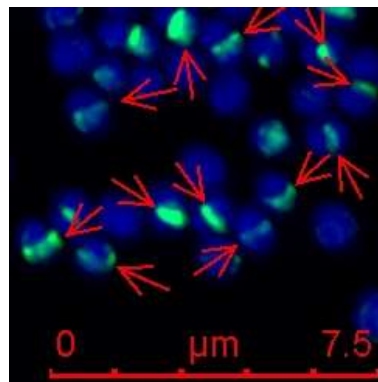
A (iv)



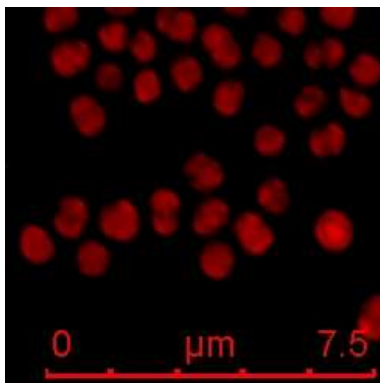
A (ii)



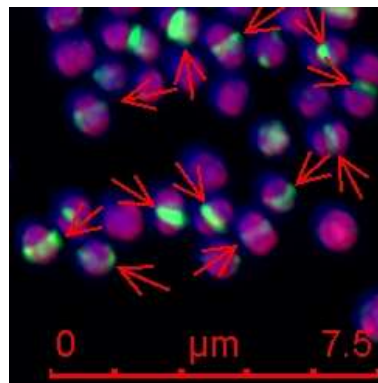
B (i)



A (iii)

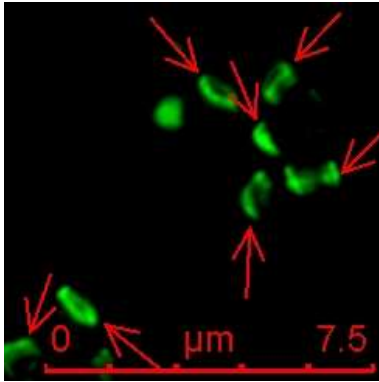


B (ii)

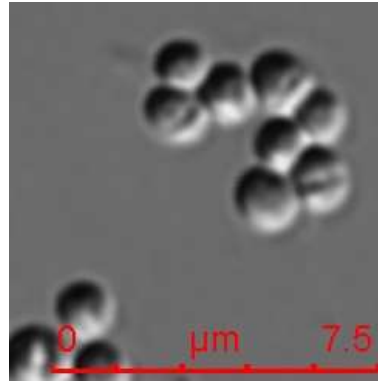


Appendix I. 13 MRSA BAA-41 was stained with single channel (A) for visualizing (i) lipid II of newly grown cell wall (green), (ii) nucleus acid (blue), (iii) cell membrane (red), (iv) DIC image; (B)(i) merged image of (A)(i) and (A)(ii); and (B)(ii) merged image of (A)(i), (A)(ii) and (A)(iii) in the presence of oxacillin at sub-lethal concentration 64 $\mu\text{g}/\text{mL}$. Scale bar is 7.5 μm .

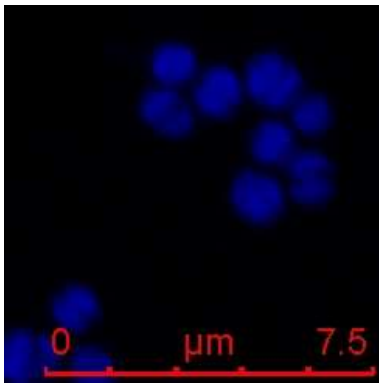
A (i)



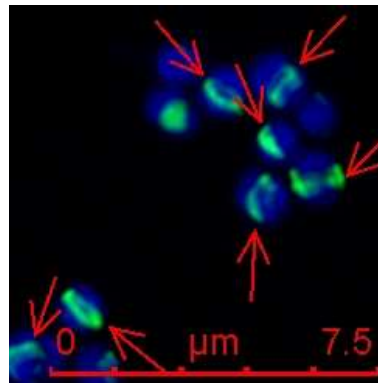
A (iv)



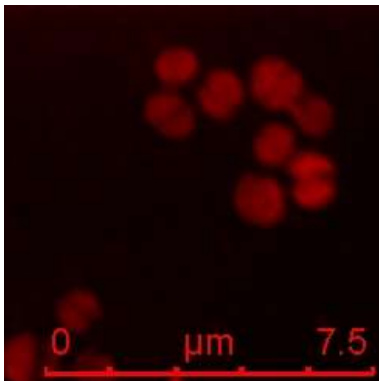
A (ii)



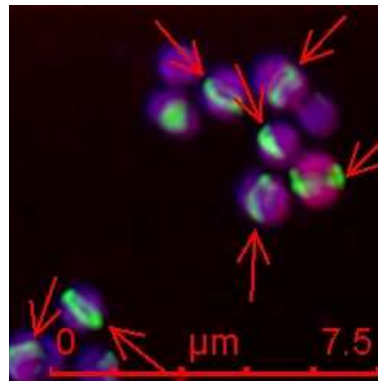
B (i)



A (iii)

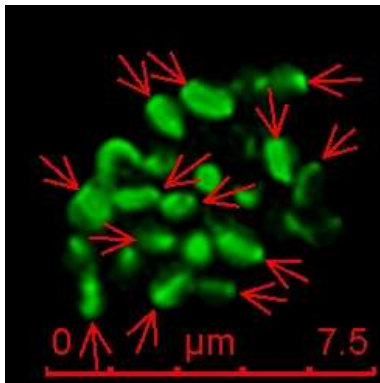


B (ii)

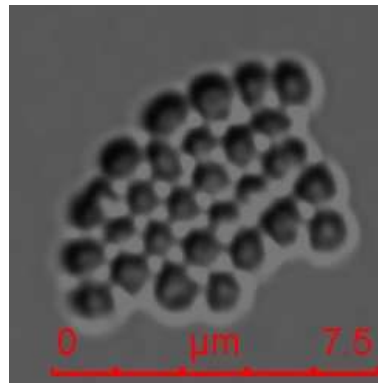


Appendix I. 14 MRSA BAA-41 was stained with single channel (A) for visualizing (i) lipid II of newly grown cell wall (green), (ii) nucleus acid (blue), (iii) cell membrane (red), (iv) DIC image; (B)(i) merged image of (A)(i) and (A)(ii); and (B)(ii) merged image of (A)(i), (A)(ii) and (A)(iii) in the presence of oxacillin at concentration $MIC \times 0.5$ (128 $\mu\text{g/mL}$). Scale bar is 7.5 μm .

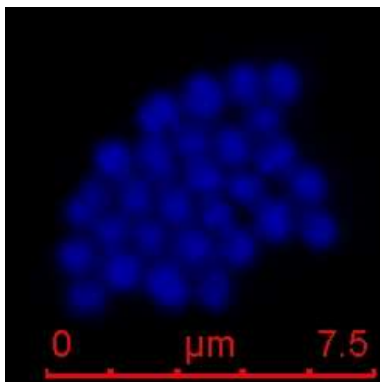
A (i)



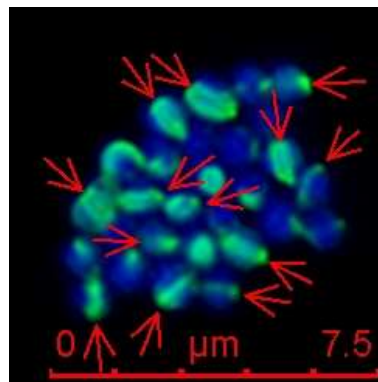
A (iv)



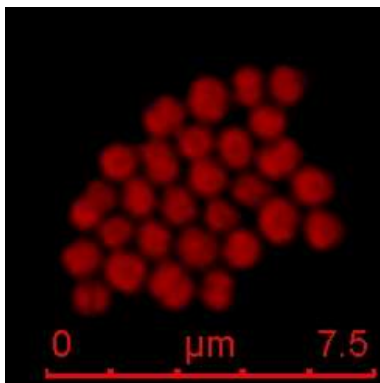
A (ii)



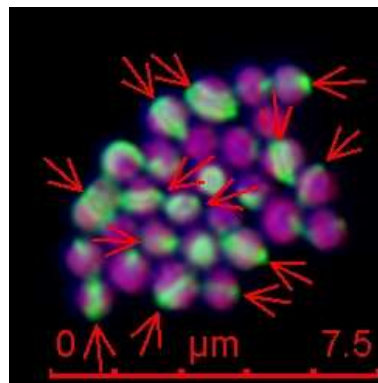
B (i)



A (iii)

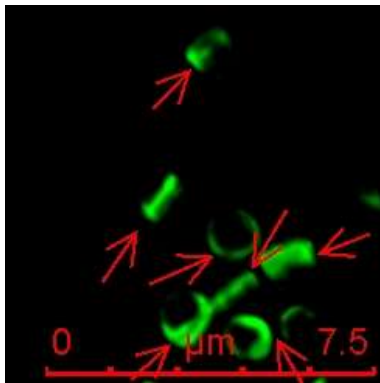


B (ii)

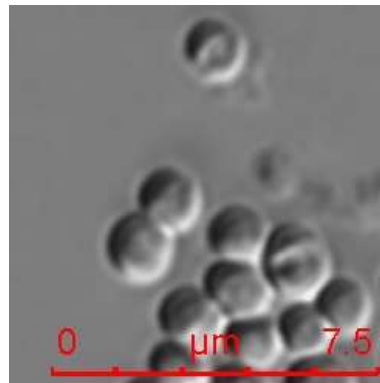


Appendix I. 15 MRSA BAA-41 was stained with single channel (A) for visualizing (i) lipid II of newly grown cell wall (green), (ii) nucleus acid (blue), (iii) cell membrane (red), (iv) DIC image; (B)(i) merged image of (A)(i) and (A)(ii); and (B)(ii) merged image of (A)(i), (A)(ii) and (A)(iii) in the presence of oxacillin at concentration $MIC \times 1$ (256 $\mu\text{g}/\text{mL}$). Scale bar is 7.5 μm .

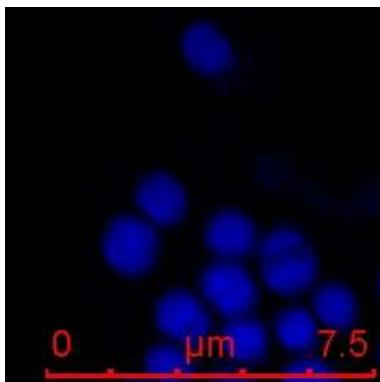
A (i)



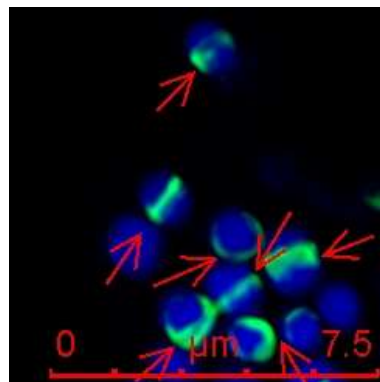
A (iv)



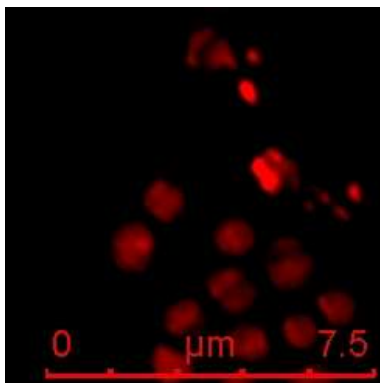
A (ii)



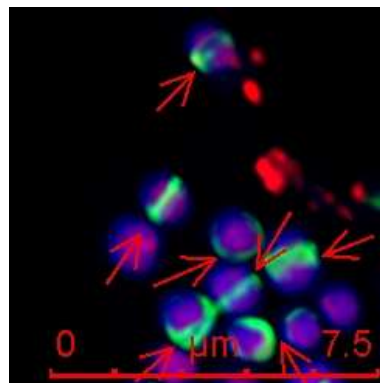
B (i)



A (iii)

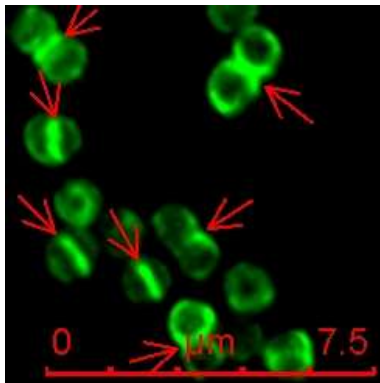


B (ii)

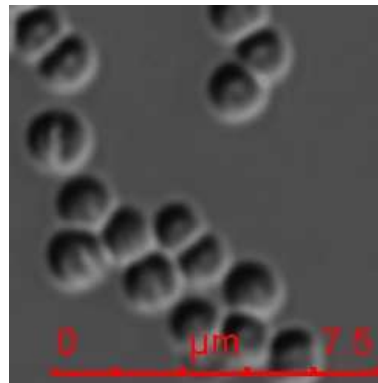


Appendix I. 16 MRSA BAA-41 was stained with single channel (A) for visualizing (i) lipid II of newly grown cell wall (green), (ii) nucleus acid (blue), (iii) cell membrane (red), (iv) DIC image; (B)(i) merged image of (A)(i) and (A)(ii); and (B)(ii) merged image of (A)(i), (A)(ii) and (A)(iii) in the presence of oxacillin at concentration $MIC \times 2$ (512 $\mu\text{g}/\text{mL}$). Scale bar is 7.5 μm .

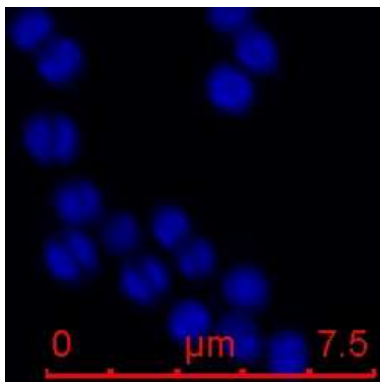
A (i)



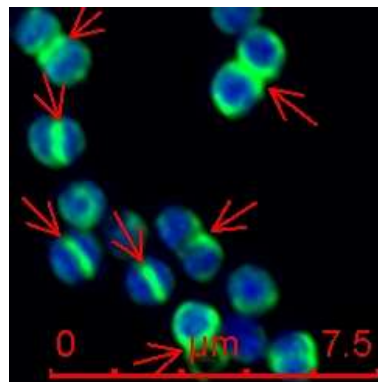
A (iv)



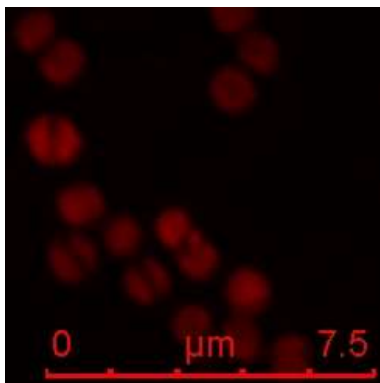
A (ii)



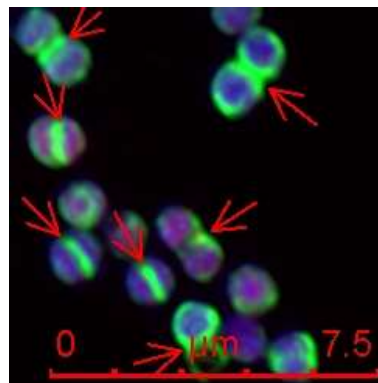
B (i)



A (iii)

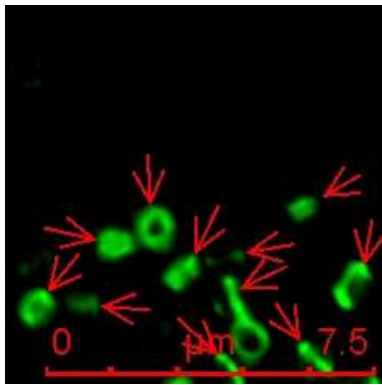


B (ii)

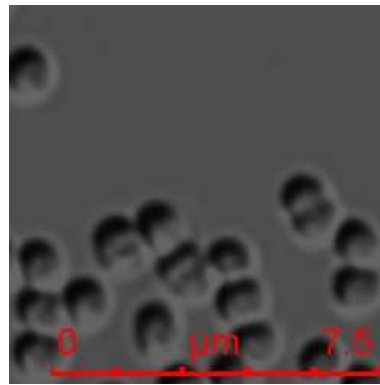


Appendix I. 17 MRSA BAA-41 was stained with single channel (A) for visualizing (i) lipid II of newly grown cell wall (green), (ii) nucleus acid (blue), (iii) cell membrane (red), (iv) DIC image; (B)(i) merged image of (A)(i) and (A)(ii); and (B)(ii) merged image of (A)(i), (A)(ii) and (A)(iii) in the presence of methicillin at sub-lethal concentration 16 $\mu\text{g}/\text{mL}$. Scale bar is 7.5 μm .

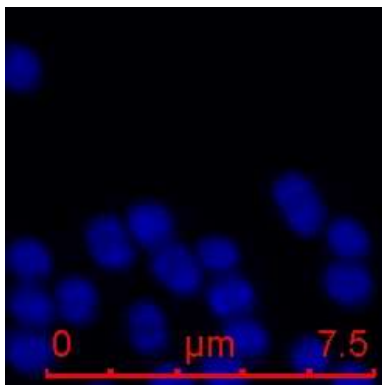
A (i)



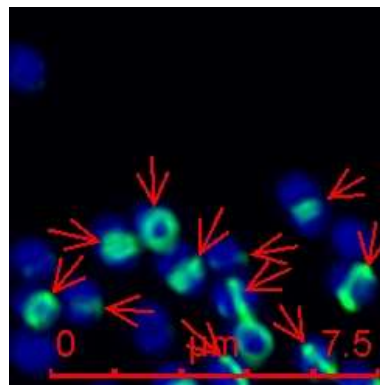
A (iv)



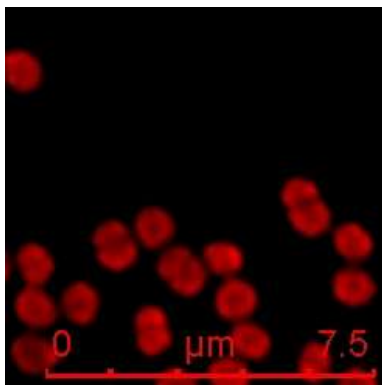
A (ii)



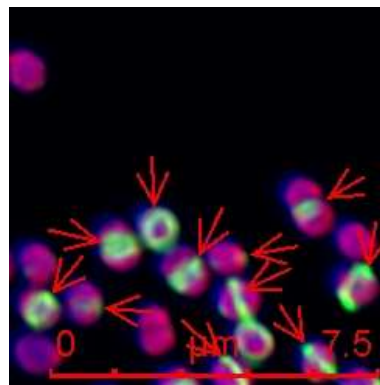
B (i)



A (iii)

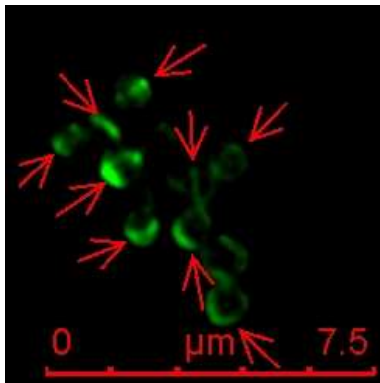


B (ii)

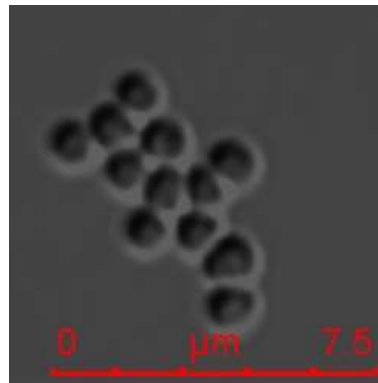


Appendix I. 18 MRSA BAA-41 was stained with single channel (A) for visualizing (i) lipid II of newly grown cell wall (green), (ii) nucleus acid (blue), (iii) cell membrane (red), (iv) DIC image; (B)(i) merged image of (A)(i) and (A)(ii); and (B)(ii) merged image of (A)(i), (A)(ii) and (A)(iii) in the presence of methicillin at sub-lethal concentration 32 $\mu\text{g}/\text{mL}$. Scale bar is 7.5 μm .

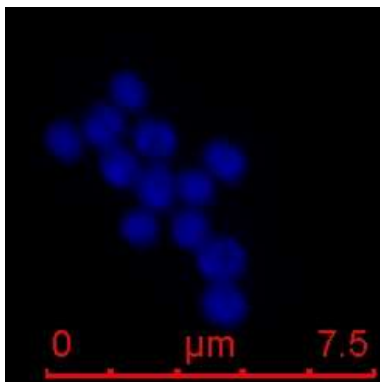
A (i)



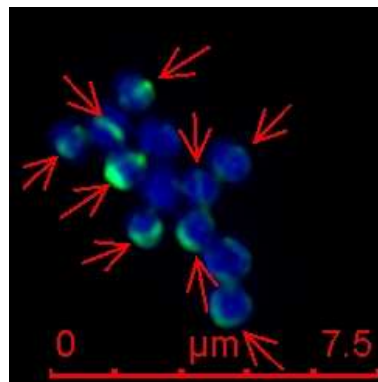
A (iv)



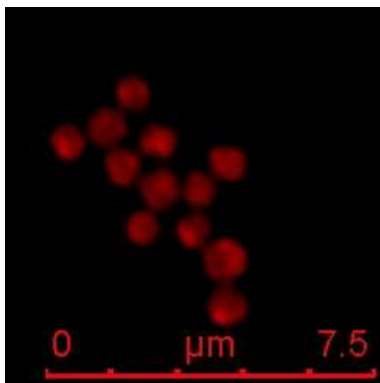
A (ii)



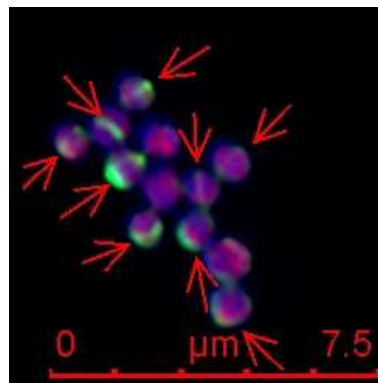
B (i)



A (iii)

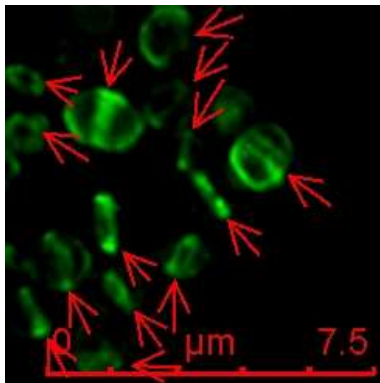


B (ii)

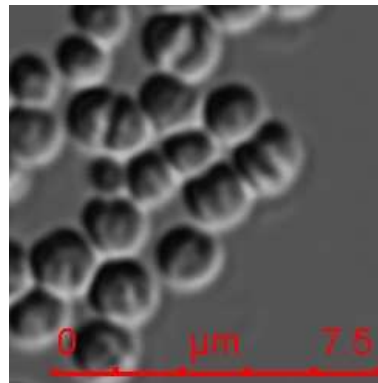


Appendix I. 19 MRSA BAA-41 was stained with single channel (A) for visualizing (i) lipid II of newly grown cell wall (green), (ii) nucleus acid (blue), (iii) cell membrane (red), (iv) DIC image; (B)(i) merged image of (A)(i) and (A)(ii); and (B)(ii) merged image of (A)(i), (A)(ii) and (A)(iii) in the presence of methicillin at sub-lethal concentration 64 $\mu\text{g}/\text{mL}$. Scale bar is 7.5 μm .

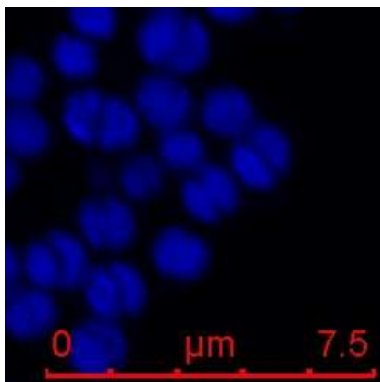
A (i)



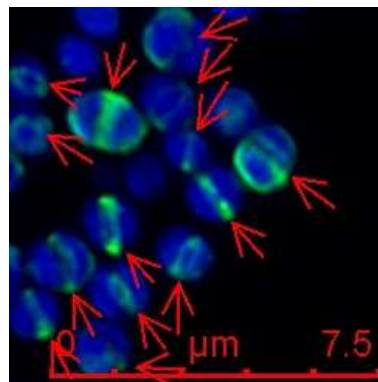
A (iv)



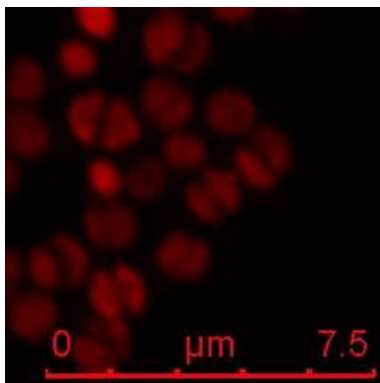
A (ii)



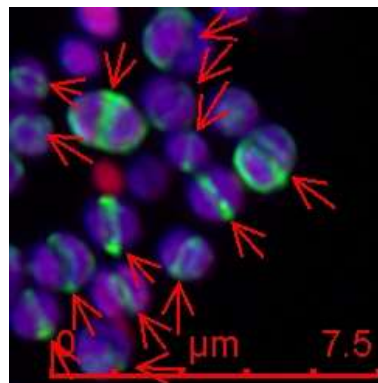
B (i)



A (iii)

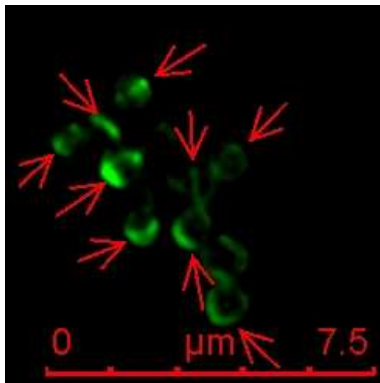


B (ii)

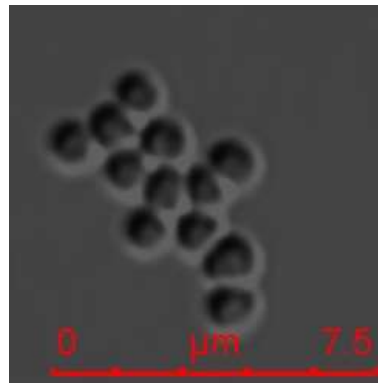


Appendix I. 20 MRSA BAA-41 was stained with single channel (A) for visualizing (i) lipid II of newly grown cell wall (green), (ii) nucleus acid (blue), (iii) cell membrane (red), (iv) DIC image; (B)(i) merged image of (A)(i) and (A)(ii); and (B)(ii) merged image of (A)(i), (A)(ii) and (A)(iii) in the presence of methicillin at sub-lethal concentration 128 $\mu\text{g}/\text{mL}$. Scale bar is 7.5 μm .

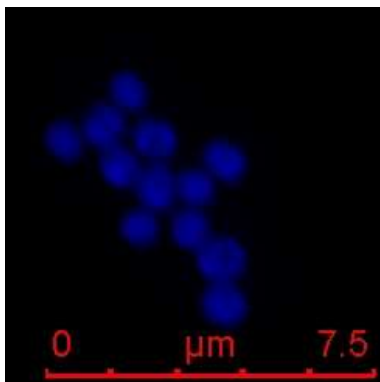
A (i)



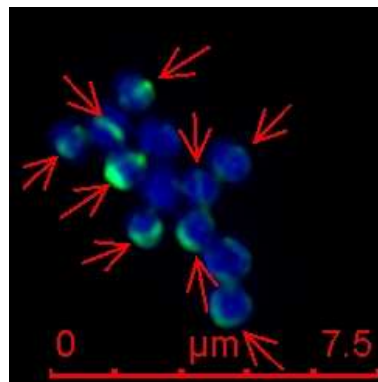
A (iv)



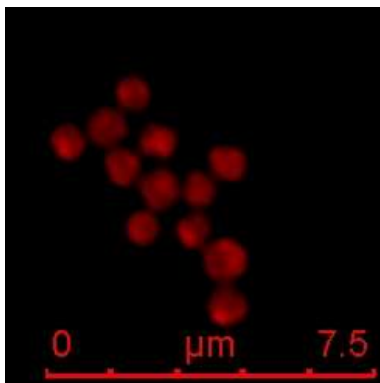
A (ii)



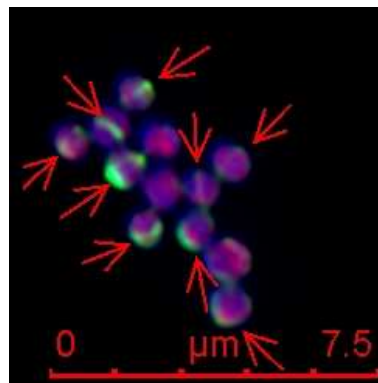
B (i)



A (iii)

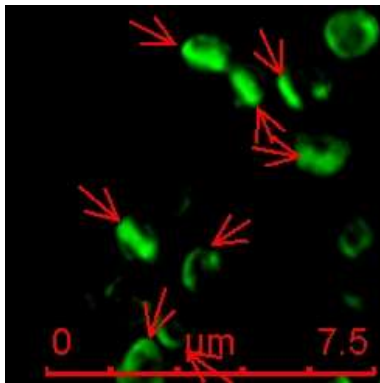


B (ii)

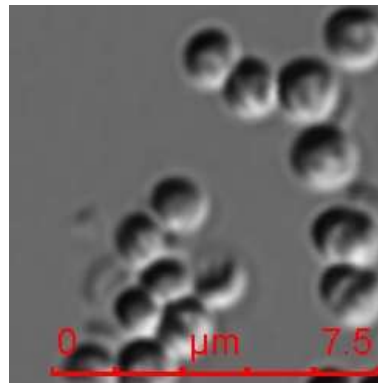


Appendix I. 21 MRSA BAA-41 was stained with single channel (A) for visualizing (i) lipid II of newly grown cell wall (green), (ii) nucleus acid (blue), (iii) cell membrane (red), (iv) DIC image; (B)(i) merged image of (A)(i) and (A)(ii); and (B)(ii) merged image of (A)(i), (A)(ii) and (A)(iii) in the presence of methicillin at sub-lethal concentration 128 $\mu\text{g}/\text{mL}$. Scale bar is 7.5 μm .

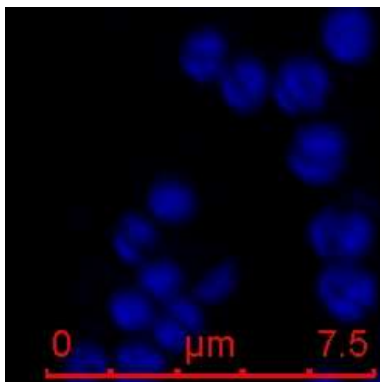
A (i)



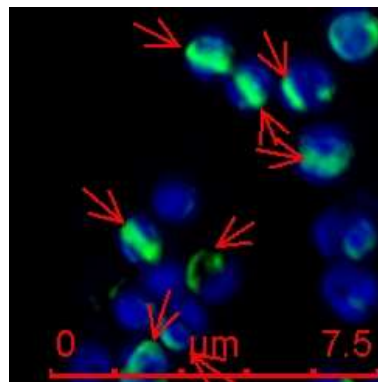
A (iv)



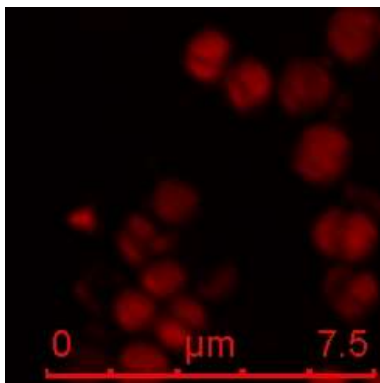
A (ii)



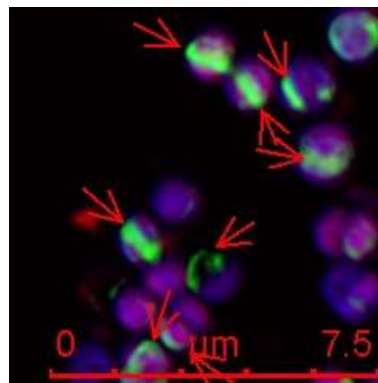
B (i)



A (iii)

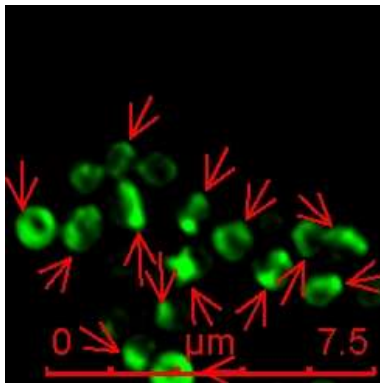


B (ii)

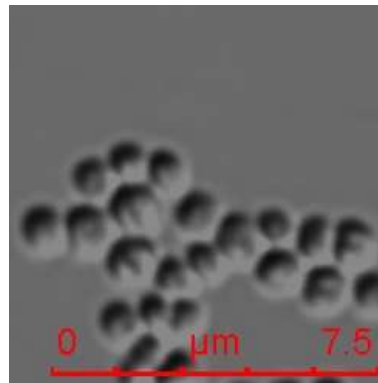


Appendix I. 22 MRSA BAA-41 was stained with single channel (A) for visualizing (i) lipid II of newly grown cell wall (green), (ii) nucleus acid (blue), (iii) cell membrane (red), (iv) DIC image; (B)(i) merged image of (A)(i) and (A)(ii); and (B)(ii) merged image of (A)(i), (A)(ii) and (A)(iii) in the presence of methicillin at $MIC \times 0.5$ (256 $\mu\text{g/mL}$). Scale bar is 7.5 μm .

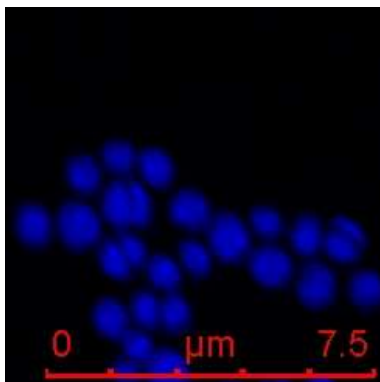
A (i)



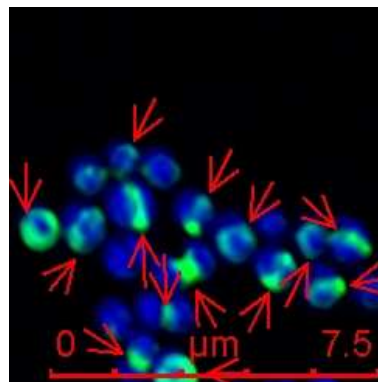
A (iv)



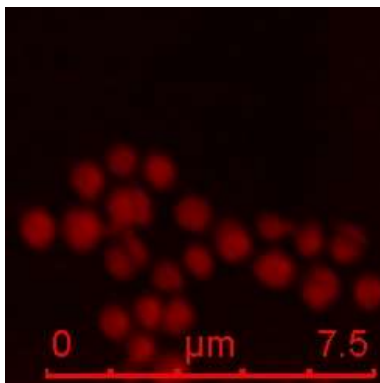
A (ii)



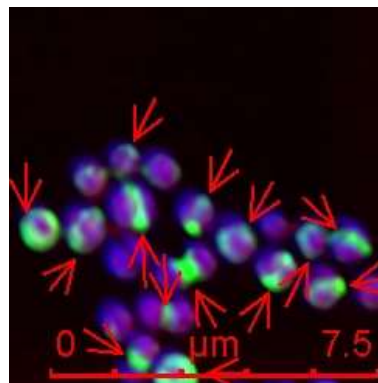
B (i)



A (iii)

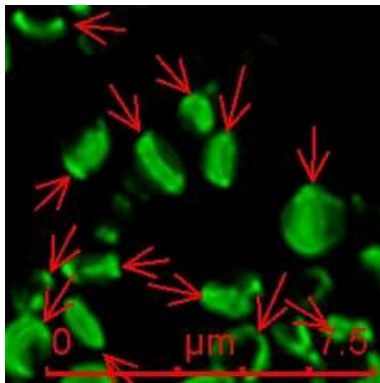


B (ii)

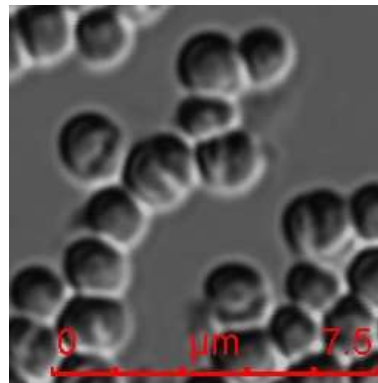


Appendix I. 23 MRSA BAA-41 was stained with single channel (A) for visualizing (i) lipid II of newly grown cell wall (green), (ii) nucleus acid (blue), (iii) cell membrane (red), (iv) DIC image; (B)(i) merged image of (A)(i) and (A)(ii); and (B)(ii) merged image of (A)(i), (A)(ii) and (A)(iii) in the presence of methicillin at MIC \times 1 (512 $\mu\text{g}/\text{mL}$). Scale bar is 7.5 μm .

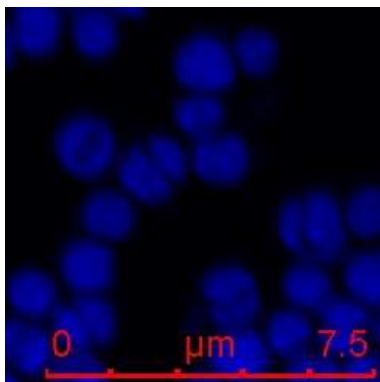
A (i)



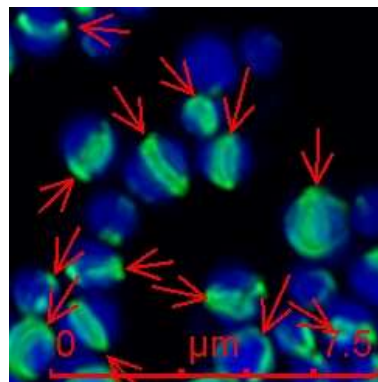
A (iv)



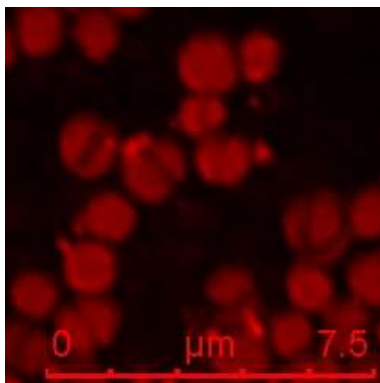
A (ii)



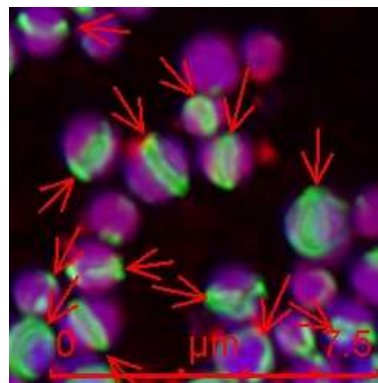
B (i)



A (iii)

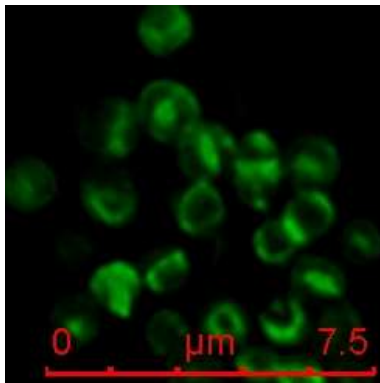


B (ii)

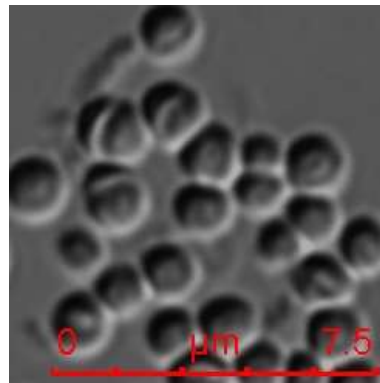


Appendix I. 24 MRSA BAA-41 was stained with single channel (A) for visualizing (i) lipid II of newly grown cell wall (green), (ii) nucleus acid (blue), (iii) cell membrane (red), (iv) DIC image; (B)(i) merged image of (A)(i) and (A)(ii); and (B)(ii) merged image of (A)(i), (A)(ii) and (A)(iii) in the presence of methicillin at MIC \times 2 (1024 $\mu\text{g}/\text{mL}$). Scale bar is 7.5 μm .

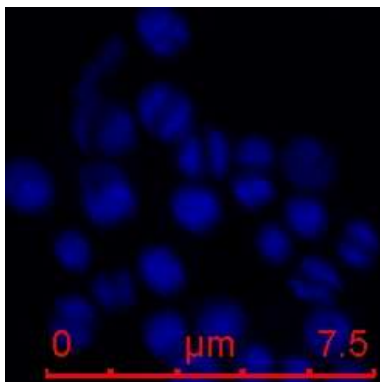
A (i)



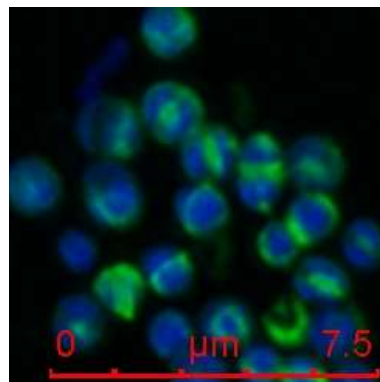
A (iv)



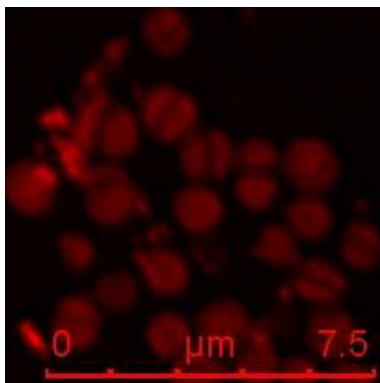
A (ii)



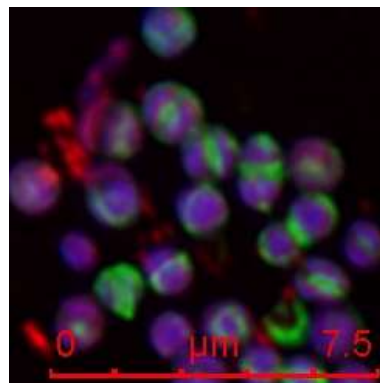
B (i)



A (iii)

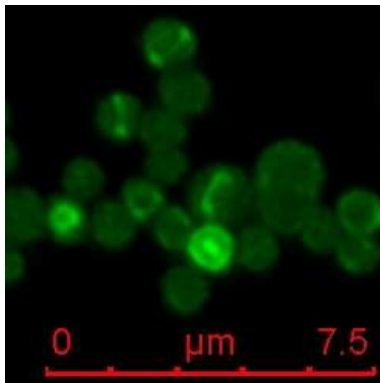


B (ii)

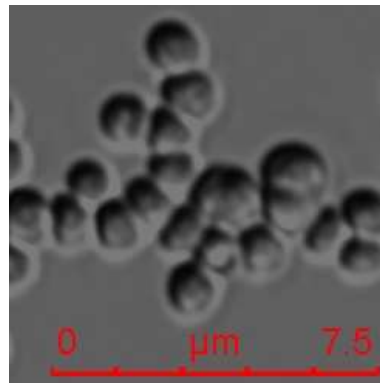


Appendix I. 25 MRSA BAA-41 was stained with single channel (A) for visualizing (i) lipid II of newly grown cell wall (green), (ii) nucleus acid (blue), (iii) cell membrane (red), (iv) DIC image; (B)(i) merged image of (A)(i) and (A)(ii); and (B)(ii) merged image of (A)(i), (A)(ii) and (A)(iii) in the presence of F332 (0.5 $\mu\text{g}/\text{mL}$) and oxacillin (8 $\mu\text{g}/\text{mL}$) combination at $\text{MIC} \times 0.5$. Scale bar is 7.5 μm .

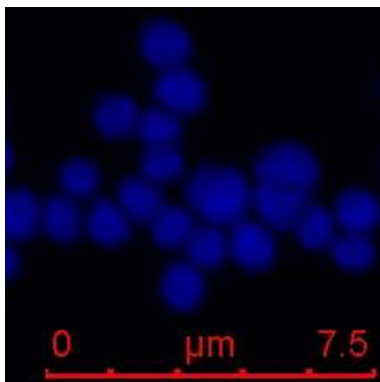
A (i)



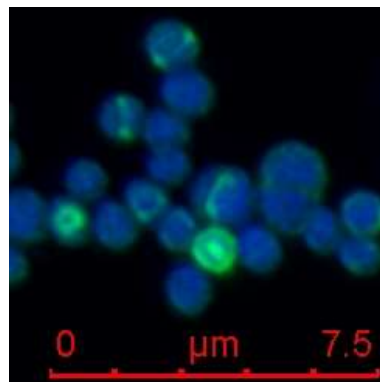
A (iv)



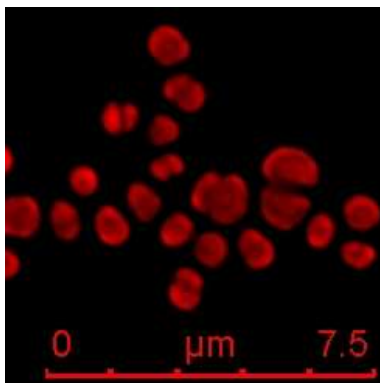
A (ii)



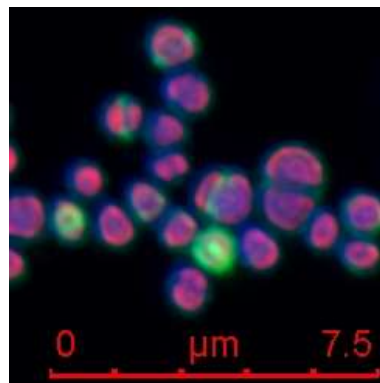
B (i)



A (iii)

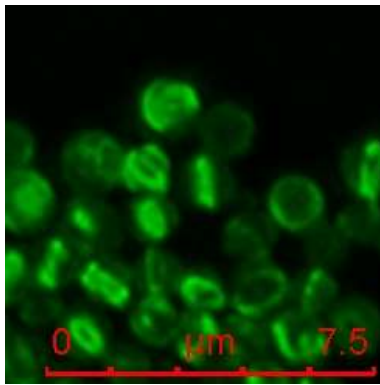


B (ii)

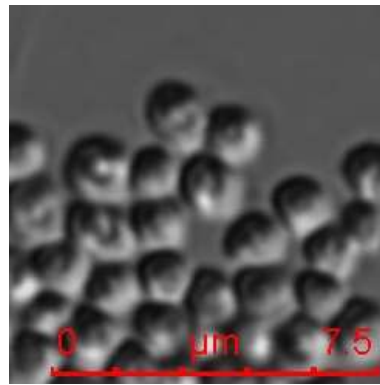


Appendix I. 26 MRSA BAA-41 was stained with single channel (A) for visualizing (i) lipid II of newly grown cell wall (green), (ii) nucleus acid (blue), (iii) cell membrane (red), (iv) DIC image; (B)(i) merged image of (A)(i) and (A)(ii); and (B)(ii) merged image of (A)(i), (A)(ii) and (A)(iii) in the presence of F332 (1 $\mu\text{g}/\text{mL}$) and oxacillin (16 $\mu\text{g}/\text{mL}$) combination at $\text{MIC} \times 1$. Scale bar is 7.5 μm .

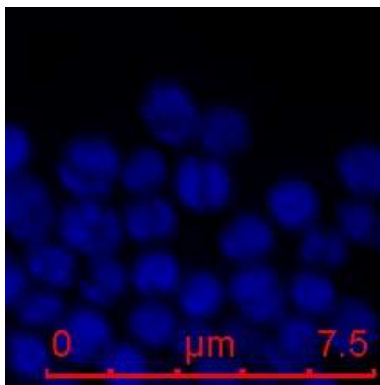
A (i)



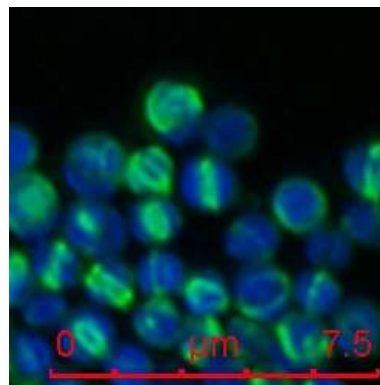
A (iv)



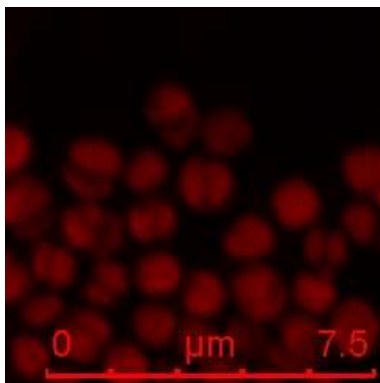
A (ii)



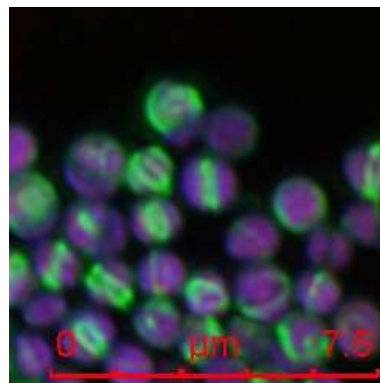
B (i)



A (iii)

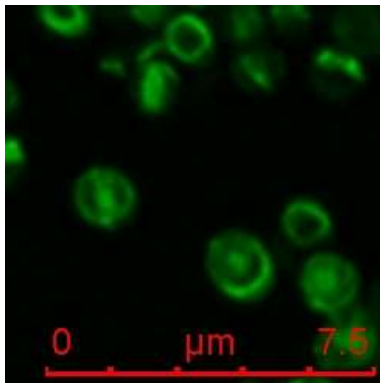


B (ii)

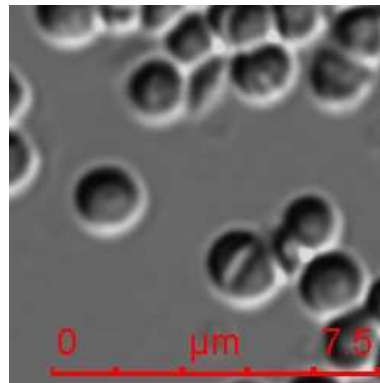


Appendix I. 27 MRSA BAA-41 was stained with single channel (A) for visualizing (i) lipid II of newly grown cell wall (green), (ii) nucleus acid (blue), (iii) cell membrane (red), (iv) DIC image; (B)(i) merged image of (A)(i) and (A)(ii); and (B)(ii) merged image of (A)(i), (A)(ii) and (A)(iii) in the presence of F332 (2 $\mu\text{g}/\text{mL}$) and oxacillin (32 $\mu\text{g}/\text{mL}$) combination at $\text{MIC} \times 2$. Scale bar is 7.5 μm .

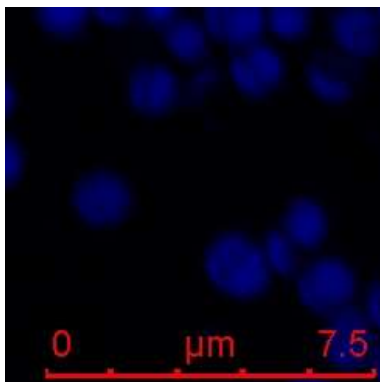
A (i)



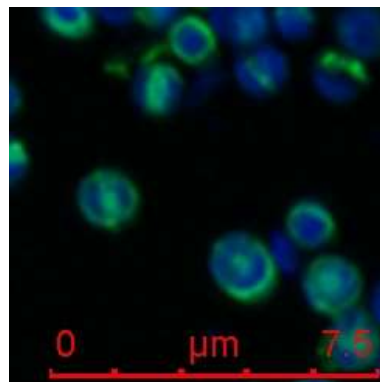
A (iv)



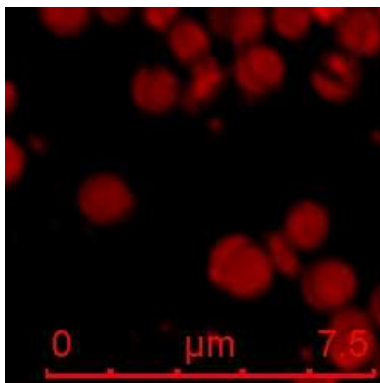
A (ii)



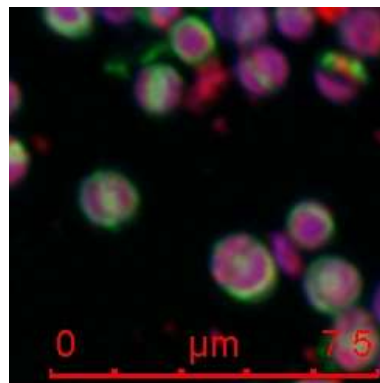
B (i)



A (iii)

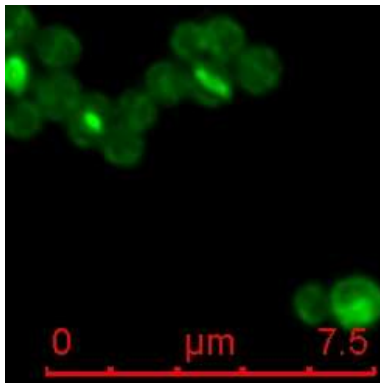


B (ii)

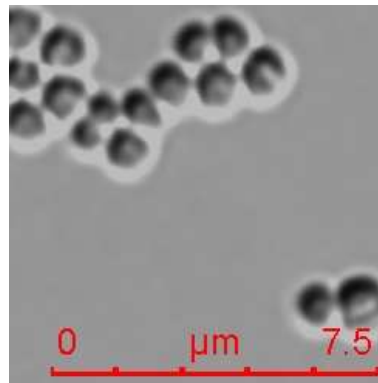


Appendix I. 28 MRSA BAA-41 was stained with single channel (A) for visualizing (i) lipid II of newly grown cell wall (green), (ii) nucleus acid (blue), (iii) cell membrane (red), (iv) DIC image; (B)(i) merged image of (A)(i) and (A)(ii); and (B)(ii) merged image of (A)(i), (A)(ii) and (A)(iii) in the presence of F332 (0.5 $\mu\text{g}/\text{mL}$) and methicillin (16 $\mu\text{g}/\text{mL}$) combination at $\text{MIC} \times 0.5$. Scale bar is 7.5 μm .

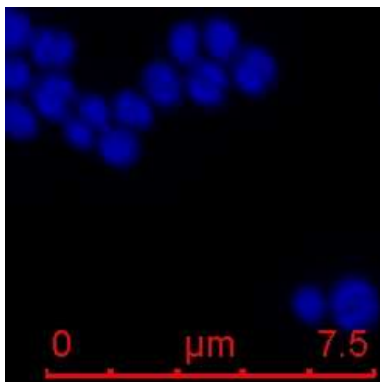
A (i)



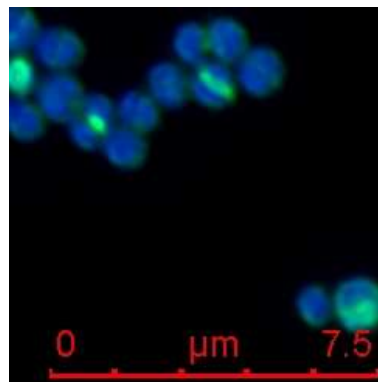
A (iv)



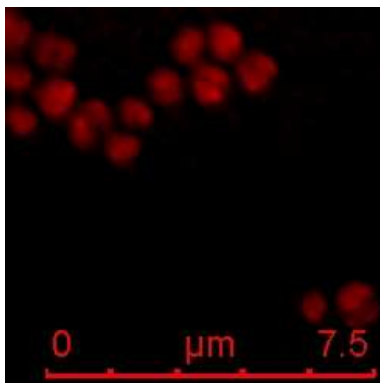
A (ii)



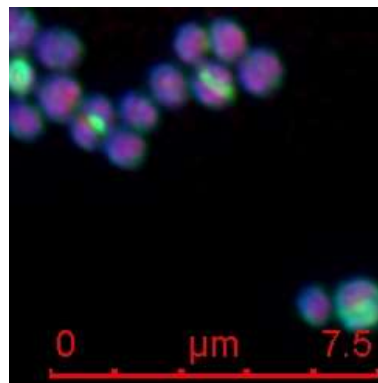
B (i)



A (iii)

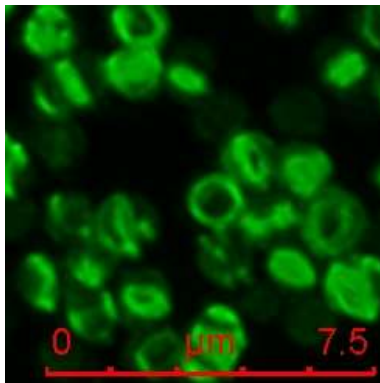


B (ii)

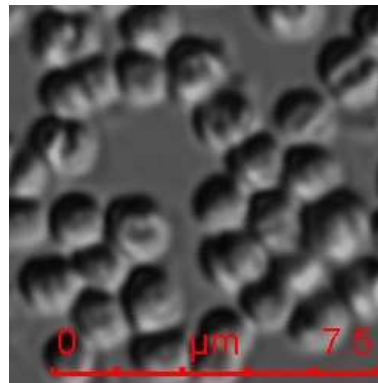


Appendix I. 29 MRSA BAA-41 was stained with single channel (A) for visualizing (i) lipid II of newly grown cell wall (green), (ii) nucleus acid (blue), (iii) cell membrane (red), (iv) DIC image; (B)(i) merged image of (A)(i) and (A)(ii); and (B)(ii) merged image of (A)(i), (A)(ii) and (A)(iii) in the presence of F332 (1 $\mu\text{g}/\text{mL}$) and methicillin (32 $\mu\text{g}/\text{mL}$) combination at $\text{MIC} \times 1$. Scale bar is 7.5 μm .

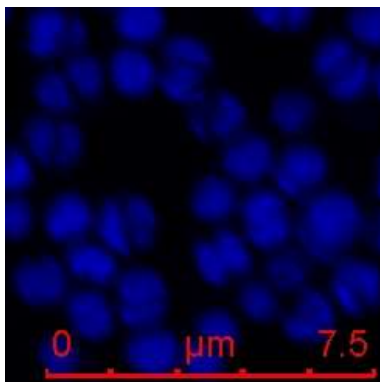
A (i)



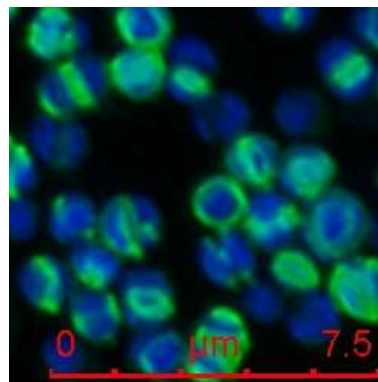
A (iv)



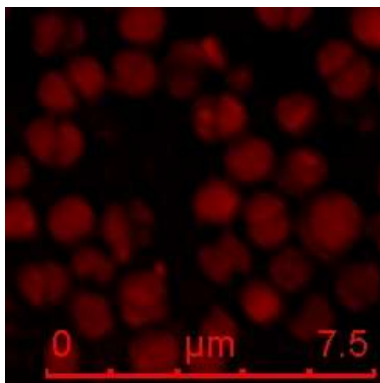
A (ii)



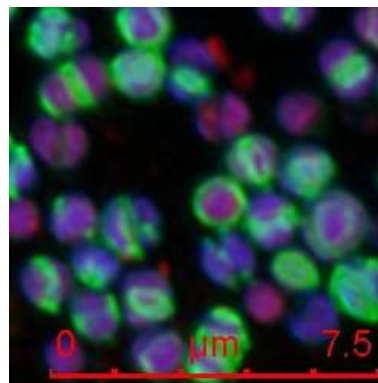
B (i)



A (iii)

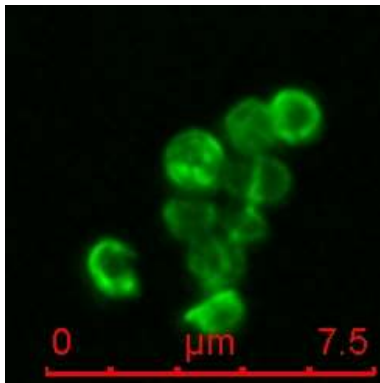


B (ii)

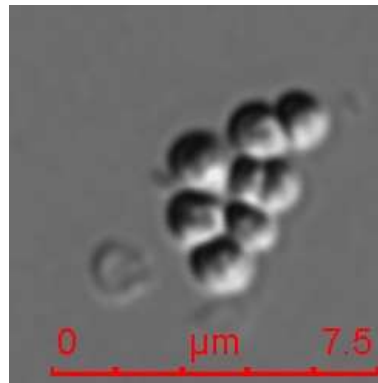


Appendix I. 30 MRSA BAA-41 was stained with single channel (A) for visualizing (i) lipid II of newly grown cell wall (green), (ii) nucleus acid (blue), (iii) cell membrane (red), (iv) DIC image; (B)(i) merged image of (A)(i) and (A)(ii); and (B)(ii) merged image of (A)(i), (A)(ii) and (A)(iii) in the presence of F332 (2 $\mu\text{g}/\text{mL}$) and methicillin (64 $\mu\text{g}/\text{mL}$) combination at $\text{MIC} \times 2$. Scale bar is 7.5 μm .

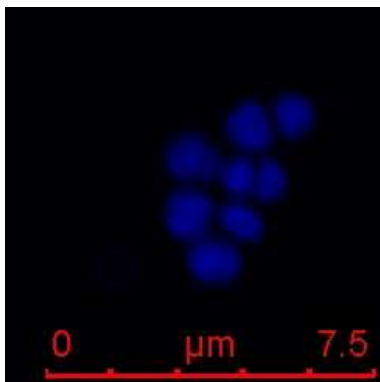
A (i)



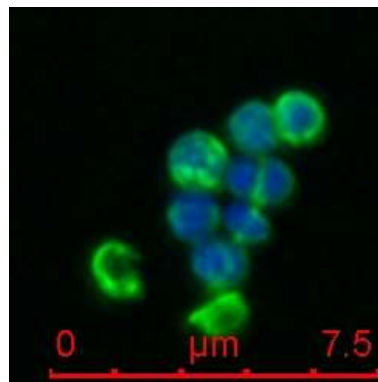
A (iv)



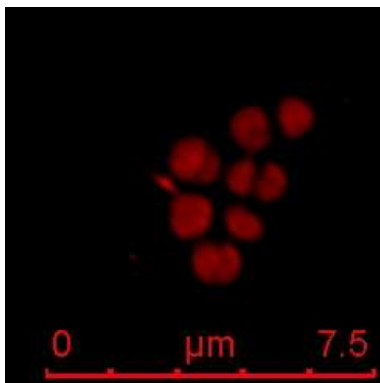
A (ii)



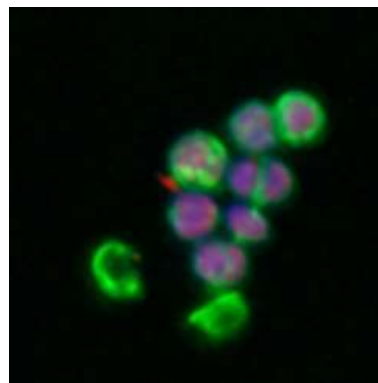
B (i)



A (iii)

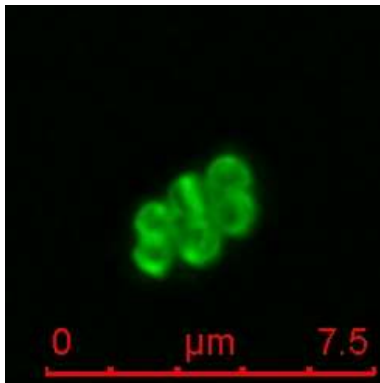


B (ii)

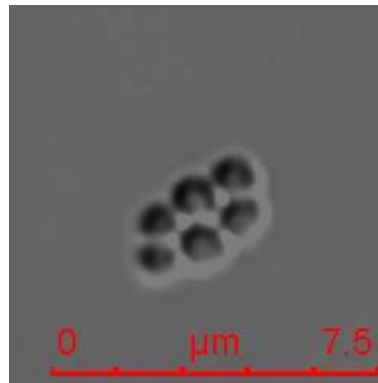


Appendix I. 31 MRSA BAA-41 was stained with single channel (A) for visualizing (i) lipid II of newly grown cell wall (green), (ii) nucleus acid (blue), (iii) cell membrane (red), (iv) DIC image; (B)(i) merged image of (A)(i) and (A)(ii); and (B)(ii) merged image of (A)(i), (A)(ii) and (A)(iii) in the presence of PC190723 (0.0623 $\mu\text{g}/\text{mL}$) and oxacillin (32 $\mu\text{g}/\text{mL}$) combination at $\text{MIC} \times 0.5$. Scale bar is 7.5 μm .

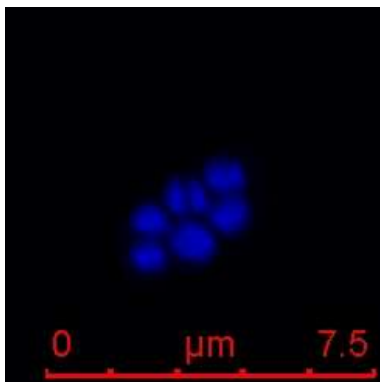
A (i)



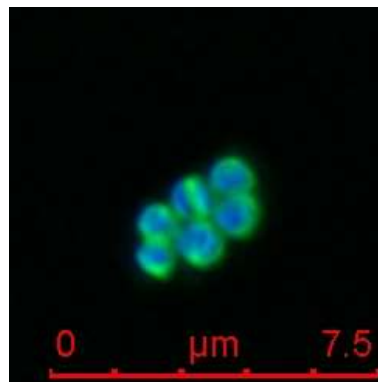
A (iv)



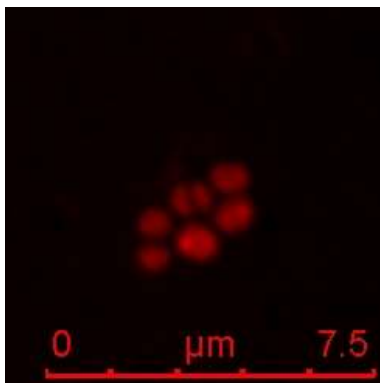
A (ii)



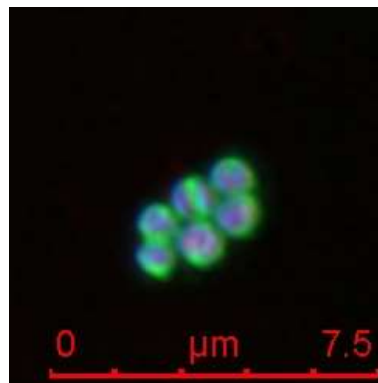
B (i)



A (iii)

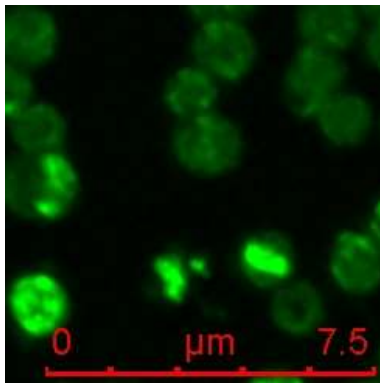


B (ii)

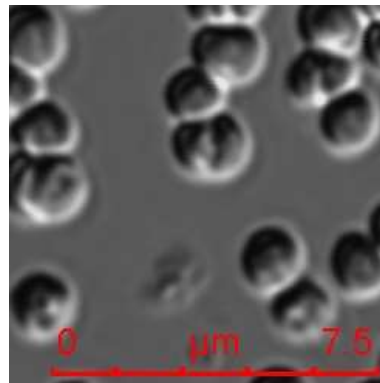


Appendix I. 32 MRSA BAA-41 was stained with single channel (A) for visualizing (i) lipid II of newly grown cell wall (green), (ii) nucleus acid (blue), (iii) cell membrane (red), (iv) DIC image; (B)(i) merged image of (A)(i) and (A)(ii); and (B)(ii) merged image of (A)(i), (A)(ii) and (A)(iii) in the presence of PC190723 (0.125 $\mu\text{g}/\text{mL}$) and oxacillin (64 $\mu\text{g}/\text{mL}$) combination at $\text{MIC} \times 1$. Scale bar is 7.5 μm .

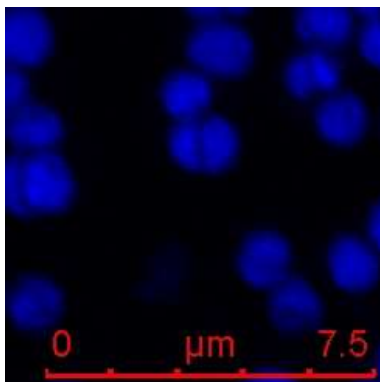
A (i)



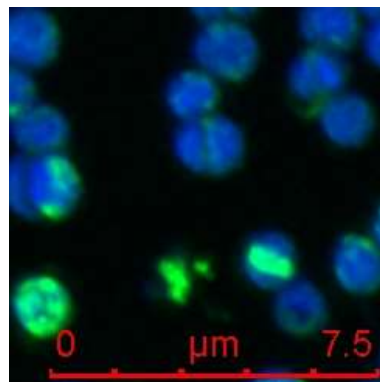
A (iv)



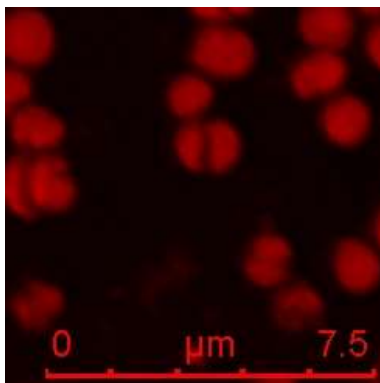
A (ii)



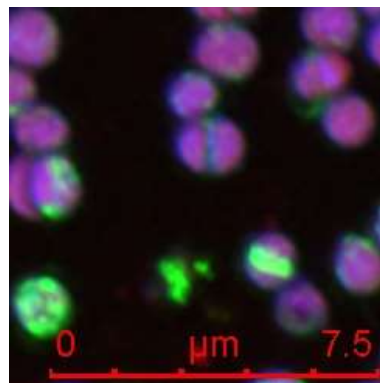
B (i)



A (iii)

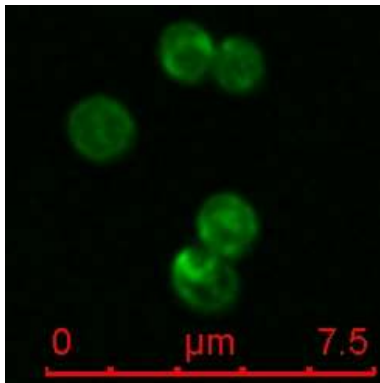


B (ii)

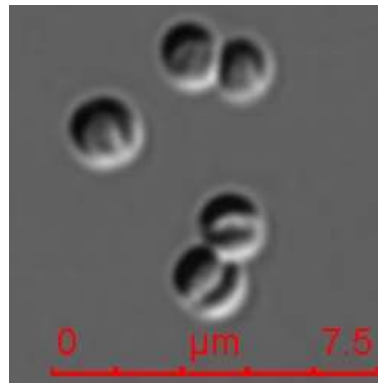


Appendix I. 33 MRSA BAA-41 was stained with single channel (A) for visualizing (i) lipid II of newly grown cell wall (green), (ii) nucleus acid (blue), (iii) cell membrane (red), (iv) DIC image; (B)(i) merged image of (A)(i) and (A)(ii); and (B)(ii) merged image of (A)(i), (A)(ii) and (A)(iii) in the presence of PC190723 (0.25 $\mu\text{g}/\text{mL}$) and oxacillin (128 $\mu\text{g}/\text{mL}$) combination at $\text{MIC} \times 1$. Scale bar is 7.5 μm .

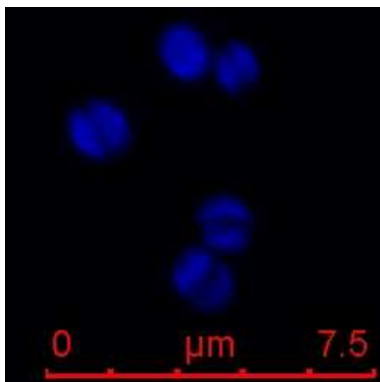
A (i)



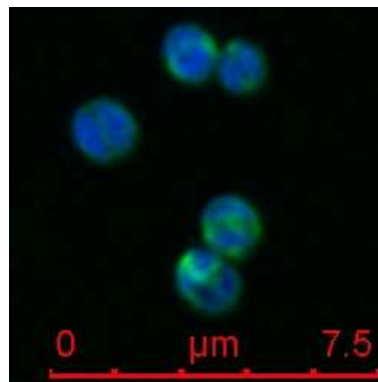
A (iv)



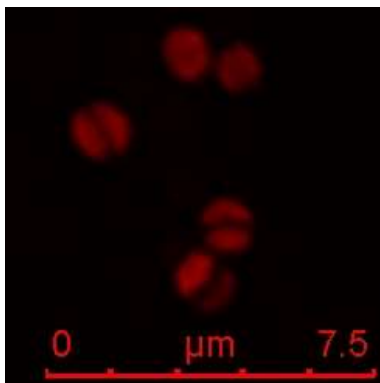
A (ii)



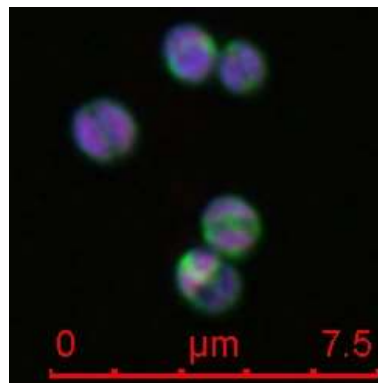
B (i)



A (iii)

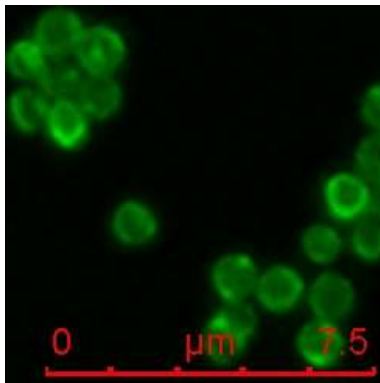


B (ii)

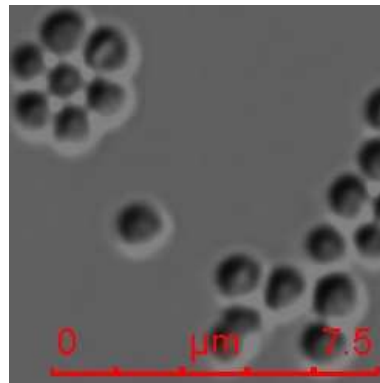


Appendix I. 34 MRSA BAA-41 was stained with single channel (A) for visualizing (i) lipid II of newly grown cell wall (green), (ii) nucleus acid (blue), (iii) cell membrane (red), (iv) DIC image; (B)(i) merged image of (A)(i) and (A)(ii); and (B)(ii) merged image of (A)(i), (A)(ii) and (A)(iii) in the presence of PC190723 (0.125 $\mu\text{g}/\text{mL}$) and methicillin (32 $\mu\text{g}/\text{mL}$) combination at $\text{MIC} \times 0.5$. Scale bar is 7.5 μm .

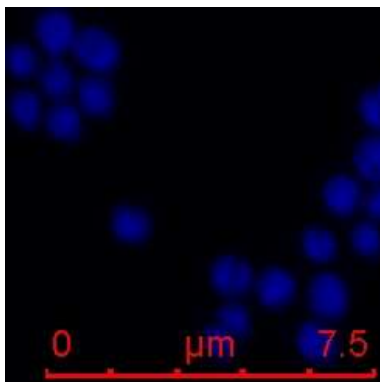
A (i)



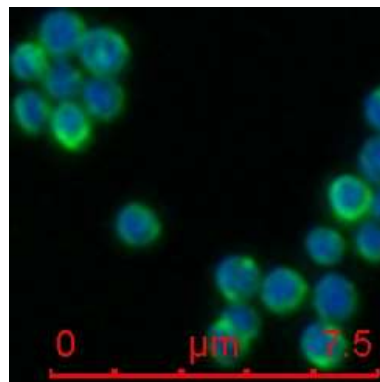
A (iv)



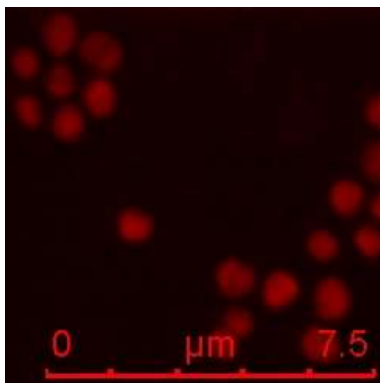
A (ii)



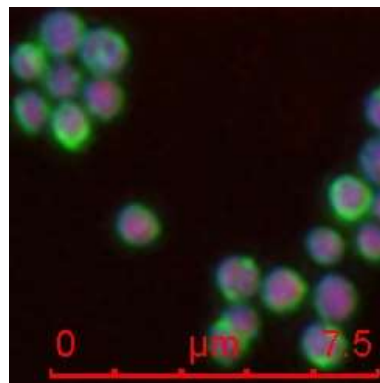
B (i)



A (iii)

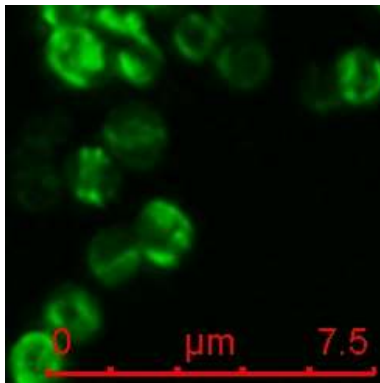


B (ii)

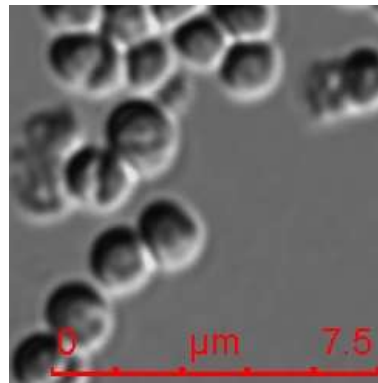


Appendix I. 35 MRSA BAA-41 was stained with single channel (A) for visualizing (i) lipid II of newly grown cell wall (green), (ii) nucleus acid (blue), (iii) cell membrane (red), (iv) DIC image; (B)(i) merged image of (A)(i) and (A)(ii); and (B)(ii) merged image of (A)(i), (A)(ii) and (A)(iii) in the presence of PC190723 (0.25 $\mu\text{g}/\text{mL}$) and methicillin (64 $\mu\text{g}/\text{mL}$) combination at $\text{MIC} \times 1$. Scale bar is 7.5 μm .

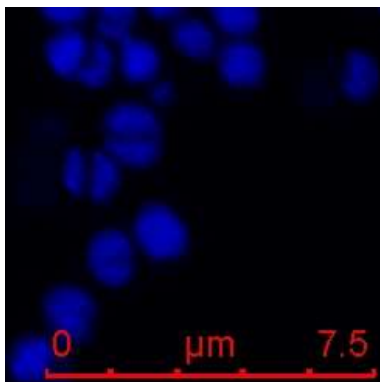
A (i)



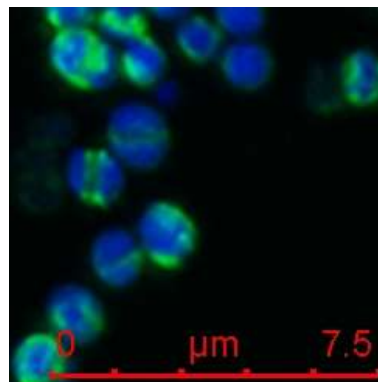
A (iv)



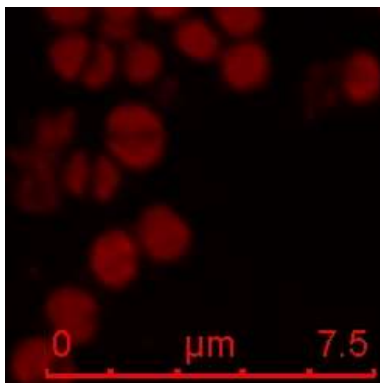
A (ii)



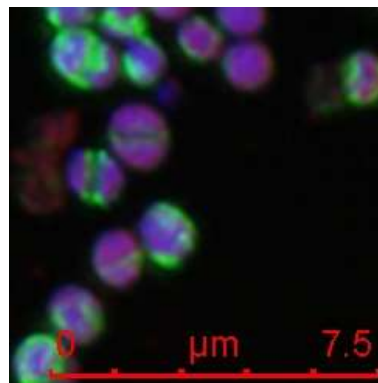
B (i)



A (iii)

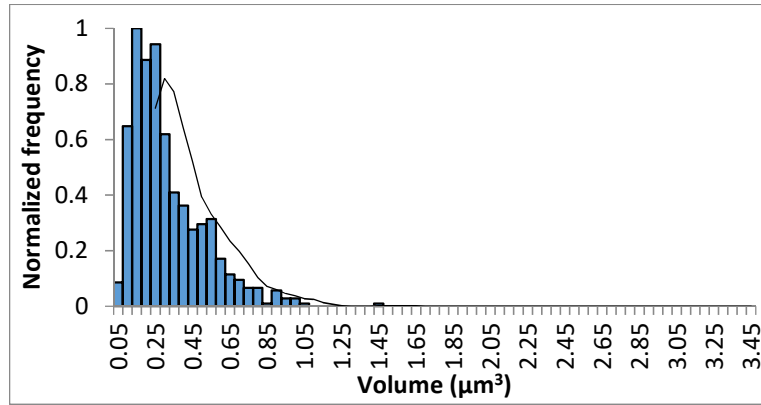


B (ii)

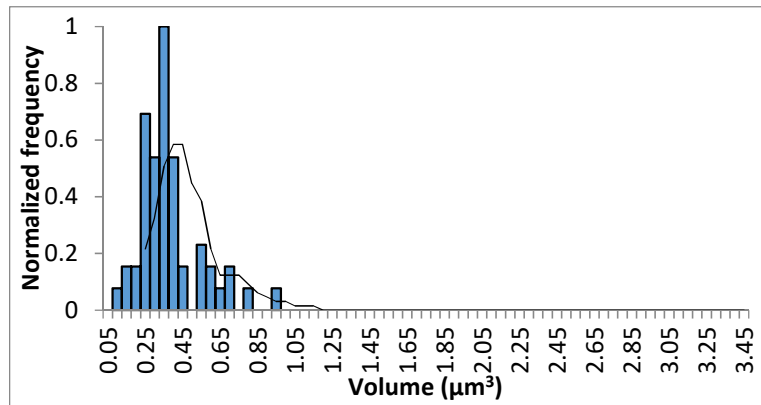


Appendix I. 36 MRSA BAA-41 was stained with single channel (A) for visualizing (i) lipid II of newly grown cell wall (green), (ii) nucleus acid (blue), (iii) cell membrane (red), (iv) DIC image; (B)(i) merged image of (A)(i) and (A)(ii); and (B)(ii) merged image of (A)(i), (A)(ii) and (A)(iii) in the presence of PC190723 (0.5 $\mu\text{g}/\text{mL}$) and methicillin (128 $\mu\text{g}/\text{mL}$) combination at $\text{MIC} \times 2$. Scale bar is 7.5 μm .

**Appendix II Histogram showing
the frequency distribution of cell
volume in MRSA**

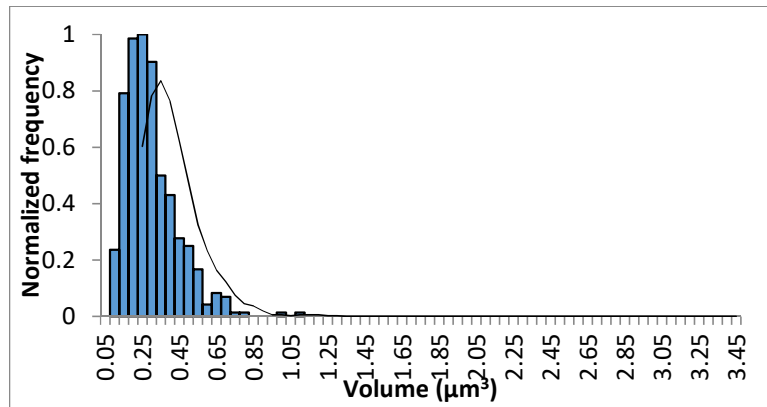


Appendix II. 1 Frequency distribution histogram of cell volume in MRSA in the absence of antibiotic compound.

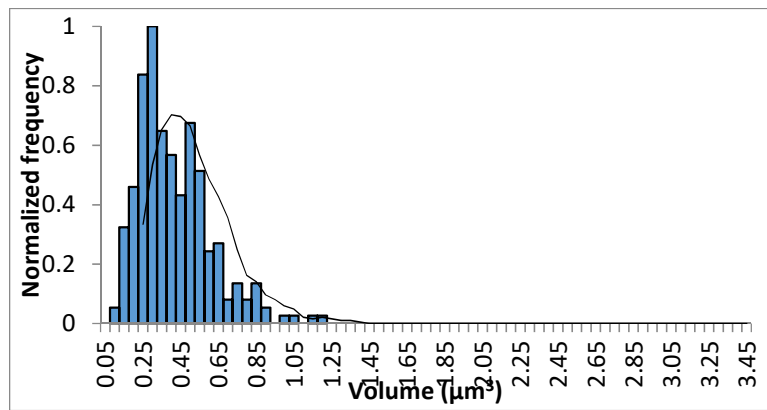


Appendix II. 2 Frequency distribution histogram of cell volume in MRSA in the presence of FtsZ inhibitor F332 at sub-lethal concentration 0.5 μg/mL.

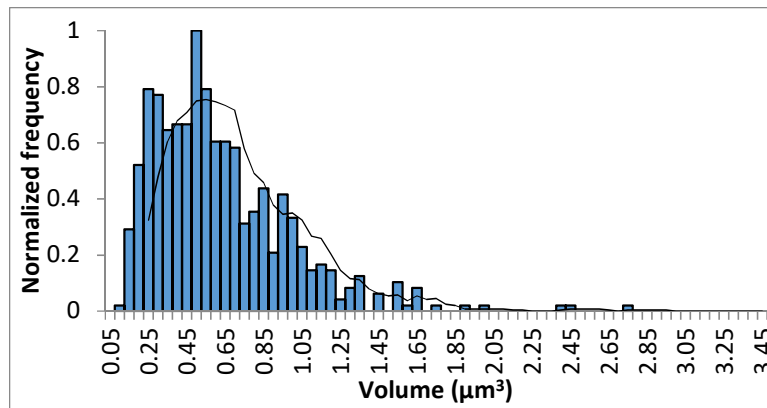
A



B

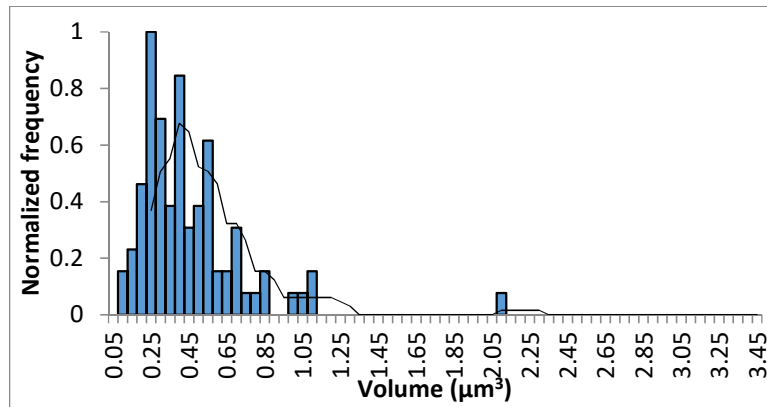


C

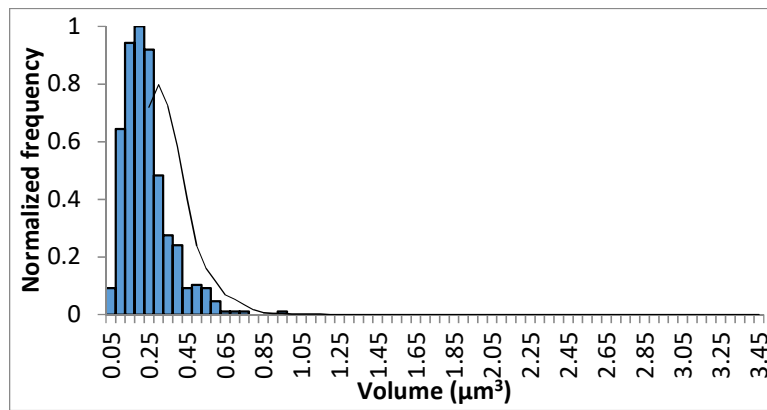


Appendix II. 3 Frequency distribution histograms of cell in the presence of FtsZ inhibitor F332 at concentrations (A) $\text{MIC} \times 0.5$, (B) $\text{MIC} \times 1$ and (C) $\text{MIC} \times 2$.

A

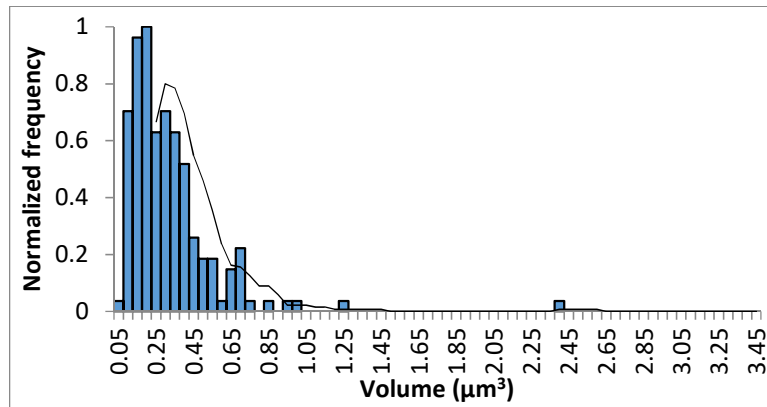


B

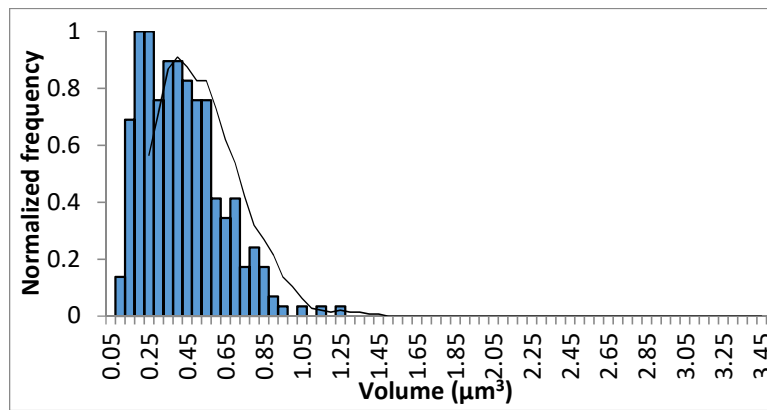


Appendix II. 4 Frequency distribution histograms of cell in the presence of FtsZ inhibitor PC190723 at sub-lethal concentrations (A) 0.065 $\mu\text{g}/\text{mL}$, (B) 0.25 $\mu\text{g}/\text{mL}$.

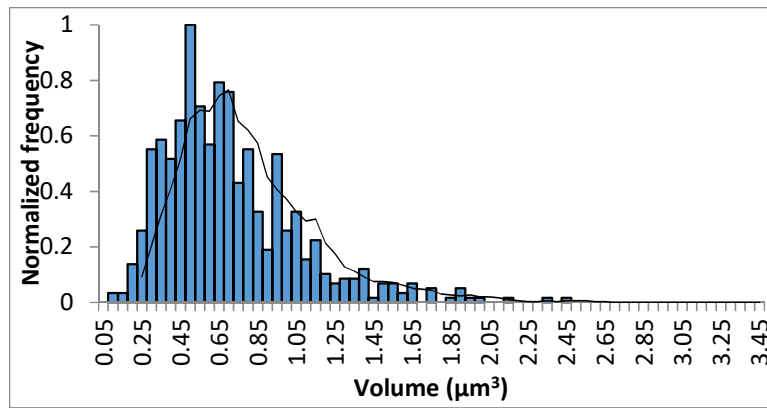
A



B

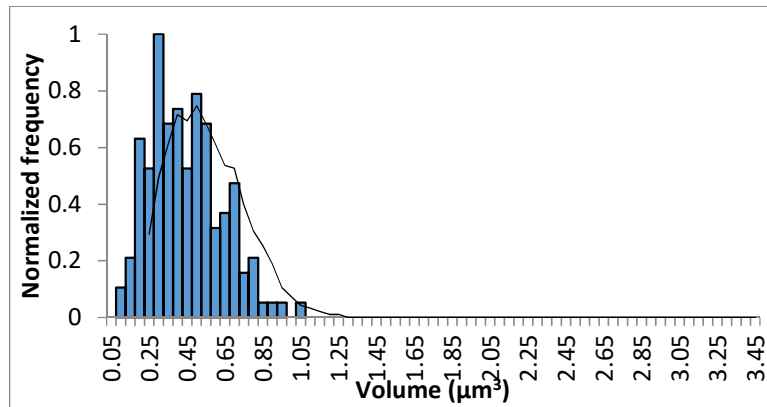


C

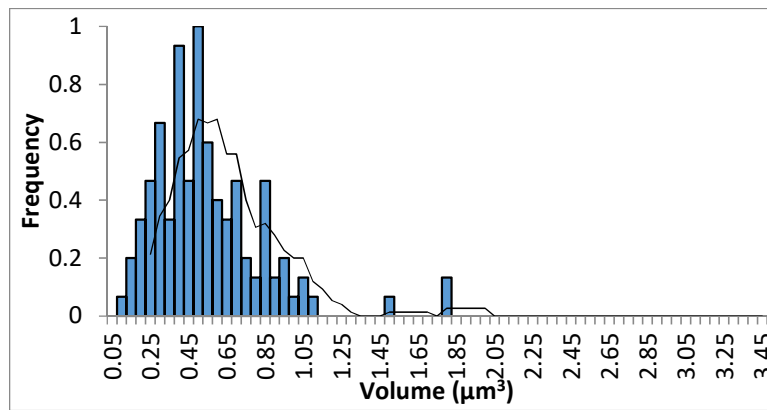


Appendix II. 5 Frequency distribution histograms of cell in the presence of FtsZ inhibitor PC190723 at concentrations (A) $\text{MIC} \times 0.5$, (B) $\text{MIC} \times 1$ and (C) $\text{MIC} \times 2$.

A

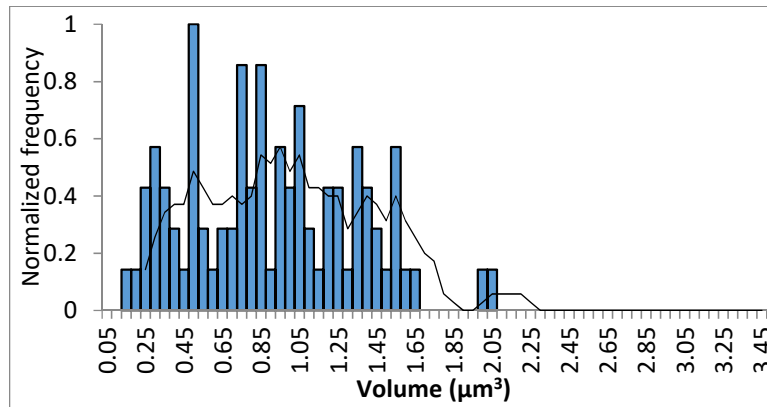


B

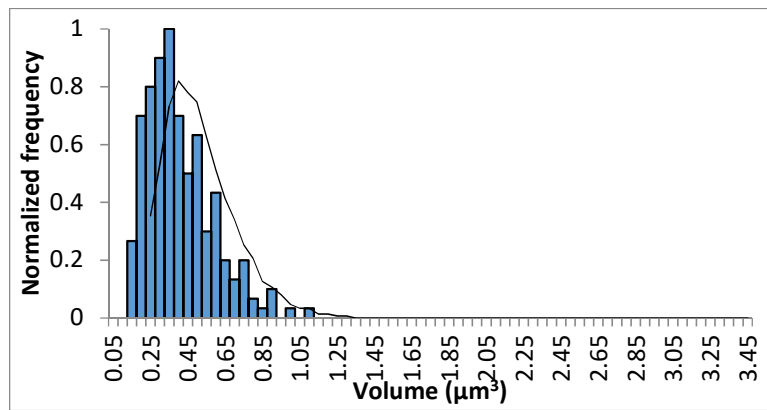


Appendix II. 6 Frequency distribution histograms of cell in the presence of oxacillin at sub-lethal concentrations (A) 8 $\mu\text{g}/\text{mL}$ and (B) 16 $\mu\text{g}/\text{mL}$.

A

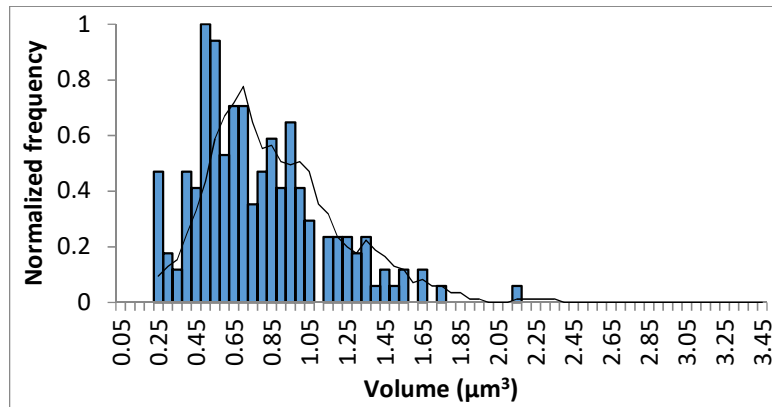


B

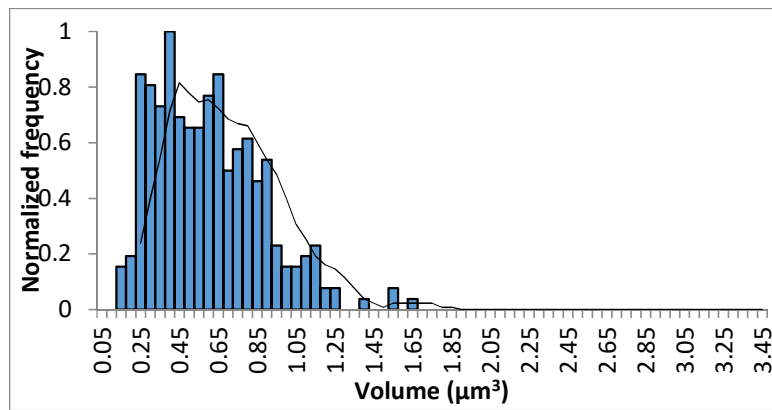


Appendix II. 7 Frequency distribution histograms of cell in the presence of oxacillin at sub-lethal concentrations (A) 32 $\mu\text{g}/\text{mL}$ and (B) 64 $\mu\text{g}/\text{mL}$.

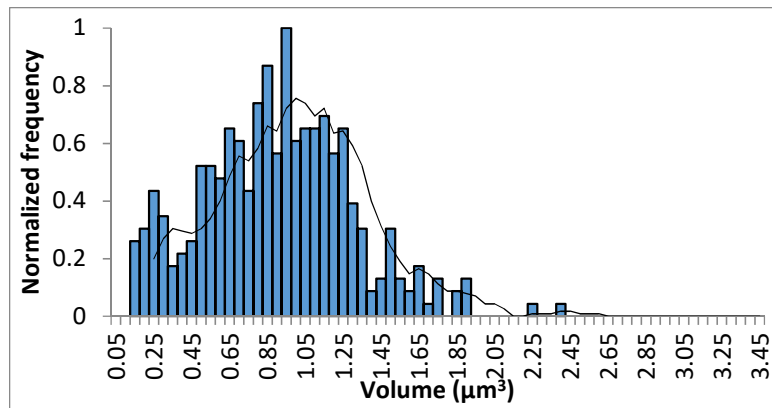
A



B



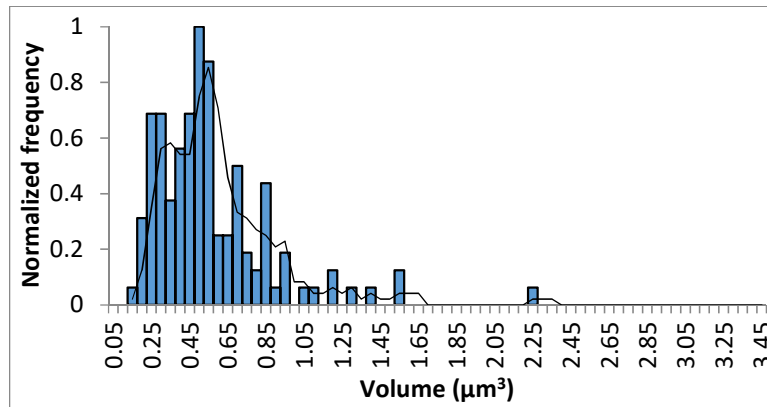
C



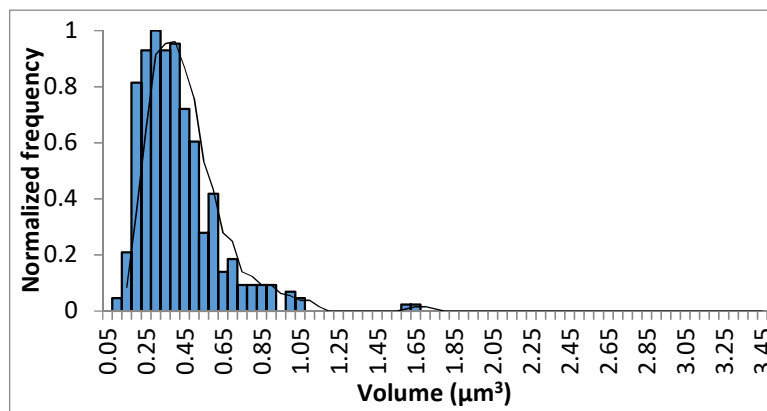
Appendix II. 8 Frequency distribution histograms of cell in the presence of oxacillin

at concentrations (A) $\text{MIC} \times 0.5$, (B) $\text{MIC} \times 1$ and (C) $\text{MIC} \times 2$.

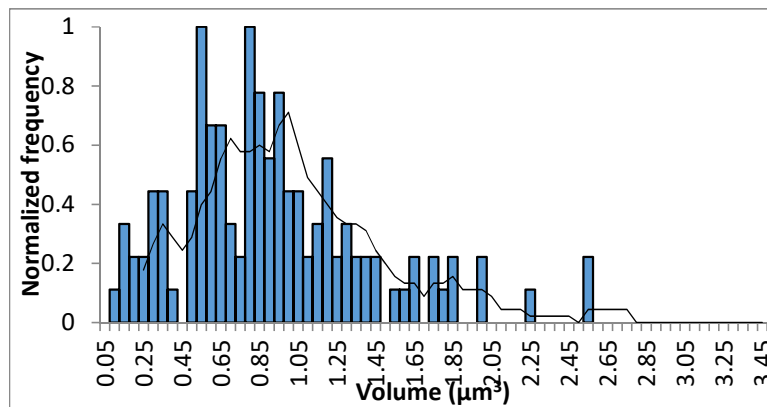
A



B

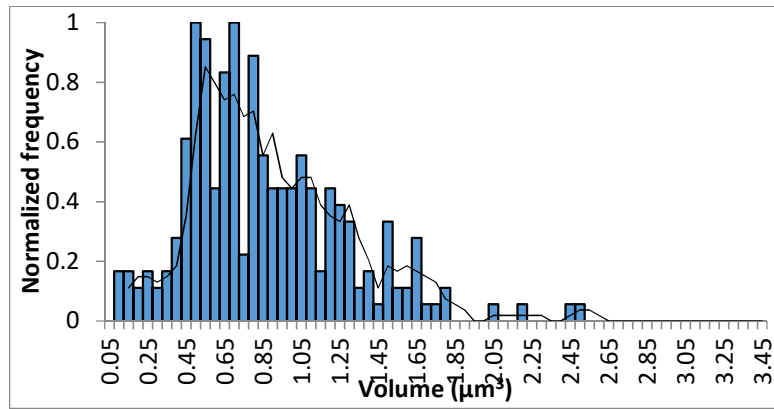


C

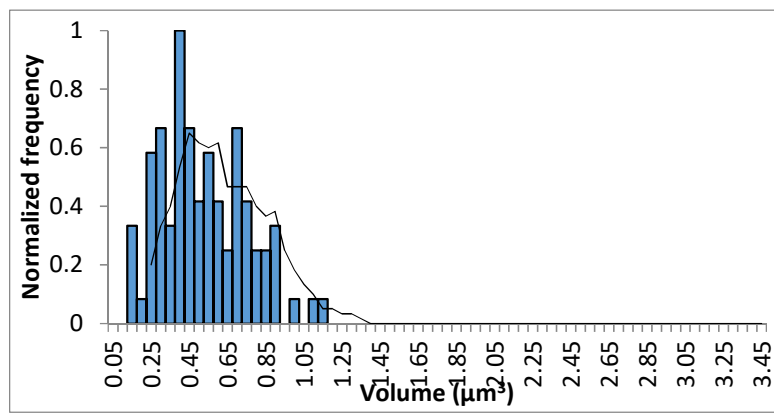


Appendix II. 9 Frequency distribution histograms of cell in the presence of methicillin at sub-lethal concentrations (A) 32 $\mu\text{g/mL}$, (B) 64 $\mu\text{g/mL}$ and (C) 128 $\mu\text{g/mL}$.

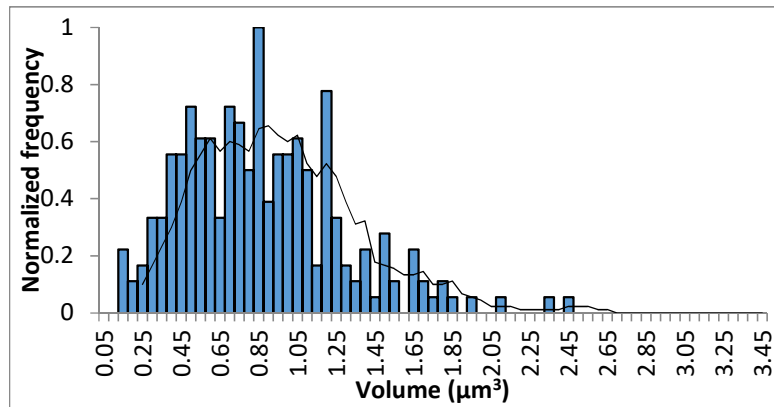
A



B



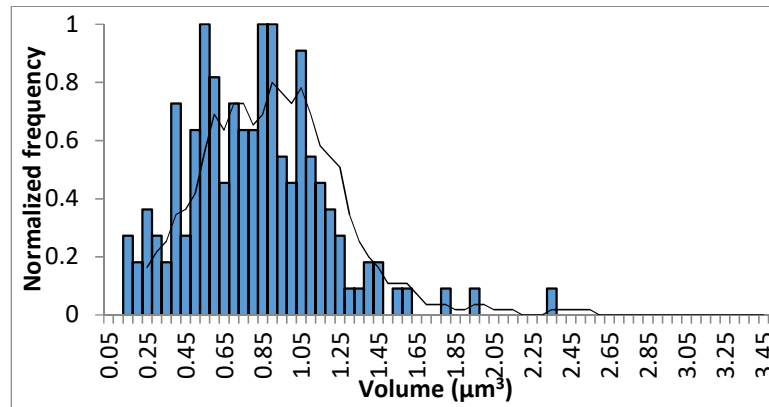
C



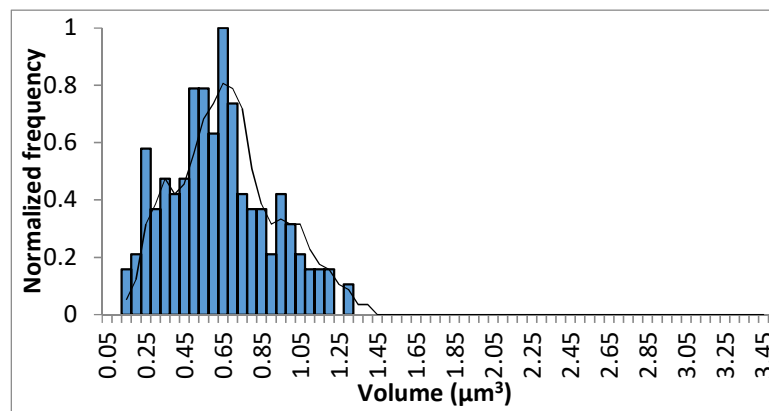
Appendix II. 10 Frequency distribution histograms of cell in the presence of methicillin

at concentrations (A) $\text{MIC} \times 0.5$, (B) $\text{MIC} \times 1$ and (C) $\text{MIC} \times 2$.

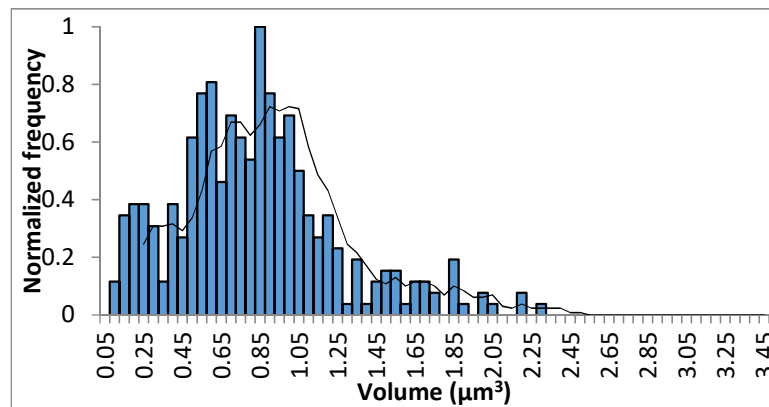
A



B

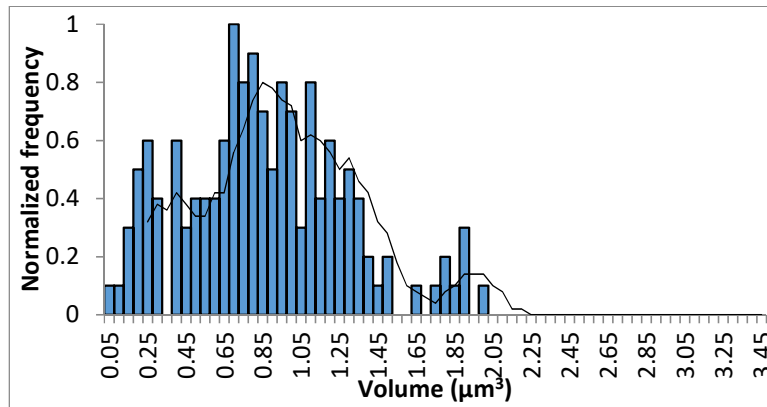


C

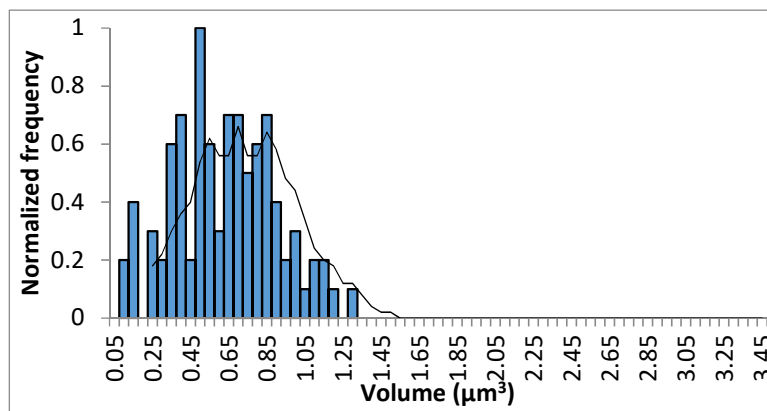


Appendix II. 11 Frequency distribution histograms of cell in the presence of F332 and oxacillin combination at concentrations (A) $\text{MIC} \times 0.5$, (B) $\text{MIC} \times 1$ and (C) $\text{MIC} \times 2$.

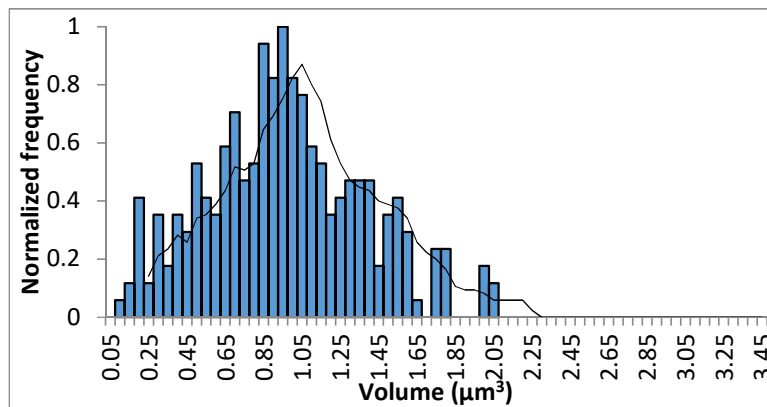
A



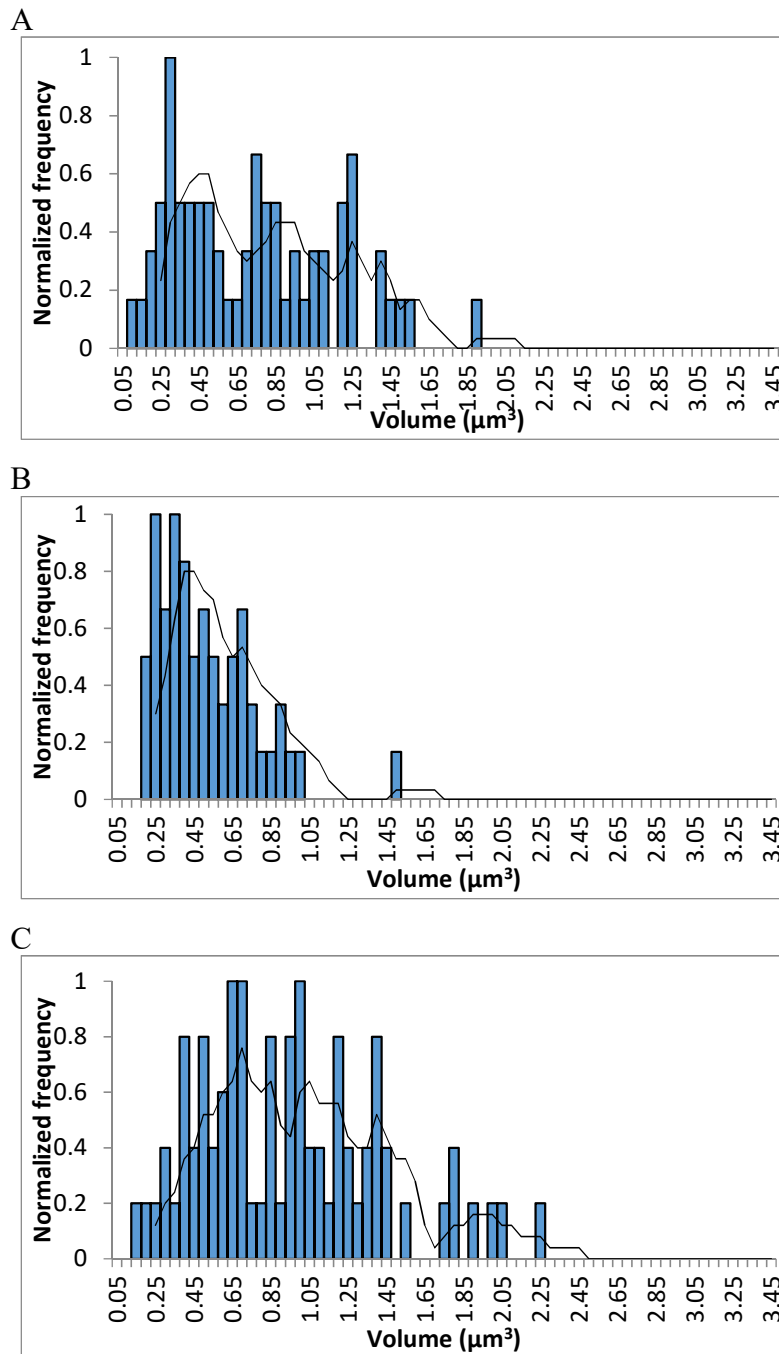
B



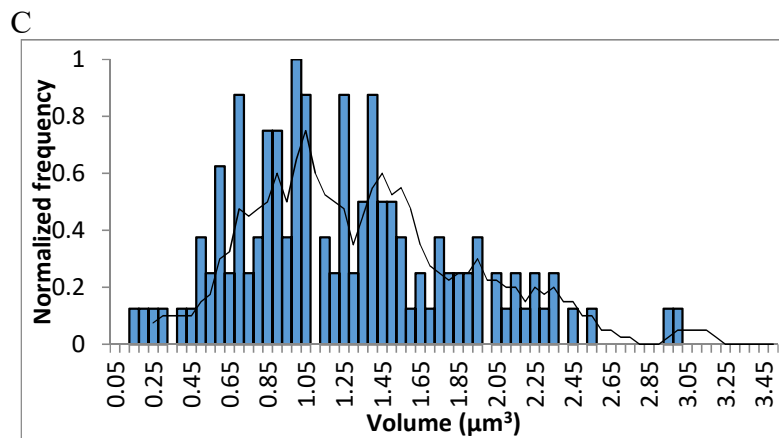
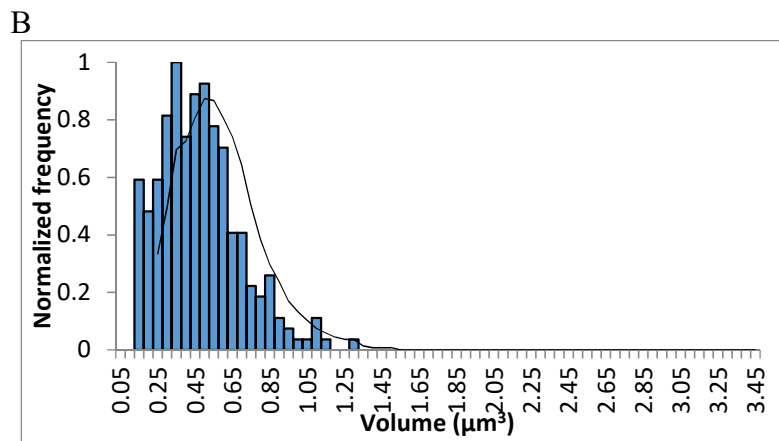
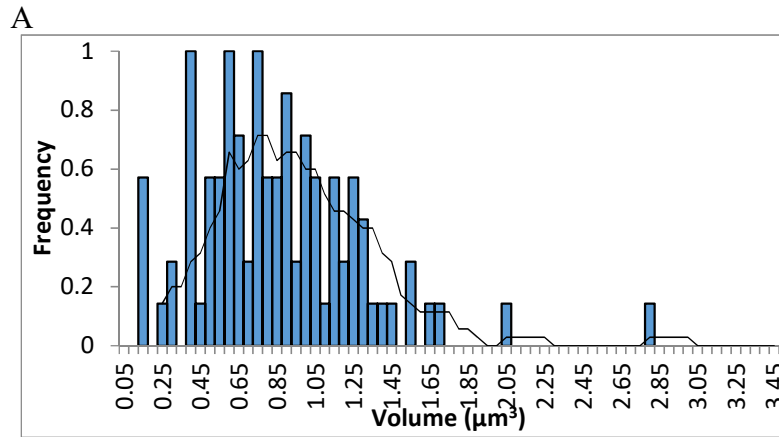
C



Appendix II. 12 Frequency distribution histograms of cell in the presence of F332 and methicillin combination at concentrations (A) $\text{MIC} \times 0.5$, (B) $\text{MIC} \times 1$ and (C) $\text{MIC} \times 2$.



Appendix II. 13 Frequency distribution histograms of cell in the presence of PC190723 and oxacillin combination at concentrations (A) $\text{MIC} \times 0.5$, (B) $\text{MIC} \times 1$ and (C) $\text{MIC} \times 2$.



Appendix II. 14 Frequency distribution histograms of cell in the presence of PC190723 and methicillin combination at concentrations (A) $\text{MIC} \times 0.5$, (B) $\text{MIC} \times 1$ and (C) $\text{MIC} \times 2$.

References

1. Boucher H, Miller LG, & Razonable RR (2010) Serious Infections Caused by Methicillin-Resistant *Staphylococcus aureus*. *Clinical Infectious Diseases* 51(Supplement 2):S183-S197.
2. Archer GL (1998) *Staphylococcus aureus*: a Well-Armed Pathogen. *Clinical Infectious Diseases* 26(5):1179-1181.
3. Rehm SJ & Tice A (2010) *Staphylococcus aureus*: Methicillin-Susceptible *S. aureus* to Methicillin-Resistant *S. aureus* and Vancomycin-Resistant *S. aureus*. *Clinical Infectious Diseases* 51(Supplement 2):S176-S182.
4. Neu HC (1992) The Crisis in Antibiotic Resistance. *Science* 257(5073):1064-1073.
5. Kobayashi SD & DeLeo FR (2009) An Update on Community-Associated MRSA Virulence. *Current Opinion in Pharmacology* 9(5):545-551.
6. Walsh C (2000) Molecular Mechanisms That Confer Antibacterial Drug Resistance. *Nature* 406(6797):775-781.
7. Walsh C (2003) *Antibiotics: Actions, Origins, Resistance* (American Society for Microbiology (ASM)).
8. Kaatz GW, McAleese F, & Seo SM (2005) Multidrug Resistance in *Staphylococcus aureus* Due to Overexpression of a Novel Multidrug and Toxin Extrusion (MATE) Transport Protein. *Antimicrobial Agents and Chemotherapy* 49(5):1857-1864.
9. Pootoolal J, Neu J, & Wright GD (2002) Glycopeptide Antibiotic Resistance. *Annual Review of Pharmacology and Toxicology* 42(1):381-408.
10. Hawkey PM (1998) The Origins and Molecular Basis of Antibiotic Resistance. *British Medical Journal* 317(7159):657.
11. Daschner FD (1976) Combination of Bacteriostatic and Bactericidal Drugs:

- Lack of Significant *In Vitro* Antagonism between Penicillin, Cephalothin, and Rolitetracycline. *Antimicrobial Agents and Chemotherapy* 10(5):802-808.
12. Bayer A & Morrison J (1984) Disparity Between Timed-Kill and Checkerboard Methods for Determination of *In Vitro* Bactericidal Interactions of Vancomycin Plus Rifampin Versus Methicillin-Susceptible and Resistant-*Staphylococcus aureus*. *Antimicrobial Agents and Chemotherapy* 26(2):220-223.
 13. Chou T-C (2006) Theoretical Basis, Experimental Design, and Computerized Simulation of Synergism and Antagonism in Drug Combination Studies. *Pharmacological Reviews* 58(3):621-681.
 14. Townsend CA (2002) New Reactions in Clavulanic Acid Biosynthesis. *Current Opinion in Chemical Biology* 6(5):583-589.
 15. Baggaley KH, Brown AG, & Schofield CJ (1997) Chemistry and Biosynthesis of Clavulanic Acid and Other Clavams. *Natural Product Reports* 14(4):309-333.
 16. Tan CM, *et al.* (2012) Restoring Methicillin-Resistant *Staphylococcus aureus* Susceptibility to β -Lactam Antibiotics. *Science Translational Medicine* 4(126):126ra135-126ra135.
 17. Tzagoloff H & Novick R (1977) Geometry of Cell Division in *Staphylococcus aureus*. *Journal of Bacteriology* 129(1):343-350.
 18. Marshall JH & Wilmoth GJ (1981) Pigments of *Staphylococcus aureus*, a Series of Triterpenoid Carotenoids. *Journal of Bacteriology* 147(3):900-913.
 19. Cui L, *et al.* (2006) Novel Mechanism of Antibiotic Resistance Originating in Vancomycin-Intermediate *Staphylococcus aureus*. *Antimicrobial Agents and Chemotherapy* 50(2):428-438.
 20. Dmitriev BA, Toukach FV, Holst O, Rietschel E, & Ehlers S (2004) Tertiary Structure of *Staphylococcus aureus* Cell Wall Murein. *Journal of Bacteriology*

- 186(21):7141-7148.
21. Errington J, Daniel RA, & Scheffers D-J (2003) Cytokinesis in Bacteria. *Microbiology and Molecular Biology Reviews* 67(1):52-65.
 22. Scheffers D-J & Pinho MG (2005) Bacterial Cell Wall Synthesis: New Insights from Localization Studies. *Microbiology and Molecular Biology Reviews* 69(4):585-607.
 23. Pinho MG, Kjos M, & Veening J-W (2013) How to Get (A)round: Mechanisms Controlling Growth and Division of Coccoid Bacteria. *Nature Reviews Microbiology* 11(9):601-614.
 24. Daniel RA & Errington J (2003) Control of Cell Morphogenesis in Bacteria: Two Distinct Ways to Make a Rod-Shaped Cell. *Cell* 113(6):767-776.
 25. van den Ent F, Amos LA, & Löwe J (2001) Prokaryotic Origin of the Actin Cytoskeleton. *Nature* 413(6851):39-44.
 26. Salje J, van den Ent F, de Boer P, & Löwe J (2011) Direct Membrane Binding by Bacterial Actin MreB. *Molecular Cell* 43(3):478-487.
 27. Doi M, *et al.* (1988) Determinations of the DNA Sequence of the *mreB* Gene and of the Gene Products of the *mre* Region That Function in Formation of the Rod Shape of *Escherichia coli* Cells. *Journal of Bacteriology* 170(10):4619-4624.
 28. Abhayawardhane Y & Stewart GC (1995) *Bacillus subtilis* possesses a Second Determinant with Extensive Sequence Similarity to the *Escherichia coli* MreB Morphogene. *Journal of Bacteriology* 177(3):765-773.
 29. Figge RM, Divakaruni AV, & Gober JW (2004) MreB, the Cell Shape-Determining Bacterial Actin Homologue, Co-ordinates Cell Wall Morphogenesis in *Caulobacter crescentus*. *Molecular Microbiology*

- 51(5):1321-1332.
30. Jones LJ, Carballido-López R, & Errington J (2001) Control of Cell Shape in Bacteria: Helical, Actin-like Filaments in *Bacillus subtilis*. *Cell* 104(6):913-922.
 31. Garner EC, *et al.* (2011) Coupled, Circumferential Motions of the Cell Wall Synthesis Machinery and MreB Filaments in *B. subtilis*. *Science* 333(6039):222-225.
 32. Domínguez-Escobar J, *et al.* (2011) Processive Movement of MreB-Associated Cell Wall Biosynthetic Complexes in Bacteria. *Science* 333(6039):225-228.
 33. Typas A, Banzhaf M, Gross CA, & Vollmer W (2012) From the Regulation of Peptidoglycan Synthesis to Bacterial Growth and Morphology. *Nature Reviews Microbiology* 10(2):123-136.
 34. Giesbrecht P, Wecke J, & Reinicke B (1976) On the Morphogenesis of the Cell Wall of *Staphylococci*. *International Review of Cytology* 44:225-318.
 35. Pinho MG & Errington J (2003) Dispersed Mode of *Staphylococcus aureus* Cell Wall Synthesis in the Absence of the Division Machinery. *Molecular Microbiology* 50(3):871-881.
 36. Lutkenhaus J & Addinall S (1997) Bacterial Cell Division And the Z Ring. *Annual Review of Biochemistry* 66(1):93-116.
 37. Møller-Jensen J & Löwe J (2005) Increasing Complexity of the Bacterial Cytoskeleton. *Current Opinion in Cell Biology* 17(1):75-81.
 38. de Boer PA (2016) Classic Spotlight: Discovery of FtsZ. *Journal of Bacteriology* 198(8):1184-1184.
 39. Margolin W (2000) Themes and Variations in Prokaryotic Cell Division. *FEMS microbiology reviews* 24(4):531-548.
 40. Begg KJ & Donachie WD (1985) Cell Shape and Division in *Escherichia coli*:

- Experiments with Shape and Division Mutants. *Journal of Bacteriology* 163(2):615-622.
41. Sun Q & Margolin W (1998) FtsZ Dynamics During the Division Cycle of Live *Escherichia coli* Cells. *Journal of Bacteriology* 180(8):2050-2056.
 42. Scheffers D-J, de Wit JG, den Blaauwen T, & Driessen AJ (2002) GTP Hydrolysis of Cell Division Protein FtsZ: Evidence that the Active Site Is Formed by the Association of Monomers. *Biochemistry* 41(2):521-529.
 43. Nogales E, Downing KH, Amos LA, & Löwe J (1998) Tubulin and FtsZ form a Distinct Family of GTPases. *Nature Structural & Molecular Biology* 5(6):451-458.
 44. Erickson HP (1998) Atomic Structures of Tubulin and FtsZ. *Trends in Cell Biology* 8(4):133-137.
 45. van den Ent F, Amos L, & Löwe J (2001) Bacterial Ancestry of Actin and Tubulin. *Current Opinion in Microbiology* 4(6):634-638.
 46. Erickson HP (1995) FtsZ, a Prokaryotic Homolog of Tubulin? *Cell* 80(3):367-370.
 47. Löwe J & Amos LA (1998) Crystal Structure of the Bacterial Cell-Division Protein FtsZ. *Nature* 391(6663):203-206.
 48. De Boer P, Crossley R, & Rothfield L (1992) The Essential Bacterial Cell-Division Protein FtsZ Is a GTPase. *Nature* 359(6392):254-256.
 49. Mukherjee A, Dai K, & Lutkenhaus J (1993) *Escherichia coli* Cell Division Protein FtsZ Is a Guanine Nucleotide Binding Protein. *Proceedings of the National Academy of Sciences* 90(3):1053-1057.
 50. de Pereda JM, Leynadier D, Evangelio JA, Chacón P, & Andreu JM (1996) Tubulin Secondary Structure Analysis, Limited Proteolysis Sites, and

- Homology to FtsZ. *Biochemistry* 35(45):14203-14215.
51. Adams DW & Errington J (2009) Bacterial Cell Division: Assembly, Maintenance and Disassembly of the Z Ring. *Nature Reviews Microbiology* 7(9):642-653.
 52. Matsui T, *et al.* (2012) Structural Reorganization of the Bacterial Cell-Division Protein FtsZ from *Staphylococcus aureus*. *Acta Crystallographica Section D* 68(9):1175-1188.
 53. Trueba FJ (1982) On the Precision and Accuracy Achieved by *Escherichia coli* Cells at Fission about Their Middle. *Archives of Microbiology* 131(1):55-59.
 54. Migocki MD, Freeman MK, Wake RG, & Harry EJ (2002) The Min System is Not Required for Precise Placement of the Mid cell Z Ring in *Bacillus subtilis*. *EMBO Reports* 3(12):1163-1167.
 55. Raskin DM & de Boer PA (1999) MinDE-Dependent Pole-to-Pole Oscillation of Division Inhibitor MinC in *Escherichia coli*. *Journal of Bacteriology* 181(20):6419-6424.
 56. Hu Z, Mukherjee A, Pichoff S, & Lutkenhaus J (1999) The MinC Component of the Division Site Selection System in *Escherichia coli* Interacts with FtsZ to Prevent Polymerization. *Proceedings of the National Academy of Sciences* 96(26):14819-14824.
 57. Rowlett VW & Margolin W (2013) The Bacterial Min System. *Current Biology* 23(13):R553-R556.
 58. Lutkenhaus J (2007) Assembly Dynamics of the Bacterial MinCDE System and Spatial Regulation of the Z Ring. *Annual Reviews Biochemistry* 76:539-562.
 59. Wu LJ & Errington J (2004) Coordination of Cell Division and Chromosome Segregation by a Nucleoid Occlusion Protein in *Bacillus subtilis*. *Cell*

- 117(7):915-925.
60. Bernhardt TG & De Boer PA (2005) SlmA, a Nucleoid-Associated, FtsZ Binding Protein Required for Blocking Septal Ring Assembly Over Chromosomes in *E. coli*. *Molecular Cell* 18(5):555-564.
 61. Wu LJ & Errington J (2012) Nucleoid Occlusion and Bacterial Cell Division. *Nature Reviews Microbiology* 10(1):8-12.
 62. Veiga H, Jorge AM, & Pinho MG (2011) Absence of Nucleoid Occlusion Effector Noc Impairs Formation of Orthogonal FtsZ Rings During *Staphylococcus aureus* Cell Division. *Molecular Microbiology* 80(5):1366-1380.
 63. Löwe J & Amos LA (1999) Tubulin-Like Protofilaments in Ca²⁺-Induced FtsZ Sheets. *The EMBO Journal* 18(9):2364-2371.
 64. Mukherjee A, Saez C, & Lutkenhaus J (2001) Assembly of an FtsZ Mutant Deficient in GTPase Activity Has Implications for FtsZ Assembly and the Role of the Z Ring in Cell Division. *Journal of Bacteriology* 183(24):7190-7197.
 65. Mukherjee A & Lutkenhaus J (1998) Dynamic Assembly of FtsZ Regulated by GTP Hydrolysis. *The EMBO Journal* 17(2):462-469.
 66. Stricker J, Maddox P, Salmon E, & Erickson HP (2002) Rapid Assembly Dynamics of the *Escherichia coli* FtsZ-Ring Demonstrated by Fluorescence Recovery after Photobleaching. *Proceedings of the National Academy of Sciences* 99(5):3171-3175.
 67. Scheffers D-J, Den Blaauwen T, & Driessen AJ (2000) Non-Hydrolysable GTP- γ -S Stabilizes the FtsZ Polymer in a GDP-Bound State. *Molecular Microbiology* 35(5):1211-1219.
 68. Bi E & Lutkenhaus J (1991) FtsZ Ring Structure Associated with Division in

- Escherichia coli*. *Nature* 354:161-164.
69. Hale CA & de Boer PA (1997) Direct Binding of FtsZ to ZipA, an Essential Component of the Septal Ring Structure That Mediates Cell Division in *E. coli*. *Cell* 88(2):175-185.
 70. Hale CA & De Boer PA (1999) Recruitment of ZipA to the Septal Ring of *Escherichia coli* Is Dependent on FtsZ and Independent of FtsA. *Journal of Bacteriology* 181(1):167-176.
 71. Pichoff S & Lutkenhaus J (2002) Unique and Overlapping Roles for ZipA and FtsA in Septal Ring Assembly in *Escherichia coli*. *The EMBO Journal* 21(4):685-693.
 72. Ortiz C, Natale P, Cueto L, & Vicente M (2016) The Keepers of the Ring: Regulators of FtsZ Assembly. *FEMS Microbiology Reviews* 40(1):57-67.
 73. Ebersbach G, Galli E, Møller-Jensen J, Löwe J, & Gerdes K (2008) Novel Coiled-Coil Cell Division Factor ZapB Stimulates Z Ring Assembly and Cell Division. *Molecular Microbiology* 68(3):720-735.
 74. Galli E & Gerdes K (2010) Spatial Resolution of Two Bacterial Cell Division Proteins: ZapA Recruits ZapB to the Inner Face of the Z-Ring. *Molecular Microbiology* 76(6):1514-1526.
 75. Huang K-H (2016) Molecular Analysis of FtsZ-Ring Assembly in *E. coli* cytokinesis. Ph.D. (The Graduate Center, City University of New York).
 76. Durand-Heredia JM, Helen HY, De Carlo S, Lesser CF, & Janakiraman A (2011) Identification and Characterization of ZapC, a Stabilizer of the FtsZ Ring in *Escherichia coli*. *Journal of Bacteriology* 193(6):1405-1413.
 77. Hale CA, *et al.* (2011) Identification of *Escherichia coli* ZapC (YcbW) as a Component of the Division Apparatus that Binds and Bundles FtsZ Polymers.

- Journal of Bacteriology* 193(6):1393-1404.
78. Addinall SG & Lutkenhaus J (1996) FtsA Is Localized to the Septum in an FtsZ-Dependent Manner. *Journal of Bacteriology* 178(24):7167-7172.
 79. Ma X, Ehrhardt DW, & Margolin W (1996) Colocalization of Cell Division Proteins FtsZ and FtsA to Cytoskeletal Structures in Living *Escherichia coli* Cells by using Green Fluorescent Protein. *Proceedings of the National Academy of Sciences* 93(23):12998-13003.
 80. Yan K, Pearce KH, & Payne DJ (2000) A Conserved Residue at the Extreme C-Terminus of FtsZ Is Critical for the FtsA-FtsZ Interaction in *Staphylococcus aureus*. *Biochemical and Biophysical Research Communications* 270(2):387-392.
 81. Bottomley AL, *et al.* (2014) *Staphylococcus aureus* DivIB Is a Peptidoglycan-Binding Protein that Is Required for a Morphological Checkpoint in Cell Division. *Molecular Microbiology* 94(5):1041-1064.
 82. Hale CA & De Boer PA (2002) ZipA Is Required for Recruitment of FtsK, FtsQ, FtsL, and FtsN to the Septal Ring in *Escherichia coli*. *Journal of Bacteriology* 184(9):2552-2556.
 83. Bigot S, Sivanathan V, Possoz C, Barre FX, & Cornet F (2007) FtsK, a Literate Chromosome Segregation Machine. *Molecular Microbiology* 64(6):1434-1441.
 84. Müller P, *et al.* (2007) The Essential Cell Division Protein FtsN Interacts with the Murein (Peptidoglycan) Synthase PBP1B in *Escherichia coli*. *Journal of Biological Chemistry* 282(50):36394-36402.
 85. Crozat E & Grainge I (2010) FtsK DNA Translocase: the Fast Motor That Knows Where It's Going. *Chembiochem* 11(16):2232-2243.
 86. Spratt BG (1977) Temperature-Sensitive Cell Division Mutants of *Escherichia*

- coli* with Thermolabile Penicillin-Binding Proteins. *Journal of Bacteriology* 131(1):293-305.
87. Mohammadi T, *et al.* (2011) Identification of FtsW as a Transporter of Lipid-Linked Cell Wall Precursors Across the Membrane. *The EMBO Journal* 30(8):1425-1432.
 88. Ikeda M, *et al.* (1989) Structural Similarity Among *Escherichia coli* FtsW and RodA Proteins and *Bacillus subtilis* SpoVE Protein, Which Function in Cell Division, Cell Elongation, and Spore Formation, Respectively. *Journal of Bacteriology* 171(11):6375-6378.
 89. Mercer KL & Weiss DS (2002) The *Escherichia coli* Cell Division Protein FtsW Is Required to Recruit Its Cognate Transpeptidase, FtsI (PBP3), to the Division Site. *Journal of Bacteriology* 184(4):904-912.
 90. Zapun A, Vernet T, & Pinho MG (2008) The Different Shapes of Cocci. *FEMS Microbiology Reviews* 32(2):345-360.
 91. Chung HS, *et al.* (2009) Rapid β -Lactam-Induced Lysis Requires Successful Assembly of the Cell Division Machinery. *Proceedings of the National Academy of Sciences* 106(51):21872-21877.
 92. Beall B & Lutkenhaus J (1991) FtsZ in *Bacillus subtilis* Is Required for Vegetative Septation and for Asymmetric Septation During Sporulation. *Genes & Development* 5(3):447-455.
 93. Dai K & Lutkenhaus J (1991) *ftsZ* Is an Essential Cell Division Gene in *Escherichia coli*. *Journal of Bacteriology* 173(11):3500-3506.
 94. Huo Y, Lu Q, Zheng X, Ma Y, & Lu F (2016) E75, R78 and D82 of *Escherichia coli* FtsZ Are Key Residues for FtsZ Cellular Self-Assembly and FtsZ-MreB Interaction. *Acta microbiologica Sinica* 56(2):264.

95. Cabeen MT & Jacobs-Wagner C (2005) Bacterial Cell Shape. *Nature Reviews Microbiology* 3(8):601-610.
96. Spratt B, Boyd A, & Stoker N (1980) Defective and Plaque-Forming Lambda Transducing Bacteriophage Carrying Penicillin-Binding Protein-Cell Shape Genes: Genetic and Physical Mapping and Identification of Gene Products from the *lip-dacA-rodA-pbpA-leuS* Region of the *Escherichia coli* Chromosome. *Journal of Bacteriology* 143(2):569-581.
97. Henriques AO, Glaser P, Piggot PJ, & Moran Jr CP (1998) Control of Cell Shape and Elongation by the *rodA* Gene in *Bacillus subtilis*. *Molecular Microbiology* 28(2):235-247.
98. Boyle DS, Khattar MM, Addinall SG, Lutkenhaus J, & Donachie WD (1997) *ftsW* Is an Essential Cell-Division Gene in *Escherichia coli*. *Molecular Microbiology* 24(6):1263-1273.
99. Beuria TK, Santra MK, & Panda D (2005) Sanguinarine Blocks Cytokinesis in Bacteria by Inhibiting FtsZ Assembly and Bundling. *Biochemistry* 44(50):16584-16593.
100. Wolff J & Knipling L (1993) Antimicrotubule Properties of Benzophenanthridine Alkaloids. *Biochemistry* 32(48):13334-13339.
101. Slaninová I, Táborská E, Bochořáková H, & Slanina J (2001) Interaction of Benzo[c]Phenanthridine and Protoberberine Alkaloids with Animal and Yeast Cells. *Cell Biology and Toxicology* 17(1):51-63.
102. Jaiswal R, Beuria TK, Mohan R, Mahajan SK, & Panda D (2007) Totarol Inhibits Bacterial Cytokinesis by Perturbing the Assembly Dynamics of FtsZ. *Biochemistry* 46(14):4211-4220.
103. Plaza A, Keffer JL, Bifulco G, Lloyd JR, & Bewley CA (2010) Chrysopaentins

- A-H, Antibacterial Bisdiarylbutene Macrocycles That Inhibit the Bacterial Cell Division Protein FtsZ. *Journal of the American Chemical Society* 132(26):9069-9077.
104. Schaffner-Barbero C, Martín-Fontecha M, Chacón P, & Andreu JM (2011) Targeting the Assembly of Bacterial Cell Division Protein FtsZ with Small Molecules. *ACS chemical biology* 7(2):269-277.
105. Wang J, *et al.* (2003) Discovery of a Small Molecule That Inhibits Cell Division by Blocking FtsZ, a Novel Therapeutic Target of Antibiotics. *Journal of Biological Chemistry* 278(45):44424-44428.
106. Anderson DE, *et al.* (2012) Comparison of Small Molecule Inhibitors of the Bacterial Cell Division Protein FtsZ and Identification of a Reliable Cross-Species Inhibitor. *ACS Chemical Biology* 7(11):1918-1928.
107. Fabiano RJ & Tu AT (1981) Purification and Biochemical Study of Viriditoxin, Tissue Damaging Toxin, from Prairie Rattlesnake Venom. *Biochemistry* 20(1):21-27.
108. Rai D, Singh JK, Roy N, & Panda D (2008) Curcumin Inhibits FtsZ Assembly: an Attractive Mechanism for Its Antibacterial Activity. *Biochemical Journal* 410(1):147-155.
109. Kaur S, Modi NH, Panda D, & Roy N (2010) Probing the Binding Site of Curcumin in *Escherichia coli* and *Bacillus subtilis* FtsZ -a Structural Insight to Unveil Antibacterial Activity of Curcumin. *European Journal of Medicinal Chemistry* 45(9):4209-4214.
110. Kunwar A, *et al.* (2008) Quantitative Cellular Uptake, Localization and Cytotoxicity of Curcumin in Normal and Tumor Cells. *Biochimica et Biophysica Acta (BBA)-General Subjects* 1780(4):673-679.

111. Domadia PN, Bhunia A, Sivaraman J, Swarup S, & Dasgupta D (2008) Berberine Targets Assembly of *Escherichia coli* Cell Division Protein FtsZ. *Biochemistry* 47(10):3225-3234.
112. Li Z, Garner AL, Gloeckner C, Janda KD, & Carlow CK (2011) Targeting the Wolbachia Cell Division Protein FtsZ as a New Approach for Antifilarial Therapy. *PLoS Negl Trop Dis* 5(11):e1411.
113. Domadia P, Swarup S, Bhunia A, Sivaraman J, & Dasgupta D (2007) Inhibition of Bacterial Cell Division Protein FtsZ by Cinnamaldehyde. *Biochemical Pharmacology* 74(6):831-840.
114. Bhattacharya A, Jindal B, Singh P, Datta A, & Panda D (2013) Plumbagin Inhibits Cytokinesis in *Bacillus subtilis* by Inhibiting FtsZ Assembly - a Mechanistic Study of Its Antibacterial Activity. *FEBS Journal* 280(18):4585-4599.
115. Thorén LM, Tuomi J, Kämäräinen T, & Laine K (2003) Resource Availability Affects Investment in Carnivory in *Drosera Rotundifolia*. *New Phytologist* 159(2):507-511.
116. Rischer H, Hamm A, & Bringmann G (2002) *Nepenthes insignis* Uses a C 2-portion of the Carbon Skeleton of L-Alanine Acquired Via Its Carnivorous Organs, to Build up the Allelochemical Plumbagin. *Phytochemistry* 59(6):603-609.
117. Farr SB, Natvig DO, & Kogoma T (1985) Toxicity and Mutagenicity of Plumbagin And the Induction of a Possible New DNA Repair Pathway in *Escherichia coli*. *Journal of Bacteriology* 164(3):1309-1316.
118. Lämpchen T, *et al.* (2008) Probing FtsZ and Tubulin with C8-Substituted GTP Analogs Reveals Differences in Their Nucleotide Binding Sites. *Chemistry &*

- Biology* 15(2):189-199.
119. Lappchen T, Hartog AF, Pinas VA, Koomen G-J, & den Blaauwen T (2005) GTP Analogue Inhibits Polymerization and GTPase Activity of the Bacterial Protein FtsZ without Affecting Its Eukaryotic Homologue Tubulin. *Biochemistry* 44(21):7879-7884.
 120. Possoz C, Newmark J, Sorto N, Sherratt DJ, & Tolmasky ME (2007) Sublethal Concentrations of the Aminoglycoside Amikacin Interfere with Cell Division without Affecting Chromosome Dynamics. *Antimicrobial Agents and Chemotherapy* 51(1):252-256.
 121. Wang H-Z, CHANG C-H, LIN C-P, & TSAI M-C (1996) Using MTT Viability Assay to Test the Cytotoxicity of Antibiotics and Steroid to Cultured Porcine Corneal Endothelial Cells. *Journal of Ocular Pharmacology and Therapeutics* 12(1):35-43.
 122. White EL, Suling WJ, Ross LJ, Seitz LE, & Reynolds RC (2002) 2-Alkoxy-carbonylaminopyridines: Inhibitors of Mycobacterium Tuberculosis FtsZ. *Journal of Antimicrobial Chemotherapy* 50(1):111-114.
 123. Ito H, *et al.* (2006) A 4-Aminofurazan Derivative - A189 - Inhibits Assembly of Bacterial Cell Division Protein FtsZ *In Vitro* and *In Vivo*. *Microbiology and Immunology* 50(10):759-764.
 124. Margalit DN, *et al.* (2004) Targeting Cell Division: Small-Molecule Inhibitors of FtsZ GTPase Perturb Cytokinetic Ring Assembly and Induce Bacterial Lethality. *Proceedings of the National Academy of Sciences of the United States of America* 101(32):11821-11826.
 125. Ruiz-Avila LB, *et al.* (2013) Synthetic Inhibitors of Bacterial Cell Division Targeting the GTP-Binding Site of FtsZ. *ACS Chemical Biology* 8(9):2072-

- 2083.
126. Stokes NR, *et al.* (2005) Novel Inhibitors of Bacterial Cytokinesis Identified by a Cell-Based Antibiotic Screening Assay. *Journal of Biological Chemistry* 280(48):39709-39715.
 127. Haydon DJ, *et al.* (2008) An Inhibitor of FtsZ with Potent and Selective Anti-Staphylococcal Activity. *Science* 321(5896):1673-1675.
 128. Stokes NR, *et al.* (2013) An Improved Small-Molecule Inhibitor of FtsZ with Superior *In Vitro* Potency, Drug-Like Properties, and *In Vivo* Efficacy. *Antimicrobial Agents and Chemotherapy* 57(1):317-325.
 129. Matsui T, *et al.* (2012) Structural Reorganization of the Bacterial Cell-Division Protein FtsZ from *Staphylococcus aureus*. *Acta Crystallographica Section D: Biological Crystallography* 68(9):1175-1188.
 130. Clements MO & Foster SJ (1999) Stress Resistance in *Staphylococcus aureus*. *Trends in Microbiology* 7(11):458-462.
 131. Tsai M, *et al.* (2011) *Staphylococcus aureus* Requires Cardiolipin for Survival under Conditions of High Salinity. *BMC Microbiology* 11(1):13.
 132. Sonenshein AL, Hoch JA, & Losick R eds (2002) *Bacillus subtilis* and Its closest relatives: from genes to cells (American Society for Microbiology, Washington DC), pp 21-41.
 133. Antignac A, Sieradzki K, & Tomasz A (2007) Perturbation of Cell Wall Synthesis Suppresses Autolysis in *Staphylococcus aureus*: Evidence for Coregulation of Cell Wall Synthetic and Hydrolytic Enzymes. *Journal of Bacteriology* 189(21):7573-7580.
 134. Mazmanian SK, Ton-That H, & Schneewind O (2001) Sortase-Catalysed Anchoring of Surface Proteins to the Cell Wall of *Staphylococcus aureus*.

- Molecular Microbiology* 40(5):1049-1057.
135. Perry AM, Ton-That H, Mazmanian SK, & Schneewind O (2002) Anchoring of Surface Proteins to the Cell Wall of *Staphylococcus aureus* III. Lipid II is an *In Vivo* Peptidoglycan Substrate for Sortase-Catalyzed Surface Protein Anchoring. *Journal of Biological Chemistry* 277(18):16241-16248.
 136. Schleifer KH & Kandler O (1972) Peptidoglycan Types of Bacterial Cell Walls and Their Taxonomic Implications. *Bacteriological Reviews* 36(4):407.
 137. De Kimpe SJ, Kengatharan M, Thiemermann C, & Vane JR (1995) The Cell Wall Components Peptidoglycan and Lipoteichoic Acid from *Staphylococcus aureus* Act in Synergy to Cause Shock and Multiple Organ Failure. *Proceedings of the National Academy of Sciences* 92(22):10359-10363.
 138. Suginaka H, Blumberg PM, & Strominger JL (1972) Multiple Penicillin-Binding Components in *Bacillus subtilis*, *Bacillus cereus*, *Staphylococcus aureus*, and *Escherichia coli*. *Journal of Biological Chemistry* 247(17):5279-5288.
 139. Zapun A, Contreras-Martel C, & Vernet T (2008) Penicillin-Binding Proteins and β -Lactam Resistance. *FEMS Microbiology Reviews* 32(2):361-385.
 140. Höltje J-V (1998) Growth of the Stress-Bearing and Shape-Maintaining Murein Sacculus of *Escherichia coli*. *Microbiology and Molecular Biology Reviews* 62(1):181-203.
 141. Den Blaauwen T, De Pedro MA, Nguyen-Distèche M, & Ayala JA (2008) Morphogenesis of Rod-Shaped Sacculi. *FEMS Microbiology Reviews* 32(2):321-344.
 142. Reed P, Veiga H, Jorge AM, Terrak M, & Pinho MG (2011) Monofunctional Transglycosylases Are Not Essential for *Staphylococcus aureus* Cell Wall

- Synthesis. *Journal of Bacteriology* 193(10):2549-2556.
143. Goffin C & Ghuysen J-M (1998) Multimodular Penicillin-Binding Proteins: an Enigmatic Family of Orthologs and Paralogs. *Microbiology and Molecular Biology Reviews* 62(4):1079-1093.
 144. Wyke AW, Ward JB, Hayes MV, & Curtis NA (1981) A Role *In Vivo* for Penicillin-Binding Protein-4 of *Staphylococcus aureus*. *European Journal of Biochemistry* 119(2):389-393.
 145. Meberg BM, Paulson AL, Priyadarshini R, & Young KD (2004) Endopeptidase Penicillin-Binding Proteins 4 and 7 Play Auxiliary Roles in Determining Uniform Morphology of *Escherichia coli*. *Journal of Bacteriology* 186(24):8326-8336.
 146. Ghuysen J-M (1991) Serine β -Lactamases and Penicillin-Binding Proteins. *Annual Reviews in Microbiology* 45(1):37-67.
 147. Berger-Bächi B, Strässle A, & Kayser F (1986) Characterization of an Isogenic Set of Methicillin-Resistant and Susceptible Mutants of *Staphylococcus aureus*. *European Journal of Clinical Microbiology* 5(6):697-701.
 148. Pucci MJ, Thanassi JA, Discotto LF, Kessler RE, & Dougherty TJ (1997) Identification and Characterization of Cell Wall-Cell Division Gene Clusters in Pathogenic Gram-Positive cocci. *Journal of Bacteriology* 179(17):5632-5635.
 149. Pereira S, Henriques A, Pinho M, De Lencastre H, & Tomasz A (2007) Role of PBP1 in Cell Division of *Staphylococcus aureus*. *Journal of Bacteriology* 189(9):3525-3531.
 150. Pinho MG, de Lencastre H, & Tomasz A (2000) Cloning, Characterization, and Inactivation of the Gene *pbpC*, Encoding Penicillin-Binding Protein 3 of *Staphylococcus aureus*. *Journal of Bacteriology* 182(4):1074-1079.

151. Song MD, Wachi M, Doi M, Ishino F, & Matsushashi M (1987) Evolution of an Inducible Penicillin-Target Protein in Methicillin-Resistant *Staphylococcus aureus* by Gene Fusion. *FEBS Letters* 221(1):167-171.
152. Hartman BJ & Tomasz A (1984) Low-Affinity Penicillin-Binding Protein Associated with Beta-Lactam Resistance in *Staphylococcus aureus*. *Journal of Bacteriology* 158(2):513-516.
153. Reynolds PE & Brown DF (1985) Penicillin-Binding Proteins of β -Lactam-Resistant Strains of *Staphylococcus aureus*: Effect of Growth Conditions. *FEBS Letters* 192(1):28-32.
154. Domanski T & Bayles K (1995) Analysis of *Staphylococcus aureus* Genes Encoding Penicillin-Binding Protein 4 and an ABC-Type Transporter. *Gene* 167(1):111-113.
155. Atilano ML, *et al.* (2010) Teichoic Acids are Temporal and Spatial Regulators of Peptidoglycan Cross-Linking in *Staphylococcus aureus*. *Proceedings of the National Academy of Sciences* 107(44):18991-18996.
156. Wada A & Watanabe H (1998) Penicillin-Binding Protein 1 of *Staphylococcus aureus* is Essential for Growth. *Journal of Bacteriology* 180(10):2759-2765.
157. Yoshida H, *et al.* (2012) Crystal Structures of Penicillin-Binding Protein 3 (PBP3) from Methicillin-Resistant *Staphylococcus aureus* in the Apo and Cefotaxime-Bound Forms. *Journal of Molecular Biology* 423(3):351-364.
158. Crossley KB, Archer G, Jefferson K, & Fowler V (2009) *Staphylococci in Human Disease* (Wiley Online Library) pp 1-38.
159. Curtis NA, Hayes MV, Wyke AW, & Ward JB (1980) A Mutant of *Staphylococcus aureus* H Lacking Penicillin-Binding Protein 4 and Transpeptidase Activity *In Vitro*. *FEMS Microbiology Letters* 9:263-266.

160. Henze UU & Berger-Bächli B (1996) Penicillin-Binding Protein 4 Overproduction Increases β -Lactam Resistance in *Staphylococcus aureus*. *Antimicrobial Agents and Chemotherapy* 40(9):2121.
161. Chan LC, *et al.* (2016) PBP4 Mediates High-Level Resistance to New Generation Cephalosporins in *Staphylococcus aureus*. *Antimicrobial Agents and Chemotherapy*:AAC. 00358-00316.
162. Weiss DS, Chen JC, Ghigo J-M, Boyd D, & Beckwith J (1999) Localization of FtsI (PBP3) to the Septal Ring Requires Its Membrane Anchor, the Z Ring, FtsA, FtsQ, and FtsL. *Journal of Bacteriology* 181(2):508-520.
163. Scheffers D-J & Errington J (2004) PBP1 is a Component of the *Bacillus subtilis* Cell Division Machinery. *Journal of Bacteriology* 186(15):5153-5156.
164. Pedersen LB, Angert ER, & Setlow P (1999) Septal Localization of Penicillin-Binding Protein 1 in *Bacillus subtilis*. *Journal of Bacteriology* 181(10):3201-3211.
165. Pinho MG & Errington J (2005) Recruitment of Penicillin-Binding Protein PBP2 to the Division Site of *Staphylococcus aureus* Is Dependent on Its Transpeptidation Substrates. *Molecular Microbiology* 55(3):799-807.
166. Bernal P, *et al.* (2010) Insertion of Epicatechin Gallate into the Cytoplasmic Membrane of Methicillin-Resistant *Staphylococcus aureus* Disrupts Penicillin-Binding Protein (PBP) 2a-Mediated β -Lactam Resistance by Delocalizing PBP2. *Journal of Biological Chemistry* 285(31):24055-24065.
167. Schneewind O (2016) Classic Spotlight: Molecular Biology of Methicillin Resistance in *Staphylococcus aureus*. *Journal of Bacteriology* 198(14):1903-1903.
168. Pinho MG, de Lencastre H, & Tomasz A (2001) An Acquired And a Native

- Penicillin-Binding Protein Cooperate in Building the Cell Wall of Drug-Resistant *Staphylococci*. *Proceedings of the National Academy of Sciences* 98(19):10886-10891.
169. Tipper DJ & Strominger JL (1965) Mechanism of Action of Penicillins: a Proposal Based on Their Structural Similarity to Acyl-D-Alanyl-D-Alanine. *Proceedings of the National Academy of Sciences of the United States of America* 54(4):1133.
170. Yocum RR, Waxman DJ, Rasmussen JR, & Strominger JL (1979) Mechanism of Penicillin Action: Penicillin and Substrate Bind Covalently to the Same Active Site Serine in Two Bacterial D-Alanine Carboxypeptidases. *Proceedings of the National Academy of Sciences* 76(6):2730-2734.
171. Poole K (2004) Resistance to β -Lactam Antibiotics. *Cellular and Molecular Life Sciences CMLS* 61(17):2200-2223.
172. Fisher JF, Meroueh SO, & Mobashery S (2005) Bacterial Resistance to β -lactam Antibiotics: Compelling Opportunism, Compelling Opportunity. *Chemical Reviews* 105(2):395-424.
173. Drawz SM & Bonomo RA (2010) Three Decades of β -Lactamase Inhibitors. *Clinical Microbiology Reviews* 23(1):160-201.
174. Lim D & Strynadka NC (2002) Structural Basis for the β -lactam Resistance of PBP2a from Methicillin-Resistant *Staphylococcus aureus*. *Nature Structural & Molecular Biology* 9(11):870-876.
175. Otero LH, *et al.* (2013) How Allosteric Control of *Staphylococcus aureus* Penicillin Binding Protein 2a Enables Methicillin Resistance and Physiological Function. *Proceedings of the National Academy of Sciences* 110(42):16808-16813.

176. Lui HK (2014) Alkoxy-And Amino-Benzamides as Inhibitors of the Bacterial Cell Division Protein FtsZ and Antibacterial Agents. (The Hong Kong Polytechnic University).
177. Czaplewski LG, *et al.* (2009) Antibacterial Alkoxybenzamide Inhibitors of the Essential Bacterial Cell Division Protein FtsZ. *Bioorganic & Medicinal Chemistry Letters* 19(2):524-527.
178. Levison ME (2004) Pharmacodynamics of Antimicrobial Drugs. *Infectious Disease Clinics of North America* 18(3):451-465.
179. Ohashi Y, *et al.* (1999) The Lethal Effect of a Benzamide Derivative, 3-Methoxybenzamide, Can Be Suppressed by Mutations within a Cell Division Gene, *ftsZ*, in *Bacillus subtilis*. *Journal of Bacteriology* 181(4):1348-1351.
180. Kim K & Anthony BF (1981) Importance of Bacterial Growth Phase in Determining Minimal Bactericidal Concentrations of Penicillin And Methicillin. *Antimicrobial Agents And Chemotherapy* 19(6):1075-1077.
181. Pfaller M, Sheehan D, & Rex J (2004) Determination of Fungicidal Activities against Yeasts And Molds: Lessons Learned from Bactericidal Testing And the Need for Standardization. *Clinical Microbiology Reviews* 17(2):268-280.
182. Arthur L. Barry PD, *et al.* (1999) *Methods for Determining Bactericidal Activity of Antimicrobial Agents: Approved Guideline M26-A* (National Committee for Clinical and Laboratory Standards Institute).
183. Stratton CW (1987) *Methodology for the Serum Bactericidal Test* (National Committee for Clinical and Laboratory Standards Institute).
184. Pogliano J, Pogliano N, & Silverman JA (2012) Daptomycin-Mediated Reorganization of Membrane Architecture Causes Mislocalization of Essential Cell Division Proteins. *Journal of Bacteriology* 194(17):4494-4504.

185. Cotroneo N, Harris R, Perlmutter N, Beveridge T, & Silverman JA (2008) Daptomycin Exerts Bactericidal Activity without Lysis of *Staphylococcus aureus*. *Antimicrobial Agents and Chemotherapy* 52(6):2223-2225.
186. Hutter B, *et al.* (2004) Prediction of Mechanisms of Action of Antibacterial Compounds by Gene Expression Profiling. *Antimicrobial Agents and Chemotherapy* 48(8):2838-2844.
187. Wikler MA (2006) *Methods for Dilution Antimicrobial Susceptibility Tests for Bacteria That Grow Aerobically* (National Committee for Clinical and Laboratory Standards Institute) eighth edition Ed.
188. Sung WS & Lee DG (2008) Mechanism of Decreased Susceptibility for Gram-Negative Bacteria and Synergistic Effect with Ampicillin of Indole-3-Carbinol. *Biological and Pharmaceutical Bulletin* 31(9):1798-1801.
189. Peterson L & Shanholtzer C (1992) Tests for Bactericidal Effects of Antimicrobial Agents: Technical Performance and Clinical Relevance. *Clinical Microbiology Reviews* 5(4):420-432.
190. Wikler MA (2006) *Performance Standards for Antimicrobial Susceptibility Testing: Sixteenth Informational Supplement* (National Committee for Clinical and Laboratory Standards Institute).
191. Finch RG, Greenwood D, Whitley RJ, & Norrby SR (2010) *Antibiotic and chemotherapy* (Elsevier Health Sciences).
192. Dutfield G (2009) *Intellectual Property Rights and the Life Science Industries: Past, Present and Future* (World Scientific).
193. French G (2006) Bactericidal Agents in the Treatment of MRSA Infections - the Potential Role of Daptomycin. *Journal of Antimicrobial Chemotherapy* 58(6):1107-1117.

194. Fayyaz M, *et al.* (2013) *In Vitro* Susceptibility of Chloramphenicol Against Methicillin-Resistant *Staphylococcus aureus*. *Journal of the College of Physicians and Surgeons - Pakistan* 23(9):637-640.
195. Falagas ME & Kopterides P (2007) Old Antibiotics for Infections in Critically Ill Patients. *Current Opinion in Critical Care* 13(5):592-597.
196. Idrees F, Jabeen K, Khan MS, & Zafar A (2009) Antimicrobial Resistance Profile of Methicillin Resistant *Staphylococcal aureus* from Skin and Soft Tissue Isolates. *Journal of the Pakistan Medical Association* 59(5):266.
197. Wang Z, Cao B, Liu Y-M, Gu L, & Wang C (2009) Investigation of the Prevalence of Patients Co-Colonized or Infected with Methicillin-Resistant *Staphylococcus aureus* and Vancomycin-Resistant *Enterococci* in China: a Hospital-Based Study. *Chinese medical journal* 122(11):1283-1288.
198. Ginsburg I (2002) The Role of Bacteriolysis in the Pathophysiology of Inflammation, Infection and Post-Infectious Sequelae. *Apmis* 110(11):753-770.
199. Nau R & Eiffert H (2002) Modulation of Release of Proinflammatory Bacterial Compounds by Antibacterials: Potential Impact on Course of Inflammation and Outcome in Sepsis and Meningitis. *Clinical Microbiology Reviews* 15(1):95-110.
200. Chan F-Y, Sun N, Leung Y-C, & Wong K-Y (2015) Antimicrobial Activity of a Quinuclidine-Based FtsZ Inhibitor and Its Synergistic Potential with β -Lactam Antibiotics. *The Journal of Antibiotics* 68(4):253-258.
201. Sun N, *et al.* (2014) Rational Design of Berberine-Based FtsZ Inhibitors with Broad-Spectrum Antibacterial Activity. *PloS One* 9(5):e97514.
202. Lui HK (2014) Alkoxy-and Amino-Benzamides as Inhibitors of The Bacterial Cell Division Protein FtsZ And Antibacterial Agents. (The Hong Kong

- Polytechnic University).
203. Liew AT, *et al.* (2011) A Simple Plasmid-Based System that Allows Rapid Generation of Tightly Controlled Gene Expression in *Staphylococcus aureus*. *Microbiology* 157(3):666-676.
 204. Schenk S & Laddaga RA (1992) Improved Method for Electroporation of *Staphylococcus aureus*. *FEMS Microbiology Letters* 94(1-2):133-138.
 205. Crissman HA, Wilder ME, & Tobey RA (1988) Flow Cytometric Localization within the Cell Cycle and Isolation of Viable Cells Following Exposure to Cytotoxic Agents. *Cancer Research* 48(20):5742-5746.
 206. Hurley KA, *et al.* (2016) Targeting the Bacterial Division Protein FtsZ. *Journal of Medicinal Chemistry*.
 207. Gautam S, *et al.* (2015) An Activity-Based Probe for Studying Crosslinking in Live Bacteria. *Angewandte Chemie* 127(36):10638-10642.
 208. Tiyanont K, *et al.* (2006) Imaging Peptidoglycan Biosynthesis in *Bacillus subtilis* with Fluorescent Antibiotics. *Proceedings of the National Academy of Sciences* 103(29):11033-11038.
 209. Helm JS, Chen L, & Walker S (2002) Rethinking Ramoplanin: the Role of Substrate Binding in Inhibition of Peptidoglycan Biosynthesis. *Journal of the American Chemical Society* 124(47):13970-13971.
 210. Hartman BJ & Tomasz A (1984) Low-Affinity Penicillin-Binding Protein Associated with β -Lactam Resistance in *Staphylococcus aureus*. *Journal of Bacteriology* 158(2):513-516.
 211. Stapleton PD & Taylor PW (2002) Methicillin Resistance in *Staphylococcus aureus*: Mechanisms and Modulation. *Science Progress* 85(Pt 1):57.
 212. Monteiro JM, *et al.* (2015) Cell Shape Dynamics During the Staphylococcal

Cell Cycle. *Nature Communications* 6.